GENOMIC ANALYSIS OF COHESIN DYNAMICS IN FISSION YEAST

Christine Katrin Schmidt

Thesis presented for the degree of Doctor of Philosophy to
University College London

Supervisor: Dr. Frank Uhlmann

2004 to 2008

Chromosome Segregation Laboratory
Cancer Research UK, London Research Institute
44 Lincoln's Inn Fields
London WC2A 3PX
United Kingdom

Statutory declaration

I, Christine Katrin Schmidt, confirm that the work presented in this thesis is my own. Where information has been derived from other sources, I confirm that this has been indicated in the thesis.

SOME IMPRESSIONS

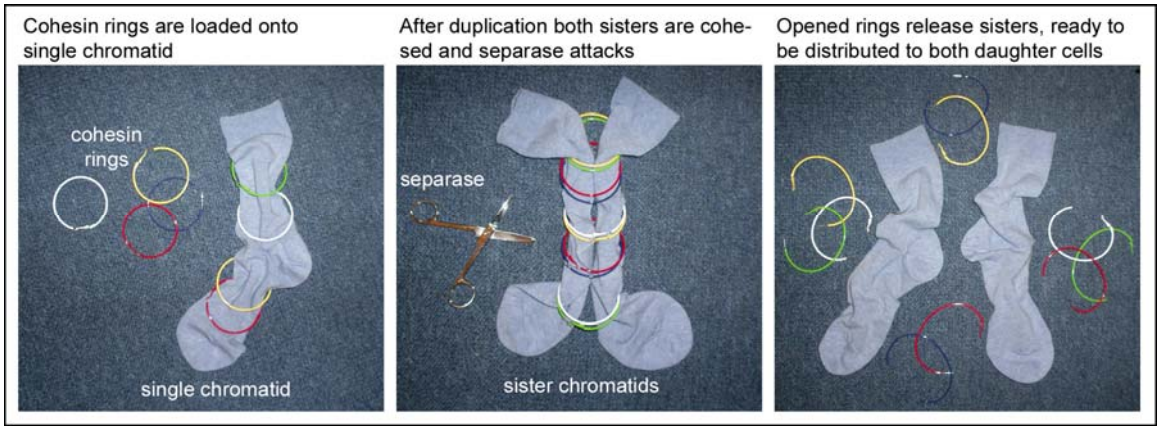

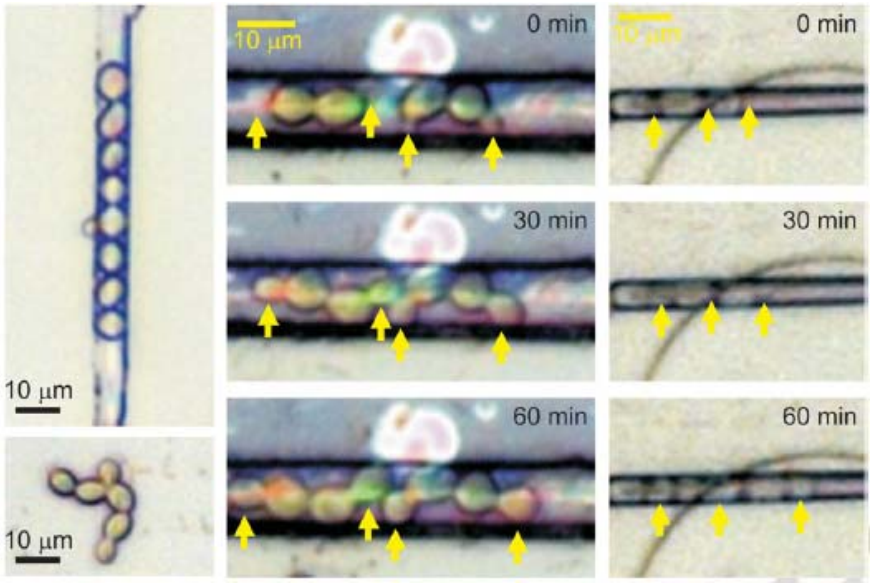

Budding yeast explores and duplicates in microtube channels.
Picture taken from Mei et al, 2008.

Publications arising from this thesis

1. Bernard P*, Schmidt CK*, Vaur S*, Dheur S, Drogat J, Genier S, Ekwall K, Uhlmann F, Javerzat JP (2008) Cell-cycle regulation of cohesin stability along fission yeast chromosomes. *EMBO J* **27**(1)**:** 111-121

2. D'Ambrosio C, Schmidt CK, Katou Y, Kelly G, Itoh T, Shirahige K, Uhlmann F (2008) Identification of *cis*-acting sites for condensin loading onto budding yeast chromosomes. *Genes Dev* **22**(16): 2215-2227

3. Schmidt CK, Brookes N, Uhlmann F (2008) Cohesin localisation along fission yeast chromosomes delineates conserved mechanisms of binding. *submitted*

* These authors contributed equally to the indicated study.

Abstract

Cohesin holds sister chromatids together and facilitates their accurate segregation in mitosis. Little is known about how and where cohesin binds to chromosomes. Recent genome-wide investigations have led to apparent disparities between different model organisms.

In this thesis, analysis of the cohesin binding pattern reveals that several determinants, thought specific for distinct organisms, collectively define the overall distribution of cohesin along fission yeast chromosomes. Like in budding yeast, cohesin is mainly detected at sites of convergent transcriptional termination, in the following termed convergent sites. However, only approximately half of these are bound whereas in budding yeast almost all of them are associated with cohesin. Furthermore, we detect cohesin at loci away from convergent sites which are characterised by the presence of the cohesin loader Mis4/Ssl3. Cohesin loading sites show a striking overlap with strongly transcribed genes, including tRNA and ribosomal protein genes. This is reminiscent of *Drosophila* cohesin and its loading factor Nipped-B that both overlap near highly transcribed genes. The cohesin loader also promotes cohesin accumulation at neighbouring convergent sites, which, together with gene arrangement and transcription, contributes to the distribution of cohesin among convergent sites.

Cohesin binding to G1 chromosomes depends on the continuous activity of the cohesin loader Mis4/Ssl3. Cohesin stability then increases during S phase independently of DNA replication but in part dependent on the acetyltransferase Eso1, a factor implicated in the establishment of cohesion. This indicates that cohesin stabilisation might be a pre-requisite for cohesion establishment rather than its consequence.

During mitosis, a fraction of cohesin leaves chromosomes in a cleavage-independent reaction in prophase similarly to what has been observed in higher eukaryotes. A substantial pool of cohesin then dissociates from chromosomes upon its cleavage at anaphase onset. As a unique feature, centromeric cohesin spreads out onto chromosome arms towards anaphase as the heterochromatin protein Swi6 dissociates from centromeres.

Taken together, our results suggest conserved mechanisms for both cohesin binding and dynamics across eukaryotes.

Table of Contents

1 Introduction 17

1.1 Sister chromatid cohesion and chromosome segregation 17

1.2 SMC complexes: chromatin modulators with various functions 19

1.2.1 General architecture of SMC complexes 19

1.3 Cohesin: a 'biological glue' that sticks sister chromatids together 22

1.3.1 The architecture of the cohesin complex 22

1.3.2 Cohesin and sister chromatid cohesion: the ring-model 22

1.3.3 Cohesin dynamics during the cell cycle 23

1.3.3.1 The cycle begins: cohesin loading onto chromatin 24

1.3.3.1.1 Cohesin loading depends on a separate loading complex 24

1.3.3.1.2 The cohesin binding pattern in budding yeast 25

1.3.3.1.3 Cohesin recruitment to fission yeast centromeres 27

1.3.3.1.4 Swi6-dependent cohesin recruitment to chromosome arms 28

1.3.3.1.5 Cohesin binding to chromosomes in *Drosophila melanogaster* 30

1.3.3.1.6 Cohesin association with chromosomes in human and mouse 30

1.3.3.2 Cohesion establishment in S phase 31

1.3.3.3 Sister chromatid cohesion in G2 33

1.3.3.3.1 Maintenance of cohesion 33

1.3.3.3.2 *De novo* cohesion establishment in response to DNA damage 33

1.3.3.4 Resolution of sister chromatid cohesion in M phase 35

1.3.3.4.1 Resolution of sister chromatid cohesion in budding yeast 35

1.3.3.4.2 Dismantling sister chromatid cohesion in higher eukaryotes 36

1.3.4 Cohesin and its regulators: expanding chromosomal functions 38

1.3.4.1 DNA repair by homologous recombination (HR) 38

1.3.4.2 Gene regulation 38

1.3.5 Cohesin and cohesin-related factors in disease 40

1.3.5.1 Cornelia de Lange syndrome 40

1.3.5.2 Roberts syndrome 40

1.4 Condensin: a chromosomal compaction machine 41
1.4.1 Chromosome condensation 41
1.4.2 The structure of the condensin complex 43
1.4.3 Condensin's various functions 44
1.5 The Smc5/Smc6 complex: a DNA repair linker 45
1.6 Bacterial SMC: three in one? 46
2 Aims 47
3 Materials and Methods 49
3.1 Fission yeast techniques 49
3.1.1 Yeast gene and protein nomenclature 49
3.1.2 Fission yeast growth conditions 50
3.1.3 Cell synchronisation 51
3.1.3.1 G1 cell cycle arrest 51
3.1.3.1.1 Nitrogen starvation 51
3.1.3.1.2 *cdc10-129* cell cycle mutants 51
3.1.3.1.3 Res1-Cter overexpression 52
3.1.3.2 HU-induced early S phase arrest 52
3.1.3.3 G2 arrest: *cdc25-22* cell cycle mutants 52
3.1.3.4 M phase arrest: *nda3-KM311* cell cycle mutants 53
3.1.4 Inactivation of Aurora B kinase activity 53
3.1.5 Strain construction 54
3.1.5.1 Random spore analysis 54
3.1.5.2 Yeast transformations 54
3.1.6 Cell cycle analysis using flow cytometry 55
3.2 Biochemistry and related techniques 56
3.2.1 Chromatin fractionation (Chromatin Pellets) 56
3.2.1.1 Spheroplastation 56
3.2.1.2 Lysis and fractionation 57
3.2.2 ChIP on chip analysis 58
3.2.2.1 Formaldehyde fixation 58
3.2.2.2 Cell breakage 58
3.2.2.3 Sonication and chromatin immunoprecipitation (ChIP) 58
3.2.2.4 Reversal of cross-linking, proteinase K and RNAse A treatment 59

3.2.2.5 DNA amplification 60
3.2.2.6 DNAse digestion 61
3.2.2.7 DNA end-labelling with biotin 61
3.2.2.8 Hybridisation to oligonucleotide microarrays 62
3.2.3 TCA yeast cell extracts 64
3.2.4 SDS-PAGE 64
3.2.5 Western blotting 65
3.2.5.1 Protein transfer 65
3.2.5.2 Immunological detection 65
3.2.5.2.1 Blocking 65
3.2.5.2.2 Primary antibody 65
3.2.5.2.3 Secondary antibody 65
3.2.5.2.4 ECL detection 65

3.3 Molecular Biology 66
3.3.1 Genomic DNA preparation 66
3.3.2 Polymerase chain reaction (PCR) 66
3.3.2.1 Endogenous C-terminal tagging of yeast proteins 66
3.3.2.2 ChIP on chip DNA amplification 68
3.3.2.2.1 Priming of genomic DNA (Round A) 68
3.3.2.2.2 DNA amplification (Round B) 69
3.3.3 Restriction digests 70
3.3.4 Phosphatase treatment 70
3.3.5 DNA ligations 71
3.3.6 Bacterial transformations 71
3.3.7 Isolation of plasmid DNA from *E. coli* 71
3.3.8 Agarose gel electrophoresis 72
3.3.9 Retrieval of DNA fragments from agarose gels 72

3.4 Cell biology and microscopy 73
3.4.1 Chromosome spreading 73
3.4.2 DNA visualisation (DAPI staining) 74
3.4.3 Septum visualisation (Calcofluor staining) 74
3.4.4 Tubulin visualisation 74

3.5 Biostatistics and Bioinformatics 75
3.5.1 Peak-picking parameters for ChIP on chip maps 75
3.5.2 Bootstrapping approach to create random cohesin binding patterns 75

3.6 Strain list 76

3.7 Vector list 78

3.8 Antibody lists 79

4 Results 80

4.1 A complex cohesin pattern along fission yeast chromosomes 80

4.1.1 Cohesin binds to an ordered subset of convergent sites 80

4.1.2 Non-random ORF arrangement along fission yeast chromosomes 83

4.1.3 Expression levels influence cohesin's binding pattern 84

4.1.4 Gene arrangement can influence cohesin's binding pattern 86

4.1.5 The role of Swi6 in defining cohesin's binding pattern 87

4.1.6 The relationship between cohesin and its loading factor Mis4/Ssl3 88

4.1.6.1 Mis4/Ssl3 overlaps with tRNA and RP genes 88

4.1.6.2 Mis4/Ssl3 coincides with other highly transcribed genes 91

4.1.6.3 An overlap of cohesin and its loader away from convergent sites 92

4.1.6.4 Cohesin clusters around its loading sites 93

4.1.6.5 The role of tRNA genes for the Mis4 and cohesin binding pattern 94

4.1.7 Mis4/Ssl3 co-localises with condensin 95

4.2 Resolution of cohesion in mitosis 97

4.2.1 Cohesin removal from fission yeast chromosomes in prophase 97

4.2.2 Cohesin-cleavage and removal at anaphase-onset 97

4.2.3 Reciprocal regulation of Mis4/Ssl3 and condensin during mitosis 100

4.2.3.1 Removal of Mis4/Ssl3 from mitotic chromosomes 100

4.2.3.2 Condensin binding to chromosomes in interphase and in mitosis 100

4.2.4 Cohesin's binding pattern during mitosis 103

4.2.4.1 Cohesin is evenly removed from mitotic chromosome arms 103

4.2.4.2 Centromeric cohesin spreads onto chromosome arms in mitosis 103

4.2.5 Heterochromatin regulates cohesin dynamics around centromeres 106

4.2.6 Cell cycle-dependent cohesin binding to the central core 109

4.3 Cell cycle regulation of cohesin stability along chromosomes 111

4.3.1 Instable cohesin binding in G1 is conserved across evolution 111

4.3.2 Cohesin binding to chromatin is stabilised in S phase cells 113

4.3.3 Cohesin stabilisation is independent of DNA replication 113

4.3.4 Eso1's contribution to cohesin stabilisation during S phase 117

5 Discussion 120

5.1 Cohesin association with fission yeast chromosomes 120

5.1.1 Similar mechanisms for cohesin loading and translocation? 120

5.1.2 Separation of function at specific cohesin sites? 122

5.1.3 A non-random cohesin distribution among convergent sites 124

5.1.4 Conserved and unique aspects of cohesin behaviour during mitosis 125

5.1.4.1 Two-step resolution of cohesion in fission yeast 125

5.1.4.2 A complex set of cohesin behaviours at centromeres 126

5.2 Condensin's chromosomal association pattern 127

5.2.1 A common loading mechanism for eukaryotic SMC complexes? 127

5.2.2 Condensin and nuclear architecture 128

5.3 Stabilisation of cohesin binding to chromosomes in S phase 129

5.3.1 A role for cohesin dynamics in gene regulation? 129

5.3.2 Cohesin stabilisation and cohesion establishment 129

6 References 132

7 Appendix 132

7.1 The cohesin binding pattern along fission yeast chromosome 2 142

7.1.1 ChIP on chip map of the cohesin subunit Rad21 142

7.1.2 Peak list of the cohesin subunit Rad21 154

7.2 Mis4 and Ssl3 binding pattern along fission yeast chromosome 2 157

7.2.1 ChIP on chip map of the cohesin loader Mis4/Ssl3 157

7.2.2 Peak list of the cohesin loader subunit Mis4 169

7.3 The condensin binding pattern along fission yeast chromosome 2 171

7.4 Sfc6 binding pattern along fission yeast chromosome 2 184

7.5 Fhl1 binding pattern along fission yeast chromosome 2 197

8 Acknowledgements 210

Table of Figures

Figure 1.1 Karyotypes of a normal human cell (A) and a human breast cancer cell (B) 18
Figure 1.2 Overview of the structure of SMC proteins and complexes 20
Figure 1.3 Cohesin forms ring-like structures. 23
Figure 1.4 Model of cohesin dynamics during the fission yeast cell cycle 24
Figure 1.5 Model of cohesin loading onto chromosomes 26
Figure 1.6 The structure of fission yeast centromere 1 27
Figure 1.7 Model of Swi6-dependent cohesin recruitment to convergent sites 29
Figure 1.8 Overview of different models of cohesin binding in various eukaryotes 31
Figure 1.9 Cohesion establishment during DNA replication 33
Figure 1.10 Model of Eco1-dependent cohesion establishment in G2 34
Figure 1.11 Dismantling sister chromatid cohesion in budding yeast 36
Figure 1.12 Resolution of cohesion in higher eukaryotes 37
Figure 1.13 Model of cohesin- and CTCF-mediated insulator function 39
Figure 1.14 Chromosome packaging of eukaryotic chromosomes 42
Figure 1.15 The architecture of the condensin I complex 43
Figure 1.16 The structure of a bacterial SMC complex 46
Figure 3.1 Schematic of the ChIP on chip procedure. 63
Figure 3.2 Oligonucleotide arrangement on chromosome 2/3 microarray. 63
Figure 4.1 A large fraction of convergent sites is not bound by cohesin. 81
Figure 4.2 Overlay of cohesin with Mis4 and convergent sites 82
Figure 4.3 Maximal distance analysis of neighbouring cohesin peaks 83
Figure 4.4 Expression levels contribute to cohesin‘s binding pattern. 85
Figure 4.5 Different cohesin patterns in mitosis and meiosis 86
Figure 4.6 The convergent site gene arrangement contributes to the cohesin pattern. 87
Figure 4.7 Swi6-independent cohesin patterning along chromosome arms 88
Figure 4.8 Mis4/Ssl3 co-localises with TFIIIC and Fhl1 at tRNA and RP genes. 89
Figure 4.9 Proximity of Mis4 sites to tRNA and RP genes on chromosome 2 90
Figure 4.10 Cytological co-localisation of Mis4/Ssl3 with Sfc3 and Fhl1 91
Figure 4.11 A link between expression and Mis4/Ssl3 association. 92
Figure 4.12 Mis4 influences cohesin’s distribution among convergent sites. 94

Figure 4.13 tRNA genes contribute to the binding patterns of Mis4 and cohesin. 95
Figure 4.14 Mis4/Ssl3 shows a striking overlap with condensin. 96
Figure 4.15 Cleavage-independent cohesin removal from chromosomes in prophase ... 98
Figure 4.16 Cleavage and removal of a cohesin fraction at anaphase-onset 99
Figure 4.17 Removal of a subfraction of Mis4/Ssl3 from mitotic chromosomes 101
Figure 4.18 Condensin binding to chromosomes in G2 and in mitosis 102
Figure 4.19 The cohesin binding pattern along chromosome arms during mitosis 104
Figure 4.20 Cohesin spreading around centromeres during mitosis 105
Figure 4.21 Swi6-regulation of cohesin dynamics during mitosis 108
Figure 4.22 Cohesin, Mis4/Ssl3 and condensin overlap at centromeres. 109
Figure 4.23 Cohesin binding to G1 chromatin requires continued Mis4/Ssl3 activity. 112
Figure 4.24 Cohesin stabilisation along chromosomes in HU-induced S phase 114
Figure 4.25 Rad21 stabilisation is independent of DNA replication. 117
Figure 4.26 Eso1 function is compromised in *eso1-H17* cells at 32°C. 118
Figure 4.27 The role of Eso1 for cohesin stabilisation in S phase 119
Figure 5.1 Model for cohesin binding in various eukaryotes 122

Table of Tables

Table 1.1 Nomenclature of cohesin and condensin complexes in different species 21
Table 3.1 Pipetting scheme for proteinase K digestion 59
Table 3.2 DNAse I digestion recipe 61
Table 3.3 Biotin-labelling pipetting recipe 61
Table 3.4 Pipetting scheme for DNA hybridisation cocktail 62
Table 3.5 PCR pipetting scheme for C-terminal tagging of yeast proteins 67
Table 3.6 PCR programme for C-terminal tagging of yeast proteins 68
Table 3.7 Pipetting schemes for ChIP on chip Round A priming reaction 69
Table 3.8 PCR pipetting recipe for ChIP on chip Round B 69
Table 3.9 PCR programme for ChIP on chip Round B 70
Table 3.10 Strains used for functional experiments in this study 76
Table 3.11 List of DNA vectors used in this study 78
Table 3.12 Primary antibodies used in this study 79
Table 3.13 Secondary antibodies used in this study 79
Table 4.1 ORF arrangement in the fission yeast genome 83
Table 4.2 Non-convergent Rad21 peaks along chromosome 2 93

List of Abbreviations

°C	Degree(s) Celsius
Δ	Deletion
ab	Antibody
ABC	ATP-binding cassette
AF	Alexa Fluor
Amp	Ampicillin
APS	Ammonium peroxodisulfate
ARS	Autonomous replicating origins
ATP	Adenosine triphosphate
AU(s)	Arbitrary unit(s)
BrdU	5-Bromo-2-deoxyuridine
BSA	Bovine serum albumin
bp	Base pairs
CAR	Cohesin associated region
CDK	Cyclin dependent kinase
CdLS	Cornelia de Lange syndrome
cen	Centromere
CIP	Calf intestinal phosphatase
ChIP	Chromatin immunoprecipitation
cnt	Central core
cs	Cold-sensitive
CS	Chromosome spreads
CTCF	CCCTC-binding factor
DAPI	4', 6-diaminidino-2-phenylindole
dH_2O	Distilled water
dNTP	Deoxyribonucleoside triphosphate
DSB	DNA double strand break
D. melanogaster	*Drosophila melanogaster*
DMSO	Dimethyl sulfoxide
DNA	Deoxyribonucleic acid
DNAse	Deoxyribonuclease
dsDNA	Double-stranded DNA
DTT	Dithiothreitol
ECL	Enhanced chemiluminescence
Eco	Establishment of cohesion
EDTA	Ethylene diamine tetra-acetic acid
EM	Electron microscopy
EMM	Edinburgh minimal medium
eGFP	Enhanced green fluorescent protein
FACS	Fluorescence activated cell sorting
5-FOA	5-Fluoroorotic acid
FRAP	Fluorescence recovery after photobleaching
G1 (2)	Gap1 (2) phase
g	Gram
GEO	Gene expression omnibus
GFP	Green fluorescent protein
HA	Hemagglutinin
HEPES	4-(2-hydroxyethyl)-1-pipeazineethansulfonic acid
HMR	Hidden MAT Right
HP1	Heterochromatin protein 1
HR	Homologous recombination
HRP	Horseradish peroxidase
HU	Hydroxyurea
hygMX6	Hygromycin B resistance gene

imr	Innermost repeats
IP	Immunoprecipitation
kanMX6	Kanamycine resistance gene
kb	Kilo base pairs
kD	Kilo Dalton
l	Litre
L	Left
LB	Luria Broth
log	Logarithm
LRI	London Research Institute, Cancer Research UK (CRUK)
µ-	Micro-
m-	Milli-
M	Molar
Mb	Megabase pairs
MEA4S	Malt extract agar plus supplements
MES	2-(N-morpholino) ethane sulfonic acid
min	Minute
n-	Nano-
NaAc	Sodium acetate
Nda	Nuclear division arrest
NEBD	Nuclear envelope breakdown
NHEJ	Non-homolgous end joining
NIPBL	Nipped-B like
1NM-PP1	4-amino-1-tert-butyl-3-(1-napthylmethyl)pyrazolo[3,4-d]pyrimidine
NOC	Nocodazole
OD	Optical density
ORF	Open reading frame
otr	Outer repeats
-p	Protein (*S. pombe* nomenclature)
PAGE	Polyacrylamide gel electrophoresis
PBS	Phophate buffered saline
PBST	Phophate buffered saline with 0.1 % Tween-20
PCR	Polymerase chain reaction
PEG	Polyethylene glycol
PIPES	1,4-Piperazinediethansulfonic acid
Plk1	Polo-like kinase 1
PMSF	Phenylmethanesulfonyl fluoride
Pol II (III)	RNA polymerase II (III)
pre-RC	Pre-replication complex
R	Right
Rad	Radiation-sensitive
RNA	Ribonucleic acid
RNAi	RNA interference
RNAse	Ribonuclease
RP genes	Ribosomal protein genes
rpm	Rotations per minute
SAPE	Phycoerythrin-streptavidin
S. cerevisiae	*Saccharomyces cerevisiae*
Scc	Sister chromatin cohesion
SDS	Sodium dodecyl sulphate
SI	Septation index
Sir	Silent information regulator
SKY	Spectral karyotyping
Smc	Structural maintenance of chromosomes
SPB	Spindle pole body
S phase	Synthesis phase
S. pombe	*Schizosaccharomyces pombe*
ssDNA	Single stranded DNA
SUP	Supernatant
Taq	*Thermus aquaticus*
TBS	Tris buffered saline
TCA	Trichloroacetic acid

Temed	N, N, N`, N`-Tetra methyl ethylene diamine
T_M	Melting temperature (of PCR primers)
Tris	Tris hydroxyl methylaminomethane
tRNA	Transfer RNA
ts	Temperature-sensitive
UTR	Untranslated region
UV	Ultraviolet
v/v	Volume per volume
Wapl	Wings-apart like
WB	Western blots
WCE	Whole cell extract
wt	Wild type
w/v	Weight per volume
YE	Yeast extract
YE4S	Yeast extract plus supplements

1 Introduction

1.1 Sister chromatid cohesion and chromosome segregation

Sister chromatids are tightly held together from their synthesis in S phase onwards, facilitating bipolar attachment of the kinetochores to the spindle during mitosis. Once chromosomes are aligned in metaphase, sister chromatid cohesion is resolved at anaphase onset, allowing the spindle to separate sisters to opposite cell poles and ensuring that an identical set of them is distributed to both daughter cells. Sister chromatids not properly associated with another therefore lead to segregation defects resulting in daughter cells with altered chromosome sets. Certain chromosomes might be missing or might have been added by mistake, a state termed aneuploidy. The importance of accurate chromosome segregation is demonstrated by the fact that aneuploidy is a hallmark of cancer cells (Lengauer et al, 1998). As an example, Figure 1.1 shows the chromosome set of a healthy human cell in which all 92 chromosomes are tightly held together in 46 pairs. Next to it, a karyotype of a human cancer cell is illustrated. Apart from numerous chromosomal translocations, the change in chromosome number due to chromosome segregation defects is striking (Figure 1.1).

But what is the biological glue made of that holds sister chromatids together and ensures their accurate segregation, thus protecting cells from genetic instability?

It is little more than a decade ago that cohesin the protein complex responsible for this process was identified. Cohesin belongs to a small group of protein complexes that contain structural maintenance of chromosomes (SMC) subunits. SMC complexes are conserved amongst the three phyla of life, and, apart from cohesin, include condensin, the Smc5/Smc6 complex and the bacterial SMC complex. All of these complexes are involved in actions related to chromosome structure and function, and the following paragraphs aim to point out some of their most important structural and functional similarities as well as their differences. The major focus will be on cohesin as it forms the main topic of interest in this thesis.

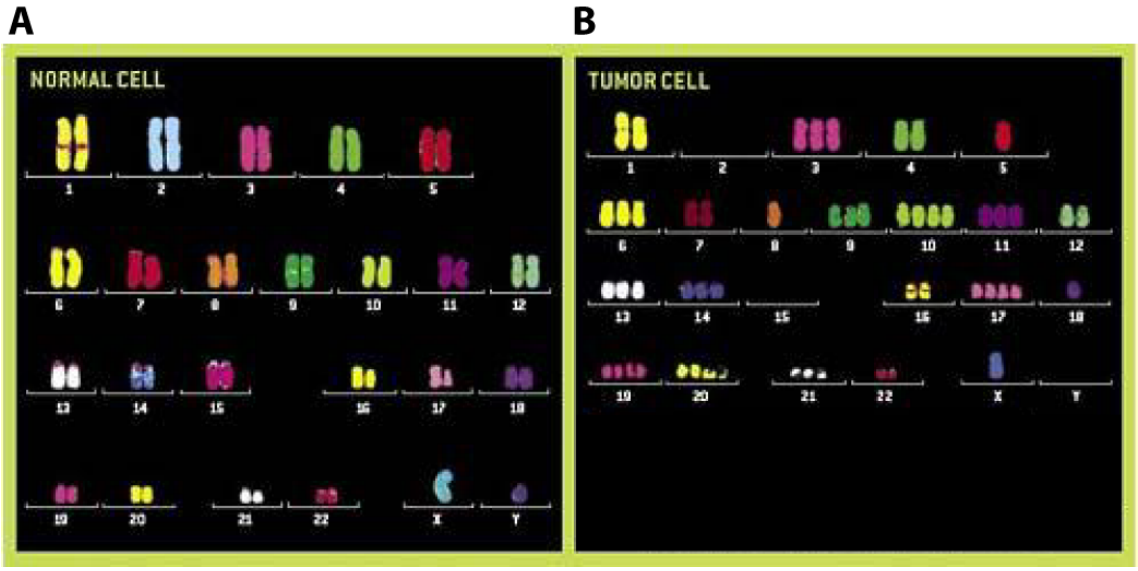

Figure 1.1 Karyotypes of a normal human cell (A) and a human breast cancer cell (B)
The 46 human chromosomes are visualised by multicolour spectral karyotyping (SKY) analysis. Due to chromosome segregation defects and chromosomal rearrangements, chromosome number and structure are highly abnormal in the tumour cell in B, characteristiscs common to most cancerous cells. Picture modified from University of California - Berkeley (2007, June 28). ScienceDaily. Retrieved August 18, 2008, from http://www.sciencedaily.com/releases/2007/06/070627130024.htm.

1.2 SMC complexes: chromatin modulators with various functions

1.2.1 General architecture of SMC complexes

SMC complexes form dimers of SMC subunits which associate with various regulatory subunits to assemble into large higher-order protein complexes. Most, if not all, bacteria and archea have one single SMC protein that dimerises to form a homodimer (1.6; Hirano, 2006). In contrast, in every eukaryote studied to date, six different SMC proteins have been discovered that form specific combinations, generating three heterodimers with different functions. Smc1/Smc3 heterodimers make up the structural basis for cohesins which hold two identical sister chromatids together from their synthesis during S phase until their segregation in mitosis (1.3; Guacci et al, 1997; Michaelis et al, 1997). Condensins, another class of SMC protein complexes composed of Smc2 and Smc4 are primarily responsible for compaction of the genome before cells divide (1.4; Hirano, 2005). The primary sequences of the two remaining SMC proteins, Smc5 and Smc6, are slightly more divergent from the other four SMC proteins. The Smc5/Smc6 complex is mainly involved in DNA repair and checkpoint responses but its exact functions remain largely unknown (1.5; Lehmann, 2005).

A common and striking feature of SMC complexes is the unusual core structure of the SMC dimers (Figure 1.2A). Each SMC subunit is composed of globular domains at its N- and C-terminus which are separated by a long α-helical structure, containing another globular domain in the middle, called the hinge domain. Each SMC subunit folds back by an antiparallel coiled coil, leading to a rod-like structure, also referred to as the arm region. The globular hinge is located at one end, and the closely associated N- and C-terminal globular domain, called the head domain, localises at the opposite end. The two rod-shaped SMC subunits then bind to another through an interaction between their hinge domains leading to characteristic heterodimers. The N-terminus of each SMC subunit contains a Walker A and the C-terminus a Walker B motif which together make up a functional ATP-binding cassette (ABC). In addition, the C-terminus contains a so-called signature motif that facilitates binding of the head domain of one SMC subunit to an ATP molecule bound to the other SMC subunit. The interaction site between the heads is much weaker than the one at the hinge (reviewed in Losada & Hirano, 2005).

Importantly, the resulting SMC dimers are very large complexes. Each coiled-coil arm is approximately 50 nm long, a length equivalent to 150 bp of double-stranded DNA (dsDNA) (Losada & Hirano, 2005).

All SMC dimers associate with a varying number of regulatory subunits that add to the specific functions of the different complexes. Generally, a member of the so-called kleisin superfamily of proteins binds to the head domains of the dimer. Kleisins include the Scc1 subunit of cohesin and the CAP-H and CAP-H2 subunits of condensin (Figure 1.2B and reviewed in Schleiffer et al, 2003).

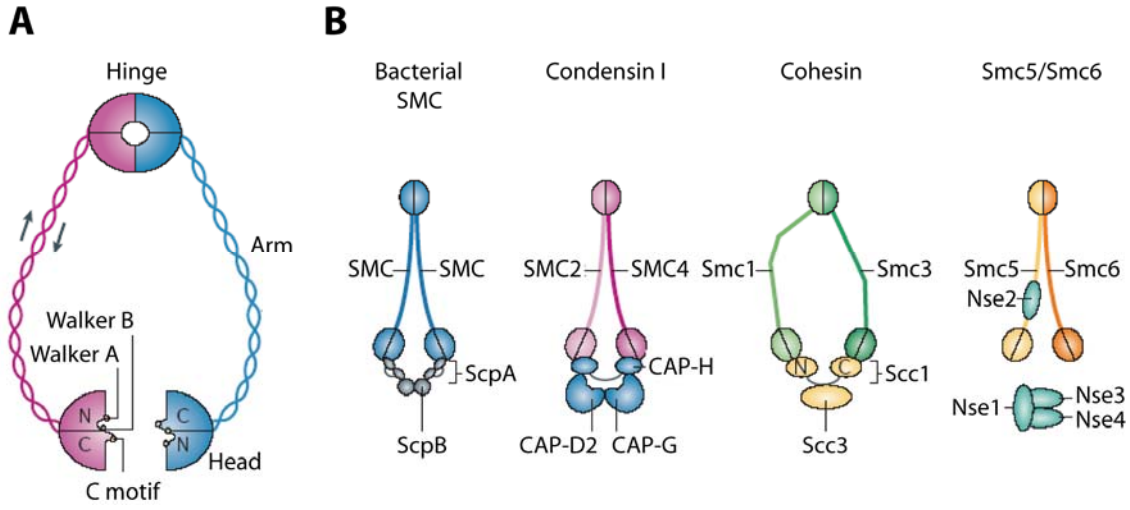

Figure 1.2 Overview of the structure of SMC proteins and complexes
(**A**) General architecture of an SMC protein dimer. The globular domains of the N- and C-terminus of each subunit fold back via an antiparallel coil (arrows) and form the ATP head domains at one end of the coil. At the other end, a globular domain, the hinge, is formed, the major dimerisation site of the two subunits. (**B**) Architecture of bacterial and eukaryotic SMC complexes. The bacterial SMC complex is the only example of two identical SMC subunits that form a homodimer. Two non-SMC subunits, SpcA and SpcB, associate with the dimer at its head region. The three eukaryotic SMC complexes are based on SMC heterodimers, Smc2 and Smc4 for condensin, Smc1 and Smc3 for cohesin and Smc5 and Smc6 for the Smc5/Smc6 complex. The number and association sites for non-SMC subunits vary between the different complexes but usually include binding of a kleisin subunit to the head domain. Picture taken from Hirano, 2006.

The naming of the SMC complex subunits is complicated by the fact that every model organism follows its own nomenclature, and many of the subunits have been individually discovered before their role as a structural basis of SMC complexes was elucidated. A table containing the names of the SMC and non-SMC subunits of cohesin and condensin in various model organisms is listed below.

Table 1.1 Nomenclature of cohesin and condensin complexes in different species

	S. cerevisiae	***S. pombe***	***Drosophila***	***X. laevis***	**Human**
Cohesin					
SMC1	Smc1	Psm1	SMC1	SMC1	SMC1α
SMC3	Smc3	Psm3	SMC3	SMC3	SMC3
SCC1	Scc1/Mcd1	Rad21	RAD21	RAD21	RAD21
SCC3	Scc3	Psc3	SA	SA1, SA2	SA1, SA2
REC8 (meiosis)	Rec8	Rec8	-	-	REC8
Condensin					
SMC2	Smc2	Cut14	DmSMC2	CAP-E	hCAP-E
SMC4	Smc4	Cut3	DmSMC4	CAP-C	hCAP-C
Condensin I-specific					
HEAT	Ycs4	Cnd1	CG1911	CAP-D2/Eg7	hCAP-D2/CNAP1
HEAT	Ycg5/Ycg1	Cnd3	CG17054	CAP-G	hCAP-G
Kleisin	Brn1	Cnd2	Barren	CAP-H	hCAP-H
Condensin II-specific					
HEAT	-	-	CG31989	-	hCAP-D3
HEAT	-	-	-	-	hCAP-G2
Kleisin	-	-	CG14685	-	hCAP-H2

1.3 Cohesin: a 'biological glue' that sticks sister chromatids together

The following paragraphs will focus in detail on what has been discovered about the cohesin complex since its discovery little more than a decade ago (Guacci et al, 1997; Michaelis et al, 1997). As all results in this thesis are based on data derived from fission yeast, particular attention will be paid to what is known about cohesin function and structure in this model organism.

1.3.1 The architecture of the cohesin complex

Cohesin consists of four essential core subunits conserved from yeast to human. Two of the subunits belong to the structural maintenance of chromosomes (SMC) family of proteins, as described previously. In fission yeast, the two SMC subunits Psm1 and Psm3 associate with the kleisin subunit Rad21 at their head domains. The fourth subunit Psc3 associates with Rad21 (Figure 1.3A; Tomonaga et al, 2000). Further subunits that are thought to associate with cohesin include Pds5 (Hartman et al, 2000; Panizza et al, 2000; Wang et al, 2002) and Wapl (Gandhi et al, 2006; Kueng et al, 2006; Wpl1 in *S. pombe* (Bernard et al, 2008)).

Vertebrate cohesin has been visualised by electron microscopy, revealing ring-like structures with the angle of the hinge wide open and the arms clearly separated. Furthermore, the regulatory subunits were visible as globular domains that associated with the head domains of the SMC heterodimers (Figure 1.3B; Anderson et al, 2002).

1.3.2 Cohesin and sister chromatid cohesion: the ring-model

The canonical function of cohesin is mediating sister chromatid cohesion from their synthesis in S phase onwards until their segregation in M phase. But how does cohesin hold the two sister chromatids together? The ring-like structure of cohesin has given rise to the hypothesis that cohesin might tether sister chromatids together by topologically embracing the two DNA double-helices inside the ring (Figure 1.4; Haering et al, 2002). Importantly, the ring has a diameter of approximately 30 - 40 nm which is theoretically large enough to accommodate the two DNA double-helices inside.

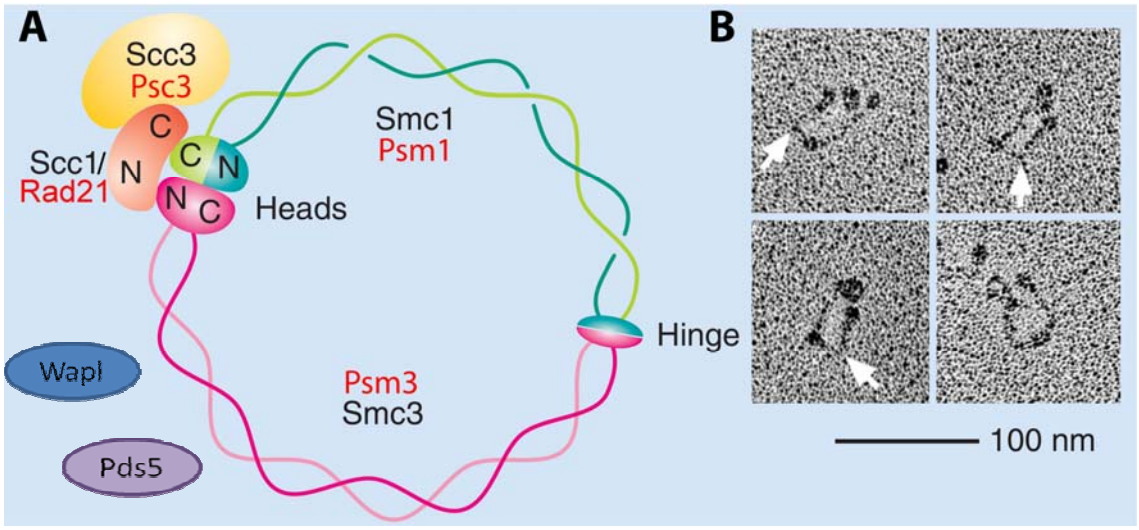

Figure 1.3 Cohesin forms ring-like structures.
(**A**) Schematic of the four core subunits of cohesin and their arrangement into a ring-like structure. Two other proteins, Pds5 and Wapl, have also been identified as cohesin subunits. It is currently unknown how stably and where exactly they associate with the cohesin ring. Names of cohesin subunits in fission yeast are indicated in red. (**B**) Electron micrographs of purified vertebrate cohesin (Anderson et al, 2002) and biochemical studies (Haering et al, 2002) provided the first evidence that gave rise to the ring-model of cohesin. Arrows indicate kinks that can often be observed at the same position in one of the two coiled-coil arms of the SMC subunits of cohesin but not of condensin. It is currently not known what functional relevance, if any, these bends might have (Haering et al, 2002). Figure modified from Uhlmann, 2003.

The ring model is intriguing as it would explain how proteolytic cleavage of the cohesin ring at anaphase onset (1.3.3.4) can lead to complete dissociation of cohesin from chromosomes and trigger sister chromatid separation. It would also explain how sister chromatid cohesion can be established concomitantly with DNA replication during S phase, as the replication machinery could be envisioned to pass through the rings (Figure 1.4). Recent compelling experimental evidence supports this idea as cohesin dissociates from engineered circular minichromosome not only upon its own proteolytic cleavage but also when the minichromosome is cut with a restriction endonuclease (Haering et al, 2008; Ivanov & Nasmyth, 2005).
Other models of how cohesin might glue sister chromatids together have been proposed, including the formation of cohesin bracelets or snaps (reviewed in Huang et al, 2005; Onn et al, 2008). However, a detailed description of the different models proposed in the literature exceeds the frame of this thesis.

1.3.3 Cohesin dynamics during the cell cycle

A complex cycle of cohesin association and dissociation to and from chromosomes takes place during every cell cycle. Cohesin is loaded onto unreplicated chromosomes in G1, followed by cohesion establishment during DNA replication in S phase and

maintenance of cohesion in G2. In M phase sister chromatid cohesion is resolved, and chromosomes segregate. An overview of the different steps is shown in Figure 1.4. In the following paragraphs each step is described in more detail.

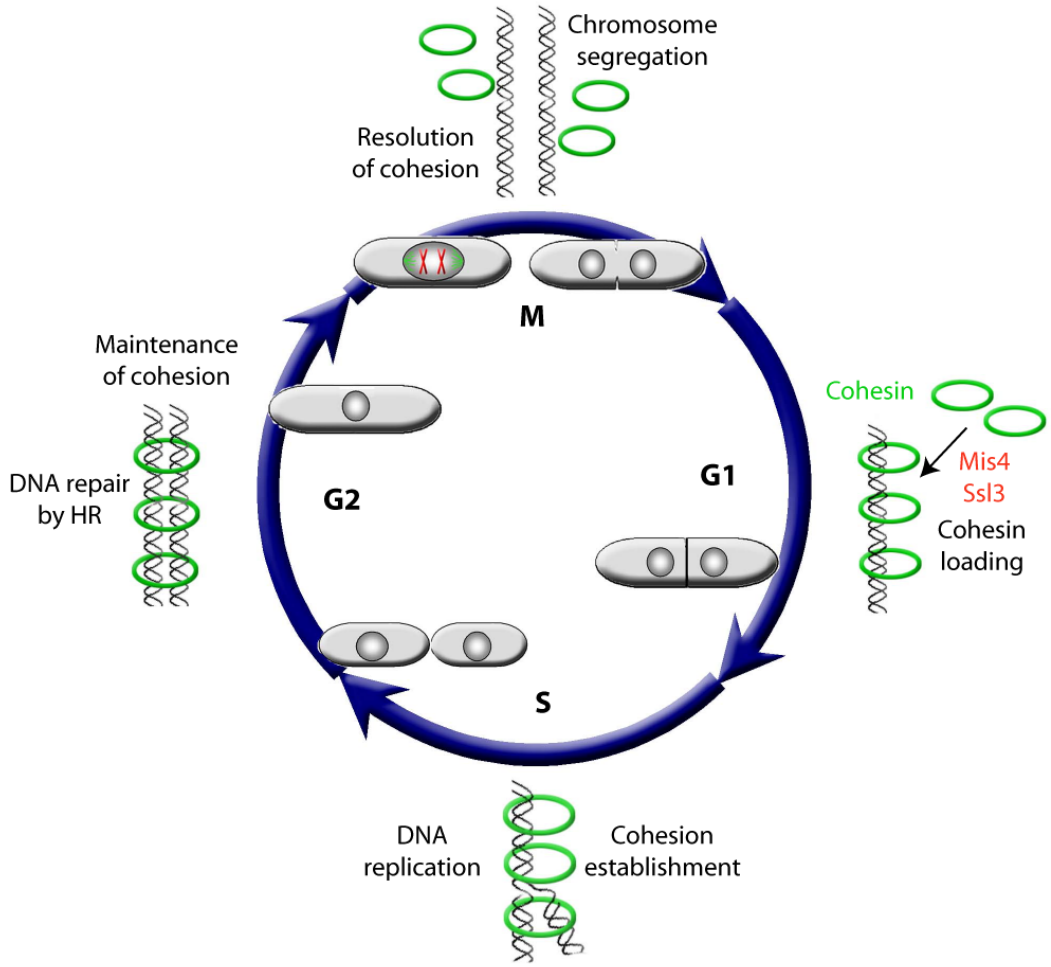

Figure 1.4 Model of cohesin dynamics during the fission yeast cell cycle
Cohesin (green rings) is loaded onto chromosomes in G1 in a process that depends on a separate loading complex constituted by Mis4 and Ssl3 in fission yeast. During DNA replication cohesion is established, possibly by topological embrace of the two sister chromatids by cohesin. Close proximity of the two sisters is maintained throughout G2. Sister chromatid cohesion helps to facilitate bipolar attachment of the spindle in M phase and thus, to ensure faithful chromosome segregation. For simplification, differences in time spans of cell cycle stages are neglected.

1.3.3.1 The cycle begins: cohesin loading onto chromatin

1.3.3.1.1 Cohesin loading depends on a separate loading complex

Cohesin loading onto chromosomes is mediated by a separate loading factor that consists of two essential subunits, Scc2 and Scc4 (Scc2/4) in budding yeast (Ciosk et al, 2000). Scc2 homologs have been discovered in fission yeast (Mis4), *Drosophila* (Nipped-B), *Xenopus* and human (NIPBL) (Furuya et al, 1998; Gillespie & Hirano, 2004; Rollins et al, 1999; Tonkin et al, 2004) and a role for Mis4 in cohesin loading to

fission yeast chromosomes has been described (Tomonaga et al, 2000). In contrary, the first Scc4 homolog, Ssl3, was only discovered in 2006 in fission yeast by Bernard et al in a screen for mutants synthetically lethal with the chromodomain containing protein Swi6, the ortholog of the heterochromatin protein HP1 in higher eukaryotes (Bernard et al, 2006). In a parallel study, Scc4 was also identified in humans (Watrin et al, 2006). Ssl3 makes a *bona fide* cohesin loading factor subunit as it is required for cohesin loading in G1 but dispensable in G2 when cohesion has already been established (Bernard et al, 2006). TIM-1, the *C. elegans* paralog of the *Drosophila timeless* clock gene functions in a similar way to the Scc2/4 cohesin loader (Chan et al, 2003). Both Scc2 and Tim-1 contain HEAT-repeats, degenerate repeating motifs involved in interactions between proteins. Furthermore, both proteins have been shown to interact with cohesin (Arumugam et al, 2003; Chan et al, 2003).

Although cohesin has been in the spotlight for many years, little is known about the molecular mechanism that leads to successful cohesin loading, and the chromosomal features that define cohesin loading sites remain elusive. It has been hypothesised that Scc2 might promote ATPase activity of the SMC heads which could lead to the opening of the cohesin ring and thereby facilitate its loading onto DNA (Arumugam et al, 2003). But where does cohesin bind to DNA? Several recent genome-wide analyses have resulted in seemingly striking differences between the rules underlying cohesin binding in distinct model organisms.

1.3.3.1.2 The cohesin binding pattern in budding yeast

Interesting insights came from a recent study in budding yeast which shows that cohesin first associates with chromosomes in G1 at sites marked by the Scc2/4 loading complex (Lengronne et al, 2004). These sites correlate with transcription strength (D'Ambrosio et al, 2008; Lengronne et al, 2004). Similarly, the *Drosophila* homolog of Scc2, Nipped-B, was also shown to co-localise with transcriptionally active genes (Misulovin et al, 2008). Interestingly, cohesin can only be detected at its loading sites during a brief time window in G1. For most of the cell cycle cohesin then localises between genes transcribed in converging directions at an average spacing of approximately 10 kb. Strikingly, cohesin is positioned to these regions by active transcription and not the underlying DNA sequence (Figure 1.5 and Figure 1.8; Glynn et al, 2004; Lengronne et al, 2004). Derived from these results and considering the ring model described above, an attractive model has emerged that envisions the transcription machinery pushing cohesin from its intial loading sites to its more permanent binding sites between conver-

gently transcribed genes (Figure 1.5; Lengronne et al, 2004). However, it is currently unclear, whether cohesin really slides along DNA or whether its translocation involves its release from DNA and its re-loading further down along the chromosome.

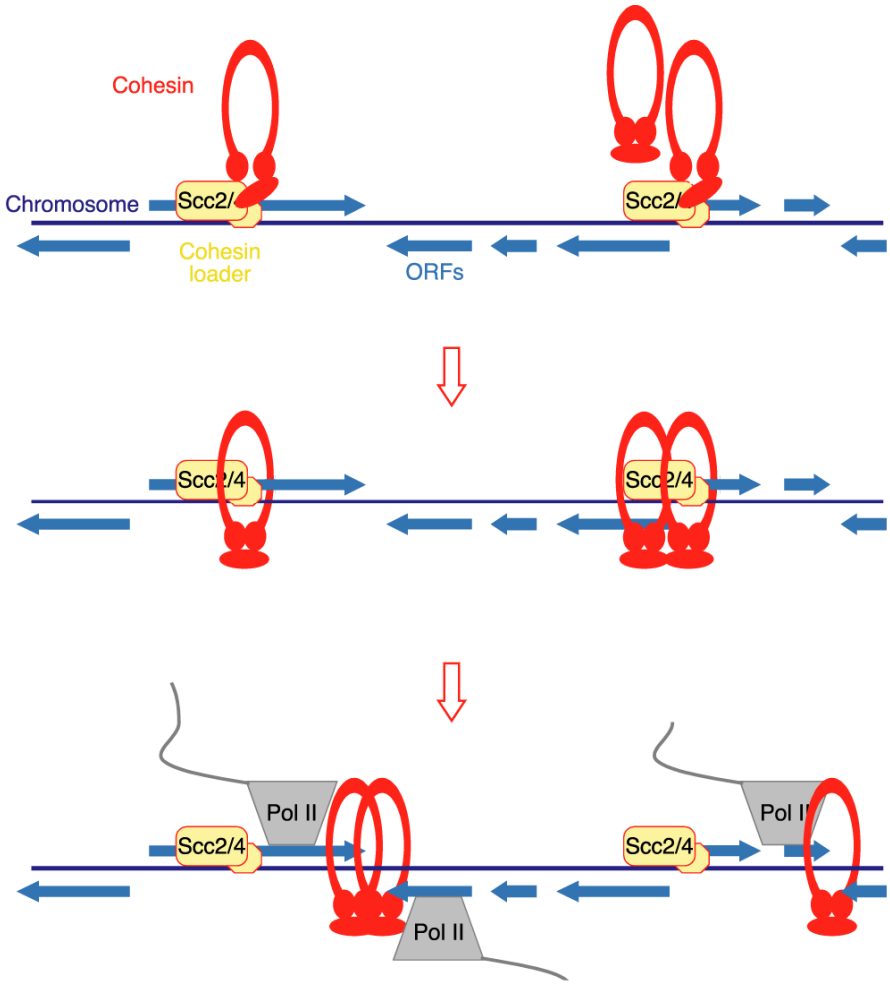

Figure 1.5 Model of cohesin loading onto chromosomes
In budding yeast, cohesin first associates with DNA at distinct loading sites characterised by the presence of the loading complex Scc2/4. Cohesin then translocates away to places between convergently transcribed genes, possibly by being pushed by the transcription machinery (Lengronne et al, 2004). Figure modified from Uhlmann, 2007.

Whereas budding yeast Scc2/4 remains chromosome-bound throughout the cell cycle, Scc2 in *Xenopus* egg extracts dissociates from chromosomes in mitosis. While its re-association with chromatin in the following cell cycle depends on the assembly of the pre-replication complex (pre-RC) it does not depend on initiation of DNA replication. As expected from these data, cohesin's association with chromatin has also been shown to be pre-RC-dependent (Ciosk et al, 2000; Gillespie & Hirano, 2004; Takahashi et al, 2004). However, this link might be specific for embryonic cells since budding yeast

cells depleted for the pre-RC component Cdc6 showed no defect in cohesin loading to chromatin in G1 (Uhlmann & Nasmyth, 1998).

1.3.3.1.3 Cohesin recruitment to fission yeast centromeres

In most organisms, cohesin is concentrated around centromeres where the pulling forces of the spindle reach their maximum. Therefore it seems plausible to have an additional loading mechanism that enriches cohesin in this area, and in fission yeast, such a mechanism has been identified. Fission yeast centromeres are made up of two silenced chromatin domains that are characterised by different groups of bound proteins (Partridge et al, 2000). The chromodomain-containing protein Swi6 (HP1 in higher eukaryotes), decorates the outer repeats (otr) while Mis6 and Cnp1 (CENP-A homolog) are confined to the central core region (cnt) (Figure 1.6). Swi6 recruitment to the otr region directly depends on the heterochromatin marker histone H3 methylated at its lysine K9 residue by the methyltransferase Clr4 (Su(var)39 in human and *Drosophila*) (Rea et al, 2000). Swi6 binding to H3 is promoted by the chromodomain that binds to the NH_2 tails of histone H3 when K9 is methylated (Bannister et al, 2001).

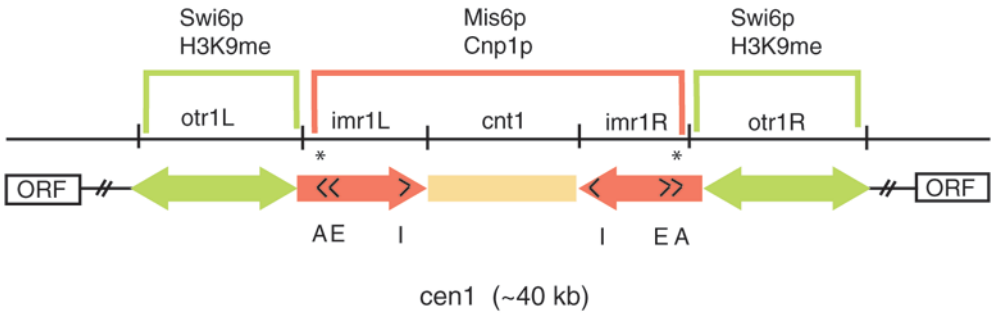

Figure 1.6 The structure of fission yeast centromere 1
The outer repeats (otr) are depicted as green bidirectional arrows. Red arrows indicate the innermost repeats (imr). The central core (cnt1) is shown as a salmon-coloured box. L stands for left, R for right, ORF for open reading frames and cen1 for centromere 1. Capital letters indicate the positions of tRNA genes and stand for the respective amino acid of the anti-codon. Asterisks indicate $tRNA^{Ala}$ genes. Heterochromatin components of the different centromere domains are shown above the brackets. Picture taken from Haldar & Kamakaka, 2006.

Strikingly, cohesin recruitment to fission yeast centromeres depends on Swi6, possibly promoted through direct physical interaction of Swi6 with the Psc3 subunit of the fission yeast cohesin complex (Bernard et al, 2001; Nonaka et al, 2002). Studies in fission yeast (Hall et al, 2003) as well as in vertebrates (Fukagawa et al, 2004) show that the

RNA interference (RNAi) machinery controls the establishment of heterochromatin which in turn recruits cohesin to these regions.

Interestingly, the bulk of Swi6/HP1 is removed from centromeric heterochromatin in mitosis. This dissociation depends on phosphorylation of serine 10 of Histone H3 (H3S10) by Aurora B kinase (Ark1 in fission yeast) (Chen et al, 2008; Petersen et al, 2001). Depletion of Aurora B by RNAi, or its inhibition through the small molecule inhibitor hesperadin, is sufficient to keep HP1 bound to chromosomes (Fischle et al, 2005; Hirota et al, 2005). Swi6/HP1 removal from mitotic chromosomes is conserved between fission yeast and human, but its biological significance remains largely unknown. A recent study in fission yeast shows that the cohesin-related condensin complex can be found at centromeric outer repeats after Swi6 has been removed (Chen et al, 2008). It is currently not known what effect a possible loss of cohesin tethering due to reduced levels of Swi6 has on cohesin's binding to these regions during mitotic progression. Swi6 only accumulates again with centromeric heterochromatin as cells enter the subsequent S phase.

In contrast to fission yeast, budding yeast centromeres are very small, consisting of a conserved sequence of 125 bp only, and no Swi6/HP1 homolog has been discovered. Likewise, no centromeric heterochromatin has been described, making fission yeast an ideal genetically tractable model organism to study the complex connection between cohesin and heterochromatin.

1.3.3.1.4 Swi6-dependent cohesin recruitment to chromosome arms

Recently, Swi6 has also been linked to recruiting cohesin to chromosome arms. Work published by Gullerova et al reveals the generation of overlapping transcripts by read-through transcription of convergent gene pairs in G1 (Gullerova & Proudfoot, 2008). The study shows that the created dsRNA is recognised by Dicer which processes it to siRNA and leads to RITS-dependent transient heterochromatin formation across the analysed convergent gene pairs. Heterochromatin structures at these regions include histone H3 lysine 9 trimethylation marks and Swi6 association. Therefore, cohesin has been proposed to be loaded to these regions by Swi6 in a way similar way to its recruitment to permanent heterochromatin structures at centromeres (Figure 1.7).

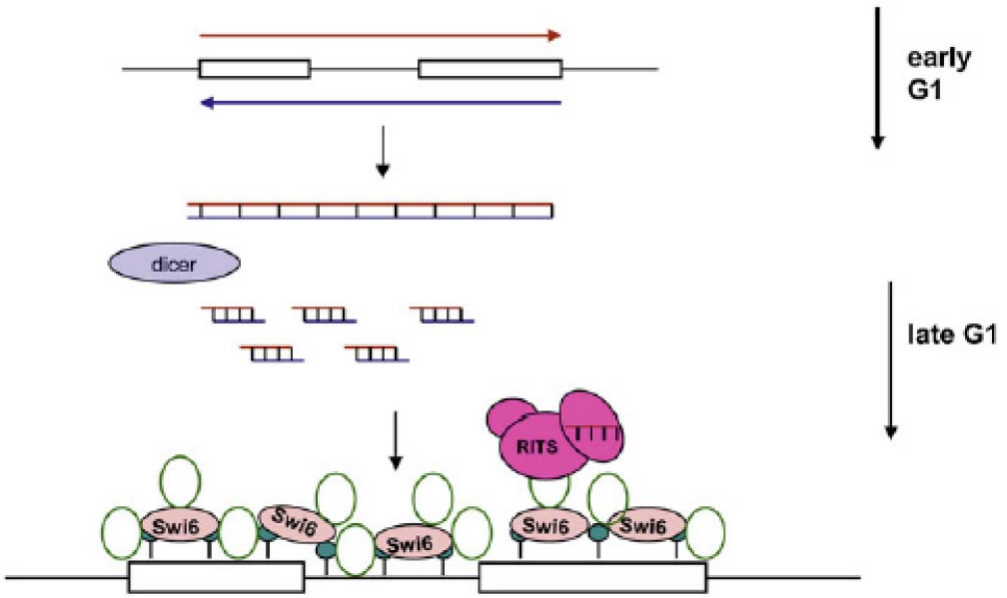

Figure 1.7 Model of Swi6-dependent cohesin recruitment to convergent sites
Overlapping transcripts (blue and red arrow) generated by bidirectional read-through transcription of convergent gene pairs (black boxes) might lead to the formation of dsRNA which is recognised and processed by Dicer (grey oval shape) into siRNA. Consequent activation of the RITS complex might lead to histone-methyltransferase-dependent methylation of lysine 9 of histone H3 (H3K9) (turquoise spots) along both convergent genes. Subsequent Swi6 recruitment via H3K9 methylation might directly lead to cohesin recruitment (green rings) prior to DNA replication in S phase. Figure adapted from Gullerova & Proudfoot, 2008.

However, it is important to state here that the study investigates three gene pairs only. Therefore, it remains unknown whether this mechanism plays a role on a genome-wide scale and whether it proves to be conserved among other eukaryotes. As there is no evidence of a Swi6 homolog in budding yeast, and the RNAi machinery is thought not to be conserved, it seems unlikely that this mechanism would follow similar rules in the two yeasts, despite their similar cohesin binding patterns. However, Sir proteins, a different type of heterochromatin proteins, required for cohesin targeting to the HMR locus in budding yeast (Chang et al, 2006), have been proposed as candidates that might mediate accumulation of cohesin at sites of convergent transcription in budding yeast (Peric-Hupkes & van Steensel, 2008).

1.3.3.1.5 Cohesin binding to chromosomes in Drosophila melanogaster

The Scc2 homolog in *Drosophila*, Nipped-B, was mapped to chromosomes and, like in budding yeast (Lengronne et al, 2004), showed a correlation with strongly transcribed genes (Misulovin et al, 2008). Whereas budding yeast cohesin was shown to rapidly translocate away from its loading sites to regions between convergently transcribed genes, cohesin along *Drosophila* chromosomes was found to overlap with its loading factor Nipped-B near highly transcribed genes, particularly at intronic sequences and 5' untranslated areas (Figure 1.8), where it co-localised (Misulovin et al, 2008).

1.3.3.1.6 Cohesin association with chromosomes in human and mouse

Three recent papers have identified the cohesin binding patterns along large parts of the genomes in mouse and in human cells (Parelho et al, 2008; Stedman et al, 2008; Wendt et al, 2008). ChIP maps of several cohesin subunits detected thousands of cohesin association sites that were slightly overrepresented on top of genes and their surrounding up- and downstream regions. The binding patterns did not significantly change between human cells synchronised in G1 and in G2 (Wendt et al, 2008). As in *Drosophila*, cohesin could be detected on top of active genes (Parelho et al, 2008; Wendt et al, 2008). A striking correlation was found between cohesin binding sites and association sites of CTCF, a sequence-specific DNA-binding protein, involved in transcriptional regulation and higher-order chromatin organisation (Figure 1.8; reviewed in Kumaran et al, 2008). Although CTCF knock-down reduced cohesin binding to its target regions, overall binding of cohesin was not affected, suggesting that CTCF might be important for concentrating cohesin to distinct regions but that it is not required for initial cohesin loading onto chromosomes (Gause et al, 2008; Wendt et al, 2008).

Whereas no sequence-specificity could be detected for cohesin association sites in yeast, cohesin binding to CTCF regions appears to depend on the CTCF binding motif. Deletion of this sequence from a certain region abolished both cohesin and CTCF binding to this area (Stedman et al, 2008). Conversely, knock-down of the Rad21 cohesin subunit did not (Parelho et al, 2008) or only weakly (Wendt et al, 2008) influence CTCF-association.

An overview of the apparent disparities of cohesin binding to chromosomes in different model organisms is shown below (Figure 1.8).

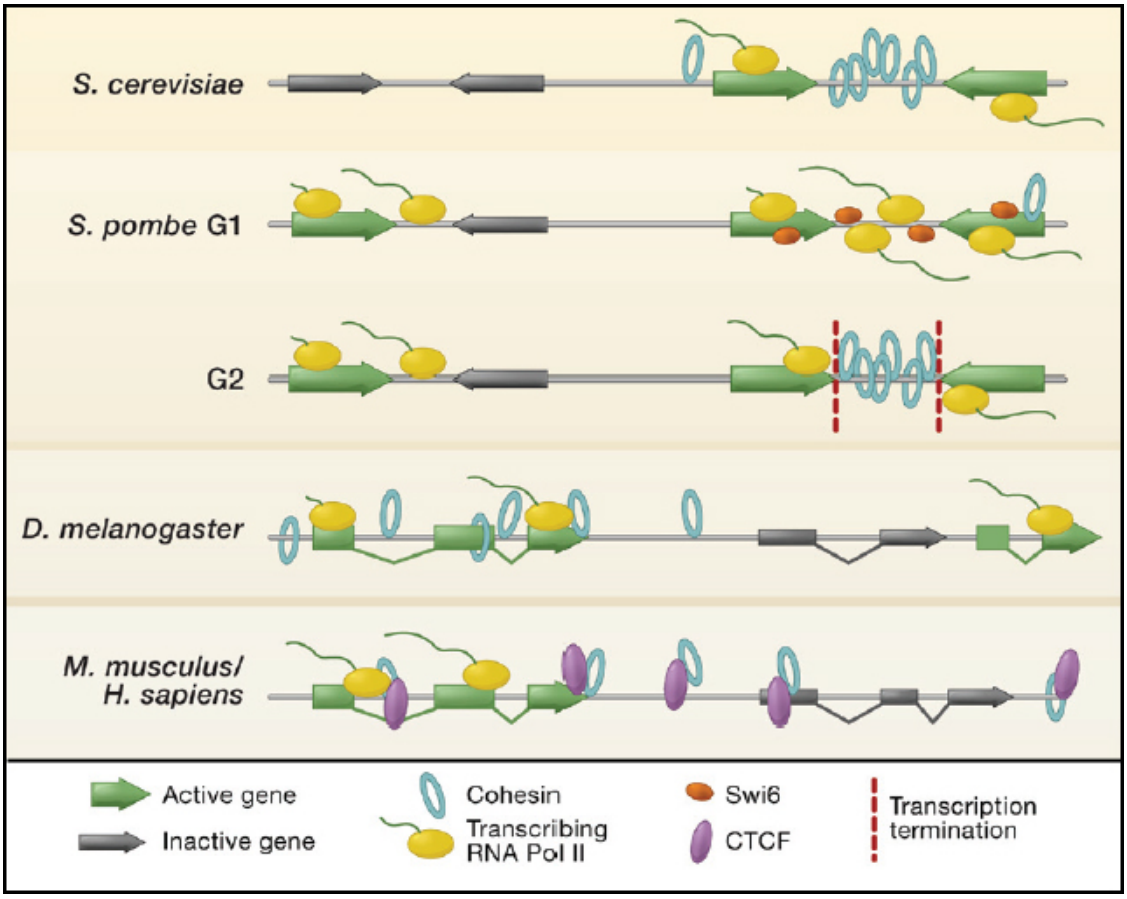

Figure 1.8 Overview of different models of cohesin binding in various eukaryotes
In budding yeast, cohesin mainly associates between convergently transcribed genes. Fission yeast shows read-through transcription at convergent genes, leading to histone H3 lysine K9 trimethylation marks and Swi6 association which in turn might recruit cohesin to these regions. In G2, heterochromatin marks at these regions are mainly lost, and a model is hypothesised that cohesin accumulation between convergently transcribed genes leads to transcriptional termination in G2. In *Drosophila*, cohesin associates both with gene-rich and intergenic regions. Only a subset of transcriptionally active genes is bound. In mammalian cells cohesin co-localises with the CTCF insulator protein at both genic and intergenic regions, although binding along genes is slightly enriched. Picture taken from Peric-Hupkes & van Steensel, 2008.

1.3.3.2 Cohesion establishment in S phase

Although cohesin has been the focus of intense studies during the last decade, the molecular basis of the mechanism of cohesion establishment still remains elusive.

After having been loaded onto unreplicated DNA, cohesin is established in S phase when DNA is replicated. Several lines of evidence point towards the direction that cohesion establishment is tightly coupled to DNA replication. Mutations in replication fork components significantly affect the process of cohesion establishment. For example, Ctf4, the DNA polymerase α-binding protein (Miles & Formosa, 1992), the heli-

case Chl1 (Petronczki et al, 2004), and several components of an alternative replication factor C complex (Mayer et al, 2001) are implicated in cohesion establishment. Furthermore, the replisome-associated acetyltransferase Eco1/Ctf7 (Eso1 in fission yeast) is essential for cohesion establishment (Kenna & Skibbens, 2003; Lengronne et al, 2006; Moldovan et al, 2006). Mutations in this factor prevent cohesion establishment during S phase although cohesin is loaded onto chromosomes in G1 (Skibbens et al, 1999; Tóth et al, 1999). In addition, recent evidence shows that Eco1-dependent acetylation of Smc3 in budding yeast promotes sister chromatid cohesion (Ben-Shahar et al, 2008; Unal et al, 2008), indicating that cohesion establishment might require the modification of cohesin into a functional acetylated form. However, it has also been shown that inactivation of the cohesin destabiliser Wapl can similarly promote sister chromatid cohesion independently of Eco1 function (Ben-Shahar et al, 2008).

Live-cell FRAP imaging studies in mammalian cells have revealed an interesting link between cohesin dynamics and S phase progression. Cohesin was shown to bind in a highly dynamic manner to G1 chromosomes. The high exchange between the chromosome-bound cohesin and the soluble nuclear pool depended on the Wapl gene product (Gerlich et al, 2006b; Kueng et al, 2006). Interestingly, a significant fraction of cohesin became stably bound during S phase progression. As cohesion is established at the same time, it could be imagined that the change in cohesin dynamics might be important for cohesion establishment. However, it is not known whether cohesin stabilisation is a manifestation of cohesion establishment or whether it is its pre-requisite.

Recent experiments in budding yeast provide evidence that cohesion establishment in S phase can proceed with no further recruitment of cohesin to chromosomes, indicating that the previously cohesin loaded onto unreplicated DNA is forming the link between the two sister chromatids (Lengronne et al, 2006). The same study shows that cohesion establishment can occur without re-engagement of an ATP hydrolysis motif that promotes initial cohesin association with chromosomes in G1 (Lengronne et al, 2006).

Despite these recent advances, the exact molecular mechanism of cohesion establishment with regards to the ring-shaped nature of cohesin still remains elusive. Two models can be imagined (Uhlmann, 2007), one of which envisions the replication fork passing through cohesin rings, a process which might be facilitated by the various replisome-associated factors mentioned above (Figure 1.9a). The other model proposes that cohesin disassembles from chromatin to allow the replication fork to progress along chromosomes. In this scenario, the replisome-associated factors shown to be important

for cohesion establishment might help to re-assemble cohesin after passage of the replication fork (Figure 1.9b).

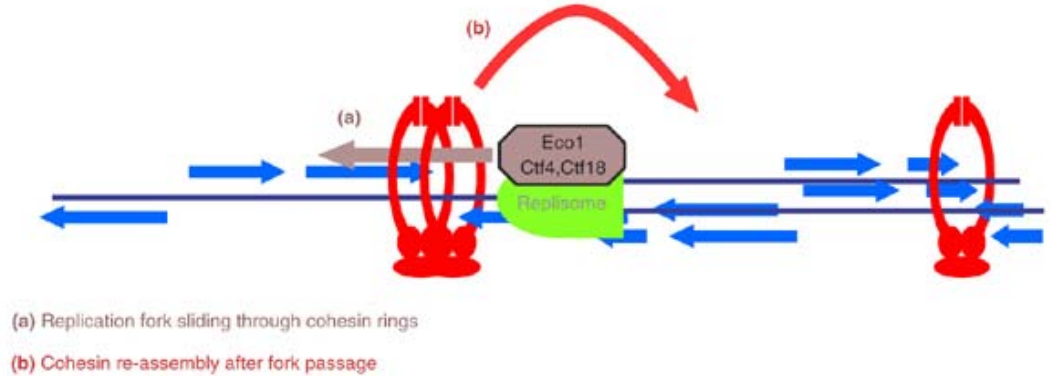

Figure 1.9 Cohesion establishment during DNA replication
Establishment of sister chromatid cohesion depends on replication fork components including the acetyltransferase Eco1 (Eso1 in *S. pombe*) and the RFC^{Ctf18} complex. Two models have been proposed how cohesion might be established (Uhlmann, 2007). The replication fork components might either help the replication fork to slide through the cohesin rings (a) or it might facilitate cohesin's re-assembly behind the replication fork (b). Figure taken from Uhlmann, 2007.

1.3.3.3 Sister chromatid cohesion in G2

1.3.3.3.1 Maintenance of cohesion

After cohesion establishment in S phase, sister chromatids are held together by cohesin throughout G2 (Figure 1.4). Maintenance of sister chromatid cohesion does not depend on cohesion establishment factors like Eco1 (Skibbens et al, 1999; Tóth et al, 1999) but in budding yeast was shown to depend on a protein called Pds5 (also known as BimD or Spo76) (Stead et al, 2003). Although Pds5 is highly conserved from yeast to human the importance of its function varies between different model organisms. While Pds5 in budding yeast is essential for viability and important for sister chromatid cohesion it is a non-essential protein in fission yeast. However, after extended G2/M arrest in the absence of Pds5, cells loose their ability to proliferate subsequently due to sister chromatid cohesion defects (Tanaka et al, 2001; Wang et al, 2002). Overall, several studies in other organisms also point in the direction that Pds5 is important for re-inforcing sister chromatid cohesion (Losada & Hirano, 2005).

1.3.3.3.2 De novo cohesion establishment in response to DNA damage

Until recently, it was generally believed that cohesion establishment could only occur at replication forks where DNA is synthesised during S phase (Uhlmann & Nasmyth,

1998). However, it has recently been shown that cohesion could also be established *de novo* in G2 in response to DNA double-strand breaks (DSBs) (Ström et al, 2004; Strom & Sjogren, 2005). Large amounts of cohesin were shown to be recruited to a defined genomic DSB site where they formed links between the two sister chromatids. As DNA repair also relies on DNA synthesis the mechanism of cohesion establishment during DNA replication in S phase and cohesion establishment at damaged DNA sites in G2 might be the same. However, two recent studies in budding yeast have shown that, despite blocking DNA synthesis for DNA repair, cohesion could still be established, indicating that cohesion establishment in G2 can fully be uncoupled from DNA synthesis (Ström et al, 2007; Ünal et al, 2007). Interestingly, cohesion was not only newly established at the site of damage but also along entire undamaged chromosomes, a process that depended on the acetyltransferase Eco1.

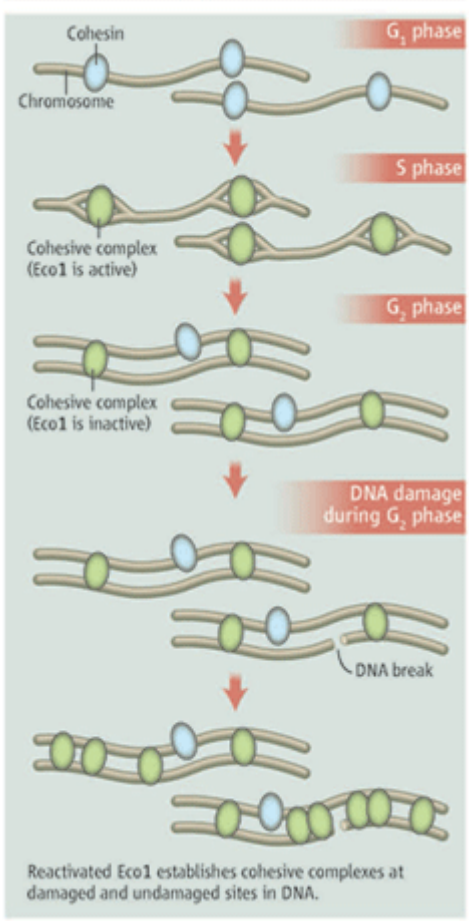

Figure 1.10 Model of Eco1-dependent cohesion establishment in G2
Cohesin (blue) first associates with chromosomes in G1, but only in S phase, when sister chromatids are generated, is cohesin transformed into cohesive links (green) between two identical chromatids. Induced by DNA damage, re-activation of Eco1 in G2 induces cohesin loading and cohesion establishment at the site of damage as well as on undamaged chromosomes. Picture taken from Watrin & Peters, 2007.

Furthermore, overexpression of Eco1 in budding yeast was sufficient to trigger cohesion establishment in G2 even if no DNA damage had occurred (Ünal et al, 2007; Watrin & Peters, 2007). Their results led Ünal et al to hypothesise that Eco1 might be rate-limiting for cohesion establishment in an unperturbed G2 phase, possibly due to the inactivation by a so far unresolved mechanism.

1.3.3.4 Resolution of sister chromatid cohesion in M phase

Having maintained sister chromatid cohesion throughout G2, cells enter M phase with tightly paired sister chromatids which forms the basis for bipolar attachment of the spindle to sister kinetochores. Only when every sister chromatid pair is attached in a bipolar manner, the spindle checkpoint is inactivated. This involves the elimination of the inhibitory form of the Mad2 checkpoint protein that inhibits Cdc20, an essential cofactor of the anaphase-promoting complex/cyclosome APC/C. How cohesion is eventually dismantled varies between different model organisms and can range from a 1-step resolution mechanism in budding yeast (1.3.3.4.1) to a more complex procedure in higher eukaryotes (1.3.3.4.2).

1.3.3.4.1 Resolution of sister chromatid cohesion in budding yeast

In budding yeast, cohesin remains on chromosomes until anaphase-onset when the protease separase cleaves cohesin's kleisin subunit Scc1. For most of the cell cycle, separase is kept inactive by being bound to an inhibitory chaperone Pds1, also called securin. Only at the meta- to anaphase transition separase is activated when the APC/C^{Cdc20} ubiquitinates Pds1 (Cohen-Fix et al, 1996), marking it for destruction by the proteasome. Once released from its inhibitor, separase cleaves Scc1 which leads to complete dissociation of cohesin from chromosomes (Uhlmann et al, 1999; Uhlmann et al, 2000). Loss of sister chromatid cohesion together with simultaneous loss of tension between the sister kinetochores allows the spindle to pull identical chromatids to opposite cell poles (Figure 1.11).

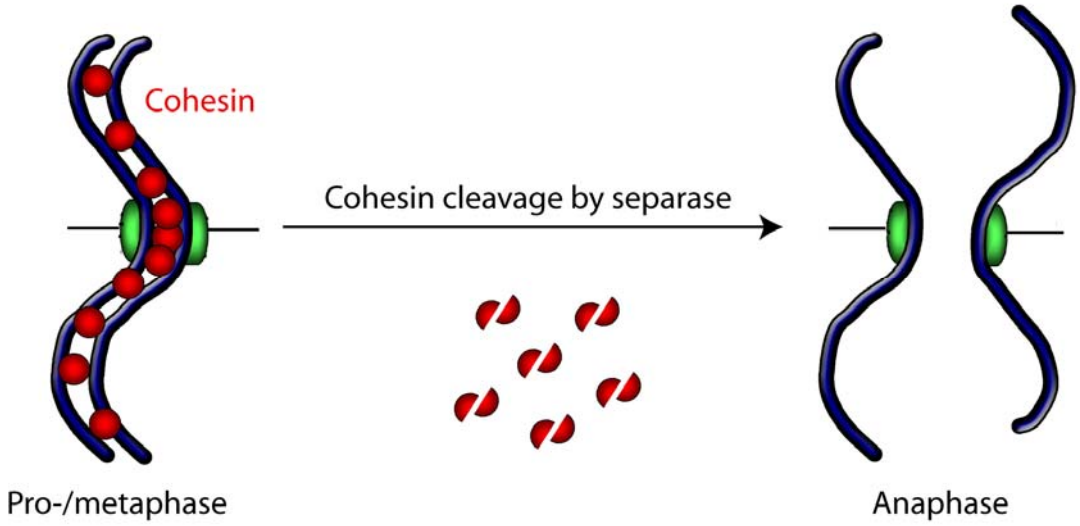

Figure 1.11 Dismantling sister chromatid cohesion in budding yeast
Cohesin is removed from both chromosomes arms and centromeres in one step at anaphase onset, when the protease separase cleaves the Scc1 (Rad21) subunit of cohesin (Uhlmann et al, 1999; Uhlmann et al, 2000).

1.3.3.4.2 Dismantling sister chromatid cohesion in higher eukaryotes

In contrast to budding yeast, the bulk of cohesin along animal chromosomes dissociates from chromosome arms but not from centromeres during pro- and prometaphase (Waizenegger et al, 2000). This initial wave of cohesin removal is commonly referred to as the 'prophase pathway' and is independent of cleavage of cohesin's kleisin subunit by the protease separase. Instead, the prophase pathway depends on the mitotic kinases Aurora B kinase (Losada et al, 2002) and Polo-like kinase Plk1 (Sumara et al, 2002) which directly or indirectly lead to hyperphosphorylation of SA2, one of the two human homologs of the Scc3 cohesin subunit (Table 1.1; Hauf et al, 2005). Since cohesin is mainly removed from chromosome arms but not from centromeres the question arises how centromeric cohesin can resist the prophase pathway. Recent studies suggest that a protein called shugoshin (the 'guardian spirit' of the genome), that associates with centromeres from prophase to anaphase-onset, protects centromeric cohesin from phosphorylation by recruiting the phosphatase PP2A (Kitajima et al, 2006; McGuinness et al, 2005; Riedel et al, 2006).

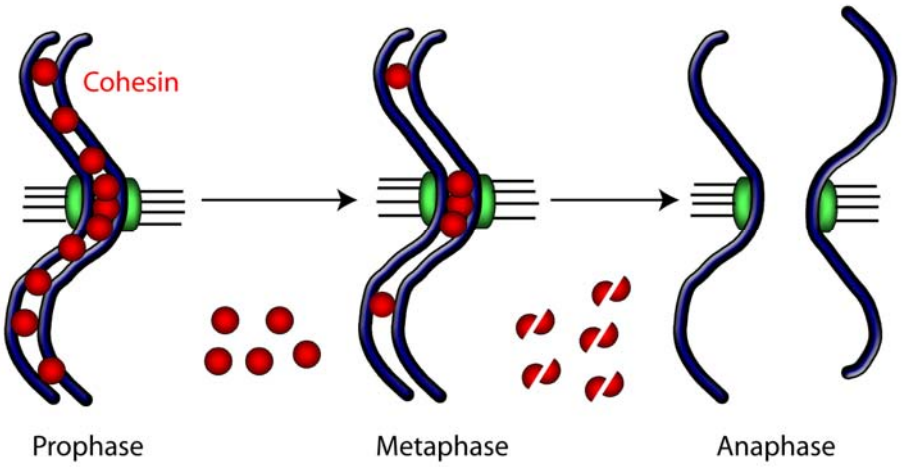

Figure 1.12 Resolution of cohesion in higher eukaryotes
At least two separate steps remove cohesin from chromosomes in higher eukaryotes. In a separase-independent manner, uncleaved cohesin is removed largely from chromosome arms in prophase dependent on phosphorylation of the cohesin SA2 (Scc3) subunit and the mitotic kinases Aurora B and Polo (Hauf et al, 2005). At anaphase-onset, the residual cohesin remaining on chromosomes, predominantly along centromeres, is cleaved by separase like in budding yeast (Waizenegger et al, 2000).

Surprisingly, inhibiting the prophase pathway e.g. by expression of a non-phosphorylatable SA2 subunit (Hauf et al, 2005) or by depletion of Plk1 (Gimenez-Abian et al, 2004) does not interfere with cell cycle progression through mitosis. Therefore, the function of the prophase pathway in higher eukaryotes still remains elusive.

After the prophase pathway has taken place, only minor amounts of cohesin (approximately 10 %) remain on chromosomes, predominantly at centromeres (Hoque & Ishikawa, 2001; Waizenegger et al, 2000). A similarly minor fraction of cohesin, presumably the chromatin-bound pool, is subsequently cleaved by separase at anaphase-onset which is essential for triggering anaphase (Figure 1.12; Hauf et al, 2001; Waizenegger et al, 2000).

1.3.4 Cohesin and its regulators: expanding chromosomal functions

1.3.4.1 DNA repair by homologous recombination (HR)

Sister chromatids are tightly paired by cohesin from their synthesis in S phase onwards. In late S and G2, cells preferably repair DNA breaks by HR rather than by non-homologous end-joining (NHEJ), by which DNA is predominantly repaired in G1. First indications of an involvement of cohesin in DNA double-strand break (DSB) repair were discovered in fission yeast in 1992, when the *rad21-45* mutant allele of cohesin's kleisin subunit was shown to be radiation-sensitive (Birkenbihl & Subramani, 1992). DSB repair was also shown to be impaired in the absence of cohesin in budding yeast and vertebrates (Losada & Hirano, 2005).

Recent results in budding yeast have detected a direct involvement of cohesin in DSB repair at a mechanistical level. Cohesin subunits were shown to be recruited to stretched-out regions of up to 100 kb around a defined DSB site (Ström et al, 2004; Unal et al, 2004). Cohesin recruitment to DSBs was dependent on the cohesin loading factor Scc2/4 and on phosphorylation of H2AX by the DNA damage checkpoint kinases Mec1/ATM and Tel1/ATR (Unal et al, 2004). Without Scc2/4 function, no cohesin accumulation at the break site could be observed, and DNA break repair was defective even though sister chromatids were linked by S phase-induced cohesion. Strikingly, cohesin recruited to DSB breaks in G2 also established cohesion between the two sister chromatids. This suggests that cohesin had two functions in these cells, one mediated by G1-loaded cohesin that led to sister chromatid cohesion in S phase, the other one employed by damage-recruited cohesin in G2 which promoted *de novo* establishment of cohesion at DSB sites, facilitating DNA repair by HR (Ström et al, 2004).

1.3.4.2 Gene regulation

Several observations suggest that cohesin may have additional roles as a regulator of gene expression (reviewed in Dorsett, 2007; Gondor & Ohlsson, 2008; Peric-Hupkes & van Steensel, 2008; Uhlmann, 2008). Budding yeast Smc1 and Smc3 have been shown to be required for preventing heterochromatin spreading from the silenced mating-type locus HMR (Hidden MAT Right). Cohesin and Nipped-B, the *Drosophila* ortholog of the cohesin loader Scc2/4, affect enhancer-promoter interactions for certain genes e.g.

the *cut* and the *Ultrabithorax* genes (Rollins et al, 2004; Rollins et al, 1999). Furthermore, engineered cohesin cleavage in a certain type of post-mitotic neurons in *Drosophila* was shown to influence the expression of the ecdysone hormone receptor. These neurons showed defects in axon pruning, and eventually, the larvae died during development (Pauli et al, 2008; Schuldiner et al, 2008). In addition, two subunits of cohesin have been shown to be involved in the regulation of the expression of the zebrafish Runx gene (Horsfield et al, 2007).

The most recent advances on cohesin's function as a gene regulator stem from studies on mammalian cells in which cohesin was shown to co-localise with the CCCTC-binding factor CTCF, a zinc-finger protein required for transcriptional insulation (Parelho et al, 2008; Stedman et al, 2008; Wendt et al, 2008). Genome-wide expression analysis in CTCF- or cohesin-depleted cells showed a striking overlap of deregulated genes, indicating a close interdependency of cohesin and CTCF function in gene-regulation. The misregulated genes were preferentially located within a 35 kb window of their closest CTCF/cohesin association site (Wendt et al, 2008). Cohesin was further shown to play a vital role for CTCF's insulator function in blocking promoter-enhancer interactions. Using reporter assays (Wendt et al, 2008) but also investigating the endogenous H19/IGF2 locus (Parelho et al, 2008), knockdown of different cohesin subunits resulted in reduced insulator activity of CTCF (Figure 1.13).

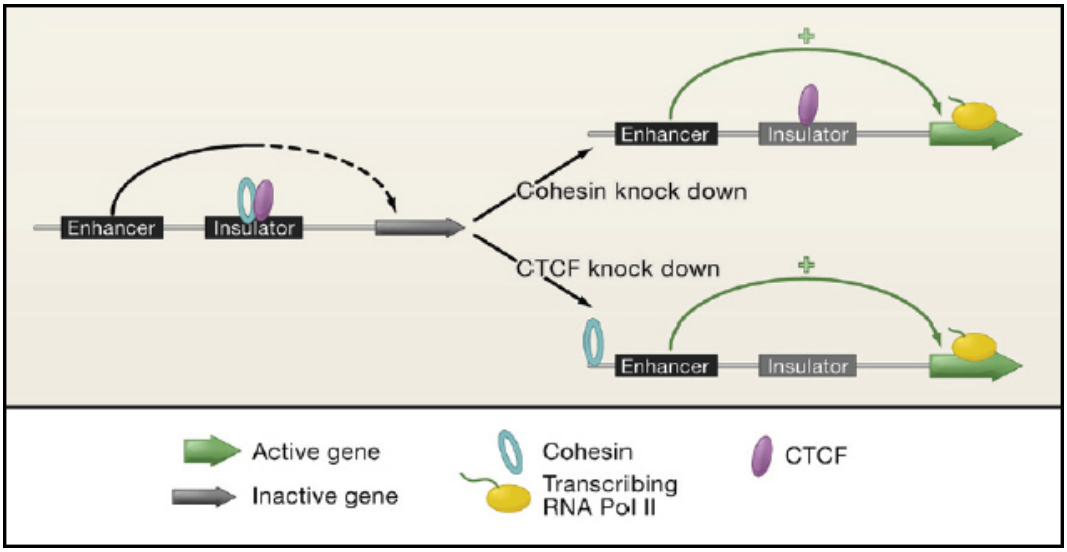

Figure 1.13 Model of cohesin- and CTCF-mediated insulator function
Removal of either cohesin or CTCF leads to loss of insulator activity and, consequently, increased enhancer-promoter interaction. The exact mechanism of cohesin binding to chromosomes, e.g. whether it binds by topological embrace or associates in a different manner with chromosomes, in each case is not known. Picture adapted from Peric-Hupkes & van Steensel, 2008.

1.3.5 Cohesin and cohesin-related factors in disease

Various diseases have been described that are caused by mutations in cohesin subunits or in its regulators.

1.3.5.1 Cornelia de Lange syndrome

Cornelia de Lange syndrome (CdLS) is a haploinsufficient human developmental disorder, frequently caused by mutations in *NIPBL* (Nipped-B like), which encodes the human ortholog of Scc2. The syndrome can also be caused by mutations in the Smc1L1 gene, which encodes the human Smc1 core subunit of cohesin (Dorsett, 2007). CdLS patients display significant defects in both physical and mental development, including diagnostic facial characteristics, upper limb abnormalities, oesophageal defects, cardiac malformations and mental retardation. Furthermore, the patient's growth is slowed down, and the affected individuals remain small in size (Dorsett, 2007). No obvious sister chromatid cohesion defects can be detected in the patients of these diseases, consistent with the rapidly growing body of evidence that cohesin plays an important role in various non-canonical processes e.g. gene-regulation.

1.3.5.2 Roberts syndrome

A similar syndrome, termed Roberts syndrome, is a recessive disease caused by mutations in Esco2, one of the human orthologs of the acetyltransferase Ctf7/Eco1 involved in cohesion establishment. Characteristics include, but are not limited to, slow growth, mental retardation and limb defects (Dorsett, 2007). In this case, affected individuals also show centromeric cohesion defects (Vega et al, 2005).

1.4 Condensin: a chromosomal compaction machine

1.4.1 Chromosome condensation

The rod-like appearance of chromosomes visible before cell division is one of the most striking characteristics of eukaryotic nuclei. But what is the function of organising the genome into compact, distinct units? The answer lies in the submission of identical copies of the genome to both daughter cells during cell division. The linear genome, consisting of a long strand of DNA, would be by far too long to fit into the nucleus without being entangled, rendering accurate sister chromatid segregation impossible. For instance, the human chromosome 22 consists of approximately 48 millions base pairs (bp) (Alberts et al, 2002). In its uncondensed form, it would span a distance of approximately 1.5 cm, about 10,000 times longer than the 2 µm it measures from end to end in mitosis (Alberts et al, 2002).

But what is the molecular basis that drives chromosome condensation prior to cell division? Compaction of eukaryotic genomes happens at various levels, and even in interphase, when chromosomes are at their most uncondensed level, the lengths of chromosomes are significantly compressed compared to their stretched out form. In fact, interphase chromosomes still show a compaction ratio of approximately 1,000-fold when compared to their uncondensed lengths (Alberts et al, 2002).

The compaction of eukaryotic chromosomes is facilitated by different chromosomal proteins: histones and additional non-histone chromosomal proteins. The most basic level of chromosome compaction relies on histones and leads to the formation of nucleosomes which were discovered in 1974 and can be seen in the electron microscope as ‘beads on a string’ (Figure 1.14; Olins & Olins, 1974). Each nucleosome is made up of a histone octamer around which 147 bp of DNA are wrapped. One nucleosome is separated from the next by a so-called ‘linker DNA’ region that makes up approximately 60 - 80 bp in length as judged by DNAse digestion of genomic DNA (Laemmli et al, 1992). The length compaction rate caused by nucleosomes is approximately 3-fold (Alberts et al, 2002).

A second level of compaction is achieved by organised packaging of nucleosomes into higher-order chromatin fibres. When nuclei are lysed onto an electron microscope grid, chromatin is visible as a fibre with a 30 nm diameter. However, the presence of this

fibre *in vivo* is still under debate. Importantly, human chromosomes curled up as 30 nm fibres, would still be approximately 0.1 cm in length, approximately 100 times too long to fit in the nucleus (Alberts et al, 2002). Therefore, higher-order condensation of chromosomes is thought to be achieved by further packaging of the 30 nm fibre into loops and coils. However, the process of higher-order chromosome condensation remains a mystery, despite its known presence for over a century (Flemming, 1882). Elucidating the mode of action of non-histone chromosomal proteins, especially that of condensin, but also that of other SMC complexes, will be crucial to understand the molecular mechanism leading to higher order condensation of chromosomes. A summarising model for the different steps of chromosome compaction is shown in Figure 1.14.

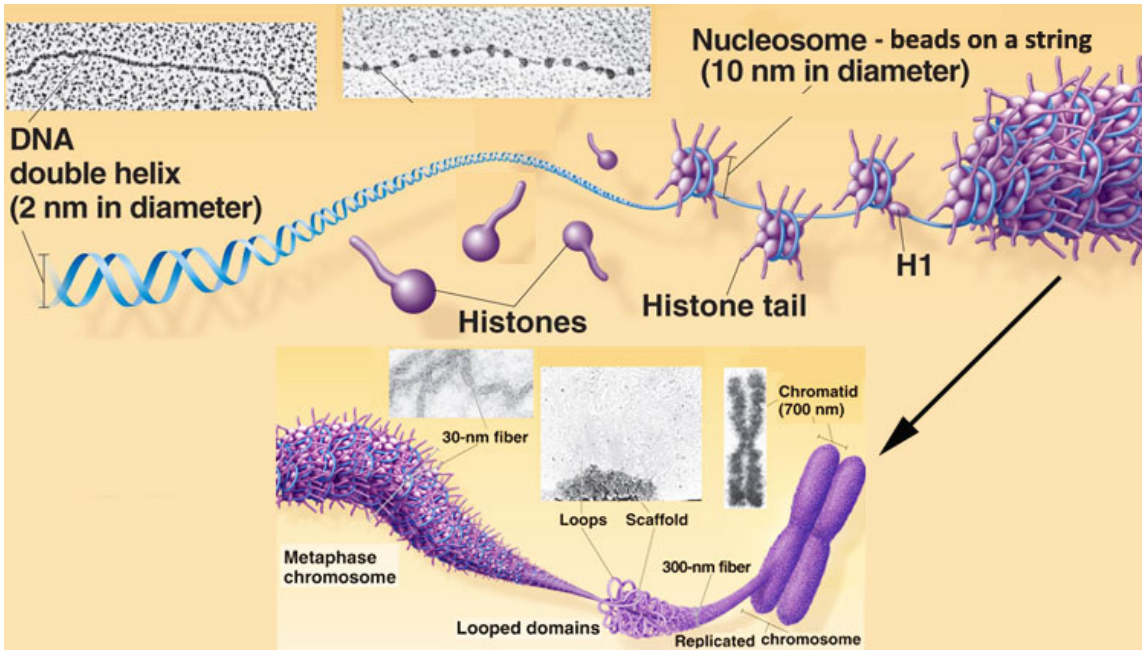

Figure 1.14 Chromosome packaging of eukaryotic chromosomes
The DNA double-helix binds around histone octameres which form nucleosomes. These are hypothesised to be further packaged into 30 nm and 300 nm fibres that eventually make up the rod-like appearance of metaphase chromosomes. Picture retrieved 31 August 2008 from:
http://fig.cox.miami.edu/~cmallery/150/cells/organelle.htm

1.4.2 The structure of the condensin complex

The core of condensin is constituted by a heterodimer of Smc2 and Smc4. Like cohesin, condensin is highly conserved from yeast to human. In vertebrates, however, two condensin complexes, condensin I and II, exist, that vary in their composition of the regulatory non-SMC subunits (Table 1.1). In general, a kleisin subunit, Cnd2 in fission yeast, associates with the head domains of the SMC heterodimer to which two HEAT-repeat containing subunits, Cnd1 and Cnd3 in fission yeast, bind (Figure 1.15). For an overview of the nomenclature of condensin subunits in different model organisms see Table 1.1. Unlike cohesin, electron micrographs of human condensin I showed different arm conformations. Whereas the SMC arms of cohesin can be seen clearly separated from each other (Figure 1.3), forming ring-like complexes, condensin's SMC arms remain in close proximity (Figure 1.15; Anderson et al, 2002). The striking differences in arm conformations displayed by condensin and cohesin could be imagined to contribute to differences in their specialised chromosomal functions (Losada & Hirano, 2005).

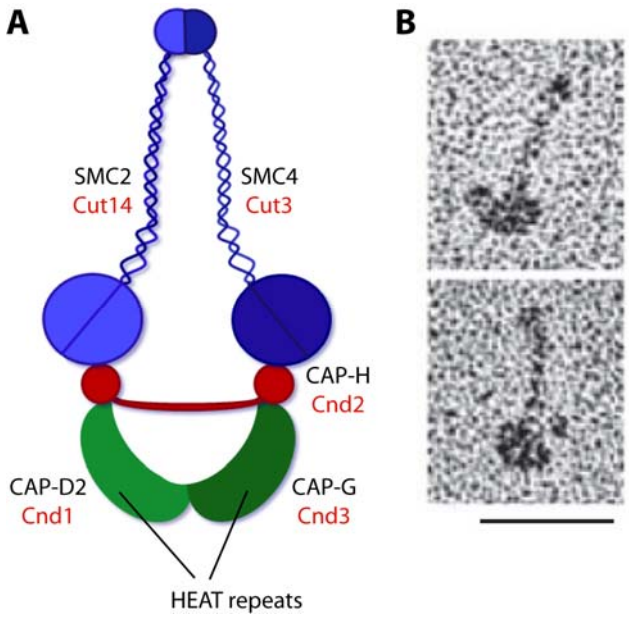

Figure 1.15 The architecture of the condensin I complex
(**A**) Schematic of the four condensin subunits and their arrangement into a V-shaped structure. Equivalent subunit names for the fission yeast condensin complex are indicated in red. (**B**) Electron micrographs of purified vertebrate cohesin. Bar, 50 nm, as taken from Anderson et al, 2002.

1.4.3 Condensin's various functions

Both the condensation of chromosomes to their thread-like structures in mitosis and sister chromatid resolution during anaphase have been shown to depend on condensin (Bhat et al, 1996; Hirano & Mitchison, 1994; Hudson et al, 2003; Ono et al, 2003; Saka et al, 1994; Strunnikov et al, 1995). Importantly, a growing body of evidence shows that condensin also plays important roles in interphase. A signalling function in the DNA replication checkpoint has been attributed to fission yeast condensin (Aono et al, 2002). In addition, interphase interactions of mammalian condensin I with PARP-1, the DNA nick-sensor poly(ADP-ribose) polymerase 1, and with XRCC1, the base excision repair (BER) factor complex, suggest a possible involvement of condensin in DNA single strand break repair (Heale et al, 2006). Furthermore, two studies have detected a role for condensin in transcriptional silencing. Budding yeast condensin has been implicated in silencing of the mating type locus, and condensin in *Drosophila* has been shown to maintain *Fab-7* PRE silencing (Bhalla et al, 2002; Lupo et al, 2001).

1.5 The Smc5/Smc6 complex: a DNA repair linker

Unlike condensin and cohesin, no function-specific name has been given to this complex, demonstrating the lack of information about its cellular function. The complex consists of a heterodimer of Smc5 and Smc6 that associates with four non-SMC subunits called Nse1, Nse2, Nse3 and Nse4 (reviewed in Losada & Hirano, 2005; Strom & Sjogren, 2007). The complex shows a significantly different structure to the ones observed for cohesin and condensin, in that Nse2 associates with the antiparallel coiled-coil arm region of the Smc5 subunit (Figure 1.2).

Although the exact cellular function of the complex is unknown it has been shown to be important for DNA repair. In fact, the gene encoding Rad18, the fission yeast homolog of Smc6, was discovered in a screen for radiation-sensitive mutants, similar to Rad21, the kleisin subunit of the cohesin complex (Birkenbihl & Subramani, 1992; Lehmann et al, 1995). The primary structure of the regulatory subunits exhibits characteristic motifs, including RING-finger motifs conserved in E3 ubiquitin and SUMO ligases. Mutations in these motifs lead to distinct phenotypes ranging from DNA damage sensitivity to irregular nucleoli and defects in telomere function (Losada & Hirano, 2005). Interestingly, cohesin and the Rad50-containing SMC related MRX complex are also implicated in DNA repair, raising the question as to why at least three different SMC-related protein complexes are needed for this process (Losada & Hirano, 2005).

1.6 Bacterial SMC: three in one?

The only SMC complex constituted of a homodimer of Smc subunits is the bacterial SMC complex. Loss of function of the *Bacillus subtilis smc* gene leads to decondensation and missegregation of chromosomes, emphasising the universal importance of SMC complexes in chromosome structure and function in all three phyla of life (Losada & Hirano, 2005). The SMC homodimer forms a complex with two non-SMC subunits, ScpA and ScpB (Figure 1.16 and Figure 1.2). ScpA belongs to the kleisin superfamily (Schleiffer et al, 2003), indicating that not only the function but also the structure of SMC complexes in bacteria and eukaryotes is closely related.

It has been proposed that the bacterial SMC complex functions in a manner reminiscent of the eukaryotic condensin complex. This hypothesis is based on a study showing that the bacterial SMC complex with its two regulatory subunits ScpA and ScpB promotes chromosome segregation in a way that involves DNA supercoiling (Lindow et al, 2002; Losada & Hirano, 2005). However, its involvement in keeping newly replicated sister DNAs together and its implications in DNA repair suggest that the bacterial SMC complex also shares features with cohesin as well as with the Smc5/Smc6 complex. Consistent with its diverse functions, purified bacterial SMC complexes display various arm conformations of the SMC homodimer, ranging from ring-like structures reminiscent of cohesin to V-shaped formations characteristic of the condensin complex (Figure 1.16).

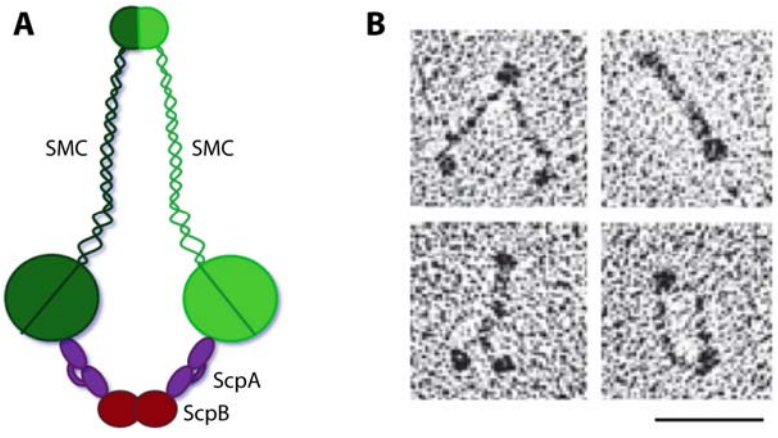

Figure 1.16 The structure of a bacterial SMC complex
(**A**) Schematic of a bacterial SMC complex composed of six subunits. (**B**) Electron micrographs show various arm conformations of purified bacterial SMC complexes, ranging from condensin-like V-shaped to cohesin-like ring arrangements. Bar, 50 nm. Micrographs taken from Anderson et al, 2002.

2 Aims

The work presented in this thesis aims to gain new insights into what parameters define and underlie the cohesin binding pattern along chromosomes. This is particularly important as several recent genome-wide surveys have revealed apparent disparities between the cohesin binding patterns of different model organisms. Fission yeast was utilised as a model organism since *S. pombe* combines features of budding yeast in terms of genetic tractability, genome size and gene density but more closely resembles higher eukaryotes regarding chromosome structure. As such, particularly heterochromatin structures at centro- and telomeres are highly conserved between fission yeast and higher eukaryotes, making *S. pombe* an attractive model organism to investigate chromosome biology. Specifically, we wanted to address the following questions:

1. Are any of the known features that determine cohesin binding along budding yeast, *Drosophila*, human and mouse chromosomes conserved in fission yeast, and/or can we detect novel characteristics that define the overall cohesin distribution along chromosomes?

2. What is the relationship between fission yeast cohesin and its loading factor Mis4/Ssl3? Little is known about the cohesin loader, and similar to the cohesin binding pattern itself, different correlations between cohesin and its loading factor have been reported in specific model organisms.

3. How is sister chromatid cohesion resolved in mitosis in fission yeast? Is a subfraction of cohesin already removed in prophase in a cleavage-independent manner like in higher eukaryotes? What happens to fission yeast cohesin when chromosomes split at anaphase-onset?

4. How does condensin fit into the picture? As cohesin and condensin are structurally related and function together in chromosome segregation during mitosis we wanted to investigate whether the functional relation between the two SMC complexes was also reflected in their binding patterns along chromosomes.

5. What happens to cohesin stability during the cell cycle? Is cohesin binding to fission yeast chromosomes highly dynamic in G1 and then stabilised during S phase, as has been observed in higher eukaryotes? How, when and where exactly during S phase would cohesin be stabilised?

3 Materials and Methods

3.1 Fission yeast techniques

3.1.1 Yeast gene and protein nomenclature

The nomenclature used for genes and proteins in this study is roughly based on (Kohli, 1987). Every gene is given a three-letter-code followed by a number, all written in lower case italics (e.g. *cdc25*). To emphasise a wild type gene, a '$^{+}$' is sometimes added at the end of the gene name (e.g. *cdc25*$^{+}$). Mutant alleles are indicated by the gene name followed by the allele number, all in lower case italics (e.g. *cdc25-22*). A deletion is marked with a '*Δ*' after the gene name (e.g. *swi6Δ*). To indicate that a particular gene has been replaced with another, the original gene name is followed by two colons and the name of the gene that replaces it (e.g. *swi6::ura4*$^{+}$).

The protein encoded by a certain gene is named with the same three-letter-and-number-code, but the first letter is written in upper-case, and all letters and numbers are typed in regular case, not italics (e.g. Rad21). In some cases a 'p' is added to the end of the protein name, standing for protein (e.g. Rad21p).

For genes fused to another DNA sequence, the name of the individual DNA sequences is expressed in the order they would appear in the genome with a hyphen separating the two sequences. *rad21-GFP-kanMX6* means that the *rad21* gene is C-terminally fused to a *GFP* gene followed by the kanamycin resistance gene *kanMX6* as a selective marker.

Some auxotrophic fission yeast markers were replaced by the equivalent budding yeast gene e.g. *swi6::LEU2*, indicating that Swi6 in a *leu1*$^{-}$ fission yeast strain has been replaced by the budding yeast *LEU2* gene. The guidelines for budding yeast gene and protein nomenclature are outlined in the *Saccharomyces* genome database on:
http://www.yeastgenome.org/

3.1.2 Fission yeast growth conditions

Haploid strains derived from the wild type h^- 972 and h^+ 975 strains (Leupold, 1950) were used for all applications. Media were as described (Moreno et al, 1991). Cells were grown in rich medium YE4S (0.5 % w/v Difco yeast extract, 3 % w/v glucose supplemented with 225 mg/l leucine, adenine, histidine and uracil each) or in minimal EMM medium (14.7 mM potassium hydrogen phthalate, 15.5 mM Na_2HPO_4, 93.5 mM NH_4Cl, 2 % glucose, 20 ml/l of 50 x salts, 1 ml/l 1000 x vitamins, 0.1 ml/l 10,000 x minerals supplemented with 225 mg/l leucine, adenine, histidine and uracil each). 50 x salts contained 0.26 M $MgCl_2 \cdot 6H_2O$, 4.99 mM $CaCl_2 \cdot 2H_2O$, 0.67 M KCl and 14.1 mM Na_2SO_4. The 1,000 x vitamins stock consisted of 4.3 mM pantothenic acid, 81.2 mM nicotinic acid, 55.5 mM inositol and 40.8 µM biotin, and the 10,000 minerals stock was constituted of 80.9 mM boric acid, 23.7 mM $MnSO_4$, 13.9 mM $ZnSO_4 \cdot 7H_2O$, 7.4 mM $FeCl_2 \cdot 6H_2O$, 2.47 mM molybdic acid, 6.02 mM KI, 1.6 mM $CuSO_4 \cdot 5H_2O$ and 47.6 mM citric acid. Standard methods were used for growth, storage and maintenance of strains (Moreno & Nurse, 1994).

Strains were kept as frozen stocks (-80°C) and thawed on agar plates when required. Liquid cultures were inoculated from a patch into the desired medium and grown overnight. For large culture volumes, precultures were grown for approximately 24 hours and used to inoculate larger cultures. All cells were grown at 25°C unless otherwise stated.

For transformations, minimal EMM medium agar plates were used, lacking the auxotrophic amino acid used for selection. Alternatively, for selection based on kanamycin or hygromycin B resistance, cells were plated on YE4S agar plates, supplemented with the kanamycin derivative Geneticin G418 (Gibco, 100 µg/ml) or hygromycin B (Roche, 300 µg/ml).

3.1.3 Cell synchronisation

Various strategies were used to arrest cells in different cell cycle stages. The techniques included the usage of cell cycle mutants (*cdc25-22*, *cdc10-129*, *nda3-KM311*), overexpression of dominant-negative cell cycle regulators (*Res1-CTer*), starvation (deprivation of nitrogen) and drug treatment (addition of hydroxyurea).

3.1.3.1 G1 cell cycle arrest

3.1.3.1.1 Nitrogen starvation

In response to nitrogen starvation, fission yeast cells arrest in G1. This method was used to probe the function of the acetyltransferase Eso1 for stabilising cohesin along chromosomes arms in an unperturbed S phase (4.3.4).

Approximately 30 ml of a mid-log phase culture (OD_{600} = 0.5) were exponentially grown in minimal EMM medium. The cells were filtered and washed 4 - 5 times with the same volume of synthetic minimal medium, lacking NH_4Cl as a nitrogen source. Cells were resuspended in 50 ml of synthetic minimal medium supplemented with 3 % glucose. The culture was shaken at 25°C for approximately 16 hours until all cells had acquired a small round shape, indicating the typical phenotype for nitrogen-starved G1 cells. Subsequent FACS analysis of DNA content (3.1.6) showed that most cells were arrested in G1. By adding excess amounts of NH_4Cl and amino acids, cells were released to progress through S phase. The release was combined with shifting to the restrictive temperature of different temperature-sensitive alleles (e.g. *eso1-H17*) (4.3.4).

3.1.3.1.2 cdc10-129 cell cycle mutants

A different type of G1 arrest was achieved, using the temperature-sensitive allele *cdc10-129*. Cdc10 is a subunit of the MBF transcription factor, the activity of which is required for entry into S phase (Nurse et al, 1976). *cdc10-129* cells were grown exponentially in complete YE4S medium at 25°C before temperature shift to 36°C, the restrictive condition for the *cdc10-129* allele. After 4 hours at the restrictive temperature the cells appeared uniformly elongated, and the septation index was close to 0. The arrest was further monitored by FACS analysis of DNA content (3.1.6).

3.1.3.1.3 Res1-Cter overexpression

Alternatively, cells were arrested in G1 by depleting the activity of the Cdc10 transcription factor, required for S phase entry, through overexpression of the C-terminal part of its binding partner Res1 (Ayte et al, 1995). To do so, cells bearing the *nmt-res1Cter* construct (strain Y2470) were grown to late-log phase in minimal EMM medium containing 20 µM thiamine to repress expression from the *nmt* promoter. Cells were then filtered to deprive the culture from thiamine and induce expression of the C-terminal part of Res1 from the *nmt1* promoter. For filtration, cells were collected on a membrane filter (Schlechter and Schuell, ME28, 1.2 µm) using a filtration apparatus from Millipore. Cells were extensively washed with at least 4 volumes of EMM and resuspended in fresh EMM medium lacking thiamine at a density of 2 x 10^5 cells/ml. Cells were small and round after approximately 7 doubling times, indicating that proliferation had stopped. The time in which cells doubled 7 times (the time before arresting) was controlled by modulating the temperature (20°C or 25°C). Once arrested, cells were shifted to 36.5°C for 2 hours. The DNA content of the cells was measured by flow cytometry before and after the temperature shift to monitor the cell cycle arrest (3.1.6). The septation index SI was determined by calcofluor staining of the septa to assess the frequency of cells undergoing cytokinesis.

3.1.3.2 HU-induced early S phase arrest

Early S phase arrest was performed by directly adding hydroxyurea (HU, Sigma, a ribonucleotide reductase inhibitor) to asynchronously growing cell cultures at a final concentration of 10 to 20 mM. Cell cycle arrest before and after the temperature shift was monitored by measuring DNA content by FACS analysis (3.1.6) and by counting the septation index SI after staining the septa with calcofluor (3.4.3). Successfully arrested cells were equal in length and started elongating depending on the duration of arrest.

3.1.3.3 G2 arrest: *cdc25-22* cell cycle mutants

The serine/threonine phosphatase Cdc25 removes the inhibitory Y15 phosphate on the cyclin dependent kinase (CDK) Cdc2, a step required for the transition from G2 to M (Gould & Nurse, 1989). Therefore, the temperature-sensitive (ts) allele *cdc25-22* can be used to synchronise cells in late G2. To do so, *cdc25-22* cells were grown exponentially in minimal EMM medium, supplemented with 225 mg/l adenine, uracil, leucine, his-

tidine and lysine before temperature shift to 36.5°C, the restrictive temperature of the *cdc25-22* allele. Cells were kept at the restrictive temperature for 6 hours, (approximately 1.5 cell cycles) when they appeared highly elongated under the microscope due to unrestricted cell growth without cell cycle progression. The arrest was assessed by calcofluor staining to determine the septation index SI (3.4.2). Typically, the septation index after 6 hours was close to 0, indicating that cells had ceased to undergo cytokinesis.

The *cdc25-22* arrest was also used for releasing cells synchronously into mitosis. After 6 hours at the restrictive temperature, cells were rapidly cooled down to 25°C by vigorously shaking the culture in ice-water. DAPI and calcofluor staining of ethanol fixed and/or methanol fixed cells were performed to determine cell synchrony. If required, cells carrying the α-tubulin Atb2 tagged with GFP at its N-terminus (Pardo & Nurse, 2005) were used to analyse the percentage of cells that contained meta- and anaphase spindles.

3.1.3.4 M phase arrest: *nda3-KM311* cell cycle mutants

The β-tubulin Nda3 forms an essential part of the spindle, required for cells to pass through mitosis. The *nda3-KM311* is a cold-sensitive allele that can be utilised to arrest cells in a metaphase-like state, showing three condensed chromosomes (Hiraoka et al, 1984; Toda et al, 1983). For the arrest, cells were exponentially grown in rich YE4S medium at 30 - 32°C followed by a 6 - 8 hour temperature-shift to 20°C, the restrictive temperature of the *nda3-KM311* allele. DAPI and calcofluor staining revealed condensed chromosomes and a septation index close to 0, respectively (3.4.2 and 3.4.3).

3.1.4 Inactivation of Aurora B kinase activity

To follow cells progress through a synchronous mitosis without Aurora B kinase (Ark1) activity we used an analog-sensitive version of the gene, *ark1-as3* (Hauf et al, 2007), that can be rapidly (within 10 minutes) inhibited by the addition of specific inhibitors that mimick ATP (4-amino-1-tert-butyl-3-(1-napthyl)pyrazolo[3,4-d]pyrimidine(1NA-PP1) or 4-amino-1-tert-butyl-3-(1-napthylmethyl)pyrazolo[3,4-d]pyrimidine (1NM-PP1)). In our case, we first arrested cells in G2 using the *cdc25-22* thermosensitive allele (3.1.3.3) and added 1NM-PP1 to the culture medium at a final concentration of 5 μM, 15 minutes before release into mitosis (3.1.3.3).

3.1.5 Strain construction

3.1.5.1 Random spore analysis

Most strains used in this study were constructed by random spore analysis. Strains of different mating types and different genotypes were crossed on malt extract agar (MEA) plates which contained a high percentage of maltose and a low percentage of nitrogen, triggering conjugation and sporulation in fission yeast. Cells were allowed to sporulate for approximately 3 days at 25°C and observed under the light microscope. In the presence of asci, a small loop of cells was resuspended in 1 ml of distilled water. 5 µl of snail juice (*Helix pomatia* juice, Biosepra) containing the enzyme helicase were added to break down the ascus walls, and the mixture was gently shaken for 5 - 6 hours at room temperature. Subsequently, the spores were pelleted at 3,000 rpm for 1 minute at room temperature in a Heraeus table-top centrifuge (Biofuge pico, Heraeus). After washing once with 1 ml of distilled water, the spores were plated on selective plates to select for the right combination of alleles.

3.1.5.2 Yeast transformations

Transformations were performed using a 1-step PCR procedure as described below and in (Bahler et al, 1998; Keeney & Boeke, 1994).

10 ml of a mid-log phase culture were pelleted in 50 ml Falcon tubes at 3,000 rpm for 1 minute at room temperature in a floor-standing centrifuge (Multifuge 4, Heraeus). The resulting cell pellet was washed with 10 ml of LiAc/TE buffer (0.1 M LiAc, 10 mM Tris/HCl pH 7.5, 1 mM EDTA pH 7.5) before resuspension in a final volume of 100 µl LiAc/TE working solution. 50 µl of salmon sperm DNA solution (10 mg/ml single stranded carrier DNA, Stratagene), and either 1 µg of linearised vector DNA or 3 - 10 µg of PCR product were added to the cell suspension and carefully mixed. After 5 minutes of incubation at room temperature, 280 µl of LiAc/TE containing 50 % PEG 3350 or 4,000 were added, and the cell suspension was carefully mixed and incubated at 30°C for 45 minutes without shaking. 48 µl of DMSO were added, and the suspension was carefully mixed. Cells were then heat-shocked at 42°C for 8 minutes, and the suspension was centrifuged in a table-top centrifuge (Biofuge pico, Heraeus) for 15 seconds at 12,000 rpm at room temperature. After washing once with 1 ml of distilled water, cells were resuspended in 200 µl of distilled water and plated on EMM agar plates, lacking

the auxotrophic amino acid used for selection. In case of selection by kanamycin and hygromycin B resistance, cells were first plated on rich YE4S medium and replica plated after 1 - 2 days onto YE4S agar plates, containing either 100 µg/ml Geneticin 418 (Gibco) or 300 µg/ml hygromycin B (Roche). Transformants were checked for the correct integration of the PCR cassette by Western bloting (3.3.2) and/or PCR analysis (3.2.5).

3.1.6 Cell cycle analysis using flow cytometry

To determine cell cycle progression, the DNA content was measured after propidium iodide staining of ethanol fixed cells (Moreno et al, 1991). Typically, 1 ml of a mid-log phase culture (OD_{600} = 0.4 - 1.0) was centrifuged at 13,000 rpm for 15 seconds in a table-top centrifuge (Biofuge pico, Heraeus) and the pellet fixed by resuspending in ice-cold 70 % ethanol and incubating on ice for at least 2 hours. Cells were resuspendend in 500 µl of 50 mM NaCitrate (pH 7.4) and treated with 0.1 mg/ml RNAse A for at least 2.5 hours at 37°C. Subsequently, 500 µl of 50 mM NaCitrate (pH 7.4), containing 8 µg/ml propidium iodide, were added to stain the DNA. After mild sonication (6 seconds at position 10, Sanyo, Soniprep 150), cells were analysed on a FACScan machine (Becton Dickinson). CellQuest software was used for subsequent image acquisition and preparation.

3.2 Biochemistry and related techniques

3.2.1 Chromatin fractionation (Chromatin Pellets)

3.2.1.1 Spheroplastation

To distinguish between soluble and chromatin-bound levels of a protein of interest, cells were gently lysed and differentially centrifuged as described in the following.

Usually, between 30 and 50 ml of a mid-log phase culture (OD_{600} = 0.5 - 0.8) were pelleted at 3,000 rpm for 5 minutes in a cooled (4°C) floor-standing centrifuge (Multifuge 4, Heraeus). The cell pellets were washed once with 10 ml of distilled ice-cold water and once with ice-cold 1.2 M sorbitol/H_2O. For spheroplastation, the cell pellet was resuspended in 800 µl of SP2 buffer (1.2 M sorbitol, 50 mM sodium citrate, 50 mM disodium hydrogen phosphate, pH 5.6 (HCl)), containing 20 - 40 µl of lysing enzymes (Sigma) and incubated at 30°C for 20 - 50 minutes, depending on the batch of lysing enzymes. Spheroplastation was checked under the light microscope by adding 2 µl of cell suspension to 2 µl of 20 % SDS/H_2O solution to lyse the successfully spheroplasted cells. When 90 % of the cells were spheroplasted (judged by their dark appearance in phase contrast) 1 M Tris/HCl pH 7.5 was added to a final concentration of 10 mM. The spheroplast resuspension was carefully underlayed with 1 ml of sucrose cushion (15 % sucrose, 1.2 M sorbitol, 10 mM Tris/HCl pH 7.5), and the spheroplasts were gently pelleted twice at 2,000 rpm for 4 minutes in a cooled (4°C) table-top centrifuge (Biofuge fresco, Heraeus), including a 180° turn of the tubes in the centrifuge to facilitate efficient pelleting. Due to the delicacy of spheroplasts, the following steps were performed with great care. 1 ml of Sorb/Tris mix (1.2 M sorbitol, 10 mM Tris/HCl pH 7.5) was added to the spheroplast pellet and the tube gently turned up and down twice. The tubes were placed into the centrifuge with the pellet facing towards the centre of the rotor. The spheroplasts were then collected by centrifugation in a cooled (4°C) table-top centrifuge (Biofuge fresco, Heraeus) (2,000 rpm for 4 minutes). The washing step with 1 ml of Sorb/Tris mix was repeated once more. The resulting spheroplast pellets were either frozen in liquid nitrogen and stored at -80°C or directly processed as described in the following paragraph.

3.2.1.2 Lysis and fractionation

Spheroplast pellets were either directly taken from 3.2.1.1 or thawed if stored at -80°C. The pellets were lysed by resuspending in 300 µl of ice-cold AX buffer (20 mM Hepes/KOH pH 7.9, 1.5 mM MgAc, 50 mM KAc, 10 % glycerol), containing 1 % Triton-X 100, 0.5 mM DTT and protease inhibitors (1 mM PMSF, 20 µg/ml leupeptin, 40 µg/ml aprotinin, 10 µg/ml pepstatin, 200 µg/ml bacitracin, 2 mM benzamidine, 2.4 µl of chymostatin, plus 1 x complete mini EDTA-free protease inhibitor tablets from Roche). The resuspension was incubated on ice for 10 minutes, including intermitted vortexing steps. To analyse the total amount of protein by Western blotting, 10 µl of this whole cell extract were mixed with the same volume of 2 x SDS loading buffer (3.2.4) and boiled for 5 - 10 minutes before storing at -20°C for SDS-PAGE. 200 µl of cell lysate were then carefully layered onto 200 µl of a sucrose cushion AXS (AX plus 30 % sucrose) and centrifuged at 4°C for 10 minutes at 12,000 rpm in a table-top centrifuge (Biofuge fresco, Heraeus) to separate the soluble from the insoluble fraction. At the top of the centrifugate, a thin lipid layer could be seen, followed by a soluble layer with a yellowish colour. The insoluble chromatin fraction at the bottom of the tube was separated from the soluble fraction by the sucrose cushion which prevented contamination of the different layers. For protein detection of the soluble fraction by Western blotting, 10 µl of the soluble extract were pooled with the same volume of 2 x SDS loading buffer followed by 5 - 10 minutes boiling and storage at -20°C. The remaining soluble fraction was discarded and the chromatin pellet washed twice in 200 µl of AX buffer. Finally, the chromatin pellet was resuspended in 200 µl of AX buffer. For detection of the protein of interest in the chromatin fraction by Western blotting, 10 µl of the resuspension were mixed with the same volume of 2 x SDS loading buffer. The samples were boiled for 5 minutes and frozen at -20°C. As loading controls for chromatin-bound and soluble proteins, antibodies against Histone H3 (rabbit polyclonal, ab1791, Abcam) and against Cdc2 (PSTAIRE, rabbit polyclonal, sc-53, Santa Cruz Biotechnology) were used for Western blotting (for dilutions see Antibody lists in 3.8).

3.2.2 ChIP on chip analysis

3.2.2.1 Formaldehyde fixation

100 ml of a late-log phase culture (OD_{600} = 0.8 - 1.0) were fixed by adding formaldehyde to a final concentration of 1 % v/v. Cells were mildly shaken for 30 minutes at room temperature followed by overnight incubation on a rotating wheel at 4°C. Cells were pelleted at 4°C and subsequently washed 3 times in 60 ml of ice-cold TBS (200 mM Tris-HCl pH 7.5, 1.5 M NaCl).

3.2.2.2 Cell breakage

The cell pellets were resuspended in 400 µl of lysis buffer (50 mM HEPES-KOH, pH 7.5, 140 mM NaCl, 1 mM EDTA/NaOH pH 8.0, 1 % Triton X-100, 0.1 % Na-deoxycholate, 1 mM PMSF), and 426 - 600 µm acid-washed glass beads (Sigma) were added up to the rim. The tubes were subsequently transferred to a multi-beads shocker (MB400U, Yasui Kikai, Osaka, Japan) for cell breakage. Engineered to work in a very cold environment (below 4°C), the multi-beads shocker allowed efficient breakage of cells with minimised protein degradation.

3.2.2.3 Sonication and chromatin immunoprecipitation (ChIP)

The resulting whole cell extract was sonicated (8 times 15 s at position 8, Sanyo, Soniprep 150) to release 400 - 800 bp long DNA fragments into the soluble fraction. After spinning for 5 minutes at 13,000 rpm at 4°C in a table-top centrifuge (Biofuge fresco, Heraeus), the supernantant was spun again under the same conditions. The pellet was discarded and the soluble extract added to a magnetic Protein-A Dynabeads pellet (Dynal) coupled to anti-PK (clone SV5-Pk1, Serotec) or anti-HA antibodies (clone 16B12, Covance) (see Antibody lists 3.8).

For the Protein-A Dynabeads pellet, 120 µl of Dynabeads for anti-HA immunoprecipitations (60 µl for anti-Pk immunoprecipitations) had been washed 3 times with PBS-BSA (5 mg/ml BSA in PBS), resuspended in 120 µl of PBS-BSA (60 µl) and incubated with 40 µl of 1 mg/ml anti-HA antibody (clone 16B12, Covance, see 3.8) (7 µl of 1 mg/ml anti-Pk antibody, clone SV5-Pk1, Serotec, see Antibody lists 3.8) for at least 3 hours on a rotating wheel in the cold room followed by two gentle washing steps with 1

ml of PBS-BSA. The resulting bead pellet coupled to the antibodies was then resuspended in the whole cell extracts and rotated on a wheel at 4°C for 3 - 6 hours.

5 µl of the supernatant (SUP sample) were taken as a comparative whole genome sample for the chromatin immunoprecipitate and kept on ice (3.2.2.8). The antibody/beads/immunprecipitate pellets were washed several times: twice with lysis buffer, twice with lysis buffer, containing an additional 360 mM NaCl, twice with washing buffer (10 mM Tris/HCl pH 8.0, 250 mM LiCl, 0.5 % NP-40, 0.5 % Na-deoxycholate, 1mM EDTA/NaOH pH 8.0) and once with TE (10 mM Tris/HCl pH 8, 1 mM EDTA), using a magnetic stand (MPC-S, Dynal). 160 µl of elution buffer (50 mM Tris/HCl pH 8.0, 10 mM EDTA, 1 % SDS) were added to the immunoprecipitates and eluted at 65°C for 15 minutes (IP sample), including a shaking step of the tubes every 3 minutes.

Small samples of the whole cell extract before and after incubation with the antibody/beads and a small sample of the eluate were kept to confirm the presence of the immunoprecipitated protein by Western blotting.

3.2.2.4 Reversal of cross-linking, proteinase K and RNAse A treatment

360 µl of TES (10 mM Tris/HCl, pH 8.0, 1 mM EDTA, 1 % SDS) were added to the 110 µl of eluate and 95 µl of TES to the 5 µl of SUP sample. The mixture was subsequently incubated overnight at 65°C to reverse the crosslinking. The immunoprecipitate was incubated with proteinase K to facilitate protein degradation as listed in the table below.

Table 3.1 Pipetting scheme for proteinase K digestion

Ingredient	Volume (µl)	
	SUP Sample	IP Sample
DNA sample	100	630
TE (pH 8)	200	432
Glycogen (10 mg/ml)	3	12
Proteinase K (20 mg/ml)	7.5	30
Total volume	303	1104

The mixture was incubated at 37°C for 2 hours. Subsequently, the DNA was extracted twice with 310 µl of buffered phenol/chloroform/isoamylalcohol (25 : 24 : 1, saturated with 10 mM Tris, pH 8.0, 1mM EDTA, Sigma) and precipitated. For precipitation, 200 mM final NaCl and 2.5 volumes of ice-cold absolute ethanol were added. The samples were vortexted and left at -20°C for at least 30 minutes, preferably overnight. After washing with 70 % ice-cold ethanol, the pellets were dried at room temperature for 30 - 60 minutes and resuspended in a final volume of 30 µl of TE.

The SUP and IP samples were then treated with a final concentration of 0.3 µg/µl RNAse A at 37°C for at least 1 hour to remove contaminating RNA before amplification of the DNA.

3.2.2.5 DNA amplification

After RNAse A digestion, the DNA was purified with QIAprep PCR purification spin columns (Qiagen) and the volume reduced by precipitation. For precipitation, 1 µl of glycogen, 1/10 volume of 3 M sodium acetate and 2.5 volumes of ice-cold absolute ethanol were added to the samples. After thorough mixing, the samples were incubated at -20°C for at least 30 minutes, preferably overnight. The DNA was pelleted at 13,000 rpm for 20 minutes at 4°C in a table-top centrifuge (Biofuge fresco, Heraeus) and the pellets washed with 70 % ice-cold ethanol. Subsequently, the DNA pellets were dried and resuspended in a final volume of 7 µl of TE. In a first step, a random primer with a fixed 3' sequence was used to prime the DNA for subsequent PCR amplification (3.3.2.2; (Iyer et al, 2001)). After this priming step, distilled water was added to the IP sample to a volume of 500 µl, and the dNTPs were removed by spinning the reaction in YM10 Microcon ultrafiltration spin columns (Millipore). To retain approximately 50 µl of DNA solution for DNA amplification (see 3.3.2.2), the columns were spun at 12.300 rpm for 25 - 45 minutes at 4°C, depending on the lot of the spin columns used. The SUP sample was processed in a slightly different way. 45 µl of distilled water were added to the 15 µl reaction. Of the 60 µl, 30.5 µl were used for PCR amplification (see 3.3.2.2).

The size range of the amplified DNA fragments was confirmed by running 5 µl of the 100 µl of PCR reaction on a 1 % agarose gel. dNTPs were removed by adding 400 µl of distilled water to the PCR reaction and subsequently spinning the DNA solution in YM10 Millipore unltrafiltration spin columns until a final volume of approximately 42 µl was retained. The flow-through was discarded, and 1 - 1.5 µl of the reaction were used to measure the DNA content with a Nanodrop spectrophotometer (ND-1000, Thermo Scientific).

3.2.2.6 DNAse digestion

Approximately 10 µg of PCR-amplified DNA were digested with DNAse I (Gibco BRL Amplification Grade) to an average size of 100 bp (Table 3.2). To do so, 40.75 µl of DNA solution were added to a PCR tube and mixed on ice with 9.25 µl of a DNAse I reaction mix (Table 3.2). The reaction was incubated for 2 minutes at 37°C in a PCR machine followed by 15 minutes incubation at 95°C to inactivate the DNAse I.

Table 3.2 DNAse I digestion recipe

Set Up Mix

Ingredient	Volume
dH_2O	7.4 µl
10 x One-Phor-All-Buffer + (Pharmacia #27-0901-0)	1 µl
25 mM $CoCl_2$	0.6 µl
DNAse I (1 U/µl) (Gibco BRL Amplification Grade #18068-015)	1 µl

Reaction Mix

Ingredient	Volume
10 x One-Phor-All-Buffer + (Pharmacia #27-0901-0)	4.85 µl
25 mM $CoCl_2$	2.9 µl
DNAse I Set Up	1.5 µl

3.2.2.7 DNA end-labelling with biotin

The DNA fragments were end-labelled with biotin-11-ddATP (NEN #NEL548).

Table 3.3 Biotin-labelling pipetting recipe

Ingredient	Volume (µl)
DNA	50
5 x TdT buffer	10
biotin	1
Terminal transferase TdT (400 U/µl)	1

The reaction was incubated at 37°C for 1 hour.

3.2.2.8 Hybridisation to oligonucleotide microarrays

202 µl of hybridisation cocktail were prepared for each sample as specified in the following table.

Table 3.4 Pipetting scheme for DNA hybridisation cocktail

Ingredient	Volume (µl)
DNA	62
3 nM control Oligo B2*	3.3
20 x eukaryotic hybridisation control	10
10 mg/ml herring sperm DNA	2
20 x SSPE (BioWhittaker Molecular Applications/Cambrex)	60
0.1 % Triton-X 100	10
dH_2O	54.7
total volume	202

*Oligo B2 hybridises to specific border regions of the microarray to facilitate alignment.

The samples were boiled at 95°C for 10 minutes before cooling on ice for 5 minutes. Meanwhile, the microarrays that had been taken out of the cold room to adjust to room temperature were loaded with 250 µl of 1 x hybridisation buffer (100 mM MES, 1 M [Na^+], 20 mM EDTA, 0.01 % Tween 20) and rotated for at least 10 minutes at 42°C and 60 rpm in a hybridisation oven (GeneChip hybridisation oven 640, Affymetrix). The 1 x hybridisation buffer was removed and the hybridisation cocktail added to the microarray. After 16 hours of hybridisation in the oven at 42°C, 60 rpm, the hybrisation buffer was carefully removed and stored at -80°C for possible rehybridisation. Staining of the biotin-labelled DNA with phycoerythrin-streptavidin (SAPE) (Molecular Probes) and subsequent washing of the microarrays were performed automatically by using the EukGe-WS1-v4-450 washing protocol on an Affymetrix fluidics station (GeneChip fluidics station 450). The stained microarrays were subsequently scanned with a Gene Chip scanner 3000 (Affymetrix).

The fission yeast chromosome 2 and 3 microarray was produced by the Affymetrix custom express service (S_pombea520106F, P/N 520106, Affymetrix). The oligonucleotide arrays were designed to contain 11 25mer probes in every 250 bp window, partially overlapping each other to fully cover both coding and non-coding sequences (Figure 3.2). Furthermore, the probes were designed with approximately equal GC amounts to

allow comparable hybridisation efficiencies. To distinguish between positive and negative binding signals we compared the ChIP fraction to a whole genome DNA sample, using the criteria as described in (Katou et al, 2003). Gene Chip operating software version 1.4 (GCOS, Affymetrix) was used to determine the signal $\log_2$ ratio, the p-value and the change p-value of every probe.

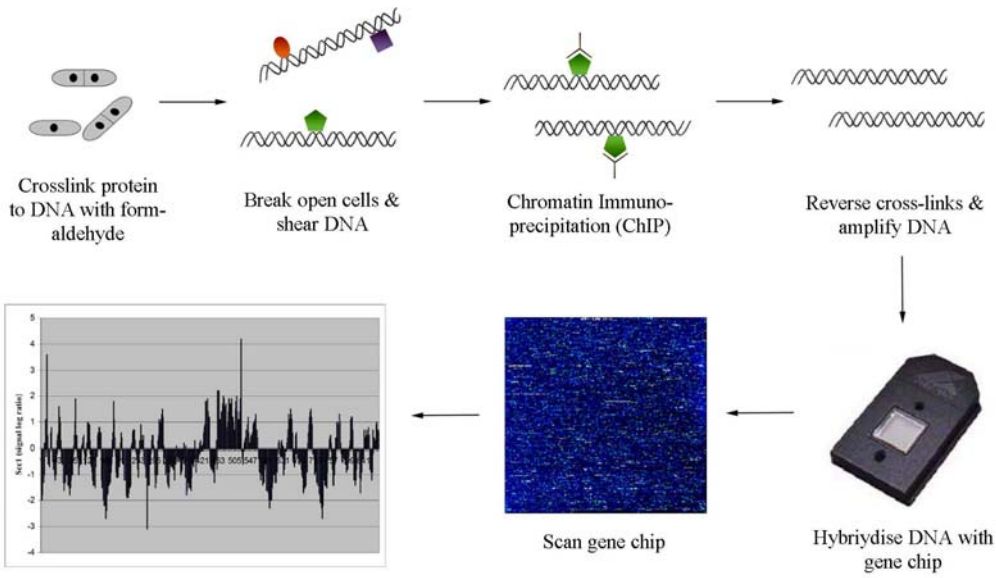

Figure 3.1 Schematic of the ChIP on chip procedure.
Fission yeast cells were fixed with formaldehyde, followed by breakage of the cells and sonication to release 400 - 800 bp DNA fragments into the supernatant. Subsequent chromatin immunoprecipitation against the protein of interest (green) was followed by reversal of the protein-DNA crosslinking. After DNA amplification and labelling, the cocktail was hybridised to a high-density oligonucleotide microarray. Gene chips were scanned, and chromosome maps were created.

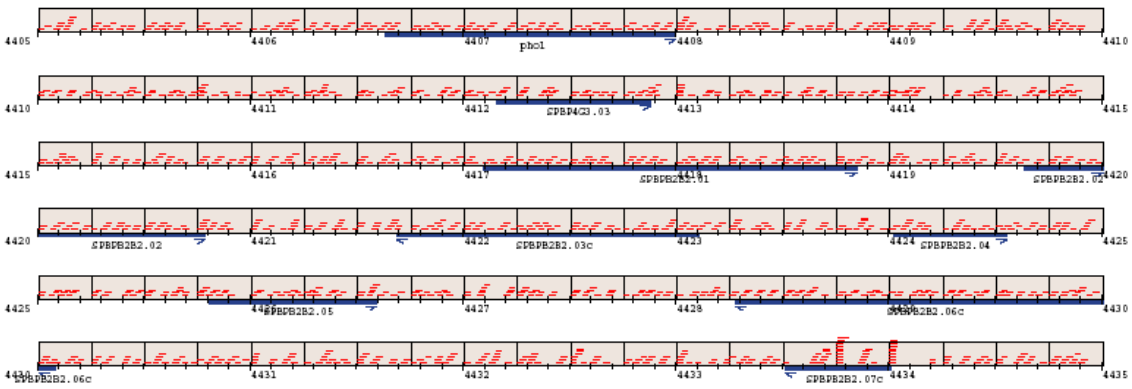

Figure 3.2 Oligonucleotide arrangement on chromosome 2/3 microarray.
A 30 kb region on the right arm of fission yeast chromosome 2 is shown. The 25mer oligonucleotide probes are depicted as red horizontal lines within 250 bp windows framed in black. Open reading frames are shown as horizontal blue bars marked with arrowheads that indicate the direction of the gene. 11 oligonucleotides are arranged within each 250 bp window.

3.2.3 TCA yeast cell extracts

Approximately 15 ml of a mid to late-log phase culture (OD_{600} = 0.5 - 0.8) were harvested in 15 ml Falcon tubes at 3,000 rpm for 5 minutes at 4°C in a Heraeus Multifuge under-bench centrifuge. The cell pellets were washed 1 time with 1 ml of cold distilled water and either stored at -20°C or directly processed for extraction. The cell pellets were thawed on ice if frozen at -20°C or directly resuspended in 200 µl of 20 % TCA. Acid-washed 426 - 600 µm glass beads (Sigma) were added up to the rim and the resuspensions subjected to cell breakage, using a multibeads shocker (Yasui Kikai, Japan). The glass beads were separated from the extract and washed twice with 200 µl of 5 % TCA. The washing fractions were pooled with the extract and the mixture pelleted at 3,000 rpm for 10 minutes in a Heraeus Biofuge pico table-top centrifuge at room temperature. The supernatant was discarded, and the TCA pellets containing all proteins were resuspended in 100 - 200 µl of SDS loading buffer. Due to the presence of TCA, the low pH induced a colour change of the bromophenol blue-containing SDS loading buffer from blue to yellow. To re-adjust the pH in the samples, approximately 50 µl of 1 M Tris base (pH unadjusted) were added until the samples changed their colour back to blue. The extracts were subsequently boiled for 10 minutes and again centrifuged for 10 minutes at 3,000 rpm in a table-top centrifuge (Biofuge pico, Heraeus). The supernatant was either frozen and stored at -20°C or directly used for SDS-PAGE (3.2.4) and Western blotting (3.2.5).

3.2.4 SDS-PAGE

Protein samples were resolved on SDS gels that were prepared with a 37.5 : 1 acrylamide to bisacrylamide solution (Amresco). Depending on the size of the protein of interest, different percentages of acrylamide/bisacrylamide gels were used. Small proteins (<30 kDa) were usually run on 10 - 15 % SDS gels and larger proteins (> 100 kDa) on 8 - 10 % gels. For higher-resolution, proteins migrated through a low-percentage stacking gel (125 mM Tris/HCl pH 6.8, 5 % bisacrylamide, 0.1 % SDS) at 100 V before progressing through the stacking gel at 120 V. SDS-PAGE running buffer was composed of 25 mM Tris, 250 mM glycine and 0.1 % SDS. The electrophoresis tanks were manufactured by CBS scientific, CA. A broad-range pre-stained protein marker (New England Biolabs) was typically run in parallel to identify the approximate size of the protein of interest.

3.2.5 Western blotting

The method was performed in a modified version from (Towbin et al, 1992).

3.2.5.1 Protein transfer

Proteins separated by SDS-PAGE (3.2.4) were transferred onto nitrocellulose membranes (Schleicher and Schuell), using a wet transfer tank (Biorad). The wet transfer buffer was composed of 3.03 g/l Tris base, 14.1 g/l glycine, 0.05 % SDS and 20 % v/v methanol. The transfer was carried out in the cold at 5.3 mA/cm^2 for 40 minutes. The efficiency of the protein transfer was checked by staining the membrane with Ponceau S solution (Sigma).

3.2.5.2 Immunological detection

3.2.5.2.1 Blocking

To limit unspecific protein binding, the membrane was shaken in 5 % skimmed milk (Marvel) in PBST (170 mM NaCl, 3 mM KCl, 10 mM Na_2HPO_4, 2 mM KH_2PO_4, 0.01 % Tween 20) for 30 - 60 minutes at room temperature.

3.2.5.2.2 Primary antibody

The membrane was then incubated for 1 hour at room temperature or overnight in the cold room with primary antibodies diluted in PBST containing 5 % w/v milk powder. For relevant antibody concentrations see Antibody lists in 3.8.

3.2.5.2.3 Secondary antibody

After 3 times washing with PBST for 5 minutes, membranes were gently shaken at room temperature for 30 - 60 minutes in PBST, containing 5 % milk powder and 1:5,000 diluted horseradish peroxidase (HRP) coupled secondary antibodies (HRP-anti-mouse or HRP-anti-rabbit, Amersham).

3.2.5.2.4 ECL detection

The membranes were washed 4 times with PBST and developed, using the ECL detection system (Amersham), according to the manufacturer's instructions.

3.3 Molecular Biology

Molecular biology techniques were performed according to (Sambrook et al, 1989). Methods included bacterial transformations, restriction enzyme digests, isolation of DNA plasmids and separation of DNA fragments by size using agarose gel electrophoresis.

3.3.1 Genomic DNA preparation

Fresh patches of yeast were grown on YE4S agar plates. For spheroplastation, a toothpick of cells was resuspended in 200 µl of SCE/ME/zymolase (1 M sorbitol, 0.1 M sodium citrate pH 7.0, 60 mM EDTA, 8 µl/ml mercaptoethanol and 2 mg/ml zymolase T-20) and incubated for 45 minutes at 37°C in a shaking thermomixer. 200 µl of SDS-solution (100 mM Tris/HCl pH 9.0, 50 mM EDTA, 2 % SDS) were added, the solution mixed and subsequently heated for 5 minutes to 65°C to lyse the cells. 200 µl of 5 M potassium acetate were added at room temperature, and the reaction was gently mixed and spun for 10 minutes at 13,000 rpm in a Heraeus Biofuge pico table-top centrifuge at room temperature. 350 µl of the supernatant were transferred to a fresh tube, and 800 µl of absolute ethanol were added at room temperature to precipitate the DNA. The sample was spun for 2 minutes at 6,000 rpm in a Heraeus table-top Biofuge pico centrifuge at room temperature, the ethanol aspirated and the DNA pellets rinsed with 70 % ethanol. After air-drying, the pellet was dissolved in 200 µl of distilled water, of which 1 µl was used for subsequent genotyping by PCR amplification.

3.3.2 Polymerase chain reaction (PCR)

3.3.2.1 Endogenous C-terminal tagging of yeast proteins

Epitope tagging of endogenous genes was performed by 1-step PCR tagging (Bahler et al, 1998). Forward primers contained approximately 80 bp of homology to the 3’ end of the gene of interest before its STOP codon, followed by an 18 nucleotides long sequence, homologous to the respective vector. The reverse primer consisted of a sequence homologous to the 3’ UTR region of the gene, followed by an 18-mer sequence that facilitated priming to the vector. The subsequent PCR product was flanked by regions homologous to the gene of interest, allowing the in-frame fusion of the epitope-containing cassette with the desired gene. Transformants were plated on selective plates,

using Geneticin G418 or hygromycin B resistence genes or auxotrophic markers. Auxotrophic markers included the *S. pombe ura4*$^+$ gene and the *S. cerevisiae LEU2* gene. The *S pombe ura4*$^+$ gene could be efficiently used as the auxotrophic mutant *ura4-D18* lacks to entire sequence of the *ura4* gene. In the case of the *S. pombe leu1-32* auxotrophic mutant allele, the *S. cerevisiae* version *LEU2* was used to minimise the chances of integration at the endogenous marker locus.

For tRNA deletion, the *K. lactis URA3* marker was initially used to replace the tRNA genes of interest and subsequently lost after counter-selection with 5-Fluoroorotic Acid (5-FOA), leaving one of the inverted repeats that had flanked the *URA3* marker integrated. Vectors used for 1-step PCR tagging are listed in table 3.7. The PCR reaction was set up as described in Table 3.5. The PCR reaction was performed in a Peltier Thermal Cycler (MJ Research), according to the programme listed in Table 3.6. After completion of the cycle, 5 µl of the reaction were run on an agarose gel to confirm the success of the reaction. Subsequently, the PCR products were precipitated by adding 1/10 volume of 3M sodium acetate (NaAc) and 2 to 2.5 volumes of ice-cold absolute ethanol to the PCR reaction. The mix was incubated at -20°C for at least 20 minutes. The DNA was then pelleted at 13,000 rpm for 15 minutes at 4°C in a table-top centrifuge (Biofuge fresco, Heraeus) before washing with 70 % ethanol and drying for approximately half an hour at 37°C. The resulting pellet was resuspended in 7 - 15 µl of distilled water and directly used for yeast transformations.

Table 3.5 PCR pipetting scheme for C-terminal tagging of yeast proteins

Ingredient	Amount
Template DNA	10 - 50 ng
Forward primer (10 µM)	1.7 µl
Reverse primer (10 µM)	1.7 µl
dNTP (10 mM for each of four)	5 µl
10 x Expand high fidelity buffer (Roche)	10 µl
25 mM $MgCl_2$	10 µl
Expand high fidelity Taq (Roche)	1 µl
dH_2O	up to 100 µl

Table 3.6 PCR programme for C-terminal tagging of yeast proteins

Step	Time and Temperature	
1	5 minutes at 95°C	
2	1 minute at 95°C	
3	2 minutes at 50°C	(depending on the T_M of the primers)
4	2 - 3 minutes at 72°C	(depending on size of the amplification product)
5	go to step 2 and repeat 7 x	
6	1 minute at 95°C	
7	2 minutes at 55 - 57°C	(depending on the T_M of the primers)
8	2 - 3 minutes at 72°C	(depending on size of the amplification product)
9	go to step 6 and repeat 20 x	
10	7 minutes at 72°C	
11	4°C forever	

3.3.2.2 ChIP on chip DNA amplification

3.3.2.2.1 Priming of genomic DNA (Round A)

15 µl of Round A set up (Table 3.7) were incubated in a PCR machine at 94°C for 2 minutes and cooled to and held at 10°C for 5 minutes while adding 5.05 µl of reaction mix (Table 3.7). The reaction was slowly (over 8 minutes) heated to 37°C, using a PCR ramp programme. After holding the temperature at 37°C for 8 minutes, the reaction was heated to 94°C for 2 minutes and subsequently cooled to and held at 10°C for 5 minutes while adding 1.2 µl of diluted sequenase (Table 3.7). The reaction was heated once more to 37°C, taking again 8 minutes for the process, and subsequently incubated at 37°C for 8 minutes before being cooled to 4°C. The samples were either frozen after this step or directly used for DNA amplification (3.3.2.2.2).

Table 3.7 Pipetting schemes for ChIP on chip Round A priming reaction

Set up in PCR tubes

Ingredient	Volume (µl)
DNA	7
5 x Sequenase buffer	2
Primer A*[1] (40 µM)	1

Reaction mix

Ingredient	Volume (µl)
5 x Sequenase buffer	1
dNTPs (3 mM each)	1.5
DTT (0.1 M)	0.75
BSA (0.5 mg/ml)	1.5
Sequenase*[2]	0.3

Diluted sequenase

Ingredient	Volume (µl)
DIL buffer	0.9
Sequenase*[2]	0.3

*[1] Primer A: GTT TCC CAG TCA CGA TCN NNN NNN NN
*[2] Sequenase Ver2.0 T7 DNA polymerase (USB #70775)

3.3.2.2.2 DNA amplification (Round B)

After dNTP removal from the IP sample and dilution of the SUP sample (see 3.2.2.5) the primed DNA was amplified by PCR as described in Table 3.8 and Table 3.9 below.

Table 3.8 PCR pipetting recipe for ChIP on chip Round B

Ingredient	Volume (µl)	
	SUP Sample	IP Sample
dH_2O	65.5	30.5
Template	15	50
10 x PCR buffer	10	10
dNTPs (2.5 mM each)	8	8
Primer B* (100 µM)	1	1
TaKaRa EX-Taq (#R0001A)	0.5	0.5
Total volume	100	100

* Primer B: GTT TCC CAG TCA CGA TC

Table 3.9 PCR programme for ChIP on chip Round B

Step	Temperature and time
1	94°C
2	95°C for 2 seconds
3	40°C for 30 seconds
4	50°C for 30 seconds
5	72°C for 3 minutes
6	go to step 2 and repeat 32 x
7	72°C for 7 minutes
8	4°C forever

3.3.3 Restriction digests

For restriction digests, New England Biolabs (NEB) enzymes and buffers were used according to the manufacturer's instructions. Typically, approximately 1 - 2 µg of plasmid DNA were digested in a 20 - 30 µl reaction by incubating for 1 - 2 hours at 37°C with 10 U of enzyme. Several enzymes required a different incubation temperature as described in the manufacturer's instructions.

3.3.4 Phosphatase treatment

Before ligation, plasmid DNA was de-phosphorylated to prevent re-ligation of the empty vector DNA. 5' phosphates were removed from plasmid DNA, using Calf Intestinal Phosphatase (CIP, New England Biolabs) according to the manufacturer's instructions. The de-phosphorylation reaction was carried out directly after the restriction digest and typically involved a 30 minute incubation at 37°C with 2 U CIP followed by 15 minutes heat-inactivation at 85°C. Subsequently, the DNA was run on an agarose gel, and the respective band containing the DNA was retrieved using a Qiagen gel electrophoresis kit (see 3.3.9) to separate the DNA from the restriction enzymes and the CIP.

3.3.5 DNA ligations

For ligations, a kit was used according to the manufacturer's instructions (Mighty Mix, TaKaRa). Typically, the same volumes (5 - 10 µl) of ligation mix and insert/vector reaction were mixed and incubated for 10 minutes at 25°C or overnight at 16°C. A 3 - 5-fold stochiometric excess of the insert was used which was determined by agarose gel electrophoresis (3.3.8) using a quantitative DNA standard (DNA Hyperladder, Bioline). To estimate re-ligation efficiency of the vector a negative control was included, using distilled water instead of insert. In a last step, the reaction mix was incubated at 65°C for 10 minutes to heat-inactivate the ligase. Subsequently, 10 µl of the reaction were transformed into 100 µl of chemically competent *E. coli* (DH5α) cells (3.3.6).

3.3.6 Bacterial transformations

DH5α *E. coli* chemical competent cells were used for plasmid DNA amplification. 10 µl of the ligation reaction were added to 100 µl of *E. coli* cells on ice. After gentle mixing and 30 minutes incubation on ice, cells were heat-shocked for 2 minutes at 42°C and subsequently incubated for 2 minutes on ice. 1 ml of liquid medium LB (10 % w/v bacto-tryptone, 5 % w/v yeast extract and 170 mM NaCl) was added, and cells were allowed to grow for 30 - 60 minutes at 37°C before plating for overnight selection on LB/Amp agar plates at 37°C (LB plus 1.5 % w/v agar, 100 µg/ml ampicillin). Resulting colonies were grown in 3 - 5 ml of LB/Amp overnight at 37°C and pelleted the next morning. DNA was isolated from the bacteria using 'miniprep' kits (Qiagen) as outlined below (3.3.7).

3.3.7 Isolation of plasmid DNA from *E. coli*

Qiagen miniprep kits were used to recover plasmid DNA from bacterial pellets, according to the manufacturer's instructions. The technique is based on alkaline lysis of the bacteria followed by adsorption of the plasmid DNA to a silica matrix in high salt conditions. After a washing step with ethanol, plasmid DNA was eluted from the column with TE (10 mM Tris, 1 mM EDTA pH 8) or distilled water.

3.3.8 Agarose gel electrophoresis

Depending on the size of the DNA fragments to be analysed, agar was added to 1 x TAE buffer at 1 - 2 % w/v (40 mM Tris base pH 7.5, 2 mM EDTA and 0.115 % v/v acetic acid). The agarose was solubilised by boiling and cooled to below 60°C, before ethidium bromide was added to a final concentration of 0.5 µg/ml. 6 x loading buffer (0.25 % w/v bromophenol blue, 0.25 % xylene cyanol FF and 30 % v/v glycerol) was used to facilitate efficient loading of DNA samples into the wells of the gels. Electrophoresis tanks manufactured by Anachem Biosciences were used, and DNA gels were run at 1 - 5 V/cm (distance between electrodes). A DNA marker (Novagene) was run in parallel to determine the position of the DNA within the gel. The visualisation of DNA fragments was performed under a UV transilluminator (BioDoc-It).

3.3.9 Retrieval of DNA fragments from agarose gels

Resolved DNA fragments were excised from agarose using a scalpel, and the DNA was recovered from the gel bands, using a gel extraction kit (Qiagen) according to the manufacturer’s instructions.

3.4 Cell biology and microscopy

3.4.1 Chromosome spreading

Spheroplasts for chromosome spreading were obtained as described for chromatin fractionation experiments (3.2.1) except for the following differences. Less cells - between 20 - 30 ml of a mid-log phase culture (OD_{600} = 0.5 - 0.8) - were used, and the cell pellet was resuspended in 400 µl of SP2 buffer (1.2 M sorbitol, 50 mM sodium citrate, 50 mM disodium hydrogen phosphate, pH 5.6 (HCl)). 200 µl of 25 mg/ml lysing enzymes (Sigma) were added and the mixture incubated at 30°C for 20 - 50 minutes, depending on the batch of lysing enzymes used. After the washing step with 1 ml of Sorb/Tris mix (3.2.1), a washing step with 1 ml of Sorb/MES mix (0.1 M MES (2-(N-morpholino) ethane sulfonic acid), 1 mM EDTA, 0.5 mM $MgCl_2$, 1 M sorbitol, pH 6.4) was performed in a similar fashion. Cells were resuspended in 200 µl of Sorb/MES mix, and 20 µl were transferred onto a glass slide (Menzel Superfrost). After consecutively adding 40 µl of fixative (4 % paraformaldehyde, 3.4 % saccharose), 80 µl of 1 % lipsol/H_2O and another 80 µl of fixative on top of the spheroplast resuspension, the mixture was gently spread on the slide using a glass rod. The slides were left overnight in the fume hood to dry. The next day, the slides were washed in PBS for 10 minutes, blocked with blocking buffer (0.5 % gelatine, 0.5 % BSA in PBS) for 20 minutes and subsequently incubated for 2 hours at room temperature with the primary antibody (diluted in blocking buffer, for dilutions see Table 3.12). Alternatively, slides were incubated with the primary antibody overnight at 4°C. After a 10 minute washing step in PBS, a 2 hour incubation period with the secondary antibody diluted in blocking buffer (see Table 3.13), and another 10 minute washing step in PBS followed. 0.1 µg/ml of DAPI, added to equal amounts of antifade reagent (FluoroGuard, BioRad) and blocking buffer, was transferred to the spread nuclei, and slides were covered and sealed with nail polish. Imaging of the slides was performed on a Zeiss Axioplan 2 fluorescence microscope using the data-acquisition software Volocity. For quantification, the fluorescence intensities of 50 - 100 spread nuclei recorded with identical exposure times were measured using the software Image J.

3.4.2 DNA visualisation (DAPI staining)

1 ml of a mid-log phase culture (OD_{600} = 0.4 - 0.8) was pelleted and resuspended in 1 ml of 70 % cold ethanol. After pelleting the fixed cells at 13,000 rpm for 15 seconds in a table-top Heraeus Biofuge pico centrifuge, 5 - 10 µl of the pellet were added to 1 ml of distilled water and pelleted as before. 1 µl of cell suspension was mixed with 1 µl of 1 µg/ml DAPI on a slide and sealed with a cover slip.

3.4.3 Septum visualisation (Calcofluor staining)

Cells were processed as described in 3.4.2 but mixed with 1 µl of a 10 mg/ml calcofluor/H_2O solution or with both 1 µl of a 10 mg/ml calcofluor/H_2O solution and 1 µl of 1 µg/ml DAPI solution.

3.4.4 Tubulin visualisation

5 ml of a mid-log phase culture (OD_{600} = 0.6 - 0.8), containing cells in which the α-tubulin subunit Atb2 had been endogenously tagged with GFP at its C-terminus (Pardo & Nurse, 2005), were filtered and collected on a methanol-resistant membrane (0.45 µm Durapore membrane filters, Millipore). The membranes were resuspended in 10 ml of methanol that had previously been cooled to -80°C for at least 2 hours. After incubation at -80°C for at least 1 hour, the membranes were removed, the cells pelleted and subsequently resuspended in 1 ml of water. On a slide, 1 µl of aqueous cell suspension was mixed with 1 µl of 1 µg/ml DAPI or with both 1 µl of 1 µg/ml DAPI and 1 µl of 10 mg/ml calcofluor solution.

3.5 Biostatistics and Bioinformatics

The tasks in this section were performed in collaboration with Neil Brookes from the LRI Biostatistics and Bioinformatics department.

3.5.1 Peak-picking parameters for ChIP on chip maps

Cohesin binding sites were assigned according to the following constraints. To reduce unspecific background signals, Rad21-Pk_9 association along the chromosomes was averaged at every point using a +/- 2,250 bp sliding window. Local maxima were identified and chosen as a peak if the raw signal intensity was above 0.3. Peaks were counted from their maximum to both sides until the raw signal $\log_2$ ratio reached a value below 0. The peak position was defined as the midpoint within the peak revealing a total of 228 sites of cohesin association along chromosome 2, as indicated by solid bars in the map (see Appendix 7.1).

The binding sites of the cohesin loader subunit Mis4, the condensin subunit Cnd2, the RNA polymerase III transcription factor subunit Sfc6 and the putative ribosomal protein gene transcription factor Fhl1 were assigned as described above, except that, due to the higher background signals, only peaks with a smoothed signal intensity above 0.5 were chosen.

Entire chromosome 2 maps of Rad21, Mis4, condensin, Sfc6 and Fhl1 can be found in the Appendix (7.1, 7.2, 7.3, 7.4 and 7.5, respectively).

3.5.2 Bootstrapping approach to create random cohesin binding patterns

To analyse the randomness, or non-randomness, of the cohesin distribution along fission yeast chromosomes, a bootstrapping approach was utilised to generate 10,000 random cohesin binding patterns along chromosome 2. For this approach, the software Pearl was used. The 228 cohesin peaks, as assigned in Appendix 7.1 and described above, were randomly distributed among the 508 available convergent sites, taking the widths of the observed peaks into account, as described in the following. This was done by distributing the peaks in a non-overlapping manner and allowing them to cover more than one intergene.

3.6 Strain list

Table 3.10 Strains used for functional experiments in this study

Strain	Genotype
Y252	*h⁻ leu1-32 nda3-KM311 cnd2-Pk9-kanMX6*
Y2197	*h90 leu1-32 ade6-M216 rad21-HA3-kanMX6*
Y2447	*h90 leu1-32 psc3-Pk9-kanMX6*
Y2460	*h90 leu1-32*
Y2463	*h⁻ leu1-32 ura4-D18 ade6-210 ssl3::ura4⁺ ars1-ssl3⁺-LEU2 rad21-HA3-kanMX6*
Y2464	*h⁻ leu1-32 ura4-D18 ade6-210 ssl3::ura4⁺ ars1-ssl3-29ts-LEU2 rad21-HA3-kanMX6*
Y2468	*h90 leu1-32 mis4-Pk9-kanMX6*
Y2470	*h⁻ leu1-32 ade6-M210 ssl3Δ::ura4⁺ ars1-ssl3-29ts-LEU2 rad21-HA3-kanMX6 ura4⁺-pREP2res1*
Y2699	*h⁻ leu1-32 cdc25-22 rad21-Pk9-kanMX6 SV40p-GFP-atb2-LEU2*
Y2703	*h90 nda3-KM311 rad21-Pk9-kanMX6*
Y2828	*h⁻ pds5-Pk9-kanMX6*
Y2863	*h⁻ leu1-32 cdc10-129 rad21-Pk9-kanMX6*
Y3071	*h⁺ ssl3-Pk9-kanMX6*
Y3127	*h⁻ ura4-D18 rad21-3eGFP-kanMX6 mis4-Pk9-kanMX6*
Y3169	*h⁺ leu1-32 cdc25-22 ssl3-Pk9-kanMX6 SV40p-GFP-atb2-LEU2*
Y3250	*h90 leu1-32 cdc25-22 cnd2-Pk9-kanMX6 SV40p-GFP-atb2-LEU2*
Y3272	*h⁻ leu1-32 ura4-D18 cdc25-22 rad21-Pk9-kanMX6 SV40p-GFP-atb2-LEU2 swi6::ura4⁺*
Y3298	*h90 leu1-32 ura4-D18 his3-D1 lys1 ade6-M210 mis4-Pk9-kanMX6 mis6-GFP-LEU2*
Y3300	*h90 leu1-32 ura4-D18 rad21-Pk9-kanMX6 mis6-GFP-LEU2*
Y3302	*h90 leu1-32 ura4-D18 cnd2-Pk9-kanMX6 mis6-GFP-LEU2*
Y3303	*h90 leu1-32 his3-D1 smc2-Pk9-kanMX6 mis6-GFP-LEU2*
Y3350	*h90 leu1-32 mis4-Pk9-kanMX6 fhl1-GFP-hygMX6*
Y3351	*h90 leu1-32 mis4-Pk9-kanMX6 sfc3-GFP-hygMX6*
Y3359	*h90 leu1-32 sfc6-Pk9-kanMX6*
Y3384	*h90 leu1-32 mis4-GFP-hygMX6 cnd2-Pk9-kanMX6*
Y3385	*h⁻ leu1-32 mis4-GFP-hygMX6 ssl3-Pk9-kanMX6*

Y3403	*h^{90} leu1-32 fhl1-Pk$_9$-kanMX6*
Y3470	*h^- ura4-D18 ade6-210 mis4-367 rad21-HA$_3$-kanMX6*
Y3493	*h^- ura4-D18 ade6-210 mis4-367eso1-H17 rad21-HA$_3$-kanMX6*
Y3586	*h^- leu1-32 cdc25-22 rad21-Pk$_9$-kanMX6 SV40p-GFP-atb2-LEU2 ark1-as3-hygMX6*
Y3650	*h^- leu1-32 ura4-D18 ade6-M210 mis4-Pk$_9$-kanMX6 SPBTRNAGLY.05D SPBTRNAARG.04D*
Y3724	*h^{90} leu1-32 ura4-D18 cdc25-22 rad21-Pk$_9$-kanMX6 SPBTRNAGLY.05D SPBTRNAARG.04D*
Y3785	*h^+ leu1-32 ura4-D18 cdc25-22 rad21-Pk$_9$-kanMX6 swi6-GFP-kanMX6 SV40p-GFP-atb2-LEU2*
Y3786	*h^+ leu1-32 ark1-as3-hygMX6 cdc25-22 rad21-Pk$_9$-kanMX6 swi6-GFP-kanMX6 SV40p-GFP-atb2-LEU2*

The strain numbers listed in the left column refer to the respective entry numbers in the Uhlmann Lab strain database.

SV40p represents the constitutive SV40 promoter. The following constructs and mutations have previously been described: *mis4-367* and *ssl3-29* (Bernard et al, 2006), *eso1-H17* (Tanaka et al, 2000), *nda3-KM311* (Hiraoka et al, 1984; Toda et al, 1983), *ars1-ssl3-29ts-LEU2* and *pREP2res1* (Bernard et al, 2008), *SV40p-GFP-atb2-LEU2* (Pardo & Nurse, 2005), *ark1-as3* (Hauf et al, 2007), *cdc10-129* (Nurse et al, 1976) and *cdc25-22* (Gould & Nurse, 1989). The *mis6-GFP-LEU2* strain was a kind gift from Kazu Tomita.

3.7 Vector list

Table 3.11 List of DNA vectors used in this study

Number	Name	Description	Origin
626	pWJ1077	Plasmid for PCR-based gene disruption. *K. lactis* URA3 flanked by 2 repeats (URA3 can be popped-out on 5-FOA)	(Reid et al, 2002)
694	pUC19-Pk_9	1-step C-terminal Pk_9 tagging vector (kanamycin resistance marker)	Wolfgang Zachariae
-	pFA6a-3HA-kanMX6	1-step C-terminal HA_3 tagging vector (kanamycin resistance marker)	(Bahler et al, 1998)
-	-	1-step C-terminal $eGFP_3$ tagging vector (kanamycin resistance marker)	John McIntyre
-	pFA6a-GFP(S65T)-kanMX6	1-step C-terminal GFP tagging vector (kanamycin resistance marker)	(Bahler et al, 1998)
-	KS-ura4	1-step gene disruption vector (*ura4 pombe* marker)	(Bahler et al, 1998)

The vector numbers listed in the left column refer to the respective entry numbers in the Uhlmann Lab DNA database.

3.8 Antibody lists

Table 3.12 Primary antibodies used in this study

				Dilution/amount		
Epitope	**Host**	**Catalog number, Description**	**Manufacturer**	**WB***	**CS***	**ChIP***
V5-´tag (Pk)	mouse	MCA1360, clone SV5-Pk1, purified IgG (1 mg/ml)	Serotec	1:5,000	1:500 - 1:1,000	7 µg
HA	mouse	MMS-101P, clone 16B12, purified IgG1 (1mg/ml)	Covance	1:5,000	1:500 - 1:1,000	20 µg
GFP	rabbit	TP401, polyclonal, purified IgG (1 mg/ml)	AMS Biotech-nology	1:3,000	1:1,000	-
PSTAIRE	rabbit	sc-53, polyclonal, purified IgG (0.2 mg/ml)	Santa Cruz	1:500	-	-
Histone H3	rabbit	ab1791, poly-clonal, purified IgG (0.5 mg/ml)	Abcam	1:5,000	-	-

Table 3.13 Secondary antibodies used in this study

Antigen	**Host**	**Description**	**Manufacturer**	**WB***	**CS***
rabbit IgG	donkey	HRP-coupled ab	Amersham	1:5,000	-
mouse IgG	donkey	HRP-coupled ab	Amersham	1:5,000	-
rabbit IgG	goat	Alexa Fluor AF488 ab	Molecular Probes	-	1:1,000
mouse IgG	goat	Alexa Fluor AF568 ab	Molecular Probes	-	1:300

* WB, Western blots; CS, chromosome spreads; ChIP, chromatin immunoprecipitation

4 Results

4.1 A complex cohesin pattern along fission yeast chromosomes

Several analyses have investigated cohesin's chromosomal binding pattern in different model organisms, but despite its highly conserved function no apparently common rule has emerged. Recent studies along mammalian chromosomes show that cohesin associates with CTCF, a zinc-finger protein required for transcriptional insulation (Parelho et al, 2008; Rubio et al, 2008; Stedman et al, 2008; Wendt et al, 2008). Although CTCF is conserved in the fruit fly, cohesin exhibits a different binding pattern, associating with highly transcribed genes throughout the non-repetitive genome (Misulovin et al, 2008). This is in contrast to budding yeast, where cohesin hardly overlaps with open reading frames (ORFs) but almost exclusively binds to convergent sites (Glynn et al, 2004; Lengronne et al, 2004). Preliminary studies also found cohesin to locate between convergently transcribed genes along fission yeast chromosomes 2 and 3 (Lengronne et al, 2004). At fission yeast centromeres, however, Swi6 (HP1 in higher eukaryotes) is essential for cohesin recruitment (Bernard et al, 2001; Nonaka et al, 2002). A recent ChIP study of several chromosomal loci suggests that Swi6 might also recruit cohesin to convergent sites along fission yeast chromosome arms (Gullerova & Proudfoot, 2008).

4.1.1 Cohesin binds to an ordered subset of convergent sites

While cohesin binding to budding yeast chromosomes has been well characterised (Glynn et al, 2004; Lengronne et al, 2004), a thorough analysis of the binding pattern in fission yeast is lacking. To characterise the binding pattern, we have hybridised cohesin chromatin immunoprecipitates to high-density oligonucleotide microarrays, covering fission yeast chromosomes 2 and 3 (Katou et al, 2003). Using these arrays, we retrieved a refined and highly reproducible binding pattern, using three different cohesin subunits (Rad21, Psc3 and Pds5) as well as the same subunit tagged with two different epitopes (Rad21-Pk_9 and -HA_3) (Figure 4.1 and Appendix). The binding patterns were indistinguishable between exponentially growing cell populations and cells arrested in G2 using the temperature-sensitive *cdc25-22* allele.

Using a peak-picking algorithm (3.5.1 and Appendix 7.1), we identified 228 binding sites along chromosome 2, of which the majority (214 peaks, 94 %) overlapped with convergent sites along chromosome arms. This indicates a conserved cohesin binding mechanism between budding and fission yeast.

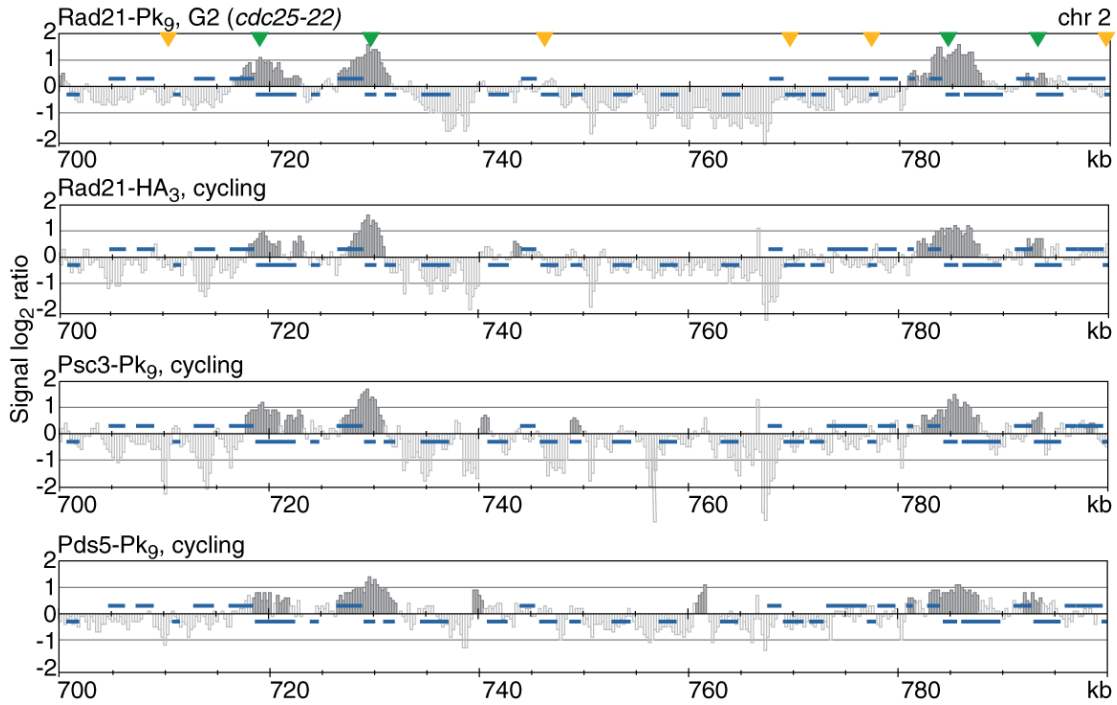

Figure 4.1 A large fraction of convergent sites is not bound by cohesin.
Chromatin immunoprecipitation (ChIP) against three different cohesin subunits of the cohesin complex, fused to two different epitope tags (Rad21-Pk_9, Rad21-HA_3, Psc3-Pk_9 and Pds5-Pk_9), yielded a reproducible binding pattern. Cells of strain Y2699 (Rad21-Pk_9, *cdc25-22*) were arrested in G2 by shifting to the restrictive temperature of 36.5°C for 6 hours. Cultures of the strain Y2197 (Rad21-HA_3), Y2447 (Psc3-Pk_9) and Y2828 (Pds5-Pk_9) were grown exponentially and, due to a short G1 phase in fission yeast, represent largely G2 cells (Alfa et al, 1993). Cells were processed for chromatin immunoprecipitation against the Pk and HA epitope-tagged cohesin subunits. Enrichment of DNA fragments in the immunoprecipitate relative to a whole genome DNA sample is shown along a 100 kb region of the left arm of chromosome 2. Each bar represents the average of 11 oligonucleotide probes within adjacent 250 bp windows. The y-axis scale is $\log_2$. Dark grey signals represent significant binding as described (Katou et al, 2003). Blue bars above and below the midline represent open reading frames (ORFs) transcribed from left to right and opposite, respectively. Green and orange arrowheads mark convergent sites that are bound or not bound by cohesin, respectively.

However, unlike in budding yeast where cohesin is found at almost every convergent site (Glynn et al, 2004; Lengronne et al, 2004), only 52 % of all convergent sites (263 of 508) were associated with cohesin along fission yeast chromosome 2 (Figure 4.2). In addition, we detected 14 cohesin peaks away from convergent sites which are characterised in paragraph 4.1.6.3.

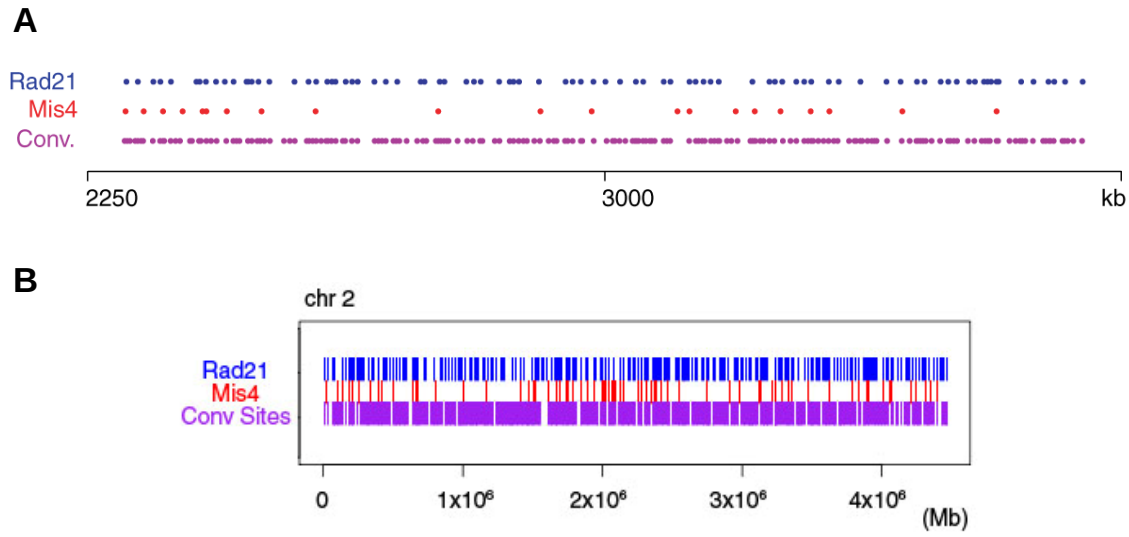

Figure 4.2 Overlay of cohesin with Mis4 and convergent sites
(**A**) The location of cohesin peaks (blue), assigned as described in Appendix 7.1, along 1.5 Mb of chromosome 2 is compared to the binding sites of the cohesin loader Mis4/Ssl3 (red; compare Figure 4.8) and the distribution of convergent sites (purple). (**B**) Entire chromosome view of cohesin association (blue), Mis4 association (red) and convergent sites (purple).

Sister chromatid cohesion along chromosome arms facilitates DNA repair of double strand breaks (DSBs) by homologous recombination (HR) (Sjögren & Nasmyth, 2001). Although no studies have directly addressed whether the distance to cohesion sites influences the efficiency of DNA repair, it is conceivable that frequent cohesion sites may help the process of HR.

We calculated a median distance of 16.5 kb between two neighbouring cohesin peaks. To test whether there was an organising principle that would ensure chromosomal cohesion sites at frequent intervals we used a bootstrapping approach to generate 10,000 random cohesin binding patterns along chromosome 2 (3.5.2). As most cohesin peaks locate to convergent sites, we distributed the 228 assigned cohesin peaks randomly among all available convergent sites. The average median distance between two neighbouring cohesin peaks calculated from the 10,000 randomised cohesin patterns was 14.5 kb, comparable to the 16.5 kb in the observed cohesin pattern. More strikingly, the maximal distances between neighbouring cohesin peaks derived from the random distributions ranged from 64.9 to 230.4 kb, on average 104.6 kb, almost twice as high as the 60.9 kb distance between two cohesin peaks at convergent sites in the observed pattern (Figure 4.3). This suggests that a mechanism exists that ensures the even distribution of cohesin binding sites along chromosome arms ($p < 0.0001$).

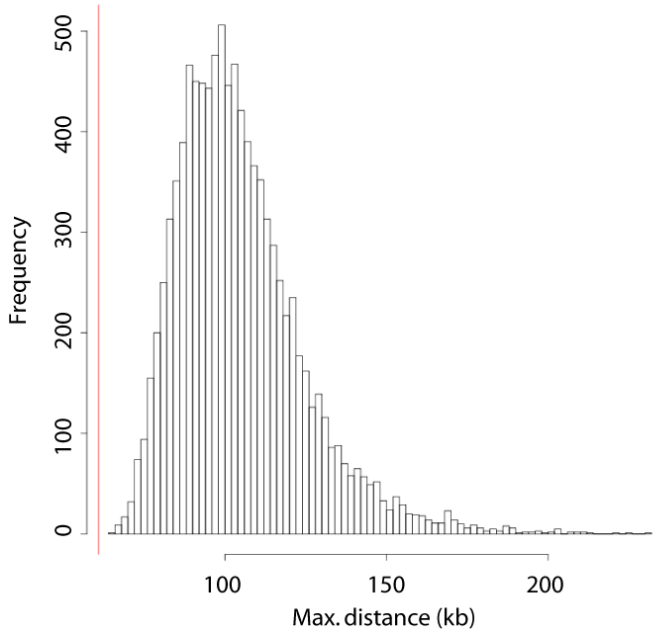

Figure 4.3 Maximal distance analysis of neighbouring cohesin peaks
10,000 random cohesin patterns along fission yeast chromosome 2 were created, using a bootstrapping approach. Number and widths of cohesin peaks were adopted from the observed binding pattern, as assigned in Appendix 7.1. Cohesin peaks were randomly distributed among all available convergent sites. The red line indicates the maximal distance between cohesin peaks at convergent sites in the observed cohesin pattern.

4.1.2 Non-random ORF arrangement along fission yeast chromosomes

We next wanted to test whether the sequence of open reading frames (ORFs) along chromosomes, which determines the pattern of convergent sites, and with that the distribution of possible cohesin binding sites, was in any way ordered to create a non-random pattern of convergent sites. A previous analysis of ORF orientations in the budding yeast genome found that the actual pattern was consistent with a random distribution (Lengronne et al, 2004). Indeed, we found that the succession of right- and left-facing genes was not random but that any gene was more likely to be followed by one in the opposite direction (54.13 %) rather than in the same direction (45.87 %, Table 4.1).

Table 4.1 ORF arrangement in the fission yeast genome

ORFs	% observed	No observed	% expected	No expected	Obs. vs exp.
Total	100,00	5189	100	5189,00	0
Convergent	27,06	1404	25	1297,25	107
Divergent	27,08	1405	25	1297,25	108
Parallel	45,87	2380	50	2594,50	-215

This suggests that a mechanism exists that reduces the occurance of parallel gene runs along fission yeast chromosomes and that creates an increased number of convergent sites (107 more than expected, Table 4.1). This leads to more potential binding sites for cohesin and raises the possibility that the limited maximal distance between neighbouring cohesin sites might, at least partially, be a consequence of the non-random gene order.

4.1.3 Expression levels influence cohesin's binding pattern

Although the non-random gene order might influence the cohesin binding pattern, it cannot explain why cohesin can locate to places away from convergent sites or why only approximately half of all available convergent sites are bound by cohesin.

To understand why only some but not all convergent sites were bound by cohesin we first wanted to test whether, like in budding yeast (Glynn et al, 2004; Lengronne et al, 2004), cohesin in fission yeast also responds to Pol II transcription by downstream translocation. As an example we analysed the convergent site between the *rad21* and the *pof3* gene. In cells arrested in G2, using the temperature-sensitive *cdc25-22* allele, *rad21* is known to be transcribed at very low levels (Birkenbihl & Subramani, 1995). In these cells, only a small cohesin peak could be detected on top of the *rad21* gene (Figure 4.4A). In contrast, in G1 cells, arrested using the *cdc10-129* mutant, *rad21* is strongly transcribed (Birkenbihl & Subramani, 1995), and no cohesin could be detected on the gene but an increased peak downstream of the *rad21* was detected. This observation corresponds to downstream translocation of cohesin upon transcription (Figure 4.4A) and is consistent with a recent study of the *nmt1*/*gut2* locus under conditions when *nmt1* expression is induced in the absence of thiamine (Gullerova & Proudfoot, 2008). Furthermore, the increased peak size of cohesin as a result of *rad21* expression indicates that transcription promotes cohesin accumulation at convergent sites and therefore contributes to the distribution of cohesin among these areas.

We next wanted to test whether the strength of transcription generally correlates with cohesin positioning among convergent sites. As an indicator for transcriptional activity we used the transcript abundance measured under growth conditions similar to the ones in our experiments (Lackner et al, 2007). Wilcoxon signed ranks testing revealed that convergent gene pairs surrounding cohesin binding sites were indeed significantly more strongly transcribed than convergent genes lacking cohesin (2325 vs 1848, respectively; p-value = 0.011; Figure 4.4B).

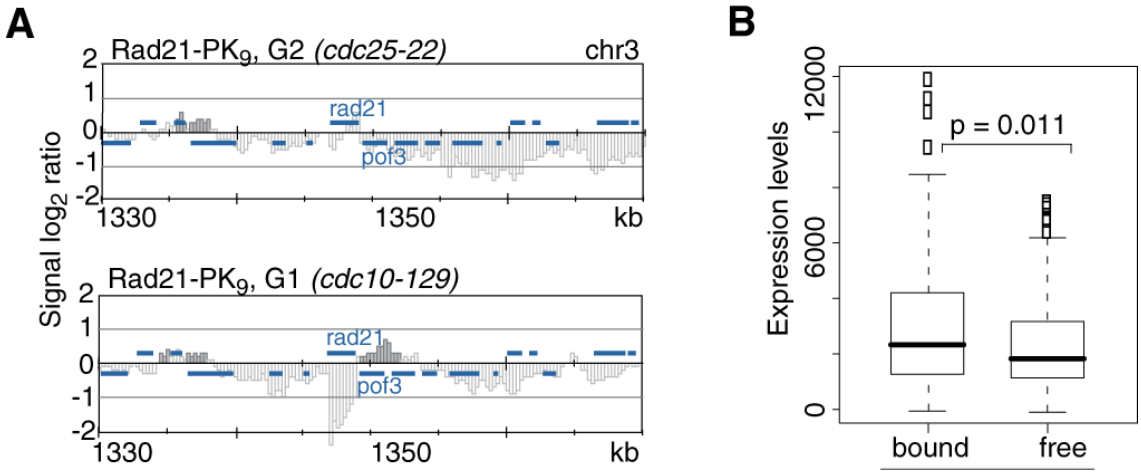

Figure 4.4 Expression levels contribute to cohesin's binding pattern.
(**A**) Cohesin corresponds to Pol II transcription by downstream translocation. Strain Y2863 (Rad21-Pk$_9$, *cdc10-129*) was arrested in G1 by shifting the culture for 4 hours to 36.5°C, the restrictive temperature of the *cdc10-129* allele. A population of Y2699 (Rad21-Pk$_9$, *cdc25-22*) cells was arrested in G2 by a 6-hour temperature shift to 36.5°C, a restrictive temperature for the *cdc25-22* mutant. A 40 kb region of the left arm of chromosome 2 is shown. (**B**) Distribution of expression levels of cohesin-bound and cohesin-free convergent genes. Boxes indicate boundaries of the 25th to the 75th percentile. The bold black line inside the boxes represents the median of the data. Whiskers reach 1.5 times the interquartile range. Outliers are marked as rectangles. The p-value was obtained by a Wilcoxon signed ranks test (Wilcox).

We also compared the observed cohesin binding pattern during the mitotic cell cycle with its meiotic counterpart, when the Rad21 subunit of cohesin is largely replaced by its meiotic paralog Rec8 (Ding et al, 2006; Kitajima et al, 2003). Interestingly, during meiosis cohesin peaks appear more evenly distributed among an overall higher fraction of convergent sites (Figure 4.5). Of all available 508 convergent sites on chromosome 2, 346 (68 %) were bound by cohesin in meiosis compared to 263 (52 %) in mitosis. This difference could be the consequence of a changed transcriptional profile during meiosis (Mata et al, 2002) or could be attributed to a distinctive chromosome architecture, e.g. a specific requirement of cohesin for homolog pairing or recombination during meiotic prophase.

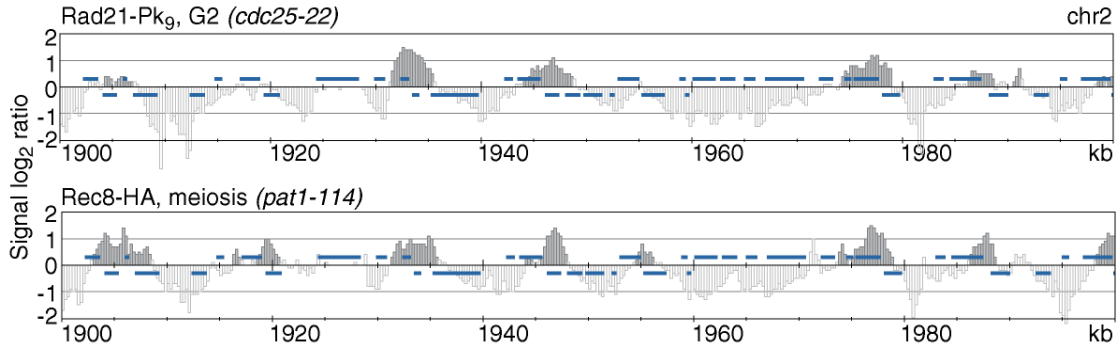

Figure 4.5 Different cohesin patterns in mitosis and meiosis
Strain Y2699 was arrested in G2, using the *cdc25-22* temperature-sensitive mutant. ChIP was performed against the cohesin subunit Rad21-Pk$_9$ (upper panel). The lower panel shows the binding pattern of the meiotic cohesin subunit Rec8-HA in *pat1-114* synchronized meiosis after the temperature was shifted up to 34°C for 3 hours. Rec8-HA ChIP on chip data were retrieved from the Gene Expression Omnibus Database (GEO) under accession number GSE5284 (Ding et al, 2006). A 100 kb region of the right arm of chromosome 2 is shown.

Taken together, these results suggest that the strength of transcription plays an important role in defining cohesin's binding pattern among convergent sites along the entire fission yeast chromosome 2.

4.1.4 Gene arrangement can influence cohesin's binding pattern

During our analysis we also noticed that convergent sites surrounded by more than one convergent gene on both sides seemed more likely to be bound by cohesin. To test this, we grouped all convergent sites into two classes. Class 1 contained all convergent sites with only one convergent gene on one or on both sides, and class 2 comprised all convergent sites with at least two convergent genes on both sides (Figure 4.6). Even though class 2 convergent sites make up only 18.9 % of all convergent sites along chromosome 2 (96 of 508), 74 % were bound by cohesin, compared to only 47 % of all class 1 convergent sites (Figure 4.6). This suggests that, in addition to the levels of transcription, the number of genes pointing towards a convergent site influence the binding pattern of cohesin along fission yeast chromosomes.

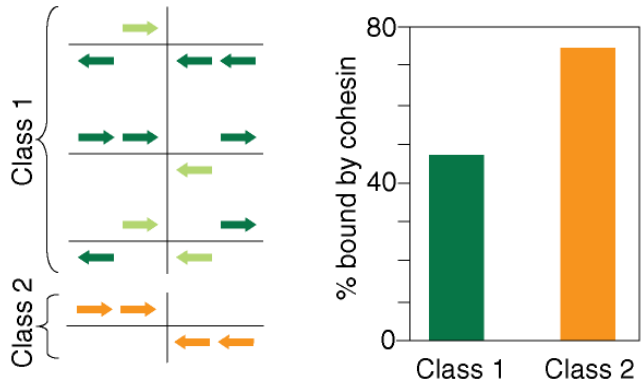

Figure 4.6 The convergent site gene arrangement contributes to the cohesin pattern.
A schematic of the two different classes of convergent sites is depicted on the left with arrows indicating the direction of transcription. Class 1 represents all convergent sites with only one convergent gene on one or on both sides (light green arrows, 18.1 % of all convergent sites on chromosome 2). Class 2 includes all convergent sites with at least two convergent genes on both sides (orange arrows, 81.9 % of all convergent sites on chromosome 2). Percentages of class 1 and class 2 convergent sites bound by cohesin along chromosome 2 are depicted on the right.

4.1.5 The role of Swi6 in defining cohesin's binding pattern

In the course of our study, evidence emerged that not only convergent transcription itself but an alternative mechanism might place cohesin to convergent sites in fission yeast (1.3.3.1.4; Gullerova & Proudfoot, 2008). The authors identify transcriptional termination sites past the 3' ends of several convergently transcribed genes which lead to read-through transcripts and dsRNA formation. They go on to show that this activates the RNAi machinery and consequently recruits Swi6/HP1 to convergent sites. Since Swi6/HP1 is known to recruit cohesin to heterochromatin, possibly through direct physical interaction with the Psc3 subunit of cohesin (Nonaka et al, 2002), the authors argue that Swi6/HP1 might also be involved in recruiting cohesin to convergent sites. As their analysis is based only on a few loci, including the *nmt2/avn2* locus on the right arm of chromosome 2, the general importance of this mechanism is not known. Using the *cdc25-22* allele to arrest cells in G2, we grew wild type and *swi6Δ* cells in synthetic medium deprived of thiamine, when *nmt2* is transcribed, and compared the two cohesin binding patterns. In contrast to the prediction, the cohesin binding pattern along chromosomes 2 and 3, including the *nmt2/avn2* convergent site, remained unchanged even when Swi6 was deleted (Figure 4.7). Only at centromeres were the levels of cohesin reduced, as expected from previous studies (Figure 4.7; Bernard et al, 2001; Nonaka et al, 2002). Therefore, in contrast to the results from Gullerova et al, our results suggest that Swi6 does not play a role in defining cohesin's chromosomal distribution among convergent sites.

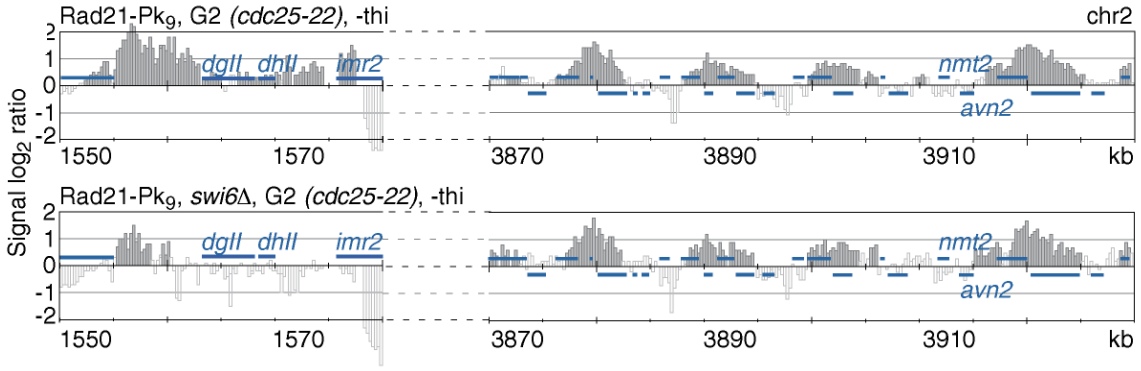

Figure 4.7 Swi6-independent cohesin patterning along chromosome arms
Strains Y2699 (Rad21-Pk$_9$, *cdc25-22*, *swi6* wild type) and Y3272 (Rad21-Pk$_9$, *cdc25-22*, *swi6Δ*) were grown in minimal EMM medium in the absence of thiamine, when *nmt2* is transcribed, and arrested in G2, using the *cdc25-22* mutant as described in 3.1.3.3. A 30 kb region of centromere 2, containing one outer *dgII* and *dhII* repeat and one inner repeat (*imr2*), is shown on the left. A 60 kb region of the right arm of chromosome 2 is depicted on the right, containing the *nmt2/avn2* convergent site studied by Gullerova et al, 2008.

4.1.6 The relationship between cohesin and its loading factor Mis4/Ssl3

4.1.6.1 Mis4/Ssl3 overlaps with tRNA and RP genes

Having discovered that cohesin binding sites are defined in their position by transcription and gene arrangement, we next wanted to test whether the sites of cohesin loading, which in budding yeast were shown to be distinct from convergent sites (Lengronne et al, 2004), contribute to cohesin's distribution among an ordered subset of convergent sites. To correlate the cohesin pattern to its likely sites of chromosomal loading, we hybridised chromatin immunoprecipitates of the cohesin loader subunits Mis4 and Ssl3 to oligonucleotide tiling arrays, covering fission yeast chromosomes 2 and 3. As expected, the two loading factor subunits showed a largely overlapping binding pattern (Figure 4.8; Appendix 7.2). Using a peak-picking algorithm and subtracting several background peaks that also appeared in an untagged strain (Appendix 7.2), we assigned 72 Mis4-specific peaks along the entire length of chromosome 2. The Mis4/Ssl3 pattern showed a largely distinct binding pattern to that of cohesin. Mis4 peaks were generally much sharper than those of cohesin (3.35 kb average width compared to 6.46 kb, respectively), and only 41.7 % overlapped with convergent sites. While the peak shape and the general binding pattern of Mis4/Ssl3 appeared different from the cohesin association pattern, 78 % of the Mis4/Ssl3 sites overlapped with cohesin along chromosome 2. In the search of an underlying determinant of Mis4/Ssl3 binding sites, we detected a strik-

ing correlation of the cohesin loader with tRNA and ribosomal protein genes, which is reminiscent of recent results from our laboratory, regarding the budding yeast cohesin loader Scc2/Scc4 (Figure 4.8 and Appendix 7.2; D'Ambrosio et al, 2008). Of the 72 Mis4 peaks identified, 34 were assigned within a 5 kb reach of either a tRNA or a ribosomal protein gene (Figure 4.9). Upon visual inspection, virtually all 38 tRNA genes and 42 ribosomal protein genes, *rpl* and *rps*, along the arms of chromosome 2 were associated with Mis4/Ssl3, even though some of the peaks fell below the detection threshold of our peak-picking algorithm. The co-localisation of the cohesin loader Mis4/Ssl3 with tRNA genes was also apparent at the extended tRNA gene clusters that flank fission yeast centromeres which were excluded from our analysis (Appendix 7.2).

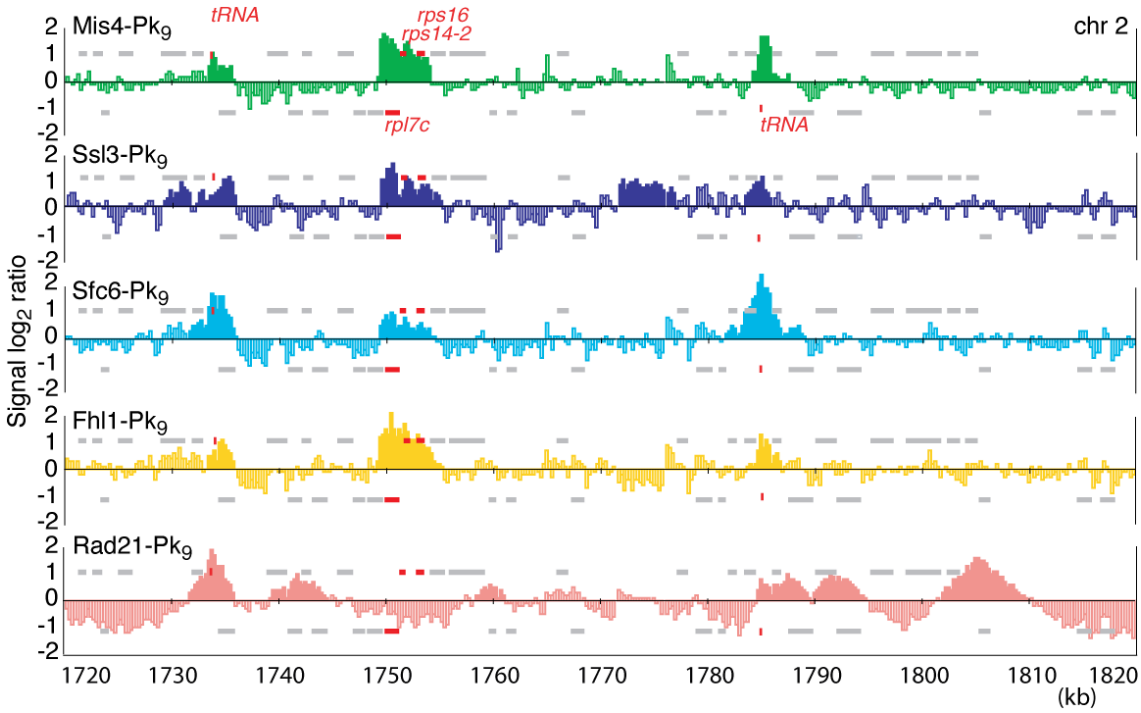

Figure 4.8 Mis4/Ssl3 co-localises with TFIIIC and Fhl1 at tRNA and RP genes.
Strains Y2468 (Mis4-Pk$_9$), Y3071 (Ssl3-Pk$_9$), Y3359 (Sfc6-Pk$_9$) and Y3403 (Fhl1-Pk$_9$) were exponentially grown in rich YE4S medium. ChIP was performed against the Pk-tagged proteins. A 100 kb region of the right arm of chromosome 2 is depicted. For comparison, the same 100 kb region of a G2 map of Rad21 (Figure 4.1) is shown. tRNA and ribosomal protein (RP) genes are highlighted in red.

Mis4/Ssl3 binding sites overlapped with the Pol III transcription factor TFIIIC subunit Sfc6 at tRNA genes, while they coincided with the forkhead domain containing protein Fhl1 at ribosomal protein genes (Figure 4.8). Fhl1 is a potential fission yeast ortholog of the budding yeast transcription factor Fhl1 that was shown to control the expression of ribosomal protein genes (Schawalder et al, 2004; Wade et al, 2004). As expected, Sfc6 mainly bound to tRNA genes (Figure 4.8; Appendix 7.4) and Fhl1 could predominantly

be detected at ribosomal protein genes (Figure 4.8; Appendix 7.5). Surprisingly, we found Sfc6 also at ribosomal protein genes and Fhl1 at tRNA genes, though to a lesser extent (Figure 4.8, Appendices 7.4 and 7.5). Whether this indicates that TFIIIC not only controls the expression of tRNA but also that of ribosomal protein genes and likewise, that Fhl1 not only regulates ribosomal protein gene expression but also the transcription of tRNA genes, remains unknown. The weaker association levels could also point towards an indirect association mechanism which might be mediated by physical DNA interactions in *trans* between ribosomal protein genes and tRNA loci within the nuclear space (see Discussion 5.2.2).

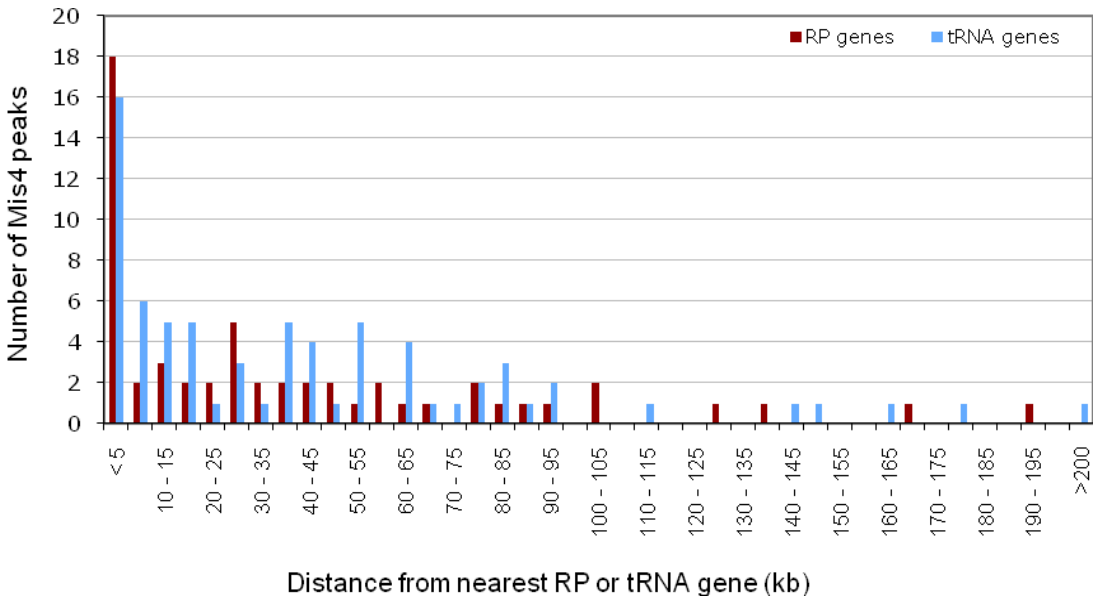

Figure 4.9 Proximity of Mis4 sites to tRNA and RP genes on chromosome 2
The distances of Mis4 peaks, as assigned in Appendix 7.2, to their nearest respective tRNA and ribosomal protein (RP) gene are shown. 16 of the 72 Mis4 peaks are within a 5 kb distance of a tRNA gene. Of the remaining 56 peaks, 18 are within 5 kb reach of a ribosomal protein gene (*rpl* or *rps*). The x-axis is split into 5 kb bins.

Using a complementary approach, immunostaining of chromosome spreads confirmed our chromatin immunoprecipitation studies. As expected, the obtained staining patterns yielded an overlapping pattern of Mis4 with Ssl3, TFIIIC and Fhl1, whereas distinct patterns of Mis4 and cohesin were observed (Figure 4.10).

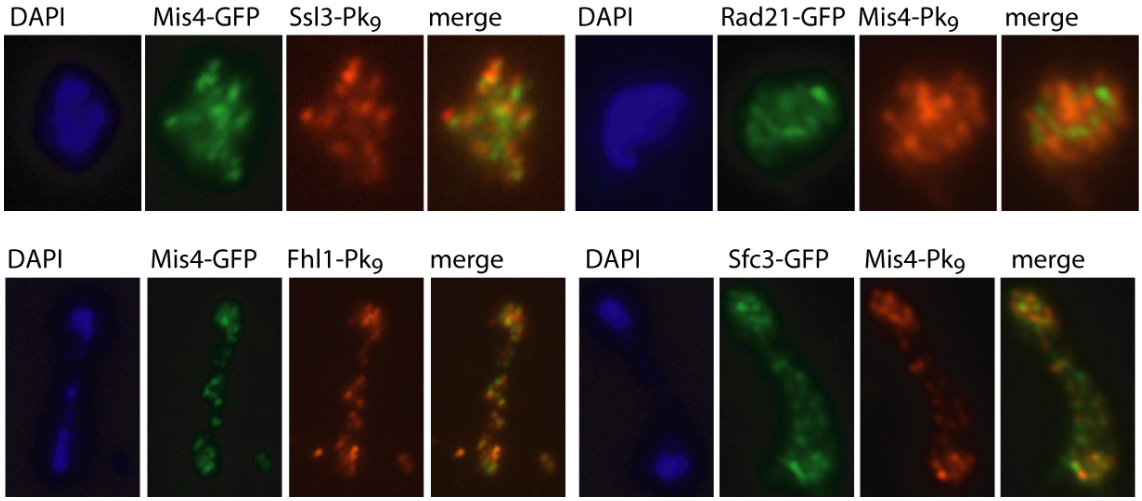

Figure 4.10 Cytological co-localisation of Mis4/Ssl3 with Sfc3 and Fhl1
Chromosome spreads of exponentially growing cells of strains Y3385 (Mis4-GFP, Ssl3-Pk$_9$), Y3127 (Mis4-Pk$_9$, Rad21-3eGFP), Y3351 (Mis4-Pk$_9$, Sfc3-GFP) and Y3350 (Mis4-Pk$_9$, Fhl1-GFP) were immunostained with 1:700 dilutions of anti-Pk antibody (mouse monoclonal, MCA1360, Serotec) or 1:1,000 dilutions of anti-GFP antibody (rabbit polyclonal, affinity purified, clone TP401, AMS Biotechnology) to detect the Pk$_9$- and GFP-tagged proteins, respectively. Secondary detection was performed with goat anti-mouse Alexa Fluor AF568 (Molecular Probes) 1:300 and with goat anti-rabbit Alexa Fluor AF488 (Molecular Probes) 1:1,000, respectively. A considerably larger fraction of overlap (yellow regions in merge pictures) could be detected between Fhl1-Pk$_9$ and Mis4-GFP, Sfc3-GFP and Mis-Pk$_9$ and Ssl3-Pk$_9$ and Mis4-GFP when compared to Rad21-GFP and Mis4-Pk$_9$.

4.1.6.2 Mis4/Ssl3 coincides with other highly transcribed genes

tRNA and ribosomal protein genes are strongly transcribed by RNA Pol III and Pol II, respectively. Approximately half of the Mis4 association sites co-localise with tRNA and/or ribosomal protein genes. We wanted to test whether the remaining Mis4/Ssl3 binding sites were also characterised by high expression levels. Therefore, we determined all the genes that were covered by Mis4 peaks, excluding tRNA and ribosomal protein gene peaks and calculated the median expression level of these genes.The median was 1.8-fold above that of all other genes, excluding tRNA and ribosomal protein genes (Figure 4.11, p-value = 8.81×10^{-6}; (Lackner et al, 2007)). However, the genes ascribed to these Mis4 sites were 2.2-fold less expressed than the ribosomal protein genes *rpl* and *rps* (Figure 4.11, p-value = 2.43×10^{-12}). Importantly, not all highly transcribed genes are Mis4/Ssl3 association sites. At least 389 genes are expressed at levels higher than the median of all Mis4/Ssl3-bound genes, yet, they are not associated with the cohesin loader Mis4/Ssl3. This suggests that high expression itself is not a sufficient determinant of Mis4/Ssl3 binding to chromosomes. Rather, our results indicate that certain groups of highly transcribed genes may contain features, e.g. promoter elements or associated transcription factors that can form a cohesin loading site.

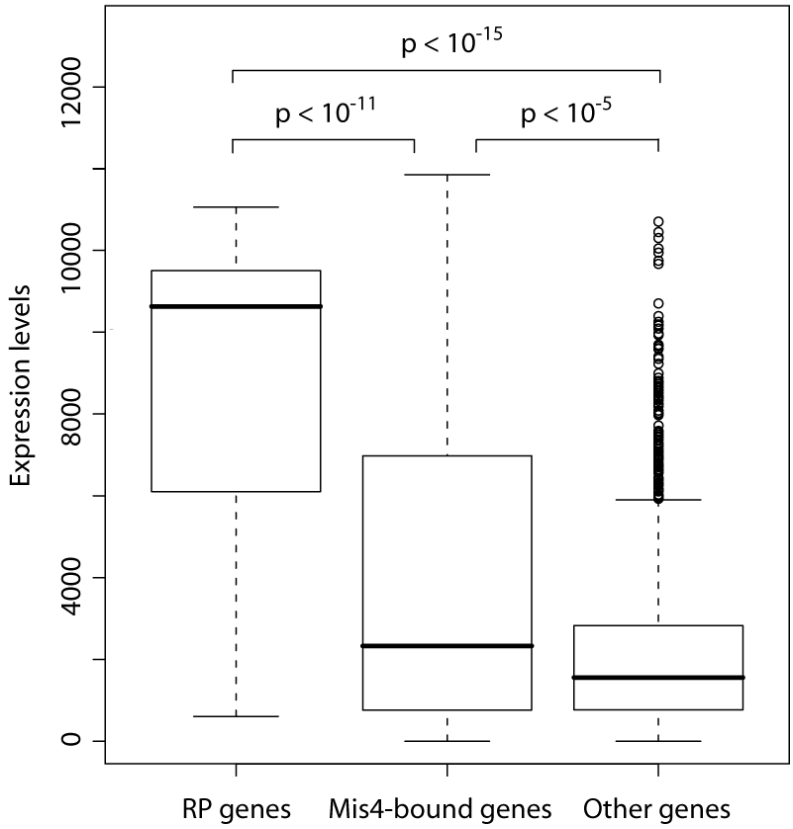

Figure 4.11 A link between expression and Mis4/Ssl3 association.
The expression levels of ribosomal protein (RP) genes, Mis4-bound genes (excluding tRNA and RP genes) and all other genes are compared. Boundaries of the boxes mark the 25th to 75th percentile surrounding the median (bold line). Whiskers extend to 1.5 times the interquartile range. Outliers are indicated as circles. P-values were obtained by Wilcoxon signed ranks testing.

4.1.6.3 An overlap of cohesin and its loader away from convergent sites

Having identified and characterised the binding sites of the cohesin loading complex we next wanted to analyse its relation with the cohesin distribution. As mentioned, of all 228 cohesin peaks, 14 did not overlap with convergent sites, of which 12 coincided with Mis4 (Table 4.2). Seven of them were located at tRNA genes, one at a ribosomal protein gene (see *rpl26* (red) in chapter 4.2.4.2, Figure 4.20 and Appendix 7.1), and the others bound to different sequences (Table 4.2, Figure 4.13, Appendices 7.1 and 7.2). In addition, 15 cohesin peaks that overlapped with convergent sites showed a 'shoulder' within the peak that overlapped with Mis4 and was clearly located away from the convergent site (e.g. tRNA gene between 1780 and 1790 kb in Figure 4.8, Appendices 7.1 and 7.2). Taken together, this suggests that at least some of cohesin's loading sites can function as more permanent cohesin binding sites. These observations are reminiscent of the correlation between *Drosophila* cohesin and its loader Nipped-B which were found to overlap with each other near strongly transcribed genes (Misulovin et al,

2008). In contrast, cohesin in budding yeast can only transiently be detected at its loading sites in G1 before it is rapidly translocated to its more permanent association sites between convergently transcribed genes (Lengronne et al, 2004). The above results indicate that cohesin loading sites themselves possess chromosomal features that can form more permanent cohesin binding sites. It is currently not known whether these loading sites also resemble cohesion sites, at which cohesin is stably bound to chromatin. Cohesin at these sites could alternatively reflect an intermediate of loading which might not establish sister chromatid cohesion before translocating to convergent sites.

Table 4.2 Non-convergent Rad21 peaks along chromosome 2

Peak no	Midpoint/bp	Bound tRNA	Bound RP gene	Mis4 overlap
1	246126	2	0	1
2	636626	1	0	1
3	1229376	0	0	1
4	1283126	0	0	-
5	1515876	0	1	1
6	1558126	12	0	1
7	1571876	0	0	1
8	1869876	0	0	-
9	1991251	1	0	1
10	3599001	0	0	1
11	3773376	2	0	1
12	3897876	1	0	1
13	3916876	0	0	1
14	4168501	1	0	1

4.1.6.4 Cohesin clusters around its loading sites

We next wanted to test whether the distribution of Mis4/Ssl3 binding sites also has an effect on the cohesin distribution among convergent sites. To do so, we compared the distances of cohesin-bound and cohesin-free convergent sites to their respective nearest Mis4/Ssl3 association site. Interestingly, our analysis revealed that the median of cohesin-bound convergent sites was on average almost twice as close to a cohesin loading site as the one of convergent sites lacking cohesin (3.90 to 7.38, respectively, p-value = 0.033, Figure 4.12). This suggests that apart from expression (4.1.3) and gene arrangement (4.1.4) also the loading site distribution contributes to determining the cohesin pattern among convergent sites.

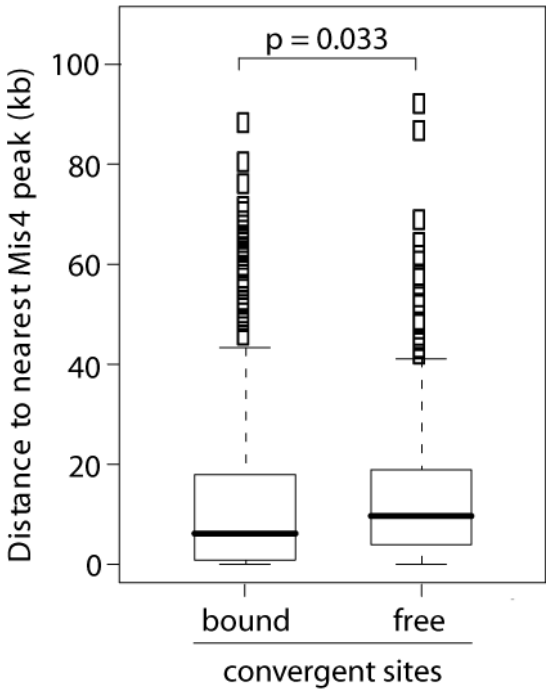

Figure 4.12 Mis4 influences cohesin's distribution among convergent sites. Boxes indicate boundaries of the 25th to the 75th percentile. The bold black line inside the boxes represents the median of the data. Error bars indicate the spread of the data. Outliers are marked as rectangles and are defined as values further away from the median than 1.5 times the width of the boxes. The p value was obtained by Wilcoxon signed rank testing.

4.1.6.5 The role of tRNA genes for the Mis4 and cohesin binding pattern

We next wanted to directly probe a possible interdependency between the distribution of cohesin and that of its loading factor Mis4/Ssl3. If the Mis4/Ssl3 loading sites define the neighbouring patterning of cohesin among convergent sites as suggested above, deletion of a loading site would be expected to change that pattern. To test this hypothesis, we deleted a 489 bp sequence, containing two neighbouring tRNA genes that form both a cohesin loader and a cohesin binding site (Figure 4.13). In response to the deletion, the cohesin loader Mis4/Ssl3 disappeared from this region as did cohesin, confirming the theory that the function of Mis4/Ssl3 as a cohesin loader had been removed from this region. However, deletion of the two tRNA genes had no significant effect on the neighbouring cohesin distribution among convergent sites (Figure 4.13). This could be due to several reasons. Even though no Mis4/Ssl3 could be detected at the region where the two tRNA genes had been deleted, weak Mis4 binding signals appeared on top of the two ORFs neighbouring the deletion site. Therefore, we cannot exclude that cohesin might still be loaded proximal to the initial loading site and that loading to these regions accounts for the cohesin signals at the neighbouring convergent sites. Furthermore, we

cannot exclude that cohesin loading by Mis4/Ssl3 is less well restricted to its chromosomal association peaks than the pattern suggests. Alternatively, neighbouring cohesin loading sites might compensate each other. We can currently not distinguish between these three possibilities.

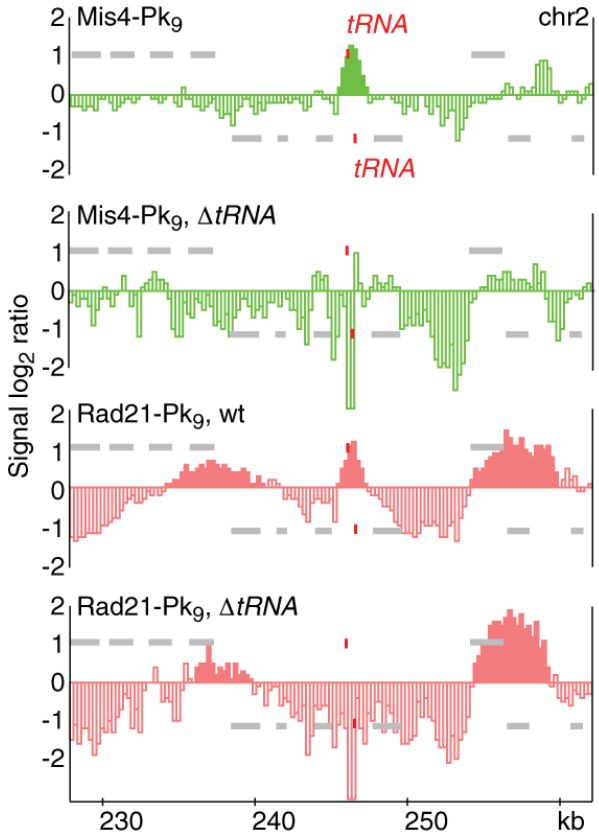

Figure 4.13 tRNA genes contribute to the binding patterns of Mis4 and cohesin.
Cultures of strain Y2468 (Mis4-Pk$_9$) and Y3650 (Mis4-Pk$_9$, *SPBTRNAGLY.05Δ, SPBTRNAARG.04Δ*) were grown exponentially, and ChIP was performed against the cohesin loading factor subunit Mis4-Pk$_9$. ChIPs of the cohesin subunit Rad21-Pk$_9$ were processed from cells of strains Y2699 (Rad21-Pk$_9$, *cdc25-22*) and Y3724 (Rad21-Pk$_9$, *cdc25-22*, *SPBTRNAGLY.05Δ, SPBTRNAARG.04Δ*) that were arrested in G2 according to 3.1.3.3. A 35 kb region surrounding the two tRNA genes on the left arm of chromosome 2 is shown with the tRNA genes marked in red.

4.1.7 Mis4/Ssl3 co-localises with condensin

Interestingly, we found a striking overlap of the cohesin loader Mis4/Ssl3 with the Cnd2 subunit of the cohesin-related condensin complex (Figure 4.14 and Appendix 7.3). Like cohesin, condensin belongs to the essential SMC subunit containing protein complexes and fulfils important roles related to chromosome condensation, structural stability of chromosomes and high-fidelity chromosome segregation in mitosis (1.4; Bhat et al, 1996; Hirano & Mitchison, 1994; Hudson et al, 2003; Ono et al, 2003; Saka et al, 1994;

Strunnikov et al, 1995). Our finding suggests that the recently reported hypothesis of cohesin and condensin loading to identical chromosomal sites is conserved between the two distantly related yeasts (D'Ambrosio et al, 2008).

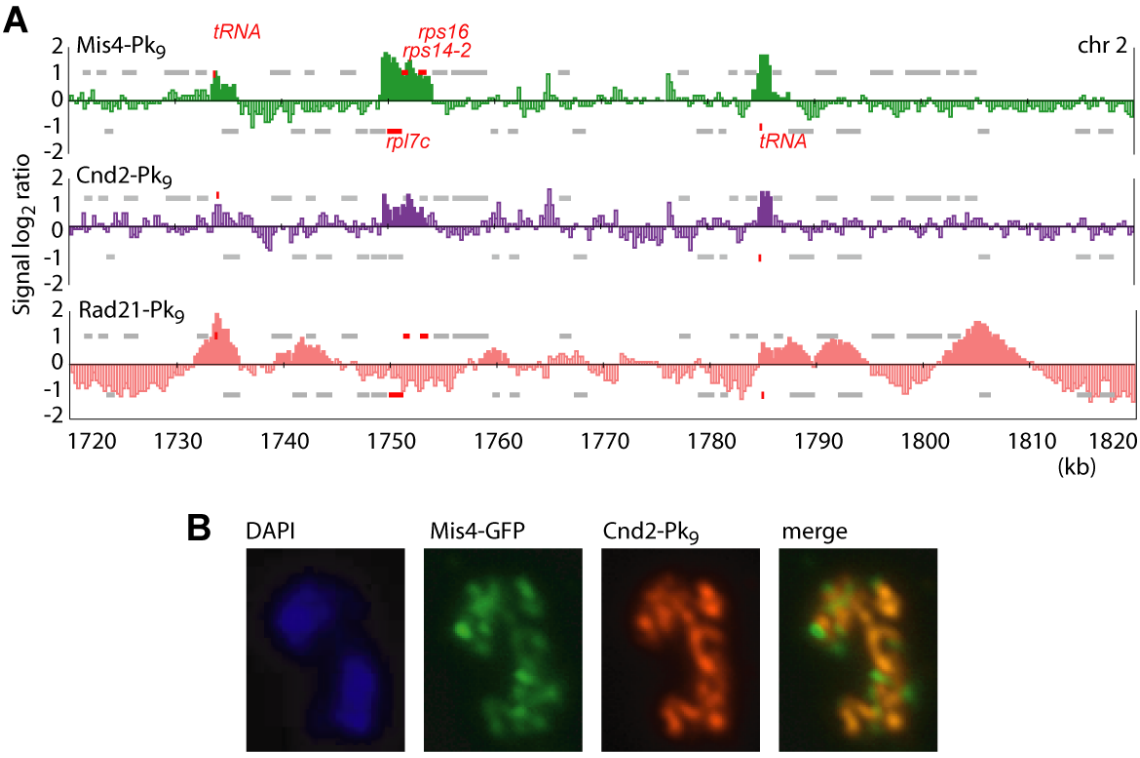

Figure 4.14 Mis4/Ssl3 shows a striking overlap with condensin.
(**A**) Co-localisation by chromatin immunoprecipitation. Cells of strain Y252 (Cnd2-Pk$_9$, *nda3-KM311*) were arrested in metaphase according to 3.1.3.4. ChIP was performed against the condensin subunit Cnd2-Pk$_9$ (purple). A 100 kb region of the right arm of chromosome 2 is depicted. For comparison the association patterns of Mis4-Pk$_9$ (green) and Rad21- Pk$_9$ (red), as obtained in 4.1.1 and 4.1.6.1, along the same region are shown. tRNA and ribosomal protein genes are highlighted in red. (**B**) Confirmation of co-localisation by cytology. Chromosome spreads of exponentially growing cells of strain Y3384 (Mis4-GFP, Cnd2-Pk$_9$) were stained to detect the Pk$_9$- and GFP-tagged proteins. Large areas appear yellow in the merge image indicating overlap of the two proteins in these regions.

4.2 Resolution of cohesion in mitosis

Having characterised various parameters that define cohesin's binding pattern in interphase we were curious to analyse if and how this binding pattern would be affected during mitosis when sister chromatid cohesion is lost.

4.2.1 Cohesin removal from fission yeast chromosomes in prophase

In higher eukaryotes, first signs of sister chromatid cohesion loss can be observed in prophase when the majority of cohesin along chromosome arms, but not from centromeres, is removed in a separase-independent manner (1.3.3.4; Losada et al, 1998; Sumara et al, 2000; Waizenegger et al, 2000). As it is thought that only a small part of fission yeast cohesin is cleaved by separase at anaphase-onset (Tomonaga et al, 2000), we wanted to test whether cohesin, like in higher eukaryotes, is in part already removed from chromosomes in prophase. To test this hypothesis, we compared the distribution of cohesin between chromatin-bound and soluble cellular fractions as cells entered mitosis. In an exponentially growing cell population, that, due to fission yeast's short G1 phase mainly contains G2 cells (Alfa et al, 1993), the majority of cohesin was detected in the chromatin-bound fraction (Figure 4.15). After these cells had been arrested in metaphase, using the *nda3-KM311* cold-sensitive β-tubulin-mutant, an increased level of cohesin could be detected in the soluble cellular fraction, while a substantial pool of cohesin remained chromatin-bound (Figure 4.15). This suggests that, like in higher eukaryotes, a small fraction of cohesin may be removed from chromosomes in prophase. However, the majority of cohesin remains chromatin-bound even when cells had entered metaphase.

4.2.2 Cohesin-cleavage and removal at anaphase-onset

We next wanted to investigate cohesin dynamics at later stages during mitosis. To follow cohesin through mitosis, we arrested cells in G2, using the *cdc25-22* temperature-sensitive allele, followed by a subsequent release of the culture into synchronous progression through mitosis at the permissive temperature of 25°C. As cells entered mitosis we again detected an increased pool of cohesin in the soluble fraction (10 minutes 25°C,

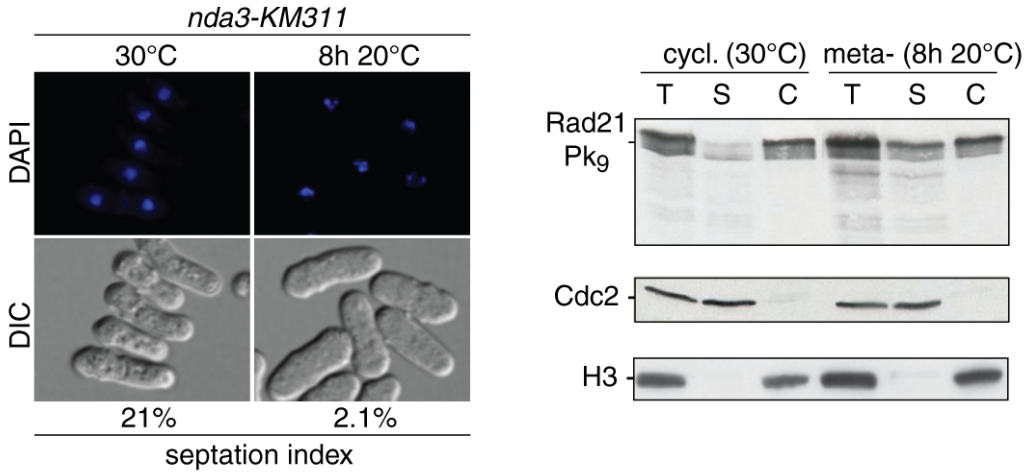

Figure 4.15 Cleavage-independent cohesin removal from chromosomes in prophase
Strain Y2703 (Rad21-Pk$_9$, *nda3-KM311*) was arrested in metaphase by shifting the culture for 8 hours to 20°C, the restrictive temperature of the *nda3-KM311* allele. Chromatin fractionation was performed before (30°C, mainly G2 cells) and after the arrest (8 hours 20°C, mainly metaphase cells). The arrest was monitored by DAPI staining of condensed chromosomes and by determining the septation index after calcofluor staining of the septa (left panel).The cohesin subunit Rad21-Pk$_9$ was detected by immunoblotting to compare its levels in the total cell extract (T), the soluble (S) and the chromatin (C) fractions. Detection of Cdc2 and Histone H3 served as controls for the soluble and the chromatin fractions, respectively (right panel).

Figure 4.16A), consistent with the results obtained from metaphase-arrested *nda3-KM311* cells (4.2.1; Figure 4.15) that indicated that some cohesin was removed from chromosomes in prophase. At anaphase-onset (20 minutes 25°C, Figure 4.16A) the C-terminal cleavage product of Rad21 could be detected, mainly in the soluble fraction. At the same time the chromatin-bound levels of cohesin decreased to approximately half of what they were in G2. As the Rad21 cleavage product is likely unstable in cells due to its degradation by the N-end rule pathway (Rao et al, 2001), it is difficult to estimate how much cohesin is actually cleaved in anaphase. As the cleavage product mainly appears in the soluble fraction, cohesin seems likely to be removed from chromosome upon cleavage. Therefore, considering the loss of cohesin from the chromatin-bound fraction, it appears likely that approximately half of the cohesin pool on chromosomes is cleaved, considerably more than previously anticipated (Tomonaga et al, 2000). As cells started to exit mitosis, cohesin accumulated again in the chromatin-bound fraction (30 - 50 minutes 25°C, Figure 4.16A). We could also detect cohesin loss from chromosomes on a single cell basis by immunostaining of spread chromosomes to visualise the cohesin subunit Rad21 together with the kinetochore marker Mis6. The decreased signal intensity of Rad21 is apparent in anaphase cells, marked by the two separate signals of Mis6 (Figure 4.16B). Rad21 stained the entire length of anaphase chromosomes, indicating that cohesin was uniformly reduced along entire chromosomes. The observation

that cohesin remains on chromosomes even in anaphase indicates that it cannot be involved in sister chromatid cohesion and therefore does not need to be cleaved and/or removed from chromosomes to initiate anaphase. This non-cohesive cohesin might have been loaded in G2 phase which takes up a considerable time period of the fission yeast cell cycle. In consistency with this, cohesin in budding yeast has been shown to be loaded onto chromosomes in G2 when usually no sister chromatid cohesion is established anymore (Lengronne et al, 2006; Uhlmann & Nasmyth, 1998). Therefore, it appears that at least two different populations of cohesin exist along chromosomes during anaphase, cohesin loaded before S phase that establishes sister chromatid cohesion and cohesin loaded after S phase, in G2, which does not link sister chromatids together. What distinguishes these two pools of cohesin on a molecular level is currently not known, but different post-translational modifications e.g. phosphorylation or acetylation might be involved.

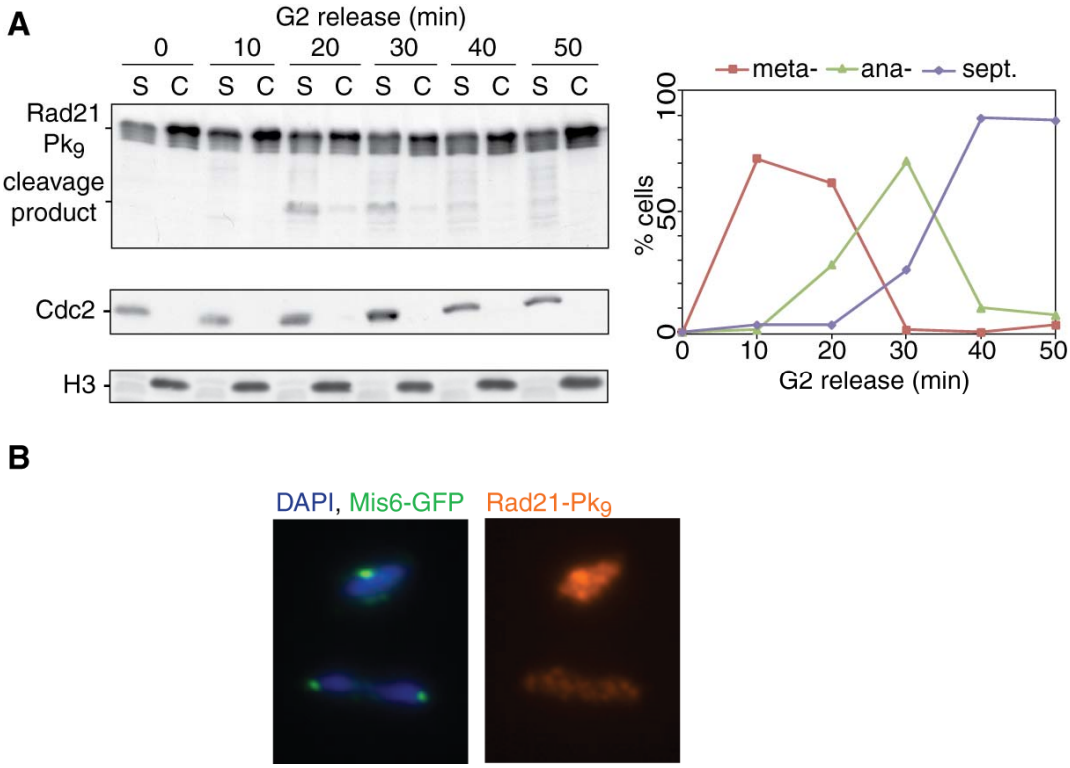

Figure 4.16 Cleavage and removal of a cohesin fraction at anaphase-onset
(**A**) Cells of strain Y2699 (Rad21-Pk$_9$, *cdc25-22*, GFP-Atb2) were arrested in G2 and released into synchronous progression through mitosis as described in 3.1.3.3. Chromatin fractionation was performed at the indicated time points, and soluble (S) and chromatin-bound fractions (C) were immunoblotted for Rad21-Pk$_9$. Detection of Cdc2 and Histone H3 served as soluble and chromatin loading controls, respectively. The synchrony of the arrest release experiment was monitored in methanol fixed cells by visualisation of the α-tubulin fusion protein GFP-Atb2. DNA was stained with DAPI, and septa were visualised with calcofluor. Cells containing spindles with non-separated DNA masses were counted as metaphase cells, cells with separating DNA masses as anaphase cells. Calcofluor staining was used to determine the septation index. (**B**) Cohesin is uniformly reduced along anaphase chromosomes. Chromosome spreads of exponentially growing Rad21-Pk$_9$ Mis6-GFP cells (Y3300) were stained against the Pk$_9$- and GFP-tagged proteins. The presence of two separate Mis6-GFP dots was used as a marker for anaphase cells.

4.2.3 Reciprocal regulation of Mis4/Ssl3 and condensin during mitosis

4.2.3.1 Removal of Mis4/Ssl3 from mitotic chromosomes

It has been observed that in vertebrates the cohesin loading complex dissociates from chromosomes as cells enter mitosis, while it remains constitutively chromosome-bound throughout the cell cycle in budding yeast (Ciosk et al, 2000; Gillespie & Hirano, 2004; Watrin et al, 2006). To follow the dynamics of the fission yeast loading factor Mis4/Ssl3 through mitosis we repeated the chromatin fractionation experiment of the *cdc25-22* G2 arrest and release experiment and analysed the subcellular distribution of Ssl3 during synchronous mitotic progression. In G2-arrested cells, the majority of Ssl3 was detected in the soluble pool while a smaller amount was found in the chromatin fraction (0 minutes 25°C, Figure 4.17A). Upon entry into mitosis as cells reached anaphase (10 - 30 minutes 25°C, Figure 4.17A), the Ssl3 levels in the chromatin fraction were slightly reduced but not completely abolished and increased again when cells started to exit mitosis (40 - 50 minutes 25°C, Figure 4.17A). Cytological staining of spread chromosomes confirmed reduced binding of the cohesin loader Mis4/Ssl3 in mitosis. Again, staining of the kinetochore marker Mis6 was used to identify mitotic cells (Figure 4.17B). Consistent with our chromatin fractionation results, no chromosome spreads were observed that had entirely lost the signal for the cohesin loader Mis4/Ssl3.

4.2.3.2 Condensin binding to chromosomes in interphase and in mitosis

As shown above, the fission yeast cohesin loader Mis4/Ssl3, like in higher eukaryotes, dissociates from chromosomes during mitosis when chromosomes condense. Furthermore, the cohesin loading complex Mis4/Ssl3 and condensin show an overlapping binding pattern along chromosomes, and the budding yeast cohesin loader Scc2/4 is implicated in chromosome condensation (D'Ambrosio et al, 2008). Due to these links between the cohesin loader and condensin we wanted to analyse the subcellular localisation of condensin when cells progress through mitosis and chromosomes condense. As fission yeast cells enter mitosis, condensin accumulates in the nucleus due to mitotic phosphorylation of its Cut3 subunit (Sutani et al, 1999). In G2-arrested cells the majority of the condensin subunit Cnd2 was localised in the soluble fraction, while a small

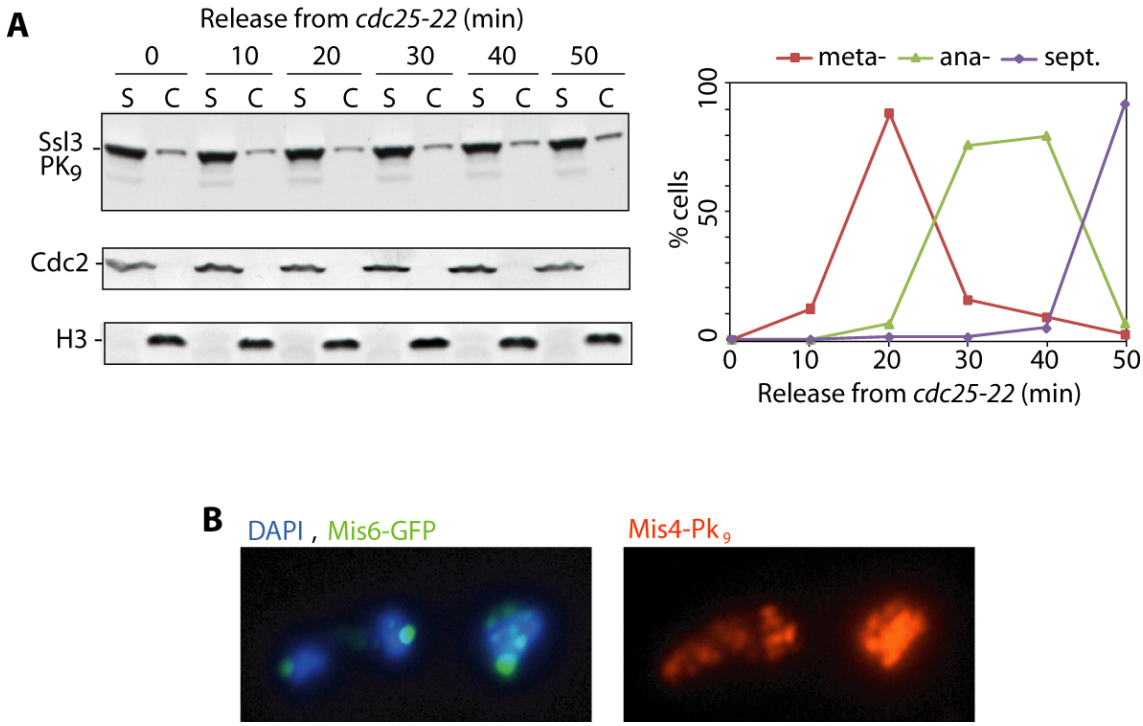

Figure 4.17 Removal of a subfraction of Mis4/Ssl3 from mitotic chromosomes
(**A**) Ssl3-Pk$_9$ *cdc25-22* GFP-Atb2 cells (Y3169) were arrested in G2 and released into mitosis as described in Figure 4.15. Cell extracts were separated into soluble (S) and chromatin (C) fractions, and the Pk$_9$-tagged cohesin loader Ssl3 was detected by immunoblotting. Cdc2 and Histone H3 detection were used as soluble and chromatin loading controls, respectively. The synchrony of the arrest and release was determined as described in Figure 4.15. (**B**) Chromosome spreads of exponentially growing Mis4-Pk$_9$ Mis6-GFP (Y3298) cells were stained for the Pk$_9$- and GFP-tagged proteins. The kinetochore marker Mis6 served to identify spreads from mitotic cells when chromosomes segregate. Note: One of the two Mis6-GFP signals of the left cell is slightly out of focus and therefore appears weaker in intensity.

portion was detected in the chromatin fraction (0 minutes 25°C, Figure 4.18A). This fraction increased as cells progressed through mitosis when chromosomes condensed (10 - 30 minutes 25°C, Figure 4.18A) and decreased again during mitotic exit (40 - 50 minutes 25°C, Figure 4.18A).

Immunostaining of spread chromosomes confirmed that the majority of condensin was recruited to chromosomes in mitosis. Like before, the kinetochore protein Mis6 was used to identify mitotic cells with segregating chromosomes. Bright staining of the condensin subunit Smc2 was observed in spreads that contained two separate Mis6 signals. In interphase cells, reduced but significant condensin staining along the entire length of chromosomes could be detected (Figure 4.18B), consistent with condensin having a role in chromosome organisation and function already in interphase.

Taken together, our results show that, as cells enter mitosis, a part of the cohesin loader Mis4/Ssl3 dissociates from chromosomes, while condensin binding to chromosomes

increases, suggesting reciprocal regulation of the two complexes during mitotic progression, despite their overlap in chromosomal distribution.

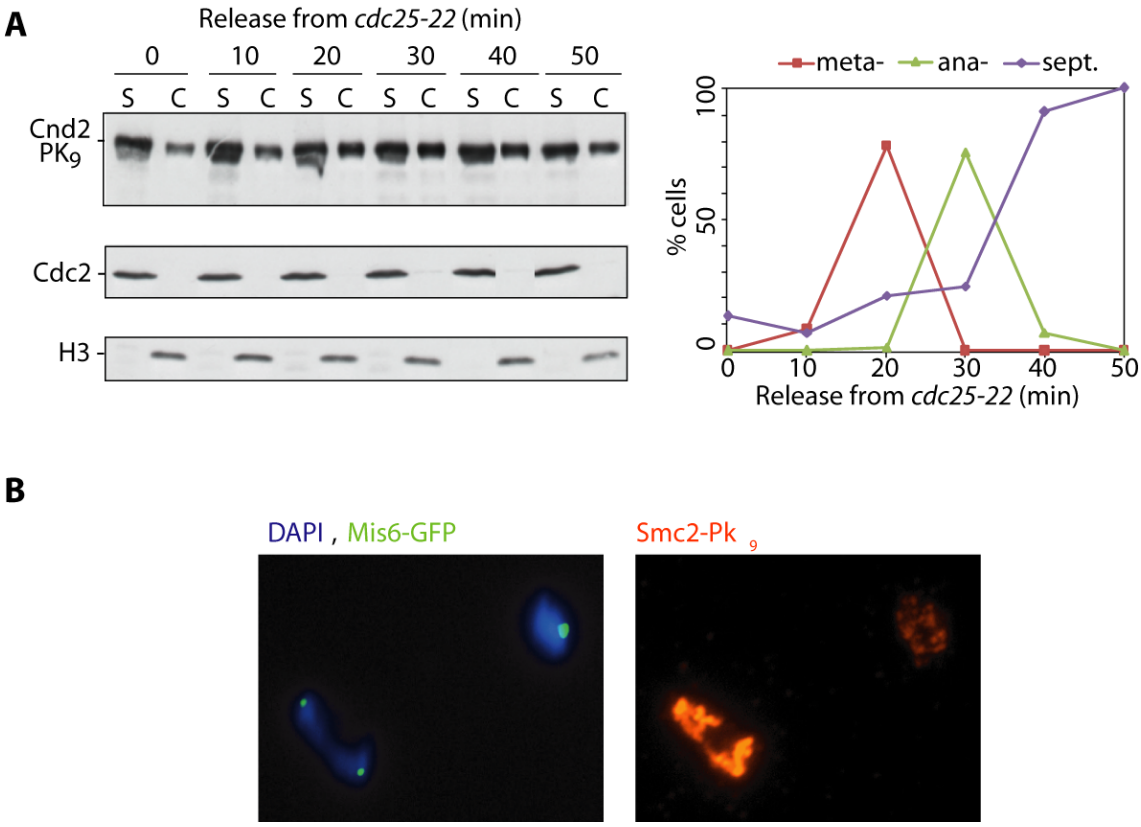

Figure 4.18 Condensin binding to chromosomes in G2 and in mitosis
(**A**) Cnd2-Pk$_9$ *cdc25-22* GFP-Atb2 cells (Y3250) were arrested in G2 and released into mitosis as described in Figure 4.16. Cell extracts were separated into soluble (S) and chromatin (C) fractions, and the Pk$_9$-tagged condensin subunit Cnd2 was detected by immunoblotting. Cdc2 and Histone H3 detection were used as soluble and chromatin loading controls, respectively. The synchrony of the arrest and release was determined as described in Figure 4.16. (**B**) Chromosome spreads of exponentially growing Smc2-Pk$_9$ Mis6-GFP (Y3303) cells were stained for the Pk$_9$- and GFP-tagged proteins. Mitotic cells with segregated chromosomes were identified by the presence of two separate signals of the kinetochore protein Mis6.

4.2.4 Cohesin's binding pattern during mitosis

The previous paragraphs suggest that a small part of cohesin dissociates from chromosomes in prophase and that a larger fraction is cleaved and removed from chromosomes at anaphase-onset. In the following we wanted to address whether the two steps of cohesin removal affected certain regions along chromosomes more than others.

4.2.4.1 Cohesin is evenly removed from mitotic chromosome arms

We followed the cohesin binding pattern during synchronous progression through mitosis, by ChIP on chip analysis, employing the *cdc25-22* arrest and release approach as described above (4.2.2). The distribution of cohesin along most of the chromosome arms remained unchanged throughout mitotic progression, indicating that cohesin is not removed from a certain subset of its binding sites, neither during cleavage-independent prophase nor during cleavage-induced anaphase removal. Rather, this result suggests that cohesin is evenly removed from most, if not all its association sites along chromosome arms (Figure 4.19).

4.2.4.2 Centromeric cohesin spreads onto chromosome arms in mitosis

In contrast to the unchanging binding pattern of cohesin along chromosomes during mitosis, we noticed a striking change in cohesin distribution around heterochromatic regions. Starting to spread in metaphase (20 minutes 25°C, Figure 4.20), cohesin covered regions of up to 50 kb around centromeres in anaphase (30 minutes 25°C, Figure 4.20), with no restriction to convergent sites. We also observed a similar, although less pronounced, spreading in cells arrested in G1 using the temperature-sensitive *cdc10-129* allele. The binding regions were more fragmented than in the anaphase sample but more expanded than in G2-arrested cells (Figure 4.20). This suggests that the changes in cohesin distribution around heterochromatin are cell cycle stage specific.

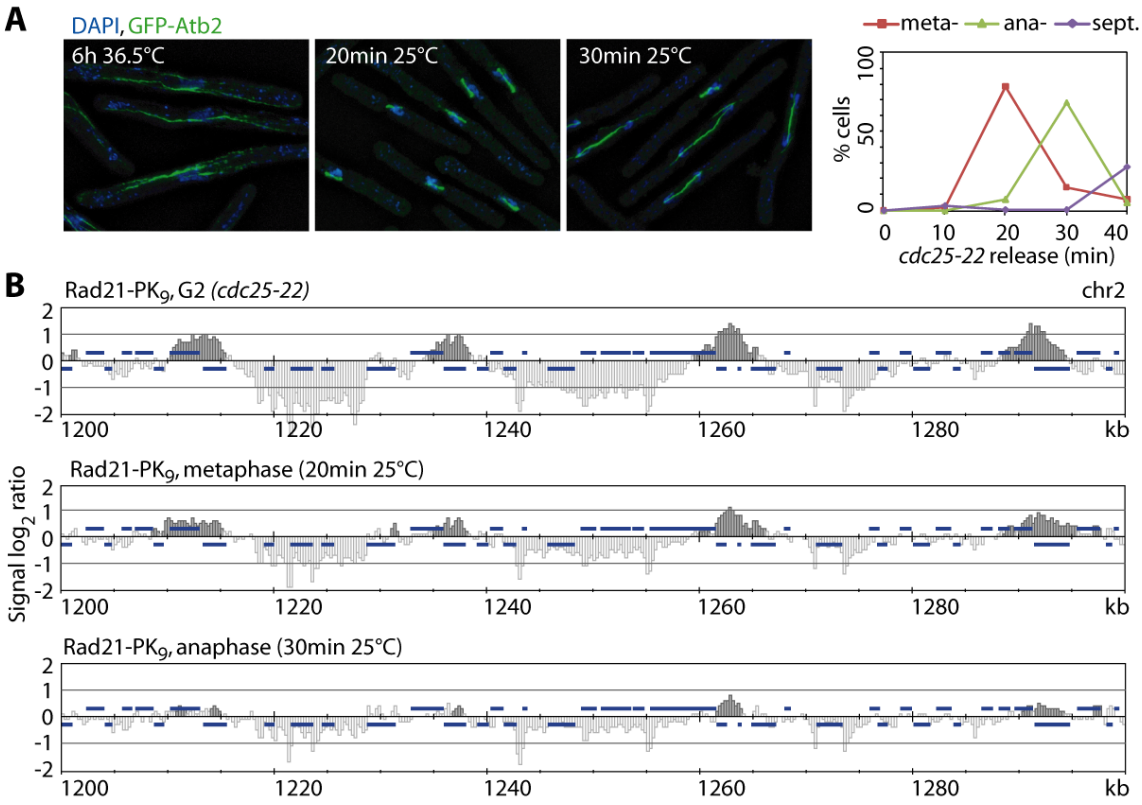

Figure 4.19 The cohesin binding pattern along chromosome arms during mitosis
(**A**) Highly synchronous progression through mitosis. Rad21-Pk$_9$ *cdc25-22* GFP-Atb2 cells (Y2699) were arrested in G2 and released into mitosis as described in Figure 4.16. DAPI staining of DNA, calcofluor staining of septa and GFP-Atb2 signals of interphase microtubules (6 hours 36.5°C), meta- (20 minutes 25°C) and anaphase spindles (30 minutes 25°C) in methanol fixed cells are shown. The synchrony of the arrest and release was determined as described in Figure 4.16. (**B**) ChIP against the cohesin subunit Rad21-Pk$_9$ was performed in cells derived from the time-points illustrated in A. The cohesin binding patterns of a 100 kb region along the left arm of chromosome 2 are depicted.

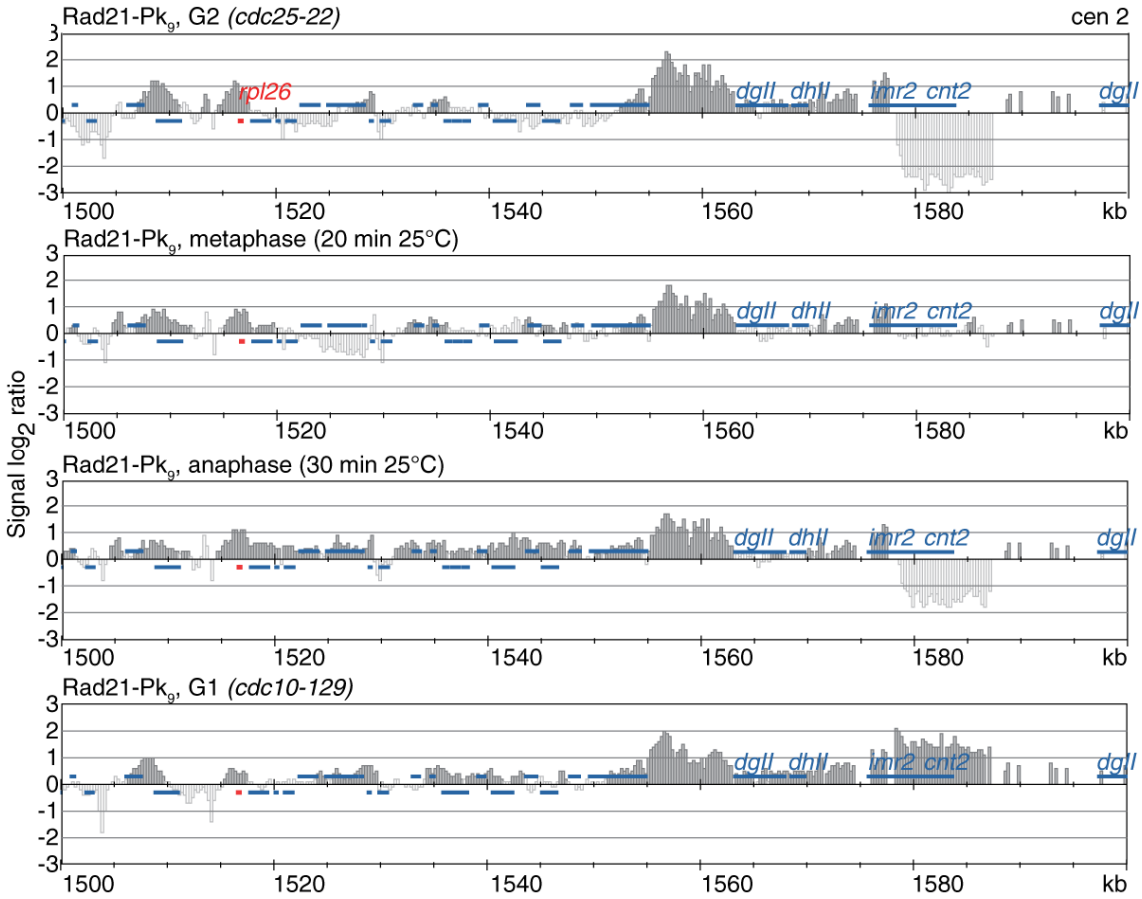

Figure 4.20 Cohesin spreading around centromeres during mitosis
ChIP against the cohesin subunit Rad21-Pk$_9$ was performed in cells treated as described in Figure 4.19. The cohesin binding pattern of a 100 kb region, including one *dgII* and one *dhII* repeat of the outer repeats, one *imr2* repeat and the central core region (*cnt2*), are shown. Note, a clear cohesin peaks associates with a ribosomal protein gene away from convergent sites, highlighted in red. Mis4/Ssl3 is also detected in this region (Appendix 7.2.1).

4.2.5 Heterochromatin regulates cohesin dynamics around centromeres

Cohesin is enriched along heterochromatic centromeric repeats. This enrichment depends on the heterochromatin protein Swi6 which is thought to largely dissociate from centromeric heterochromatin after Aurora B kinase phosphorylation of histone H3 (Chen et al, 2008; Fischle et al, 2005; Hirota et al, 2005). Swi6 then reaccumulates when cells enter the subsequent S phase (1.3.3.1.4). Mitotic Swi6 removal from heterochromatin happens with similar timing as the observed cohesin spreading around these regions. Furthermore, Swi6 removal from heterochromatin could cause a loss of anchoring for cohesin to heterochromatin. To test whether the two events were causally linked, we repeated the experiment but inactivated the activity of Aurora B, using an analog-sensitive Aurora B mutant, *ark1-as3* (Hauf et al, 2007). When the ATP-analog 1NM-PP1 was added to G2-arrested cells, 15 minutes before they were released into mitosis, no spreading of cohesin was observed during mitosis. Swi6 removal from chromosomes in these cells was inhibited as signals of the fusion protein Swi6-GFP, visible as several bright fluorescent foci within the nucleus, failed to dissolve in mitosis (Figure 4.21A). In contrast, the majority of Swi6-GFP foci had disappeared in *ark1* wild type cells, both in the presence and absence of 1NM-PP1 (Figure 4.21A and B). This suggests that mitotic Swi6 dissociation from chromosomes triggers a change in cohesin mobility that causes it to spread from centromeric heterochromatin onto neighbouring sequences. So far, this is a unique feature of fission yeast cohesin.

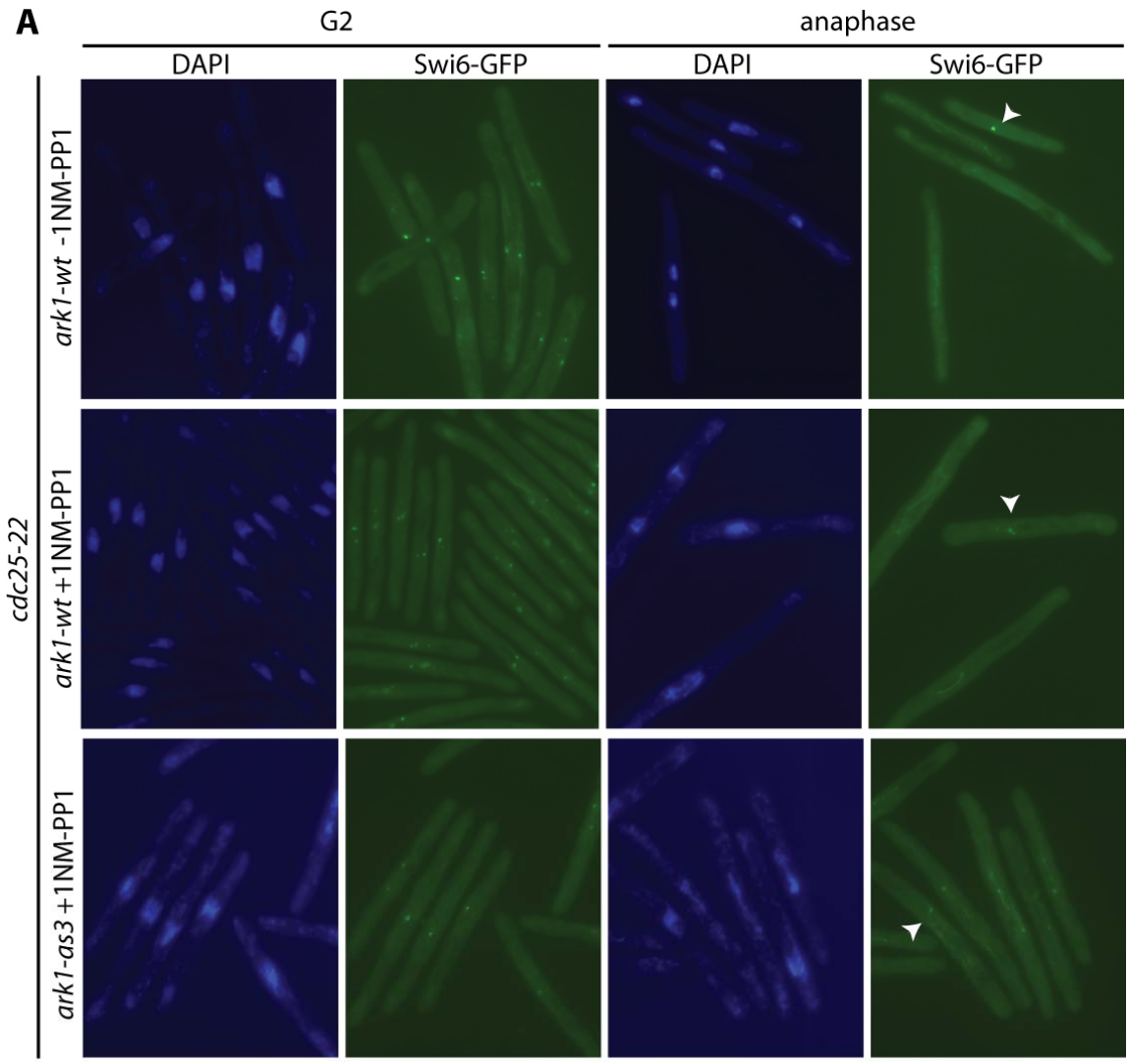
A
G2
anaphase
DAPI
Swi6-GFP
DAPI
Swi6-GFP
cdc25-22
ark1-wt -1NM-PP1
ark1-wt +1NM-PP1
ark1-as3 +1NM-PP1

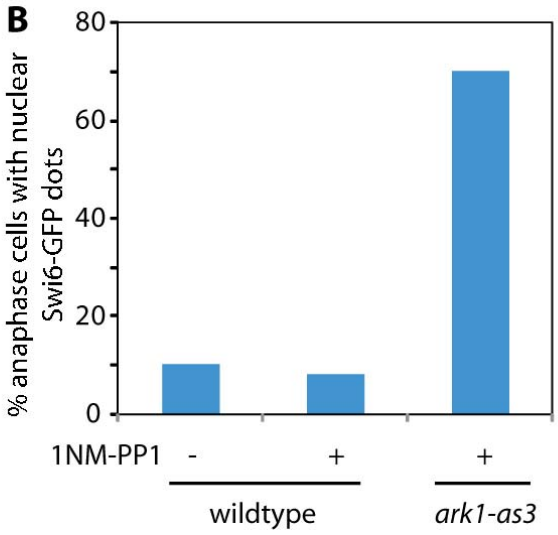
B
% anaphase cells with nuclear Swi6-GFP dots
80
60
40
20
0
1NM-PP1 - + +
wildtype
ark1-as3

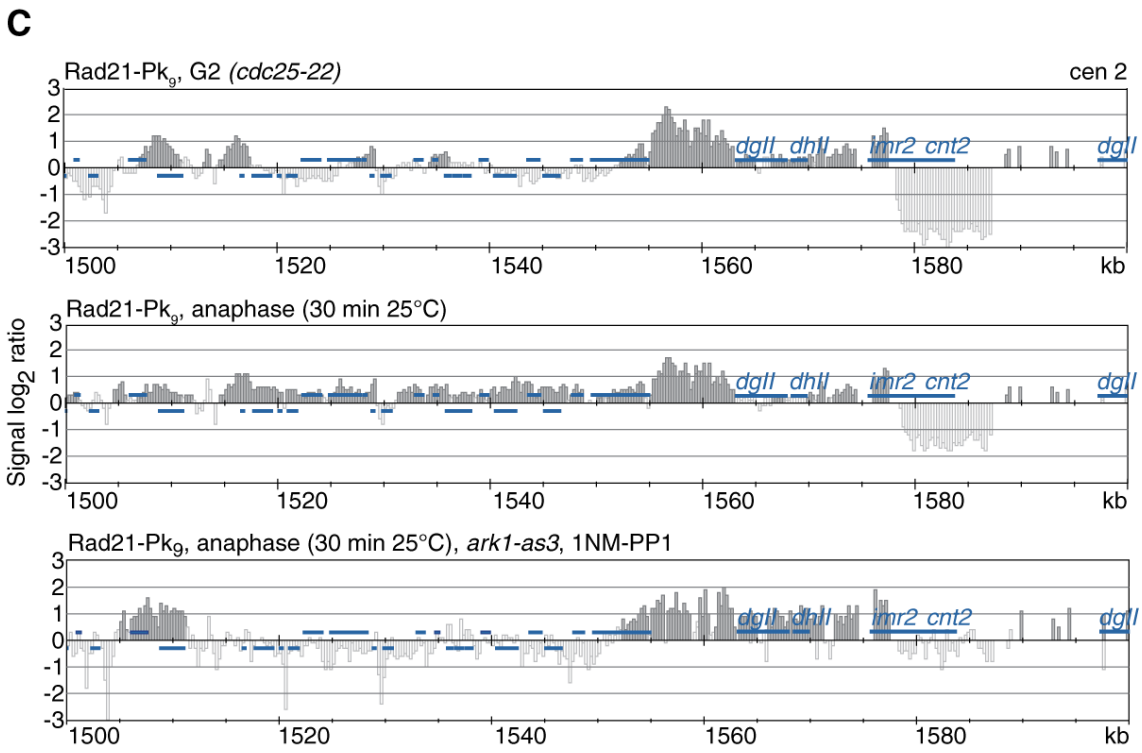

Figure 4.21 Swi6-regulation of cohesin dynamics during mitosis
(**A**) Swi6 dissociation from fission yeast chromosomes depends on Aurora B kinase activity. Rad21-Pk$_9$ *cdc25-22 ark1-as3* Swi6-GFP cells (3785) and Rad21-Pk$_9$ *cdc25-22 ark1* wild type Swi6-GFP cells (3786) were arrested in G2 and released into mitosis as described in Figure 4.20. To inactivate Aurora B kinase activity, 5µM 1NM-PP1 were added to the *ark1-as3* culture and, as a control, to half of the cells of the *ark1* wild type culture, 15 minutes before release into mitosis (Hauf et al, 2007). Visual inspection of the fusion protein Swi6-GFP confirmed that, compared to *ark1* wild type control cells in the presence or absence of 1NM-PP1, Swi6-GFP accumulation at heterochromatic centromeres, apparent as punctate fluorescent staining within the nucleus, failed to dissolve during mitosis. In the anaphase samples, Swi6-GFP signals in the nuclei of cells that have not yet entered anaphase are marked with arrowheads and serve as an internal control. Weaker fluorescent signals of α-tubulin (GFP-Atb2) are visible in the background. (**B**) Quantification of A. At least 100 anaphase cells were counted, and the percentages, displaying punctate fluorescence Swi6-GFP signals in the nucleus, are graphed. (**C**) Aurora B kinase-dependent spreading of centromeric cohesin during mitosis. The G2 (*cdc25-22*) and anaphase (30 minutes after release) cohesin binding patterns of *ark1* wild type cells in the absence of 1NM-PP1, taken from Figure 4.16, are compared to the anaphase binding pattern of *ark1-as3* cells in which Aurora B kinase activity had been inactivated. A 100 kb region, containing the centromere region of chromosome 2, including one *dgII* and one *dhII* repeat of the outer repeats, one inner *imr2* repeat and the central core (*cnt2*) sequence, are illustrated.

4.2.6 Cell cycle-dependent cohesin binding to the central core

Cohesin accumulation at fission yeast centromeres has mainly been attributed to its recruitment to the centromeric repeats by the heterochromatin protein Swi6. Using our ChIP on chip approach, we detected cohesin also at the central core of centromeres. No cohesin could be observed when cells were arrested in G2 while cohesin accumulated at the central core in G1-arrested cells (Figure 4.22A). This suggests that cohesin enrichment at the central core region underlies cell cycle regulation. We also found the cohesin loader Mis4/Ssl3 enriched at the central core, suggesting that cohesin might be loaded to this region in G1 but might then translocate away to its more permanent association site at centromeric repeats. Condensin also overlapped with the central core region, confirming previous reports (Nakazawa et al, 2008). Co-localisation of all three protein complexes, cohesin, condensin and the cohesin loader Mis4/Ssl3, at centromeres was confirmed by double-immunostaining of spread chromosomes with the kinetochore marker Mis6 (Figure 4.22B).

Figure 4.22 Cohesin, Mis4/Ssl3 and condensin overlap at centromeres.
(**A**) The cohesin loader and condensin overlap at the central core of centromere 2. Cells of strain Y2699 (Rad21-Pk_9 *cdc25-22*) were grown in minimal EMM medium at 25°C and subsequently shifted to 36.5°C for 6 hours to arrest cells in G2. Rad21-Pk_9 *cdc10-129* (Y2863) cells were grown in minimal EMM medium at 25°C and subsequently arrested in G1 by shifting the cultures to 36.5°C for 4 hours. Mis4-Pk_9 cells (Y2468) were exponentially grown in rich YE4S medium at 25°C. Cnd2-Pk_9 *nda3-KM311* cells (Y252) were grown in rich YE4S medium at 32°C and subsequently arrested in metaphase by growing the cultures for 6 hours at 20°C, the restrictive temperature of the *nda3-KM311* allele. ChIP was performed against the Pk-tagged proteins. A 50 kb region including the central core (*cnt2*) of the centromere of chromosome 2 is shown. (**B**) Flow cytometry analysis showed that Rad21-Pk_9 *cdc10-129* (Y2863) cells were efficiently arrested in G1 when the ChIP sample was taken. (**C**) Confirmation of co-localisation of the cohesin loading complex and condensin with centromeres. Mis4-Pk_9 Mis6-GFP cells (Y3298), Cnd2-Pk_9 Mis6-GFP cells (Y3302) and Smc2-Pk_9 Mis6-GFP cells (Y3303) were exponentially grown in rich YE4S medium at 25°C and processed for chromosome spreads. Staining against the Pk- and GFP-tagged proteins was performed to detect the cohesin loading complex subunit Mis4-Pk_9, the condensin subunits Cnd2-Pk_9 and Smc2-Pk_9 together with the kinetochore marker Mis6-GFP. Separate Mis6-GFP dots indicate mitotic cells with segregating chromosomes (Figure next page).

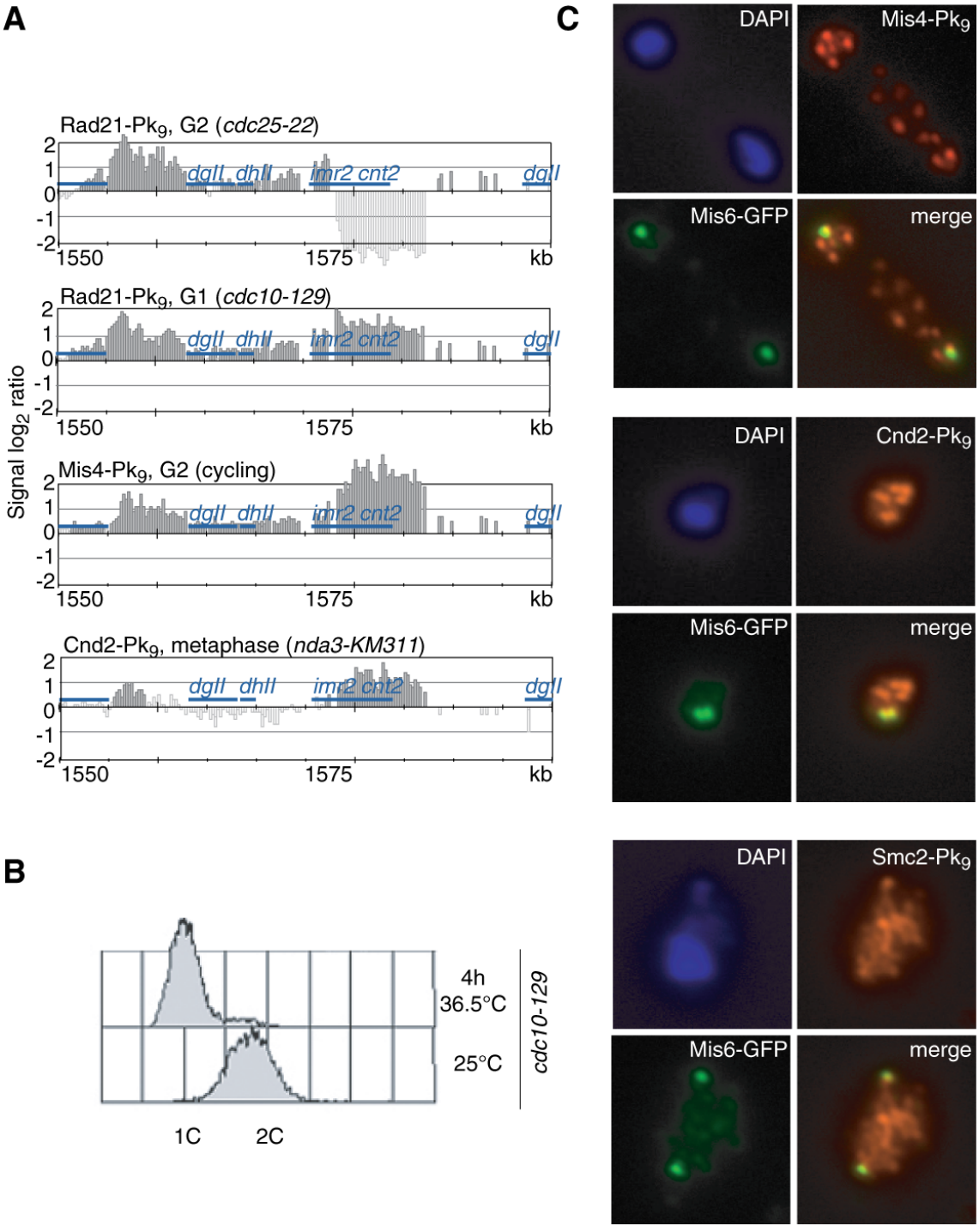
A
Rad21-Pk9, G2 (cdc25-22)
Rad21-Pk9, G1 (cdc10-129)
Mis4-Pk9, G2 (cycling)
Cnd2-Pk9, metaphase (nda3-KM311)
Signal log2 ratio
dgtI dhtI
imr2 cnt2
dgtI
1550
1575
kb
B
4h
36.5°C
25°C
cdc10-129
1C
2C
C
DAPI
Mis4-Pk9
Mis6-GFP
merge
Cnd2-Pk9
Smc2-Pk9

4.3 Cell cycle regulation of cohesin stability along chromosomes

In mammalian cells cohesin binds to G1 chromosomes in a highly dynamic fashion. FRAP experiments revealed that chromatin-bound cohesin was in a constant exchange with the soluble pool during G1. Approximately a third of the cohesin pool then became stabilised concomitantly with DNA replication in S phase, dependent on the cohesin destabiliser Wapl (Gerlich et al, 2003; Kueng et al, 2006). Sister chromatid cohesion is established at the same time during DNA replication in S phase (Uhlmann & Nasmyth, 1998), and little is known about how this is exactly achieved. Stabilisation of cohesin binding to chromosomes could be the consequence of cohesion establishment, possibly caused by the replication fork progressing through cohesin sites. Alternatively, cohesin stabilisation could be the pre-requisite of cohesion establishment. We wanted to dissect the mechanism of cohesion stabilisation during the cell cycle, using fission yeast as a model organism. The following work was performed in collaboration with Jean-Paul Javerzat's laboratory in Bordeaux (Bernard et al, 2008).

4.3.1 Instable cohesin binding in G1 is conserved across evolution

We first wanted to test whether, like in mammalian cells, cohesin in fission yeast was also bound to chromosomes in an instable manner in G1. If cohesin was only loosely associated with chromosomes and was in frequent exchange with its soluble pool, it could be imagined that the cohesin loader Mis4/Ssl3 might continuously be required to reload cohesin onto chromosomes. To test this, we arrested cells, carrying the temperature-sensitive alleles *mis4-367* and *ssl3-29* in G1 by titrating out the Cdc10 transcription factor, required for S phase entry, through overexpression of the C-terminal part of its binding partner Res1 (3.1.3.1.3; Ayte et al, 1995). We then inactivated the cohesin loader Mis4/Ssl3 in G1 and measured cohesin binding by Rad21-HA immunofluorescence on spread chromosomes. Strikingly, cohesin binding to G1 chromosomes was almost completely abolished after inactivation of the loading factor Mis4/Ssl3 (Figure 4.23). Dissociation of cohesin from centromeres and three cohesin associated regions (CARs) along the arm of chromosome 2 could be confirmed using chromatin immunoprecipation combined with real-time PCR (Bernard et al, 2008). This suggests that an active cohesin loading machinery is continuously required for maintaining cohesin lev-

els on chromosomes in G1. Theoretically, this observation could be explained if the cohesin loader would directly tether cohesin to chromosomes. However, our previous observations indicate that cohesin and its loading machinery show largely distinct distributions along chromosome arms (4.1.6). Our result therefore rather suggests that cohesin undergoes repetitive loading cycles during G1 to maintain chromosome association. Importantly, this indicates that cohesin instability is conserved among eukaryotes, underlining its functional importance.

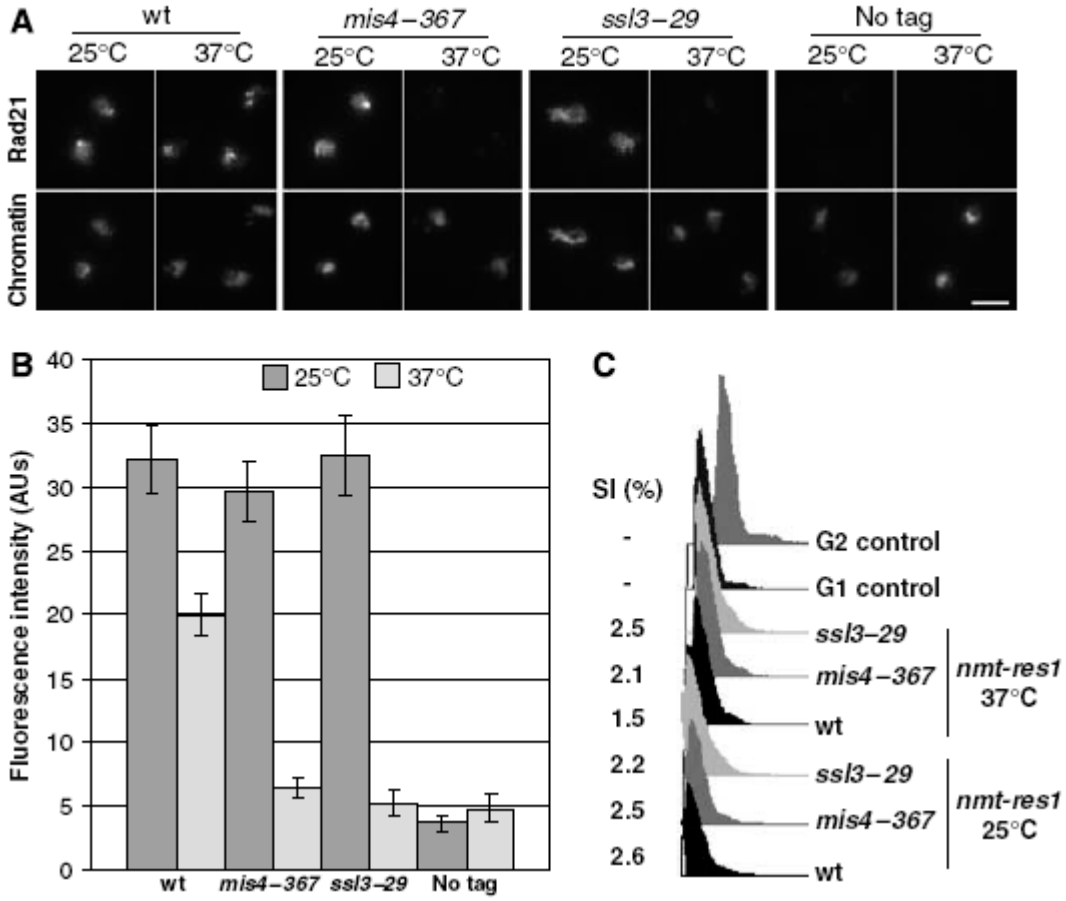

Figure 4.23 Cohesin binding to G1 chromatin requires continued Mis4/Ssl3 activity.
(**A**) Wild type cells (JP2596; Bernard et al, 2008) and cells carrying the temperature-sensitive *mis4-367* (JP2598; Bernard et al, 2008) and *ssl3-29* (Y2470) alleles of the cohesin loader factor were arrested in G1 at 25°C by overexpressing the C-terminal moiety of Res1 (Ayte et al, 1995) under control of the inducible *nmt1* promoter. The G1-arrested cultures were shifted to 37°C for 2 hours to inactivate the cohesin loader Mis4/Ssl3. Cohesin association with chromatin was visualised before and after the temperature shift to 37°C by immunofluorescence of spread chromosomes. DNA was counterstained with DAPI. Scale bar, 5 µm. (**B**) The fluorescence of 50 to 100 spread nuclei was quantified. Error bars show the confidence intervals. (**C**) FACS analysis of DNA content and septation indices (SI) indicate that the majority of cells remained arrested in a 1C cell cycle stage throughout the course of the experiment. The final experiment was performed by Jean-Paul Javerzat's group. Graph taken from Bernard et al, 2008.

4.3.2 Cohesin binding to chromatin is stabilised in S phase cells

We next wanted to address at what time during cell cycle progression cohesin binding to chromosomes was stabilised. Previous reports had shown that both in budding yeast and fission yeast the cohesin loading machinery became dispensable for viability once cells had entered G2 (Bernard et al, 2006; Ciosk et al, 2000). Furthermore, no Mis4/Ssl3 activity was required to maintain cohesin bound to chromosomes as assayed by ChIP analysis (Bernard et al, 2006) and by our immunofluorescence assay of spread chromosomes (Bernard et al, 2008). We were therefore interested to address at what time and how cohesin was stabilised between G1 and G2. Cohesin stabilisation could be a manifestation of cohesion establishment or it could be the consequence of cell cycle regulation, independently of DNA replication and cohesion establishment. To test this, we arrested cells, bearing the thermosensitive *mis4-367* or *ssl3-29* alleles, at the permissive temperature in early S phase, using the ribonucleotide reductase inhibitor hydroxyurea (HU) that leads to rapid depletion of deoxynucleotides. Once arrested in S phase at the permissive temperature, we shifted the cultures to the restrictive temperature to inactivate cohesin loading. In contrast to our observation in G1-arrested cells, immunostaining of chromosome spreads showed that a significant fraction of cohesin remained on chromosomes even after the loading machinery had been inactivated (Figure 4.24). This suggests that cohesin became stabilised in HU-arrested early S phase cells.

4.3.3 Cohesin stabilisation is independent of DNA replication

We next wanted to test whether cohesin was equally stabilised along its association sites on chromosome arms. Therefore, we repeated the HU experiment from above (4.3.2) and analysed the cohesin binding pattern on entire chromosomes by performing chromatin immunoprecipitation against epitope-tagged Rad21, followed by hybridisation to fission yeast chromosome 2 and 3 tiling oligonucleotide arrays, as described previously (4.1). As expected from our previous analyses, cohesin was mainly detected at convergent sites. Interestingly, its binding pattern remained unchanged both with regards to its relative peak heights and its chromosomal positions, when the loading factor subunit Ssl3 was inactivated (Figure 4.25A). This suggests that there are no regions along chromosome arms where cohesin is preferentially stabilised during early S phase, confirming

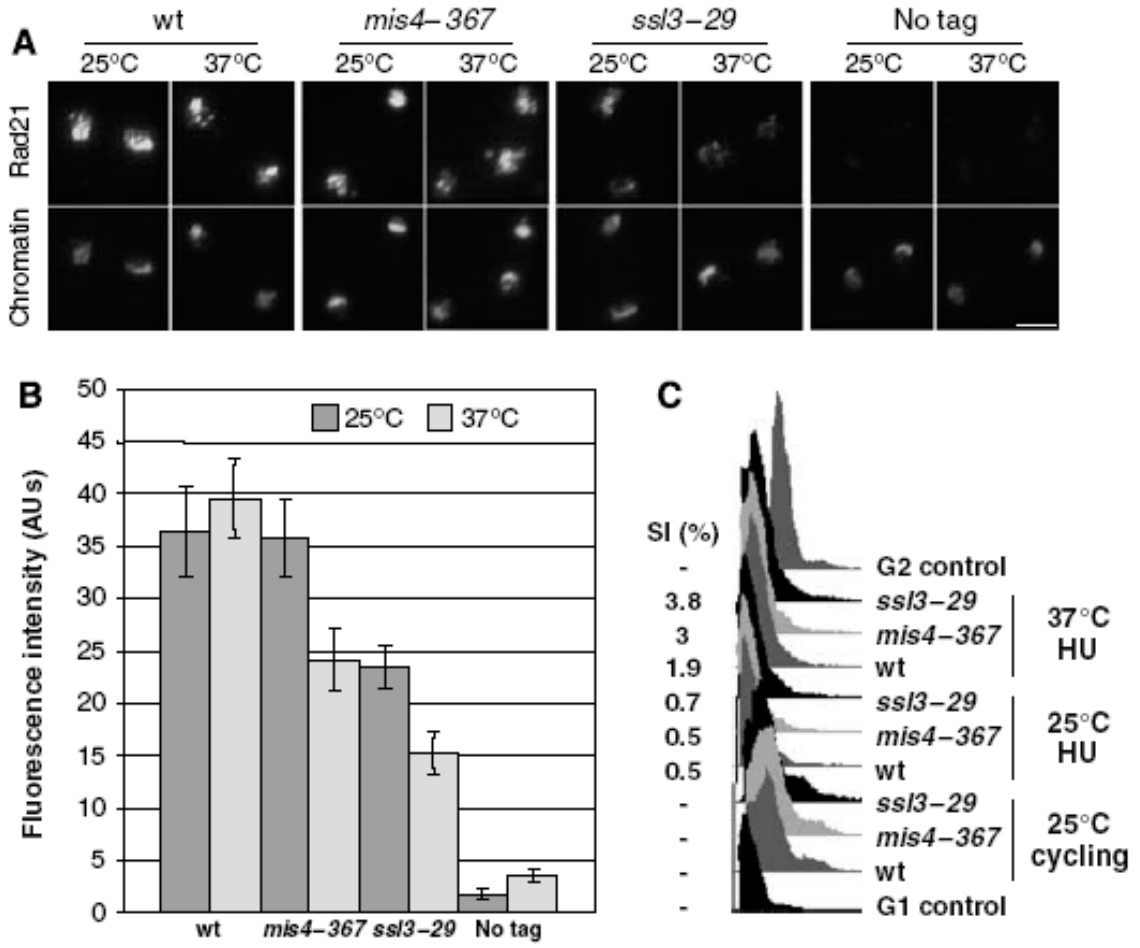

Figure 4.24 Cohesin stabilisation along chromosomes in HU-induced S phase
(**A**) Wild type (Y2464), *mis4-367* (Y3470) and *ssl3-29* (Y2463) were treated with hydroxyurea (HU) to arrest cells in early S-phase at 25°C. In the presence of HU, the cultures were shifted to 37°C for 2 hours to inactivate the cohesin loader subunits Mis4 and Ssl3 while cells remained in early S-phase. Rad21-HA binding to chromosomes was assessed by immunostaining of cohesin on spread chromosomes before and after the temperature shift to 37°C. The scale bar marks 5 µl in length (**B**) Quantification of the Rad21-HA fluorescence in the spread nuclei obtained in A. The nuclei of 50 - 100 cells were measured. Error bars indicate the confidence interval. (**C**) FACS analysis and septation indices (SI) show that the cultures arrested with a close to 1C DNA content throughout HU treatment. The final experiment was performed by Jean-Paul Javerzat's group (Bernard et al, 2008).

that, unlike in G1, the cohesin loading factor Mis4/Ssl3 is not required for maintaining cohesin's binding to chromosomes in S phase. This result was surprising, as only small regions, approximately 4 to 5 kb, surrounding early replicating origins on both sides, are replicated in HU treated cells (Patel et al, 2006). Therefore, the intriguing idea that cohesin stabilisation might be a consequence of cohesion establishment, possibly due to the replication fork passing through cohesin binding sites, seemed unlikely. Nevertheless, it remained possible that cohesin binding sites could be closely assembled around early firing origins and might therefore be replicated in HU-arrested cells. However, analysis of the distances of cohesin binding sites to origins, known to initiate DNA replication in HU-arrested cells (Heichinger et al, 2006), revealed that only approximately

half the cohesin binding sites were located within 10 kb reach of these origins, a conservative estimate of how far DNA replication might have progressed in HU treated cells. The other half was detected too far away from an origin to have been replicated. As all cohesin peaks along chromosome arms were equally stabilised during HU, our observation suggests that cohesin stabilisation occurred independently of the replication status of the respective cohesin association site.

To directly probe this hypothesis, the replication status of four different CARs, two in close proximity to predicted early firing origins (CAR1979 and CAR438) and two distant to any known origin (CAR758 and CAR1806), were determined in HU treated cells. Cells able to take up and incorporate 5-bromo-2-deoxyuridine (BrdU) during DNA replication (Patel et al, 2006) were arrested in G1 by nitrogen starvation and subsequently released into rich medium at 25°C in the presence of BrdU and HU. Once arrested in S phase, the culture was shifted to 37°C for 2 hours. Subsequently, HU was washed away to allow cells to complete replication at 37°C in the presence of BrdU. DNA was extracted from cells just before the release from HU (HU37) and from cells that had completed replication at 37°C (REL37). ChIP was performed using an anti-BrdU antibody, followed by real-time PCR to quantify the immunoprecipitated DNA. The ratio of REL37/HU37 indicated the extent of DNA replication of the respective CARs (Figure 4.25B). As expected the two CARs close to an origin were replicated to 20 % and 50 % whereas no replication of the two CARs away from any origin could be detected. Two strong origins (ARS3003 and ARS3004) and a centromeric region, known to be early replicated (Kim et al, 2003), served as positive controls. Even strong fission yeast origins are known not to fire in every cell and similar values for ARS3003 and ARS3004 have previously been observed by DNA combing (Patel et al, 2006). Wild type, *mis4-367* and *ssl3-29* cells showed a similar replication status at the investigated regions, indicating that the inactivation of the loading machinery had no significant influence on the pattern of origin firing. Taken together, this observation confirms the hypothesis that cohesin can be stabilised along chromosomes independently of DNA replication at least in HU-induced early S phase.

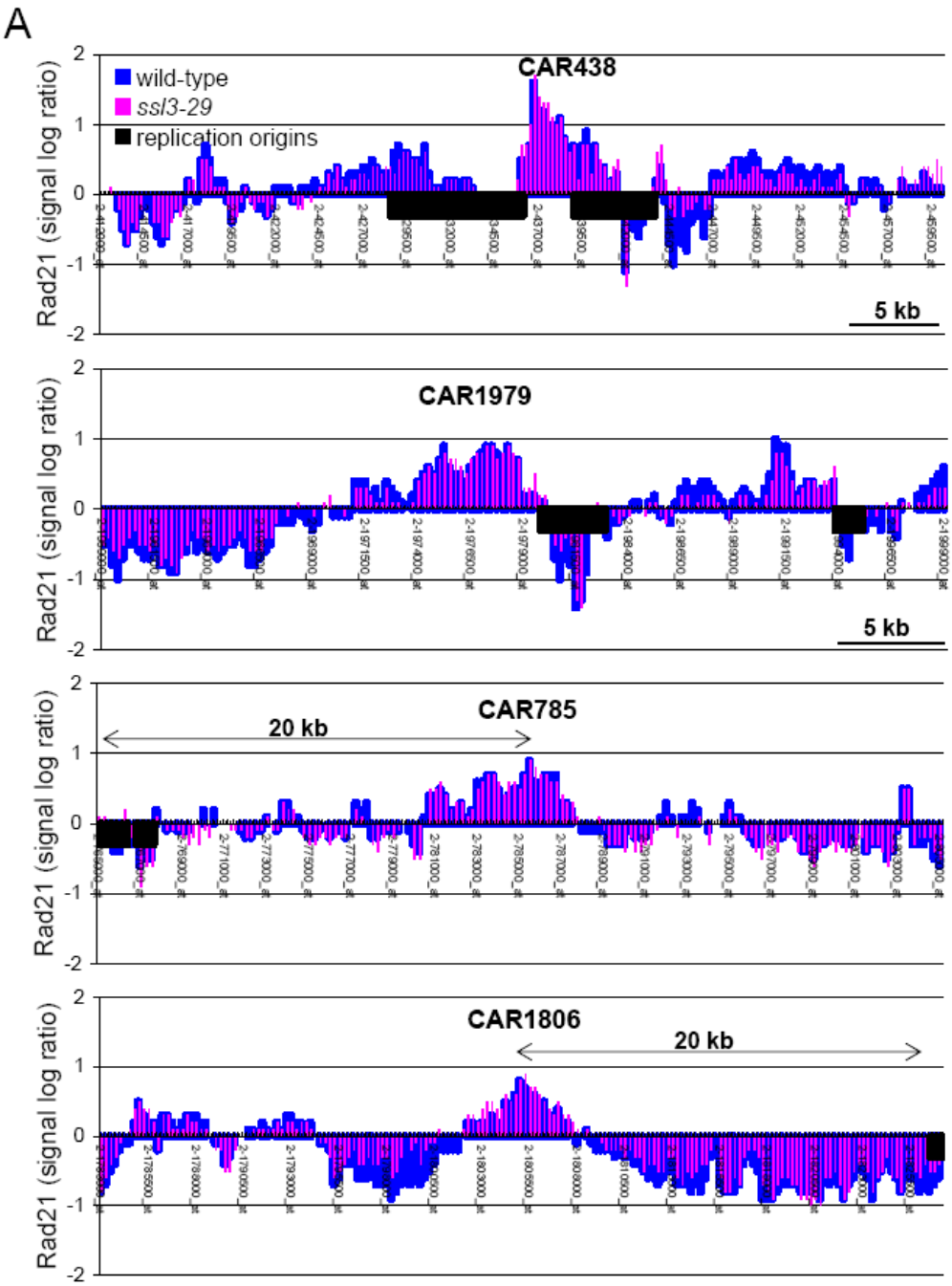
A
wild-type
ssl3-29
replication origins
CAR438
CAR1979
CAR785
CAR1806
20 kb
5 kb
Rad21 (signal log ratio)
B
wild type
mis4-367
ssl3-29
BrdU incorporation HU37 / REL 37 (%)
ARS 3003
ARS 3004-5
CAR 1806
CAR 785
CAR 1979
CAR 438
CEN (imr)

Figure 4.25 Rad21 stabilisation is independent of DNA replication.
(**A**) Wild type (Y2464) and *ssl3-29 rad21-HA* cells (Y2463) were arrested in early S-phase by hydroxyurea (HU) treatment at 25°C and then shifted to 37°C for 3 hours in the presence of HU to inactivate the cohesin loading factor Ssl3. Rad21-HA binding to chromosomes was assessed by ChIP followed by hybridisation to oligonucleotide tiling arrays, covering chromosomes 2 and 3. The data sets from the two strains were merged for comparison. Black boxes indicate replication origins in intergenic regions known to fire in HU (Heichinger et al, 2006). Four regions along chromosome 2 are shown. (**B**) Determination of the replication status of selected loci in the HU arrest. Cells were arrested in G1 by nitrogen starvation and released into the cell cycle at 25°C in the presence of HU and BrdU. After 2 hours at 37°C (HU37), HU was washed out, and cells were allowed to resume replication for 1 hour in the presence of BrdU (REL37). Replicated DNA was immunoprecipitated using anti-BrdU antibodies and quantified by real-time PCR. The extent of DNA replication in the HU arrest at 37°C is given by the ratio HU37/REL37. The replication status results were retrieved in Jean-Paul Javerzat's laboratory (Bernard et al, 2008) (see Figure on previous page).

4.3.4 Eso1's contribution to cohesin stabilisation during S phase

Two recent studies in budding yeast have reported on a genome-wide reinforcement of cohesion as a response to a single DNA double-strand break (DSB). This process is independent of DNA replication and happens outside of S phase but requires the acetyltransferase Eco1 (Ctf7) which travels with the replication fork and has recently been shown to acetylate the cohesin subunit SMC3 during S phase (Ben-Shahar et al, 2008; Ström et al, 2007; Ünal et al, 2007). We were wondering whether a similar mechanism could be responsible for the observed cohesin stabilisation during HU-induced early S phase. To test the function of Eso1, the fission yeast counterpart of Eco1, for cohesin stabilisation, we took advantage of the fact that the thermosensitive allele *eso1-H17* (Tanaka et al, 2000) becomes efficiently inactivated at a lower temperature (32°C; Figure 4.26) than the mutant loading factor allele *mis4-367*, which fully supports cell growth at 32°C.

Cultures of *mis4-367* mutant and *mis4-367*, *eso1-H17* double-mutant cells were arrested by HU treatment at 32°C to allow cells to enter S phase without Eso1 function. Cohesin was bound to chromosomes at this stage even though the levels were slightly reduced compared to wild type cells, possibly due to partial inactivation of Mis4 at 32°C. Once arrested in S phase, the cultures were shifted to 37°C to inactivate cohesin loading. Cohesin binding appeared almost unchanged after its loading had been abolished, even though Eso1 had been inactivated (Figure 4.27A). This suggests that cohesin stabilisation in HU phase is not dependent on a functional Eso1 gene and that the mechanism is different to G2 cohesin reinforcement observed in response to DSBs.

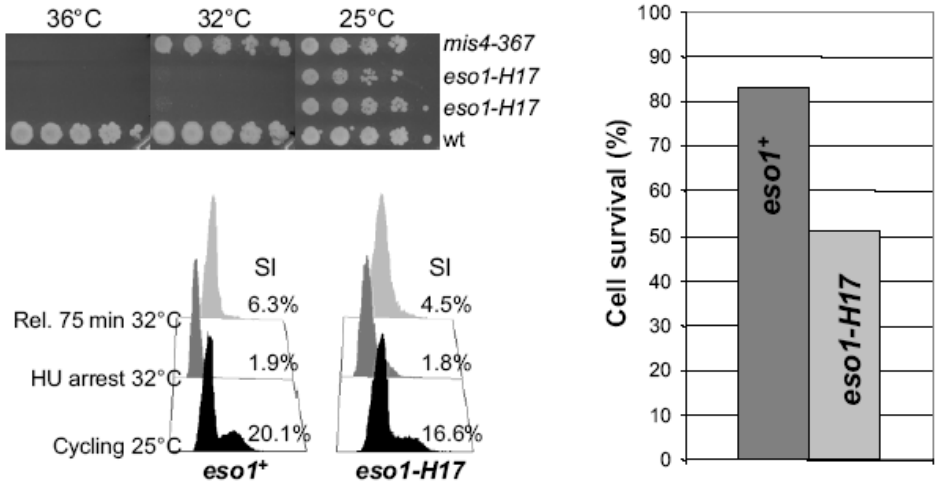

Figure 4.26 Eso1 function is compromised in *eso1-H17* cells at 32°C.
Serial dilutions of cells were spotted on agar plates and incubated at the indicated temperatures. Note that *mis4-367* but not *eso1-H17* cells can form colonies at 32°C. To estimate the extent of Eso1 inactivation within a single cell cycle, HU was added to *eso1-H17* and *eso1*$^+$ cycling cells at 25°C and shifted to 32°C to induce early S phase arrest (HU arrest 32°C). HU was washed away, and cells were incubated for 75 minutes at 32°C to allow the completion of DNA replication (Rel. 75 minutes 32°C). Cell survival was determined at that time by plating cells at 25°C. SI: septation index. The tests were conducted by Jean-Paul Javerzat's group. Figure taken from Bernard et al, 2008.

Importantly, cohesin stabilisation in HU-induced early S phase cells might not reflect what happens during unperturbed S phase progression. An alternative pathway might act in parallel or in addition that correlates cohesin stabilisation with progression through a normal S phase. Recent FRAP analyses point towards such a pathway in mammalian cells as the turnover of cohesin on chromosomes was shown to increase as cells advanced through S phase (Gerlich et al, 2006b). We therefore wanted to test whether this was also the case in fission yeast. Cultures of *mis4-367* single and *mis4-367*, *eso1-H17* double mutants were arrested in G1 by nitrogen starvation. Upon release the cultures were shifted to 32°C to allow cells to progress through S phase without Eso1 function but with an active cohesin loading machinery. After DNA replication was completed, cells were shifted to 37°C to inactivate the cohesin loader Mis4, and cohesin binding to chromosomes was monitored on immunostained chromosome spreads. In *eso1*$^+$ cells cohesin levels remained almost unchanged after inactivation of Mis4, confirming previous results that the loading machinery Mis4/Ssl3 is not required for stable cohesin binding to chromosomes in G2 (Bernard et al, 2006). In contrast, cohesin levels dropped significantly after inactivation of Mis4, when cells had passed through S phase without a functional *eso1* gene (Figure 4.27B). The reduction of cohesin levels to approximately half of what they were before is possibly an underestimate of Eso1's contribution to cohesin stabilisation, as, due to the synchronisation by nitrogen starvation,

only about two thirds of the cells progressed through S phase without Eso1 function. Our result suggests that a pathway exists in fission yeast that stabilises cohesin concomitantly with unperturbed S phase progression and dependently of a functional *eso1* gene.

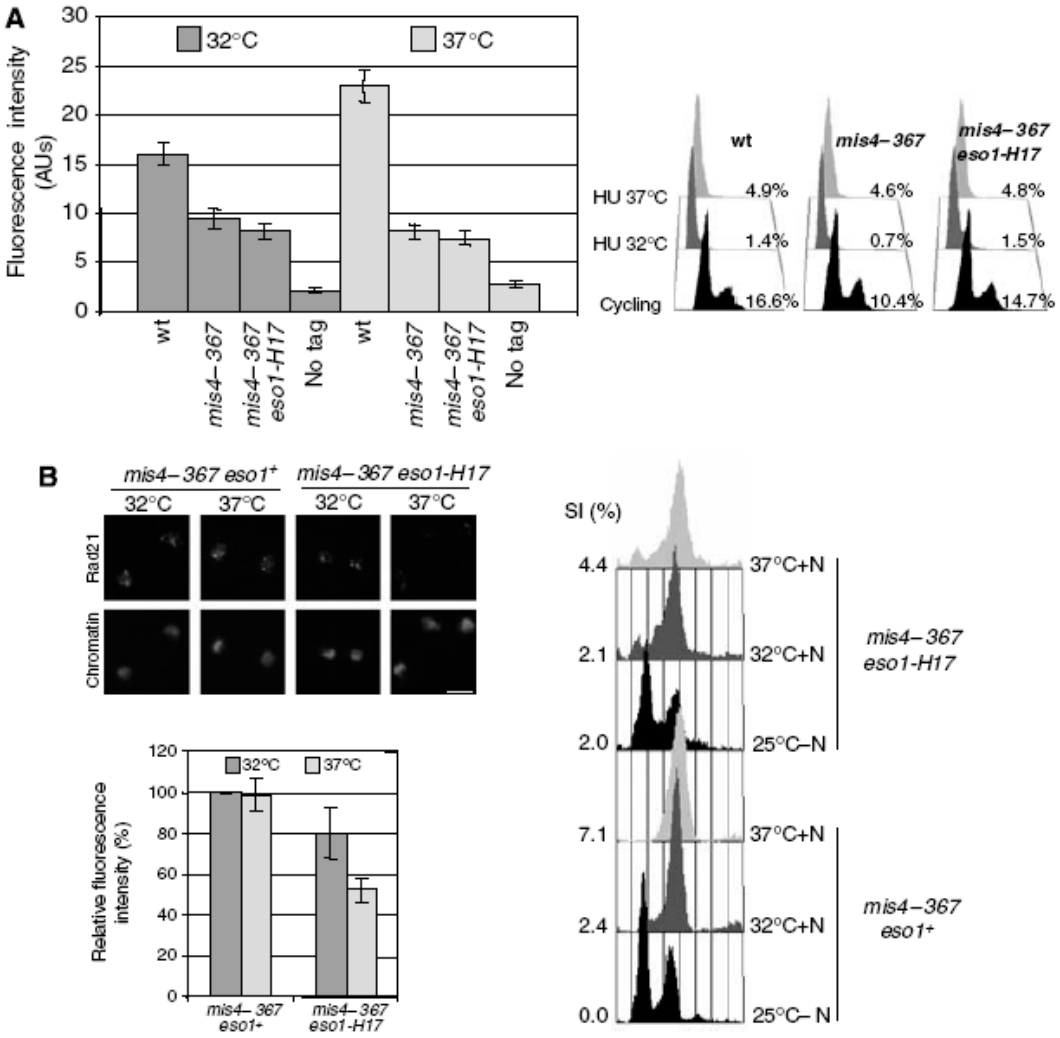

Figure 4.27 The role of Eso1 for cohesin stabilisation in S phase
(**A**) Cohesin stabilisation in HU-treated cells is independent of a functional *eso1* gene. Wild type, *mis4-367* (Y3470) and *mis4-367, eso1-H17* (3493) cultures were arrested in HU at 32°C. Cohesin loading was inactivated by temperature-shift to 37°C for 2 hours in the presence of HU. Cohesin binding to HU chromosomes at 32°C and at 37°C was assessed by quantification of immunofluorescence intensity of Rad21 on 50 - 100 spread chromosomes. Error bars show the confidence interval of the mean with $\alpha = 0.05$. DNA content analysis in the right panel indicates that all cells remained in a 1C HU state throughout the course of the experiment. (**B**) Reduced chromosomal cohesin stability after S-phase without Eso1. Cells were arrested in G1 by nitrogen starvation (25°C -N) and released to pass through S-phase at 32°C, a restrictive temperature for *eso1-H17*. 3.75 hours after release, when cells had completed S-phase (32°C +N), the temperature was raised to 37°C for 1.5 hours to inactivate Mis4 and probe the stability of cohesin on G2 chromosomes (37°C +N). Rad21-HA levels on chromatin were monitored on chromosome spreads by immunofluorescence before and after the shift to 37°C. Rad21-HA fluorescence was measured in 50 - 100 nuclei. DNA content analysis and septation index SI (%) show that most cells are in G1 after nitrogen starvation and pass through S-phase within 3.75 hours after release. Cells remain in G2 after temperature shift to 37°C for 1.5 hours. The quantification is based on two independent experiments with the error bars indicating the standard deviation of the means. The fluorescence for each sample is normalised to the value of the *mis4-367* sample before the 37°C shift. Scale bar = 5 µm.

5 Discussion

5.1 Cohesin association with fission yeast chromosomes

Cohesin is an essential chromosomal protein that mediates sister chromatid cohesion to ensure faithful chromosome segregation. Apart from this canonical function, cohesin is also involved in gene regulation and DNA repair by homologous recombination. Despite its essential function and its high conservation from yeast to human, recent genome-wide surveys have revealed striking apparent differences in the cohesin binding patterns between various model organisms. Our analyses of the cohesin binding pattern along fission yeast chromosomes allow us to reconcile different aspects of cohesin behaviour on chromosomes and suggest that disparities between organisms reflect a different emphasis of certain aspects of cohesin behaviour rather than different principles of action.

5.1.1 Similar mechanisms for cohesin loading and translocation?

Cohesin loading onto chromosomes depends on a separate loading complex Mis4/Ssl3 (Scc2/Scc4, Nipped-B, NIPL). In budding yeast, cohesin initially associates with its loader Scc2/4 along chromosomes in G1 but is then rapidly translocated to convergent sites where it can be detected throughout most of the cell cycle until mitosis when proteolytic cleavage of cohesin triggers its removal from chromosomes (Figure 5.1A; Lengronne et al, 2004; Uhlmann et al, 1999). In contrast to budding yeast, cohesin in *Drosophila* shows a more permanent overlap with its loading factor Nipped-B and was not found to be significantly enriched between convergently transcribed genes (Figure 5.1C; Misulovin et al, 2008). In fission yeast we find both, a subpool of cohesin permanently coincides with its loader Mis4/Ssl3 whereas a different fraction of cohesin responds to Pol II transcription and translocates to sites of transcriptional termination (Figure 5.1B; also see Gullerova & Proudfoot, 2008). This opens the possibility that, despite the apparent disparities described above, cohesin associates with chromosomes in a similar fashion in these organisms, with more or less emphasised retention at its loading sites.

Even though no translocation of cohesin to convergent sites has been observed along *Drosophila* chromosome arms, it cannot be excluded that a similar process takes place (Misulovin et al, 2008). It can be envisioned that, due to the larger intergenic distances in this organisms, as compared to budding and fission yeast, cohesin might not be concentrated into discrete peaks between convergently transcribed genes and might therefore have escaped detection so far. In human and mouse cells, cohesin coincides with the zinc-finger containing protein CTCF, a factor involved in gene silencing (Figure 5.1D; Parelho et al, 2008; Rubio et al, 2008; Stedman et al, 2008; Wendt et al, 2008). The cohesin loader Scc2/Scc4 has not been mapped, yet, and it will be interesting to analyse whether it co-localises with cohesin at CTCF sites or whether it binds to separate places characterised by yet other chromosomal features.

It is not known how Scc2/4 is recruited to chromosomes. Its binding sites are characterised by strong transcriptional activity both in budding yeast and in *Drosophila* which might help to rapidly distribute cohesin away from its loading sites to allow further loading reactions (D'Ambrosio et al, 2008; Lengronne et al, 2004; Misulovin et al, 2008). We find this feature conserved in fission yeast, where Mis4/Ssl3 shows a striking overlap with tRNA and ribosomal protein genes, both strongly transcribed groups of genes, although by different polymerases. But is transcription also involved in the recruitment of the cohesin loader to chromosomes arms? As a high number of Mis4/Ssl3 unbound genes (389) are more highly expressed than the median of all Mis4/Ssl3 bound genes, transcription itself is not sufficient to recruit Mis4/Ssl3 to chromosomes. It rather seems that certain subsets of highly transcribed genes might harbour features required to load Mis4/Ssl3 onto chromosomes. Transcription factors are known to control the expression of large groups of genes and as such might be involved in this process. Consistent with this idea we find a striking overlap of the cohesin loader Mis4/Ssl3 with the forkhead domain-containing protein Fhl1 that, in budding yeast, is known to regulate the expression of ribosomal protein genes. Furthermore, Mis4/Ssl3 coincides with the RNA Pol III transcription factor TFIIIC that controls the expression of tRNA genes. It will be an interesting directive for the future to test whether such factors are sufficient to recruit Mis4/Ssl3 to chromosomes. Targeting of these factors, or parts of them, to defined chromosomal regions e.g. by using the lac operator/repressor recognition system (Robinett et al, 1996) might lead to the answer of this question and may help to narrow down the essential elements for this process. Alternatively, it could be promoter sequence elements that might be involved in the recruitment of the cohesin loader

Mis4/Ssl3 to chromosomes. A recent study in budding yeast supports this idea. Budding yeast condensin coincides with the cohesin loader Scc2/4 at tRNA and ribosomal protein genes like we observed in fission yeast (D'Ambrosio et al, 2008). Insertion of a B box element, not sufficient to induce Pol III transcription without additional promoter elements, but able to recruit TFIIIC to chromosomes, induces a condensin binding site (D'Ambrosio et al, 2008). This is the first evidence for sequence-specific loading of condensin onto chromosomes. It will be interesting to address whether the same or similar elements might be sufficient to recruit the cohesin loader Scc2/4 to chromosomes and whether this mechanism is conserved in fission yeast.

5.1.2 Separation of function at specific cohesin sites?

Cohesin does not only promote sister chromatid cohesion but is also involved in transcriptional regulation. Its first role in gene regulation came from a study in budding yeast, where cohesin was detected as part of a chromosomal boundary, a region that separates an area of active expression from one of gene repression, an effect known as insulation (Donze et al, 1999). But do all cohesin binding sites act both as cohesion sites and as chromosomal insulators? Or could it be that cohesin at its loading sites participates in functions different to the ones it fulfils when bound to distant convergent sites? Cohesin loading sites in budding and fission yeast can be detected at tRNA genes (D'Ambrosio et al, 2008) which have been implicated as chromatin barriers (Haldar & Kamakaka, 2006; Valenzuela & Kamakaka, 2006). Cohesin in human and mouse cells co-localises with the chromosomal boundary and insulator element CTCF and in several cases, cohesin was directly shown to be required for CTCF's gene regulatory function

Figure 5.1 Model for cohesin binding in various eukaryotes
(**A**) Budding yeast cohesin is initially recruited to Scc2/4 sites in G1 but rapidly translocates to its more permanent association sites between convergently transcribed genes. (**B**) Fission yeast cohesin can be permanently detected at certain Mis4/Ssl3 sites but also corresponds to RNA Pol II transcription by downstream translocation to convergent sites. Only certain convergent gene pairs are bound by cohesin, characterised e.g. by strong transcriptional activity. (**C**) *Drosophila* cohesin and its loader Nipped-B overlap near strongly transcribed genes. Even though cohesin has not been detected at convergent sites, large intergenic distances in this organism might make it difficult to detect cohesin along these regions. (**D**) In human and mouse cells, cohesin coincides with CTCF but has not been found enriched between convergently transcribed genes. Like in *Drosophila*, cohesin might be translocated to convergent site but due to the large distances between genes, might not to be concentrated enough to be detected. The cohesin loader has not yet been mapped in these two organisms. Cohesin loader sites in all model organisms studied so far show a striking overlap with strong transcriptional activity e.g. tRNA genes or ribosomal protein genes (Figure next page).

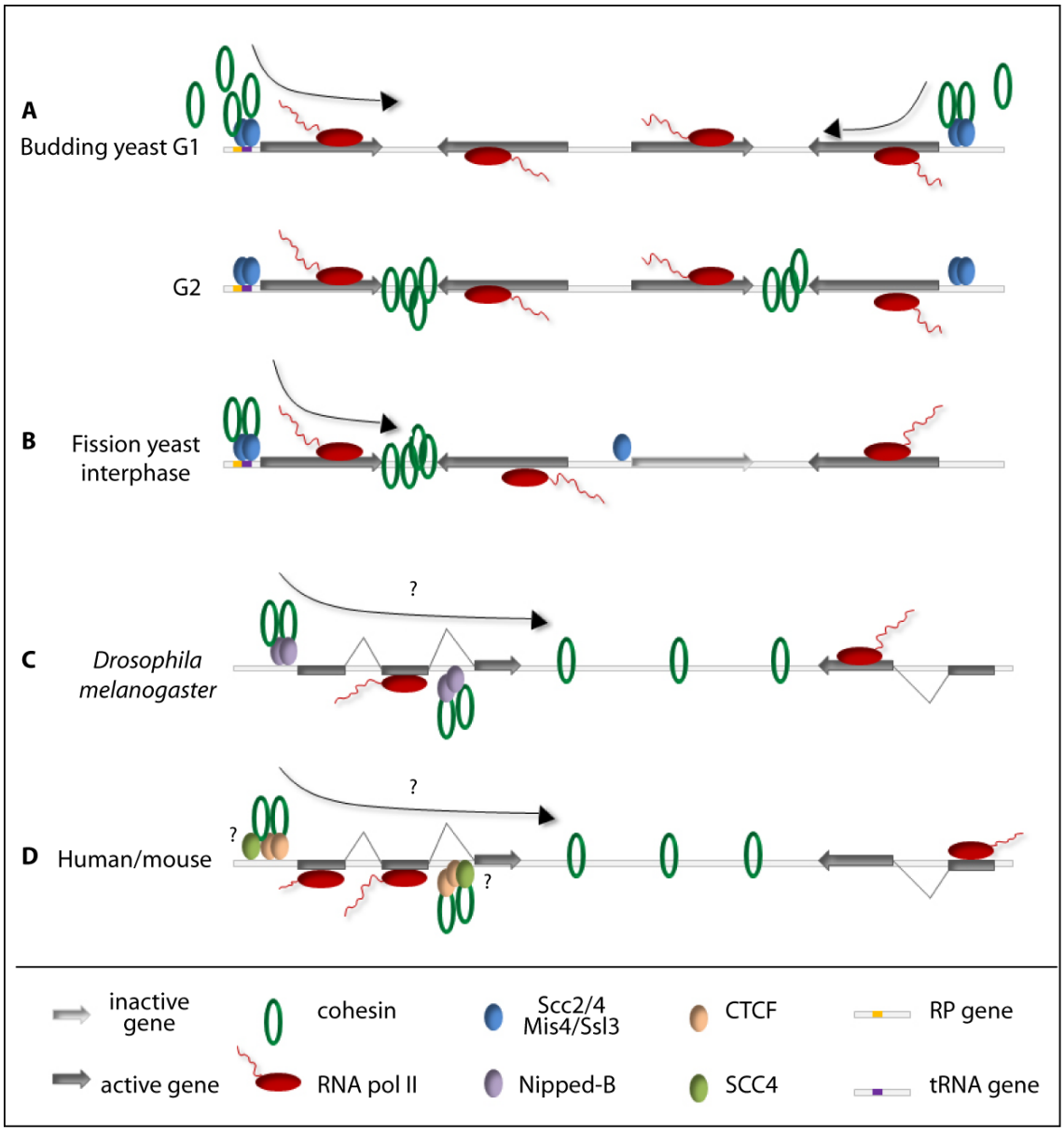

(Parelho et al, 2008; Rubio et al, 2008; Stedman et al, 2008; Wendt et al, 2008). *Drosophila* cohesin together with its loader Nipped-B is also involved in transcriptional regulation (Rollins et al, 2004; Rollins et al, 1999). These observations suggest that the subpool of cohesin bound to its loading sites might be predominantly involved in gene regulation.

But can cohesin's gene regulatory role be separated from its function in sister chromatid cohesion? Cohesin was recently detected in *Drosophila* neurons, permanently arrested cells that have no sister chromatids in their cells. Furthermore, inactivation of cohesin in a certain type of neurons in developing *Drosophila* brains had drastic effects on expression of the ecdysone hormone receptor. The neurons were defective in eliminating unwanted projections and eventually, the larvae died during development (Pauli et al,

2008; Schuldiner et al, 2008). These observations suggest that cohesin can regulate genes independently of its function in sister chromatid cohesion. Furthermore, they open up the possibility that the stability of cohesin binding may differ between cohesin at its loading sites and cohesin that associates with distant convergent sites. We predict that cohesin may associate in a more dynamic fashion with its loading sites to promote reversible interactions between gene regulatory regions. Cohesin might then be stabilised along chromosomes at distant convergent sites, a pre-requisite for enduring sister chromatid cohesion. It will be interesting to test whether either one or both of the subpools of chromosome-bound cohesin are further stabilised by acetylation of their Smc3 subunit during the establishment of sister chromatid cohesion in S phase (Ben-Shahar et al, 2008; Unal et al, 2008; Zhang et al, 2008).

5.1.3 A non-random cohesin distribution among convergent sites

Cohesin is not distributed randomly along fission yeast chromosome arms but occupies an ordered subset of convergent sites. Interestingly, we found that two neighbouring cohesin peaks at convergent sites were never as far apart from each other as would be expected if the distribution was normal. This ensures an even cohesin pattern with no large gaps between neighbouring cohesin sites. The non-random cohesin pattern seems to be achieved by various mechanisms including the gene arrangement around convergent genes, the expression levels of convergent genes and the proximity to cohesin loading sites. Furthermore, we found that not only the cohesin pattern was non-random but that the gene arrangement along fission yeast chromosomes favoured the frequent alteration of gene orientations at the expense of parallel gene runs. This raised the number of convergent sites by 107 along the entire fission yeast genome and thus increased the number of potential binding sites for cohesin. We do not know whether the benefit of regularly spaced cohesin along chromosome arms contributed to the selection of this non-random gene order. No such non-random gene arrangement has been observed in budding yeast where almost all convergent sites are bound by cohesin, thus reducing the effect of long parallel gene runs (Lengronne et al, 2004). But where does the difference in the amount of cohesin-bound convergent sites arise from? One possibility could be the higher frequency of cohesin loading sites in budding yeast e.g. as a consequence of a larger number of tRNA genes - 274 in the budding yeast genome compared to 174 in

the fission yeast genome many of which are found clustered around centromeres (Takahashi et al, 1991; Wood et al, 2002).

What could be the biological importance of an even cohesin patterning along chromosomes? As cohesin is involved in DNA repair by homologous recombination, frequent intervals of cohesin sites might ensure the close proximity of sister chromatids at any possible site of DNA damage which in turn could increase the efficiency of DNA repair.

5.1.4 Conserved and unique aspects of cohesin behaviour during mitosis

The analysis of the resolution of sister chromatid cohesion in fission yeast have revealed both conserved as well as so far unknown features.

5.1.4.1 Two-step resolution of cohesion in fission yeast

A small, but significant fraction of cohesin was released into the soluble pool when chromosomes condensed before metaphase. This happened in an apparently cleavage-independent manner similar to what has been observed in higher eukaryotes during the prophase pathway (Sumara et al, 2000; Waizenegger et al, 2000). The majority of cohesin then remained on chromosomes until anaphase onset when approximately half of the chromatin-bound fraction of cohesin was released into the soluble pool, probably upon cleavage of the Rad21 cohesin subunit. The distribution of the remaining chromosomal cohesin, both after cleavage-independent removal in prophase and cleavage-dependent removal in anaphase, appeared largely unchanged along chromosomes arms. This suggests that cohesin was evenly removed from most, if not all, cohesin sites, indicating that cohesin removal is not linked to specific locations along chromosomes. Interestingly, a substantial cohesin pool stayed on chromosomes throughout mitosis, suggesting that this subpool of cohesin was not involved in sister chromatid cohesion. It might have been loaded onto chromosomes in G2, which makes up a considerable time of the cell cyle in fission yeast (Alfa et al, 1993), and would therefore not have been involved in cohesion establishment during S phase (Haering et al, 2004; Lengronne et al, 2006; Uhlmann & Nasmyth, 1998).

What would be the biological function of such a non-cohesive cohesin pool? There are two attractive possibilities. Some cohesin of this subpool could be involved in transcriptional regulation which might continue throughout mitosis. Alternatively or additionally, persistent cohesin could be important for cohesion establishment in the subsequent

S phase as a short G1 phase in fission yeast might not allow sufficient time for *de novo* loading of cohesin onto chromosomes. Whether and how separase is able to specifically recognise and cleave the cohesin involved in sister chromatid cohesion is currently unknown. It will be interesting to test whether there are structural clues that might lead to a differential recognition pattern of cohesin such as post-translational modifications.

5.1.4.2 A complex set of cohesin behaviours at centromeres

As a unique feature, cohesin at centromeres displayed surprisingly dynamic behaviour and spread onto neighbouring sequences along chromosome arms during mitosis when Swi6 was removed from chromosomes (Chen et al, 2008; Fischle et al, 2005; Hirota et al, 2005). Cohesin spreading could therefore be the consequence of the loss of Swi6-dependent anchoring to centromeric repeats (Bernard et al, 2001; Nonaka et al, 2002). Centromeric cohesin may be loaded to the central core of the centromere where we found the cohesin loader Mis4/Ssl3 to be enriched and where we observed cohesin accumulation in G1. From there, cohesin might translocate outwards to be no longer detected at the central core in G2. Its tethering to the outer centromeres by Swi6 then ensures persisting enrichment at centromeres required for the biorientation of sister chromatids on the mitotic spindle. Release from its tether during mitosis might facilitate the dynamic centromere breathing behaviour as a part of the biorientation process (Goshima & Yanagida, 2000). The observed spreading of cohesin onto neighbouring chromosomal arm regions might therefore be a consequence of centromere breathing rather than have its own explicit function. However, it can be imagined that the released cohesin might help to redistribute cohesin along chromosome arms where it could further be translocated to convergent sites by the transcription machinery. Again, this might be particularly important in fission yeast, since, due to a short G1 phase, little time is available to ensure sufficient cohesin association along chromosomes before the following S phase.

5.2 Condensin's chromosomal association pattern

5.2.1 A common loading mechanism for eukaryotic SMC complexes?

We observed a largely overlapping binding pattern between fission yeast condensin and the cohesin loader Mis4/Ssl3, similar to what has been reported in budding yeast (D'Ambrosio et al, 2008). This has led to the hypothesis that condensin might be recruited to the same sites where cohesin is loaded onto chromosomes (D'Ambrosio et al, 2008). In line with this hypothesis, condensin levels decreased on chromosomes upon inactivation of the cohesin loader Scc2/4 in budding yeast (D'Ambrosio et al, 2008). Furthermore, a functional connection between Scc2/4 and condensin has also been detected in budding yeast, as chromosome condensation was reduced when Scc2/4 was inactivated (D'Ambrosio et al, 2008). Interestingly, the cohesin loader Scc2/4 has also been implicated in recruiting the Smc5/Smc6 complex to chromosomes (Betts Lindroos et al, 2006), suggesting that all SMC complexes might be loaded in a similar fashion. This seems reasonable as all complexes share structural similarities. However, the exact mechanism of the loading reactions remains to be determined.

If condensin is recruited to chromosomes by the cohesin loader, why does it not translocate away from its loading sites as the majority of cohesin does? Even though this difference accounts for the largely distinct distributions of cohesin and condensin along chromosomes, it might be more of a quantitative rather than a qualitative nature. In budding yeast, condensin, like cohesin, is largely excluded from ORFs (D'Ambrosio et al, 2008). Furthermore, upon induction of RNA Pol I or II transcription within the rDNA repeats, condensin has been shown to be removed from transcribed regions (Johzuka & Horiuchi, 2007; Wang et al, 2006). In addition, condensin, recruited upstream of the actively transcribed LSM4 gene, could be detected both up- and downstream of the gene (D'Ambrosio et al, 2008), suggesting that condensin, like cohesin, can respond to Pol II transcription by translocation. These observations open up the possibility that condensin may indeed be translocated from its loading sites like cohesin does but that this happens with reduced processivity. This hypothesis is in line with fluorescence recovery after photobleaching studies that revealed a faster exchange of

human condensin with the soluble pool, as compared to cohesin (Gerlich et al, 2006a; Gerlich et al, 2006b).

5.2.2 Condensin and nuclear architecture

During our analysis of the Mis4/Ssl3 distribution along chromosomes we observed that Sfc6, a subunit of the TFIIIC complex that regulates tRNA genes was not only enriched at tRNA genes but, to a weaker extent, could also be detected near ribosomal protein genes. Likewise, the forkhead domain containing protein Fhl1, a putative paralog of the budding yeast Fhl1 protein involved in the regulation of ribosomal protein genes was not only bound near ribosomal protein genes but also accumulated close to tRNA genes albeit to a lesser extent. It is not known whether TFIIIC also controls ribosomal protein genes and vice versa, whether Fhl1 can also regulates Pol III transcribed tRNA genes. The fact that we detect condensin at both tRNA and ribosomal protein genes raises the possibility that the observed interactions arise from an indirect association of these regions within the nucleus which might be mediated by condensin. In line with this hypothesis, condensin has recently been reported to be required for the physical interactions of tRNA genes that can be found clustered in the nuclear periphery in interphase (Noma et al, 2006; Thompson et al, 2003). It will be interesting to address whether ribosomal protein genes also cluster within the nuclear space and whether they also physically associate with tRNA genes. This is likely to help reveal condensin’s mode of action in compacting the genome of which surprisingly little is known so far.

5.3 Stabilisation of cohesin binding to chromosomes in S phase

5.3.1 A role for cohesin dynamics in gene regulation?

The analysis of cohesin association with chromosomes in G1 shows that continued activity of the cohesin loader Mis4/Ssl3 is required for the maintenance of cohesin along chromosomes. This is reminiscent of the cohesin behaviour in higher eukaryotes where cohesin binding to chromosomes is dynamic in G1 (Gerlich et al, 2006b). The fact that this mode of cohesin behaviour is conserved across evolution suggests an important but yet unresolved biological function for cohesin dynamics. As DNA has not been replicated in G1 and cohesin is bound to single chromatids only, it can be imagined that the dynamics of cohesin might be important for its role in gene regulation. Cohesin instability along G1 chromosomes, both in fission yeast and in higher eukaryotes, depends on the cohesin destabiliser protein Wapl (Bernard et al, 2008; Kueng et al, 2006). It is not known how Wapl achieves this but it might be involved in unloading cohesin from chromosomes. As Wapl was identified as a direct association partner of the cohesin complex it might achieve this by altering the intrinsic stability of cohesin (Gandhi et al, 2006; Kueng et al, 2006). The fission yeast *wpl* gene, although crucial for cohesin dynamics, is non-essential for viability, and cells, lacking Wapl grow indistinguishably from wild type cells (Bernard et al, 2008). Therefore, Wapl-controlled cohesin dynamics in G1 must be dispensible for the essential process of cohesion establishment during S phase. It will be interesting to directly probe whether cohesin dynamics are important for gene regulation. One possibility would be to test whether any genes are misregulated in cells in which cohesin dynamics are inhibited, e.g. in Wapl depleted cells.

5.3.2 Cohesin stabilisation and cohesion establishment

The establishment of sister chromatid cohesion usually occurs concomitantly with DNA replication during S-phase (Uhlmann & Nasmyth, 1998), and in mammalian cells, the stabilisation of cohesin is tightly linked to S phase progression (Gerlich et al, 2006b). Therefore, the question arises whether cohesin stabilisation is also linked to cohesion establishment during DNA replication. In G2 cells cohesin was only partially stabilised

along chromosomes when the acetyltransferase Eso1 was inactivated. As Eso1 is required for cohesion establishment, this result suggests that cohesin stabilisation can at least partially be attributed to the process of cohesion establishment. But what molecular events could trigger the change in the stability of cohesin binding to chromosomes? Three recent studies have reported the acetylation of Smc3 cohesin subunit by Eco1 in yeast and human during cohesion establishment in S phase (Ben-Shahar et al, 2008; Unal et al, 2008; Zhang et al, 2008), making this an attractive candidate.

But is cohesin stabilisation a pre-requisite for cohesion establishment or does it arise as a consequence of this process? Or might the reality be a combination of both? A change in the behaviour of cohesin binding might initially facilitate cohesion establishment. As cohesion between sister chromatids establishes, cohesin might further become stabilised on chromosomes. Even though our results are not able to distinguish between these possibilities they show that, using HU-arrested cells, cohesin stabilisation can clearly be uncoupled from cohesion establishment. In HU-arrested cells little DNA is replicated but cohesin is largely stabilised along chromosomes. Importantly, cohesin is evenly stabilised at its chromosomal association sites, both in unreplicated regions, where cohesion between sister chromatids has not yet been established, and in replicated regions. Therefore, cohesin stabilisation in these conditions appears to be cell-cycle regulated and independent of DNA replication and cohesion establishment.

But how does the DNA replication-independent cohesin stabilisation observed in HU-treated cells relate to the cohesin stabilisation in an unperturbed S phase? In response to HU-treatment, a separate pathway of cohesin stabilisation might be triggered that does not usually act on cohesin during normal S phase progression. Alternatively, the pathway for cohesin stabilisation in an unperturbed S phase might not be that different from the one observed in HU-induced early S phase arrest. Even during normal S phase progression RPA-bound single-stranded DNA activates the intra S checkpoint, leading to the inhibition of late origins (Marheineke & Hyrien, 2004; Miao et al, 2003; Shechter & Gautier, 2005; Sorensen et al, 2004). Therefore, it has been suggested that an HU-induced S phase arrest is a result of an amplified level of checkpoint activation that happens at milder levels during normal S phase progression (Shechter & Gautier, 2005). In this scenario, HU-mediated fork-stalling may exacerbate a cohesin stabilisation reaction that usually takes place at lower levels or exclusively in close proximity to the replication fork (Bernard et al, 2008). Therefore, our analysis allows us to suggest that co-

hesin stabilisation and DNA replication/cohesion establishment may be temporally linked but mechanistically different during normal S phase progression.

Our observations open up the possibility that cohesin stabilisation precedes DNA replication, suggesting that cohesin stabilisation might be a pre-requisite for cohesion establishment rather than its consequence. Considering the recent findings that Eco1 acetylates the Smc3 subunit of cohesin during S phase, it will be interesting to test whether acetylated cohesin is the stabilised substrate for cohesion establishment.

6 References

Alberts B, Johnson A, Lewis J, Raff M, Roberts K, Walter P (2002) *Molecular Biology of the Cell*, 4th edn. New York: Garland Science.

Alfa C, Fantes P, Hyams J, McLeod M, Warbrick E (1993) *Experiments with fission yeast: a laboratory course manual*, Cold Spring Harbor, NY: Cold Spring Harbor Laboratory Press.

Anderson DE, Losada A, Erickson HP, Hirano T (2002) Condensin and cohesin display different arm conformations with characteristic hinge angles. *J Cell Biol* **156:** 419-424

Aono N, Sutani T, Tomonaga T, Mochida S, Yanagida M (2002) Cnd2 has dual roles in mitotic condensation and interphase. *Nature* **417:** 197-202

Arumugam P, Gruber S, Tanaka K, Haering CH, Mechtler K, Nasmyth K (2003) ATP hydrolysis is required for cohesin's association with chromosomes. *Curr Biol* **13:** 1941-1953

Ayte J, Leis JF, Herrera A, Tang E, Yang H, DeCaprio JA (1995) The Schizosaccharomyces pombe MBF complex requires heterodimerization for entry into S phase. *Mol Cell Biol* **15**(5)**:** 2589-2599

Bahler J, Wu JQ, Longtine MS, Shah NG, McKenzie A, 3rd, Steever AB, Wach A, Philippsen P, Pringle JR (1998) Heterologous modules for efficient and versatile PCR-based gene targeting in Schizosaccharomyces pombe. *Yeast* **14**(10)**:** 943-951

Bannister AJ, Zegerman P, Partridge JF, Miska EA, Thomas JO, Allshire RC, Kouzarides T (2001) Selective recognition of methylated lysine 9 on histone H3 by the HP1 chromo domain. *Nature* **410**(6824)**:** 120-124

Ben-Shahar TR, Heeger S, Lehane C, East P, Flynn H, Skehel M, Uhlmann F (2008) Eco1-dependent cohesin acetylation during establishment of sister chromatid cohesion. *Science* **321**(5888)**:** 563-566

Bernard P, Drogat J, Maure J-F, Dheur S, Vaur S, Genier S, Javerzat J-P (2006) A screen for cohesion mutants uncovers Ssl3, the fission yeast counterpart of the cohesin loading factor Scc4. *Curr Biol* **16**(9)**:** 875-881

Bernard P, Maure JF, Partridge JF, Genier S, Javerzat JP, Allshire RC (2001) Requirement of heterochromatin for cohesion at centromeres. *Science* **294:** 2539-2542

Bernard P, Schmidt CK, Vaur S, Dheur S, Drogat J, Genier S, Ekwall K, Uhlmann F, Javerzat JP (2008) Cell-cycle regulation of cohesin stability along fission yeast chromosomes. *EMBO J* **27**(1)**:** 111-121

Betts Lindroos H, Ström L, Itoh T, Katou Y, Shirahige K, Sjögren C (2006) Chromosomal association of the Smc5/6 complex reveals that it functions in differently regulated pathways. *Mol Cell* **22:** 755-767

Bhalla N, Biggins S, Murray AW (2002) Mutation of *YCS4*, a budding yeast condensin subunit, affects mitotic and nonmitotic chromosome behavior. *Mol Biol Cell* **13:** 632-645

Bhat MA, Philp AV, Glover DM, Bellen HJ (1996) Chromatid segregation at anaphase requires the *barren* product, a novel chromosome-associated protein that interacts with topoisomerase II. *Cell* **87:** 1103-1114

Birkenbihl RP, Subramani S (1992) Cloning and characterization of rad21 an essential gene of Schizosaccharomyces pombe involved in DNA double-strand-break repair. *Nucleic Acids Res* **20**(24)**:** 6605-6611

Birkenbihl RP, Subramani S (1995) The *rad21* gene product of *Schizosaccharomyces pombe* is a nuclear, cell cycle-regulated phosphoprotein. *J Biol Chem* **270**(13)**:** 7703-7711

Chan RC, Chan A, Jeon M, Wu TF, Pasqualone D, Rougvie AE, Meyer BJ (2003) Chromosome cohesion is regulated by a clock gene paralogue TIM-1. *Nature* **423**(6943)**:** 1002-1009

Chang CR, Wu CS, Hom Y, Gartenberg MR (2006) Targeting of cohesin by transcriptionally silent chromatin. *Genes Dev* **19**(24)**:** 3031-3042

Chen ES, Zhang K, Nicolas E, Cam HP, Zofall M, Grewal SI (2008) Cell cycle control of centromeric repeat transcription and heterochromatin assembly. *Nature* **451**(7179)**:** 734-737

Ciosk R, Shirayama M, Shevchenko A, Tanaka T, Toth A, Shevchenko A, Nasmyth K (2000) Cohesin's binding to chromosomes depends on a separate complex consisting of Scc2 and Scc4 proteins. *Mol Cell* **5:** 1-20

Cohen-Fix O, Peters J-M, Kirschner MW, Koshland D (1996) Anaphase initiation in *Saccharomyces cerevisiae* is controlled by the APC-dependent degradation of the anaphase inhibitor Pds1p. *Genes Dev* **10:** 3081-3093

D'Ambrosio C, Schmidt CK, Katou Y, Kelly G, Itoh T, Shirahige K, Uhlmann F (2008) Identification of cis-acting sites for condensin loading onto budding yeast chromosomes. *Genes Dev* **22**(16)**:** 2215-2227

Ding DQ, Sakurai N, Katou Y, Itoh T, Shirahige K, Haraguchi T, Hiraoka Y (2006) Meiotic cohesins modulate chromosome compaction during meiotic prophase in fission yeast. *J Cell Biol* **174**(4)**:** 499-508

Donze D, Adams CR, Rine J, Kamakaka RT (1999) The boundaries of the silenced *HMR* domain in *Saccharomyces cerevisiae*. *Genes Dev* **13:** 698-708

Dorsett D (2007) Roles of the sister chromatid cohesion apparatus in gene expression, development, and human syndromes. *Chromosoma* **116**(1)**:** 1-13

Fischle W, Tseng BS, Dormann HL, Ueberheide BM, Garcia BA, Shabanowitz J, Hunt DF, Funabiki H, Allis CD (2005) Regulation of HP1-chromatin binding by histone H3 methylation and phosphorylation. *Nature* **438**(7071)**:** 1116-1122

Flemming W (1882) *Zellsubstantz, Kern und Zelltheilung*, Leipzig, Germany: F.C.W. Vogel.

Fukagawa T, Nogami M, Yoshikawa M, Ikeno M, Okazaki T, Takami Y, Nakayama T, Oshimura M (2004) Dicer is essential for formation of the heterochromatin structure in vertebrate cells. *Nat Cell Biol* **6**(8)**:** 784-791

Furuya K, Takahashi K, Yanagida M (1998) Faithful anaphase is ensured by Mis4, a sister chromatid cohesion molecule required in S phase and not destroyed in G_1 phase. *Genes Dev* **12:** 3408-3418

Gandhi R, Gillespie PJ, Hirano T (2006) Human Wapl is a cohesin-binding protein that promotes sister-chromatid resolution in mitotic prophase. *Curr Biol* **16**(24)**:** 2406-2417

Gause M, Schaaf CA, Dorsett D (2008) Cohesin and CTCF: cooperating to control chromosome conformation? *Bioessays* **30**(8)**:** 715-718

Gerlich D, Beaudouin J, Kalbfuss B, Daigle N, Eils R, Ellenberg J (2003) Global chromosome positions are transmitted through mitosis in mammalian cells. *Cell* **112:** 751-764

Gerlich D, Hirota T, Koch B, Peters J-M, Ellenberg J (2006a) Condensin I stabilizes chromosomes mechanically through a dynamic interaction in live cells. *Curr Biol* **16:** 333-344

Gerlich D, Koch B, Dupeux F, Peters J-M, Ellenberg J (2006b) Live-cell imaging reveals a stable cohesin-chromatin interaction after but not before DNA replication. *Curr Biol* **16:** 1571-1578

Gillespie PJ, Hirano T (2004) Scc2 couples replication licensing to sister chromatid cohesion in *Xenopus* egg extracts. *Curr Biol* **14:** 1598-1603

Gimenez-Abian JF, Sumara I, Hirota T, Hauf S, Gerlich D, de la Torre C, Ellenberg J, Peters JM (2004) Regulation of sister chromatid cohesion between chromosome arms. *Curr Biol* **14**(13)**:** 1187-1193

Glynn EF, Megee PC, Yu HG, Mistrot C, Unal E, Koshland DE, DeRisi JL, Gerton JL (2004) Genome-wide mapping of the cohesin complex in the yeast *Saccharomyces cerevisiae*. *PLoS Biol* **2**(9)**:** 1325-1339

Gondor A, Ohlsson R (2008) Chromatin insulators and cohesins. *EMBO Rep* **9**(4)**:** 327-329

Goshima G, Yanagida M (2000) Establishing biorientation occurs with precocious separation of the sister kinetochores, but not the arms, in the early spindle of budding yeast. *Cell* **100**(6)**:** 619-633

Gould KL, Nurse P (1989) Tyrosine phosphorylation of the fission yeast cdc2+ protein kinase regulates entry into mitosis. *Nature* **342**(6245)**:** 39-45

Guacci V, Koshland D, Strunnikov A (1997) A direct link between sister chromatid cohesion and chromosome condensation revealed through analysis of *MCD1* in S. cerevisiae. *Cell* **91:** 47-57

Gullerova M, Proudfoot NJ (2008) Cohesin complex promotes transcriptional termination between convergent genes in S. pombe. *Cell* **132**(6)**:** 983-995

Haering CH, Farcas AM, Arumugam P, Metson J, Nasmyth K (2008) The cohesin ring concatenates sister DNA molecules. *Nature* **454**(7202)**:** 297-301

Haering CH, Löwe J, Hochwagen A, Nasmyth K (2002) Molecular architecture of SMC proteins and the yeast cohesin complex. *Mol Cell* **9:** 773-788

Haering CH, Schoffnegger D, Nishino T, Helmhart W, Nasmyth K, Löwe J (2004) Structure and stability of cohesin's Smc1-kleisin interaction. *Mol Cell* **15:** 951-964

Haldar D, Kamakaka RT (2006) tRNA genes as chromatin barriers. *Nat Struct Mol Biol* **13**(3)**:** 192-193

Hall IM, Noma K, Grewal SIS (2003) RNA interference machinery regulates chromosome dynamics during mitosis and meiosis in fission yeast. *Proc Natl Acad Sci USA* **100**(1)**:** 193-198

Hartman T, Stead K, Koshland D, Guacci V (2000) Pds5p is an essential chromosomal protein required for both sister chromatid cohesion and condensation in *Saccharomyces cerevisiae*. *J Cell Biol* **151**(3)**:** 613-626

Hauf S, Biswas A, Langegger M, Kawashima SA, Tsukahara T, Watanabe Y (2007) Aurora controls sister kinetochore mono-orientation and homolog bi-orientation in meiosis-I. *EMBO J* **26**(21)**:** 4475-4486

Hauf S, Roitinger E, Koch B, Dittrich CM, Mechtler K, Peters JM (2005) Dissociation of cohesin from chromosome arms and loss of arm cohesion during early mitosis depends on phosphorylation of SA2. *PLoS Biol* **3**(3)**:** e69

Hauf S, Waizenegger IC, Peters JM (2001) Cohesin cleavage by separase required for anaphase and cytokinesis in human cells. *Science* **293**(5533)**:** 1320-1323

Heale JT, Ball AR, Jr., Schmiesing JA, Kim JS, Kong X, Zhou S, Hudson DF, Earnshaw WC, Yokomori K (2006) Condensin I interacts with the PARP-1-XRCC1 complex and functions in DNA single-strand break repair. *Mol Cell* **21**(6)**:** 837-848

Heichinger C, Penkett CJ, Bahler J, Nurse P (2006) Genome-wide characterization of fission yeast DNA replication origins. *EMBO J* **25**(21)**:** 5171-5179

Hirano T (2005) Condensins: organizing and segregating the genome. *Curr Biol* **15**(7)**:** R265-275

Hirano T (2006) At the heart of the chromosome: SMC proteins in action. *Nat Rev Mol Cell Biol* **7:** 311-322

Hirano T, Mitchison TJ (1994) A heterodimeric coiled-coil protein required for mitotic chromosome condensation in vitro. *Cell* **79:** 449-458

Hiraoka Y, Toda T, Yanagida M (1984) The NDA3 gene of fission yeast encodes beta-tubulin: a cold-sensitive nda3 mutation reversibly blocks spindle formation and chromosome movement in mitosis. *Cell* **39**(2 Pt 1)**:** 349-358

Hirota T, Lipp JJ, Toh BH, Peters JM (2005) Histone H3 serine 10 phosphorylation by Aurora B causes HP1 dissociation from heterochromatin. *Nature* **438**(7071)**:** 1176-1180

Hoque MT, Ishikawa F (2001) Human chromatid cohesin component hRad21 is phosphorylated in M phase and associated with metaphase centromeres. *J Biol Chem* **276**(7)**:** 5059-5067

Horsfield JA, Anagnostou SH, Hu JK, Cho KH, Geisler R, Lieschke G, Crosier KE, Crosier PS (2007) Cohesin-dependent regulation of Runx genes. *Development* **134**(14)**:** 2639-2649

Huang CE, Milutinovich M, Koshland D (2005) Rings, bracelet or snaps: fashionable alternatives for Smc complexes. *Philos Trans R Soc Lond B Biol Sci* **360:** 537-542

Hudson DF, Vagnarelli P, Gassmann R, Earnshaw WC (2003) Condensin is required for nonhistone protein assembly and structural integrity of vertebrate mitotic chromosomes. *Dev Cell* **5**(2)**:** 323-336

Ivanov D, Nasmyth K (2005) A topological interaction between cohesin rings and a circular minichromosome. *Cell* **122:** 849-860

Iyer VR, Horak CE, Scafe CS, Botstein D, Snyder M, Brown PO (2001) Genomic binding sites of the yeast cell-cycle transcription factors SBF and MBF. *Nature* **409**(6819)**:** 533-538

Johzuka K, Horiuchi T (2007) RNA polymerase I transcription obstructs condensin association with 35S rRNA coding regions and can cause contraction of long repeat in Saccharomyces cerevisiae. *Genes Cells* **12**(6)**:** 759-771

Katou Y, Kanoh Y, Bandoh M, Noguchi H, Tanaka H, Ashikari T, Sugimoto K, Shirahige K (2003) S-phase checkpoint proteins Tof1 and Mrc1 form a stable replication-pausing complex. *Nature* **424:** 1078-1083

Keeney JB, Boeke JD (1994) Efficient targeted integration at leu1-32 and ura4-294 in Schizosaccharomyces pombe. *Genetics* **136**(3)**:** 849-856

Kenna MA, Skibbens RV (2003) Mechanical link between cohesion establishment and DNA replication: Ctf7p/Eco1p, a cohesion establishment factor, associates with three different replication factor C complexes. *Mol Cell Biol* **23**(8)**:** 2999-3007

Kim SM, Dubey DD, Huberman JA (2003) Early-replicating heterochromatin. *Genes Dev* **17**(3)**:** 330-335

Kitajima TS, Miyazaki Y, Yamamoto M, Watanabe Y (2003) Rec8 cleavage by separase is required for meiotic nucelar divisions in fission yeast. *EMBO J* **22**(20)**:** 5643-5653

Kitajima TS, Sakuno T, Ishiguro K, Iemura S, Natsume T, Kawashima SA, Watanabe Y (2006) Shugoshin collaborates with protein phosphatase 2A to protect cohesin. *Nature* **441**(7089)**:** 46-52

Kohli J (1987) Genetic nomenclature and gene list of the fission yeast Schizosaccharomyces pombe. *Curr Genet* **11**(8)**:** 575-589

Kueng S, Hegemann B, Peters BH, Lipp JJ, Schleiffer A, Mechtler K, Peters JM (2006) Wapl controls the dynamic association of cohesin with chromatin. *Cell* **127**(5)**:** 955-967

Kumaran RI, Thakar R, Spector DL (2008) Chromatin dynamics and gene positioning. *Cell* **132**(6)**:** 929-934

Lackner DH, Beilharz TH, Marguerat S, Mata J, Watt S, Schubert F, Preiss T, Bahler J (2007) A network of multiple regulatory layers shapes gene expression in fission yeast. *Mol Cell* **26**(1)**:** 145-155

Laemmli UK, Kas E, Poljak L, Adachi Y (1992) Scaffold-associated regions: cis-acting determinants of chromatin structural loops and functional domains. *Curr Opin Genet Dev* **2**(2)**:** 275-285

Lehmann AR (2005) The role of SMC proteins in the responses to DNA damage. *DNA Repair (Amst)* **4**(3)**:** 309-314

Lehmann AR, Walicka M, Griffith DJF, Murray JM, Watts FZ, McCready S, Carr AM (1995) The *rad18* gene of *Schizosaccharomyces pombe* defines a new subgroup of the SMC superfamily involved in DNA repair. *Mol Cell Biol* **15**(12)**:** 7067-7080

Lengauer C, Kinzler KW, Vogelstein B (1998) Genetic instabilities in human cancers. *Nature* **396:** 643-649

Lengronne A, Katou Y, Mori S, Yokobayashi S, Kelly GP, Itoh T, Watanabe Y, Shirahige K, Uhlmann F (2004) Cohesin relocation from sites of chromosomal loading to places of convergent transcription. *Nature* **430:** 573-578

Lengronne A, McIntyre J, Katou Y, Kanoh Y, Hopfner K-P, Shirahige K, Uhlmann F (2006) Establishment of sister chromatid cohesion at the *S. cerevisiae* replication fork. *Mol Cell* **23:** 787-799

Leupold U (1950) Die Vererbung von Homothallie und Heterothallie bei *Schizosaccharomyces pombe*. *C R Trav Lab Carlsberg Ser Physiol* **24:** 381-480

Lindow JC, Britton RA, Grossman AD (2002) Structural maintenance of chromosomes protein of Bacillus subtilis affects supercoiling in vivo. *J Bacteriol* **184**(19)**:** 5317-5322

Losada A, Hirano M, Hirano T (1998) Identification of *Xenopus* SMC protein complexes required for sister chromatid cohesion. *Genes Dev* **12:** 1986-1997

Losada A, Hirano M, Hirano T (2002) Cohesin release is required for sister chromatid resolution but not for condensin-mediated compaction, at the onset of mitosis. *Genes Dev* **16**(23)**:** 3004-3016

Losada A, Hirano T (2005) Dynamic molecular linkers of the genome: the first decade of SMC proteins. *Genes Dev* **19**(11)**:** 1269-1287

Lupo R, Breiling A, Bianchi ME, Orlando V (2001) *Drosophila* chromosome condensation proteins topoisomerase II and barren colocalize with polycomb and maintain *Fab-7* PRE silencing. *Mol Cell* **7:** 127-136

Marheineke K, Hyrien O (2004) Control of replication origin density and firing time in Xenopus egg extracts: role of a caffeine-sensitive, ATR-dependent checkpoint. *J Biol Chem* **279**(27)**:** 28071-28081

Mata J, Lyne R, Burns G, Bahler J (2002) The transcriptional program of meiosis and sporulation in fission yeast. *Nat Genet* **32**(1)**:** 143-147

Mayer ML, Gygi SP, Aebersold R, Hieter P (2001) Identification of RFC(Ctf18p, Ctf8p, Dcc1p): an alternative RFC complex required for sister chromatid cohesion in S. cerevisiae. *Mol Cell* **7**(5)**:** 959-970

McGuinness BE, Hirota T, Kudo NR, Peters J-M, Nasmyth K (2005) Shugoshin prevents dissociation of cohesin from centromeres during mitosis in vertebrate cells. *PLoS Biol* **3**(3)**:** 433-449

Mei Y, Huang G, Solovev AA, Urena EB, Mönch I, Ding F, Reindl T, Fu RKY, Chu PK, Schmidt OG (2008) Versatile approach for integrative and functionalised tubes by strain engineering of nanomembranes on polymers. *Advanced Materials* **20:** 1-6

Miao H, Seiler JA, Burhans WC (2003) Regulation of cellular and SV40 virus origins of replication by Chk1-dependent intrinsic and UVC radiation-induced checkpoints. *J Biol Chem* **278**(6)**:** 4295-4304

Michaelis C, Ciosk R, Nasmyth K (1997) Cohesins: Chromosomal proteins that prevent premature separation of sister chromatids. *Cell* **91:** 35-45

Miles J, Formosa T (1992) Evidence that POB1, a Saccharomyces cerevisiae protein that binds to DNA polymerase alpha, acts in DNA metabolism in vivo. *Mol Cell Biol* **12**(12)**:** 5724-5735

Misulovin Z, Schwartz YB, Li XY, Kahn TG, Gause M, MacArthur S, Fay JC, Eisen MB, Pirrotta V, Biggin MD, Dorsett D (2008) Association of cohesin and Nipped-B with transcriptionally active regions of the Drosophila melanogaster genome. *Chromosoma* **117**(1)**:** 89-102

Moldovan G-L, Pfander B, Jentsch S (2006) PCNA controls establishment of sister chromatid cohesion during S phase. *Mol Cell* **23:** 723-732

Moreno S, Klar A, Nurse P (1991) Molecular genetic analysis of fission yeast Schizosaccharomyces pombe. *Methods Enzymol* **194:** 795-823

Moreno S, Nurse P (1994) Regulation of progression through the G1 phase of the cell cycle by the rum1+ gene. *Nature* **367**(6460)**:** 236-242

Nakazawa N, Nakamura T, Kokubu A, Ebe M, Nagao K, Yanagida M (2008) Dissection of the essential steps for condensin accumulation at kinetochores and rDNAs during fission yeast mitosis. *J Cell Biol* **180**(6)**:** 1115-1131

Noma K, Cam HP, Maraia RJ, Grewal SIS (2006) A role for TFIIIC transcription factor complex in genome organization. *Cell* **125:** 859-872

Nonaka N, Kitajima T, Yokobayashi S, Xiao G, Yamamoto M, Grewal SIS, Watanabe Y (2002) Recruitment of cohesin to heterochromatic regions by Swi6/HP1 in fission yeast. *Nat Cell Biol* **4**(1)**:** 89-93

Nurse P, Thuriaux P, Nasmyth K (1976) Genetic control of the cell division cycle in the fission yeast Schizosaccharomyces pombe. *Mol Gen Genet* **146**(2)**:** 167-178

Olins AL, Olins DE (1974) Spheroid chromatin units (v bodies). *Science* **183**(122)**:** 330-332

Onn I, Heidinger-Pauli JM, Guacci V, Unal E, Koshland DE (2008) Sister Chromatid Cohesion: A Simple Concept with a Complex Reality. *Annu Rev Cell Dev Biol*

Ono T, Losada A, Hirano M, Myers MP, Neuwald AF, Hirano T (2003) Differential contributions of condensin I and condensin II to mitotic chromosome architecture in vertebrate cells. *Cell* **115:** 109-121

Panizza S, Tanaka T, Hochwagen A, Eisenhaber F, Nasmyth K (2000) Pds5 cooperates with cohesin in maintaining sister chromatid cohesion. *Curr Biol* **10**(24)**:** 1557-1564

Pardo M, Nurse P (2005) The nuclear rim protein Amo1 is required for proper microtubule cytoskeleton organisation in fission yeast. *J Cell Sci* **118**(Pt 8)**:** 1705-1714

Parelho V, Hadjur S, Spivakov M, Leleu M, Sauer S, Gregson HC, Jarmuz A, Canzonetta C, Webster Z, Nesterova T, Cobb BS, Yokomori K, Dillon N, Aragon L, Fisher AG, Merkenschlager M (2008) Cohesins functionally associate with CTCF on mammalian chromosome arms. *Cell* **132**(3)**:** 422-433

Partridge JF, Borgstrom B, Allshire RC (2000) Distinct protein interaction domains and protein spreading in a complex centromere. *Genes Dev* **14**(7)**:** 783-791

Patel PK, Arcangioli B, Baker SP, Bensimon A, Rhind N (2006) DNA replication origins fire stochastically in fission yeast. *Mol Biol Cell* **17**(1)**:** 308-316

Pauli A, Althoff F, Oliveira RA, Heidmann S, Schuldiner O, Lehner CF, Dickson BJ, Nasmyth K (2008) Cell-type-specific TEV protease cleavage reveals cohesin functions in Drosophila neurons. *Dev Cell* **14**(2)**:** 239-251

Peric-Hupkes D, van Steensel B (2008) Linking cohesin to gene regulation. *Cell* **132**(6)**:** 925-928

Petersen J, Paris J, Willer M, Philippe M, Hagan IM (2001) The *S. pombe* aurora-related kinase Ark1 associates with mitotic structures in a stage dependent manner and is required for chromosome segregation. *J Cell Sci* **114:** 4371-4384

Petronczki M, Chwalla B, Siomos MF, Yokobayashi S, Helmhart W, Deutschbauer AM, Davis RW, Watanabe Y, Nasmyth K (2004) Sister-chromatid cohesion mediated by the alternative RF-$C^{Ctf18/Dcc1/Ctf8}$, the helicase Chl1 and the polymerase-⟨-associated protein Ctf4 is essential for chromatid disjunction during meiosis II. *J Cell Sci* **117:** 3547-3559

Rao H, Uhlmann F, Nasmyth K, Varshavsky A (2001) Degradation of a cohesin subunit by the N-end rule pathway is essential for chromosome stability. *Nature* **410:** 955-959

Rea S, Eisenhaber F, O'Carroll D, Strahl BD, Sun ZW, Schmid M, Opravil S, Mechtler K, Ponting CP, Allis CD, Jenuwein T (2000) Regulation of chromatin structure by site-specific histone H3 methyltransferases. *Nature* **406**(6796)**:** 593-599

Reid RJD, Sunjevaric I, Kedacche M, Rothstein R (2002) Efficient PCR-based gene disruption in *Saccharomyces* strains using intergenic primers. *Yeast* **19:** 319-328

Riedel CG, Katis VL, Katou Y, Mori S, Itoh T, Helmhart W, Galova M, Petronczki M, Gregan J, Cetin B, Mudrak I, Ogris E, Mechtler K, Pelletier L, Buchholz F, Shirahige K, Nasmyth K (2006) Protein phosphatase 2A protects centromeric sister chromatid cohesion during meiosis I. *Nature* **441**(7089)**:** 53-61

Robinett CC, Straight A, Li G, Willhelm C, Sudlow G, Murray A, Belmont AS (1996) In vivo localization of DNA sequences and visualization of large-scale chromatin organization using lac operator/repressor recognition. *J Cell Biol* **135**(6 Pt 2)**:** 1685-1700

Rollins RA, Korom M, Aulner N, Martens A, Dorsett D (2004) *Drosophila* Nipped-B protein supports sister chromatid cohesion and opposes the stromalin/Scc3 cohesion factor to facilitate long-range activation of the *cut* gene. *Mol Cell Biol* **24**(8)**:** 3100-3111

Rollins RA, Morcillo P, Dorsett D (1999) Nipped-B, a Drosophila homologue of chromosomal adherins, participates in activation by remote enhancers in the *cut* and *Ultrabithorax* genes. *Genetics* **152:** 577-593

Rubio ED, Reiss DJ, Welcsh PL, Disteche CM, Filippova GN, Baliga NS, Aebersold R, Ranish JA, Krumm A (2008) CTCF physically links cohesin to chromatin. *Proc Natl Acad Sci U S A* **105**(24)**:** 8309-8314

Saka Y, Sutani T, Yamashita Y, Saitoh S, Takeuchi M, Nakaseko Y, Yanagida M (1994) Fission yeast cut3 and cut14, members of a ubiquitous protein family, are required for chromosome condensation and segregation in mitosis. *EMBO J* **13**(20)**:** 4938-4952

Sambrook J, Maniatis T, Fritsch EF (1989) *Molecular cloning: a laboratory manual.*: Cold Spring Harbor Laboratory Press.

Schawalder SB, Kabani M, Howald I, Choudhury U, Werner M, Shore D (2004) Growth-regulated recruitment of the essential yeast ribosomal protein gene activator Ifh1. *Nature* **432**(7020)**:** 1058-1061

Schleiffer A, Kaitna S, Maurer-Stroh S, Glotzer M, Nasmyth K, Eisenhaber F (2003) Kleisins: A superfamily of bacterial and eukaryotic SMC protein partners. *Mol Cell* **11:** 571-575

Schuldiner O, Berdnik D, Levy JM, Wu JS, Luginbuhl D, Gontang AC, Luo L (2008) piggyBac-based mosaic screen identifies a postmitotic function for cohesin in regulating developmental axon pruning. *Dev Cell* **14**(2)**:** 227-238

Shechter D, Gautier J (2005) ATM and ATR check in on origins: a dynamic model for origin selection and activation. *Cell Cycle* **4**(2)**:** 235-238

Sjögren C, Nasmyth K (2001) Sister chromatid cohesion is required for postreplicative double-strand break repair in *Saccharomyces cerevisiae*. *Curr Biol* **11:** 991-995

Skibbens RV, Corson LB, Koshland D, Hieter P (1999) Ctf7p is essential for sister chromatid cohesion and links mitotic chromosome structure to the DNA replication machinery. *Genes Dev* **13:** 307-319

Sorensen CS, Syljuasen RG, Lukas J, Bartek J (2004) ATR, Claspin and the Rad9-Rad1-Hus1 complex regulate Chk1 and Cdc25A in the absence of DNA damage. *Cell Cycle* **3**(7)**:** 941-945

Stead K, Aguilar C, Hartman T, Drexel M, Meluh P, Guacci V (2003) Pds5p regulates the maintenance of sister chromatid cohesion and is sumoylated to promote the dissolution of cohesion. *J Cell Biol* **163**(4)**:** 729-741

Stedman W, Kang H, Lin S, Kissil JL, Bartolomei MS, Lieberman PM (2008) Cohesins localize with CTCF at the KSHV latency control region and at cellular c-myc and H19/Igf2 insulators. *EMBO J* **27**(4)**:** 654-666

Ström L, Karlsson C, Betts Lindroos H, Wedahl S, Katou Y, Shirahige K, Sjögren C (2007) Postreplicative formation of cohesion is required for repair and induced by a single DNA break. *Science* **317:** 242-245

Ström L, Lindroos HB, Shirahige K, Sjögren C (2004) Postreplicative recruitment of cohesin to double-strand breaks is required for DNA repair. *Mol Cell* **16:** 1003-1015

Strom L, Sjogren C (2005) DNA damage-induced cohesion. *Cell Cycle* **4**(4)**:** 536-539

Strom L, Sjogren C (2007) Chromosome segregation and double-strand break repair - a complex connection. *Curr Opin Cell Biol* **19**(3)**:** 344-349

Strunnikov A, Hogan E, Koshland D (1995) *SMC2*, a *Saccharomyces cerevisiae* gene essential for chromosome segregation and condensation, defines a subgroup within the SMC family. *Genes Dev* **9:** 587-599

Sumara I, Vorlaufer E, Gieffers C, Peters BH, Peters J-M (2000) Characterization of vertebrate cohesin complexes and their regulation in prophase. *J Cell Biol* **151**(4)**:** 749-761

Sumara I, Vorlaufer E, Stukenberg PT, Kelm O, Redemann N, Nigg EA, Peters J-M (2002) The dissociation of cohesin from chromosomes in prophase is regulated by Polo-like kinase. *Mol Cell* **9:** 515-525

Sutani T, Yuasa T, Tomonaga T, Dohmae N, Takio K, Yanagida M (1999) Fission yeast condensin complex: essential roles of non-SMC subunits for condensation and Cdc2 phosphorylation of Cut3/SMC4. *Genes Dev* **13:** 2271-2283

Takahashi K, Murakami S, Chikashige Y, Niwa O, Yanagida M (1991) A large number of tRNA genes are symmetrically located in fission yeast centromeres. *J Mol Biol* **218**(1)**:** 13-17

Takahashi TS, Yiu P, Chou MF, Gygi S, Walter JC (2004) Recruitment of Xenopus Scc2 and cohesin to chromatin requires the pre-replication complex. *Nat Cell Biol* **6**(10)**:** 991-996

Tanaka K, Hao Z, Kai M, Okayama H (2001) Establishment and maintenance of sister chromatid cohesion in fission yeast by a unique mechanism. *EMBO J* **20**(20)**:** 5779-5790

Tanaka K, Yonekawa T, Kawasaki Y, Kai M, Furuya K, Iwasaki M, Murakami H, Yanagida M, Okayama H (2000) Fission yeast Eso1p is required for establishing sister chromatid cohesion during S phase. *Mol Cell Biol* **20**(10)**:** 3459-3469

Thompson M, Haeusler RA, Good PD, Engelke DR (2003) Nucleolar clustering of dispersed tRNA genes. *Science* **302:** 1399-1401

Toda T, Umesono K, Hirata A, Yanagida M (1983) Cold-sensitive nuclear division arrest mutants of the fission yeast Schizosaccharomyces pombe. *J Mol Biol* **168**(2)**:** 251-270

Tomonaga T, Nagao K, Kawasaki Y, Furuya K, Murakami A, Morishita J, Yuasa T, Sutani T, Kearsey SE, Uhlmann F, Nasmyth K, Yanagida M (2000) Characterization of fission yeast cohesin: essential anaphase proteolysis of Rad21 phosphorylated in the S phase. *Genes Dev* **14:** 2757-2770

Tonkin ET, Wang T-J, Lisgo S, Bamshad MJ, Strachan T (2004) NIPBL, encoding a homolog of fungal Scc2-type sister chromatid cohesion proteins and fly Nipped-B, is mutated in Cornelia de Lange syndrome. *Nat Genet* **36**(6)**:** 636-641

Tóth A, Ciosk R, Uhlmann F, Galova M, Schleiffer A, Nasmyth K (1999) Yeast Cohesin complex requires a conserved protein, Eco1p (Ctf7), to establish cohesion between sister chromatids during DNA replication. *Genes Dev* **13:** 320-333

Towbin H, Staehelin T, Gordon J (1992) Electrophoretic transfer of proteins from polyacrylamide gels to nitrocellulose sheets: procedure and some applications. 1979. *Biotechnology* **24:** 145-149

Uhlmann F (2003) Chromosome cohesion and separation: from men and molecules. *Curr Biol* **13:** R104-R114

Uhlmann F (2007) What is your assay for sister-chromatid cohesion? *EMBO J* **26**(22)**:** 4609-4618

Uhlmann F (2008) Molecular biology: cohesin branches out. *Nature* **451**(7180)**:** 777-778

Uhlmann F, Lottspeich F, Nasmyth K (1999) Sister-chromatid separation at anaphase onset is promoted by cleavage of the cohesin subunit Scc1. *Nature* **400:** 37-42

Uhlmann F, Nasmyth K (1998) Cohesion between sister chromatids must be established during DNA replication. *Curr Biol* **8:** 1095-1101

Uhlmann F, Wernic D, Poupart M-A, Koonin EV, Nasmyth K (2000) Cleavage of cohesin by the CD clan protease separin triggers anaphase in yeast. *Cell* **103:** 375-386

Unal E, Arbel-Eden A, Sattler U, Shroff R, Lichten M, Haber JE, Koshland D (2004) DNA damage response pathway uses histone modification to assemble a double-strand break-specific cohesin domain. *Mol Cell* **16**(6)**:** 991-1002

Unal E, Heidinger-Pauli JM, Kim W, Guacci V, Onn I, Gygi SP, Koshland DE (2008) A molecular determinant for the establishment of sister chromatid cohesion. *Science* **321**(5888)**:** 566-569

Ünal E, Heidinger-Pauli JM, Koshland D (2007) DNA double-strand breaks trigger genome-wide sister-chromatid cohesion through Eco1 (Ctf7). *Science* **317:** 245-248

Valenzuela L, Kamakaka RT (2006) Chromatin Insulators. *Annu Rev Genet* **40:** 107-138

Vega H, Waisfisz Q, Gordillo M, Sakai N, Yanagihara I, Yamada M, van Gosliga D, Kayserili H, Xu C, Ozono K, Jabs EW, Inui K, Joenje H (2005) Roberts syndrome is caused by mutations in ESCO2, a human homolog of yeast ECO1 that is essential for the establishment of sister chromatid cohesion. *Nat Genet* **37**(5)**:** 468-470

Wade JT, Hall DB, Struhl K (2004) The transcription factor Ifh1 is a key regulator of yeast ribosomal protein genes. *Nature* **432**(7020)**:** 1054-1058

Waizenegger IC, Hauf S, Meinke A, Peters JM (2000) Two distinct pathways remove mammalian cohesin from chromosome arms in prophase and from centromeres in anaphase. *Cell* **103**(3)**:** 399-410

Wang B-D, Butylin P, Strunnikov A (2006) Condensin function in mitotic nucleolar segregation is regulated by rDNA transcription. *Cell Cycle* **5**(19)**:** 2260-2267

Wang S-W, Read RL, Norbury CJ (2002) Fission yeast Pds5 is required for accurate chromosome segregation and for survival after DNA damage or metaphase arrest. *J Cell Sci* **115:** 587-598

Watrin E, Peters JM (2007) Molecular biology. How and when the genome sticks together. *Science* **317**(5835)**:** 209-210

Watrin E, Schleiffer A, Tanaka K, Eisenhaber F, Nasmyth K, Peters J-M (2006) Human Scc4 is required for cohesin binding to chromatin, sister-chromatid cohesion, and mitotic progression. *Curr Biol* **16:** 863-874

Wendt KS, Yoshida K, Itoh T, Bando M, Koch B, Schirghuber E, Tsutsumi S, Nagae G, Ishihara K, Mishiro T, Yahata K, Imamoto F, Aburatani H, Nakao M, Imamoto N, Maeshima K, Shirahige K, Peters JM (2008) Cohesin mediates transcriptional insulation by CCCTC-binding factor. *Nature* **451**(7180)**:** 796-801

Wood V, Gwilliam R, Rajandream MA, Lyne M, Lyne R, Stewart A, Sgouros J, Peat N, Hayles J, Baker S, Basham D, Bowman S, Brooks K, Brown D, Brown S, Chillingworth T, Churcher C, Collins M, Connor R, Cronin A, Davis P, Feltwell T, Fraser A, Gentles S, Goble A, Hamlin N, Harris D, Hidalgo J, Hodgson G, Holroyd S, Hornsby T, Howarth S, Huckle EJ, Hunt S, Jagels K, James K, Jones L, Jones M, Leather S, McDonald S, McLean J, Mooney P, Moule S, Mungall K, Murphy L, Niblett D, Odell C, Oliver K, O'Neil S, Pearson D, Quail MA, Rabbinowitsch E, Rutherford K, Rutter S, Saunders D, Seeger K, Sharp S, Skelton J, Simmonds M, Squares R, Squares S, Stevens K, Taylor K, Taylor RG, Tivey A, Walsh S, Warren T, Whitehead S, Woodward J, Volckaert G, Aert R, Robben J, Grymonprez B, Weltjens I, Vanstreels E, Rieger M, Schafer M, Muller-Auer S, Gabel C, Fuchs M, Dusterhoft A, Fritzc C, Holzer E, Moestl D, Hilbert H, Borzym K, Langer I, Beck A, Lehrach H, Reinhardt R, Pohl TM, Eger P, Zimmermann W, Wedler H, Wambutt R, Purnelle B, Goffeau A, Cadieu E, Dreano S, Gloux S, Lelaure V, Mottier S, Galibert F, Aves SJ, Xiang Z, Hunt C, Moore K, Hurst SM, Lucas M, Rochet M, Gaillardin C, Tallada VA, Garzon A, Thode G, Daga RR, Cruzado L, Jimenez J, Sanchez M, del Rey F, Benito J, Dominguez A, Revuelta JL, Moreno S, Armstrong J, Forsburg SL, Cerutti L, Lowe T, McCombie WR, Paulsen I, Potashkin J, Shpakovski GV, Ussery D, Barrell BG, Nurse P (2002) The genome sequence of Schizosaccharomyces pombe. *Nature* **415**(6874)**:** 871-880

Zhang J, Shi X, Li Y, Kim BJ, Jia J, Huang Z, Yang T, Fu X, Jung SY, Wang Y, Zhang P, Kim ST, Pan X, Qin J (2008) Acetylation of Smc3 by Eco1 is required for S phase sister chromatid cohesion in both human and yeast. *Mol Cell* **31**(1)**:** 143-151

7 Appendix

7.1 The cohesin binding pattern along fission yeast chromosome 2

7.1.1 ChIP on chip map of the cohesin subunit Rad21

Rad21-Pk_9 *cdc25-22* cells (Y2699) were arrested in G2 by shifting to the restrictive temperature of 36.5°C for 6 hours in minimal EMM medium. Cells were processed for ChIP against the cohesin subunit Rad21-Pk_9. The binding profile of Rad21-Pk_9 along fission yeast chromosome 2, relative to a whole genome DNA sample, is shown in the following pages. Every bar represents the average of 11 oligonucleotide probes within 250 bp windows. Peaks in dark red were assigned according to the following criteria: Signal intensities were smoothed using a sliding 2.25 kb window. Local maxima were identified, and those with a raw signal intensity above 0.3 were chosen as a peak. Peaks extend from their maximum to both sides until the raw signal $\log_2$ ratio reaches a value below 0. The peak position was defined as the midpoint within the peak. Using these criteria 228 peaks were identified along chromosome 2, highlighted as solid red bars. Open reading frames (ORFs) are shown as grey bars above and below the midline, transcribed from left to right and right to left, respectively. tRNA and ribosomal protein genes of the large (*rpl*) and the small subunit (*rps*) are highlighted in red.

Rad21-Pk$_9$, G2 *(cdc25-22)*

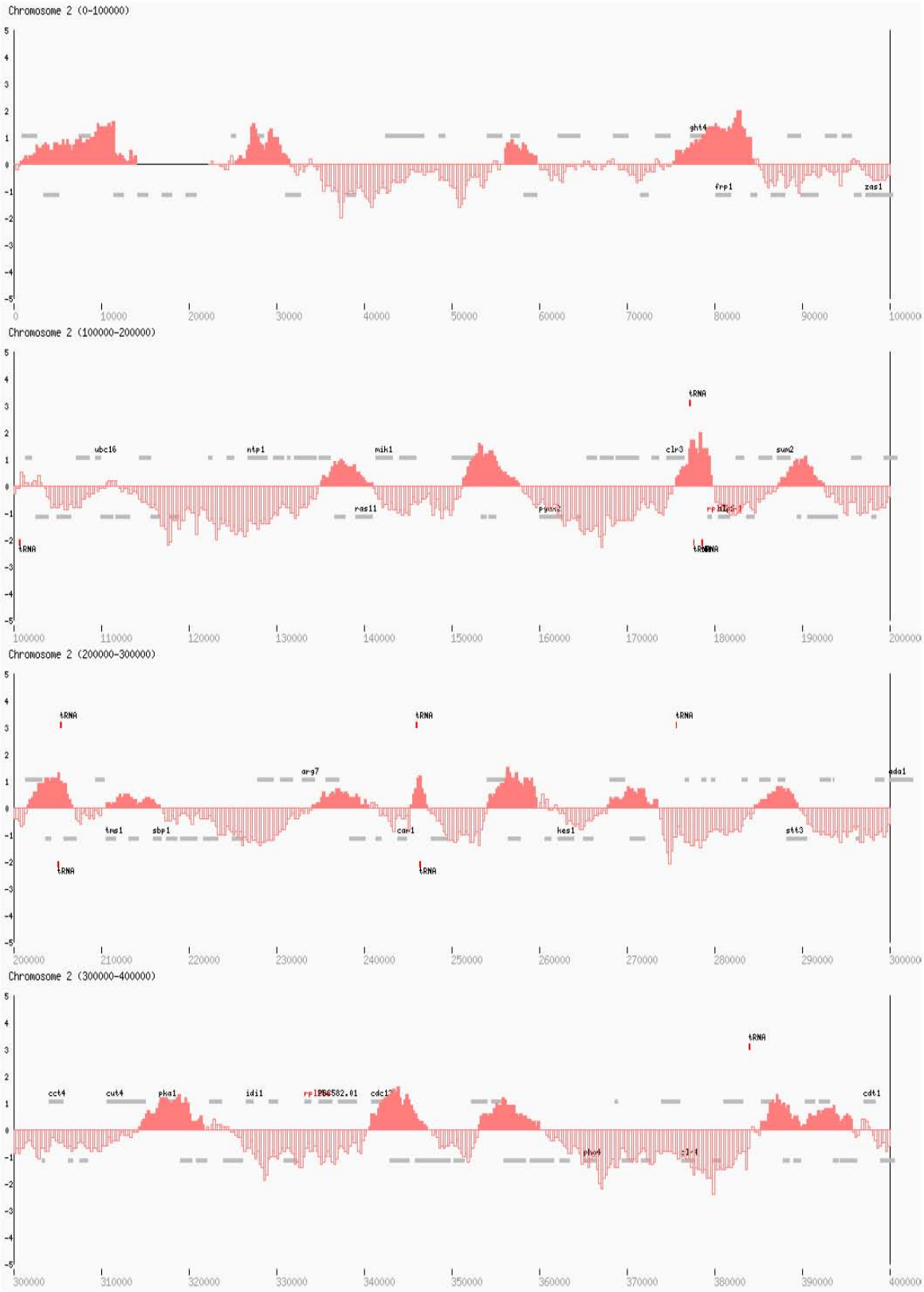

Rad21-Pk$_9$, G2 *(cdc25-22)*

Rad21-Pk$_9$, G2 *(cdc25-22)*

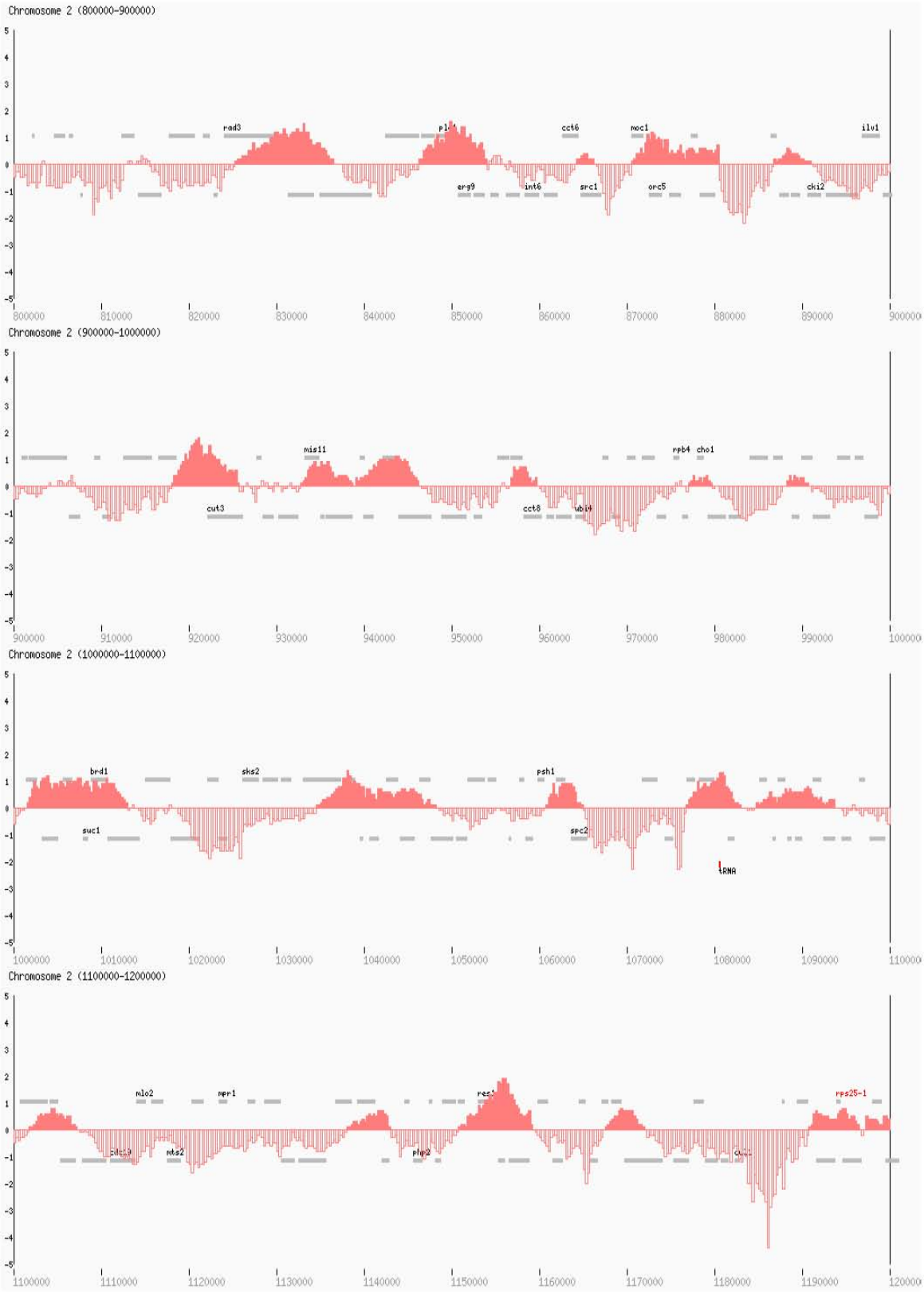

Rad21-Pk$_9$, G2 *(cdc25-22)*

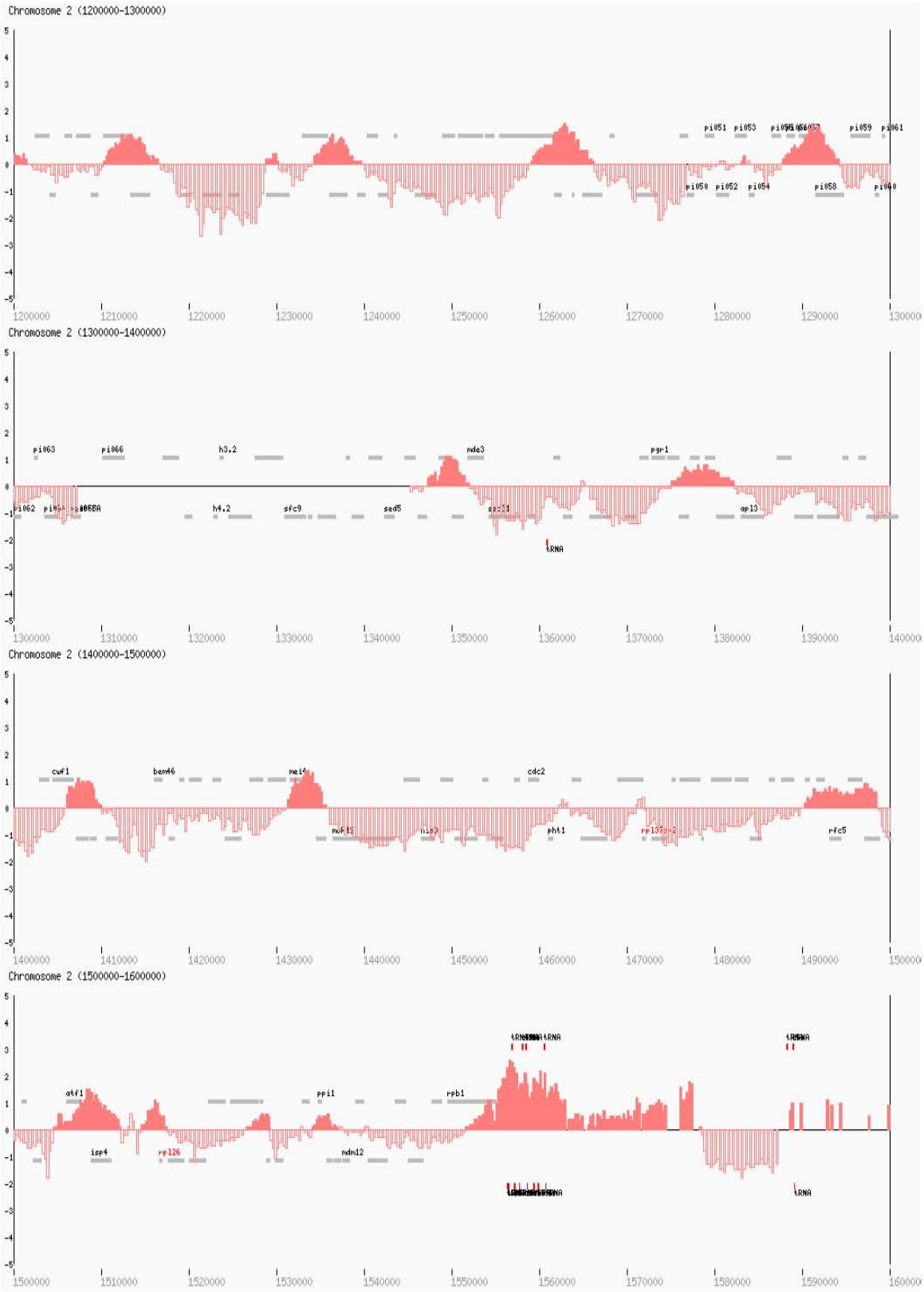

Rad21-Pk$_9$, G2 *(cdc25-22)*

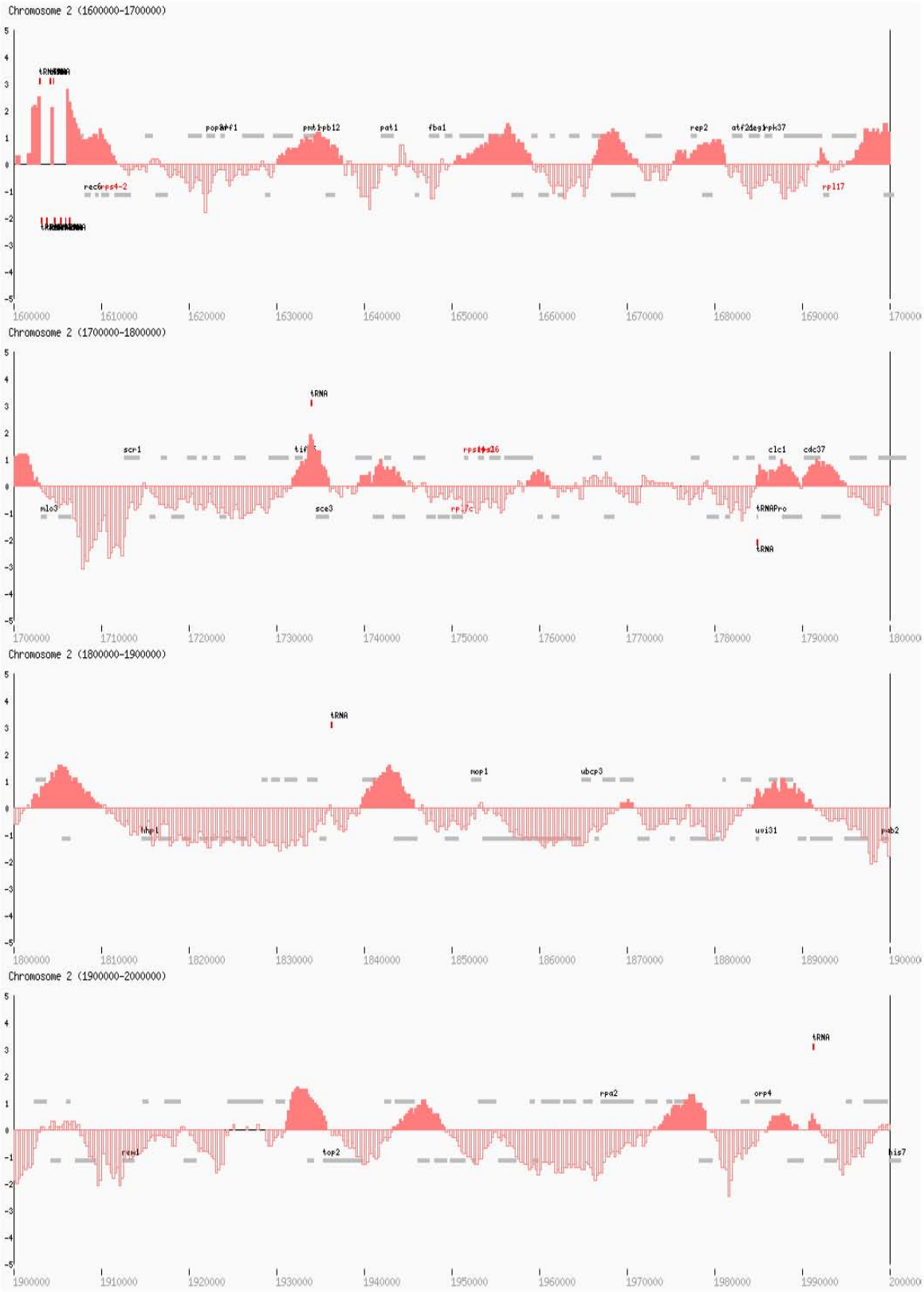

Rad21-Pk9, G2 *(cdc25-22)*

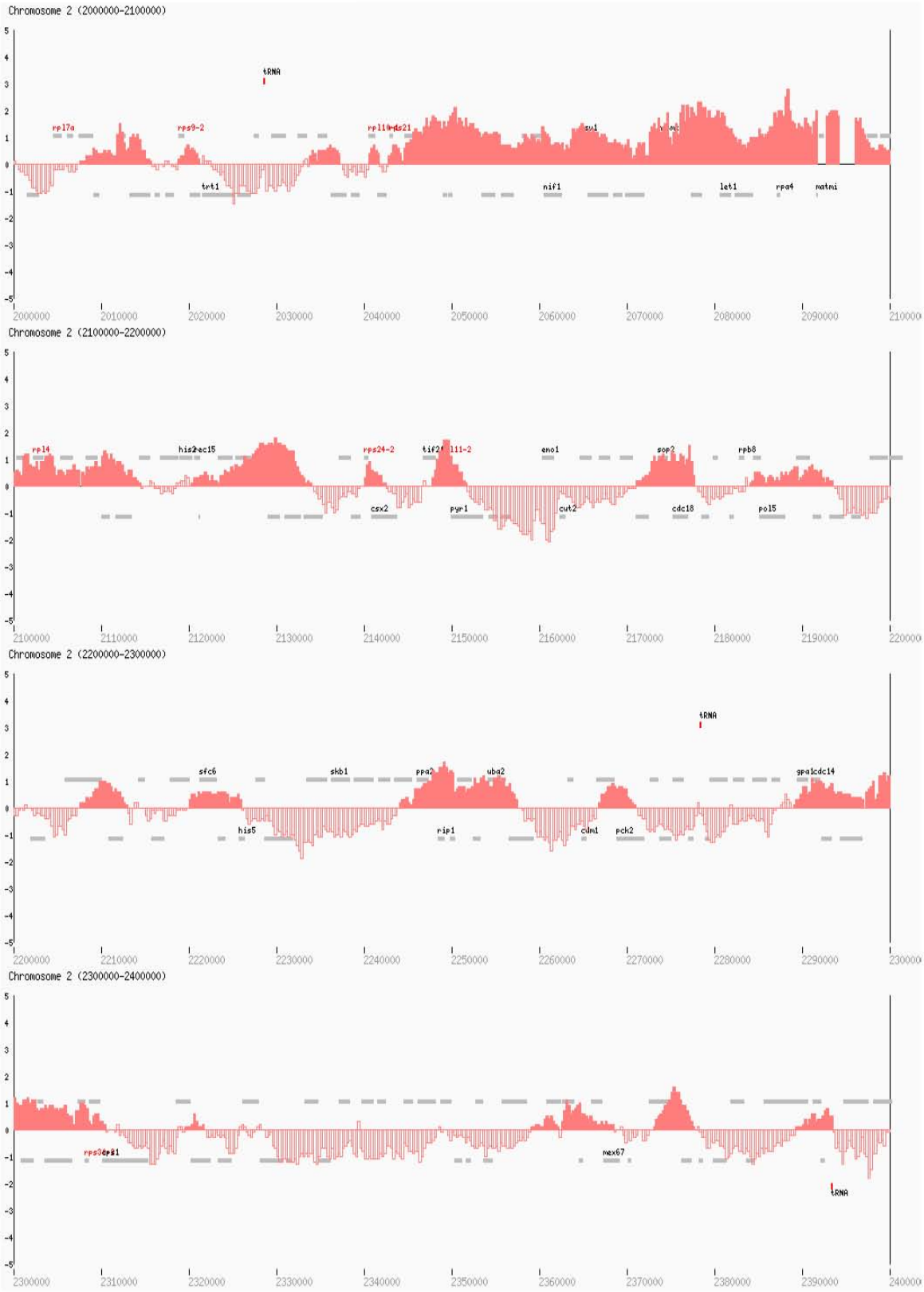

Rad21-Pk$_9$, G2 *(cdc25-22)*

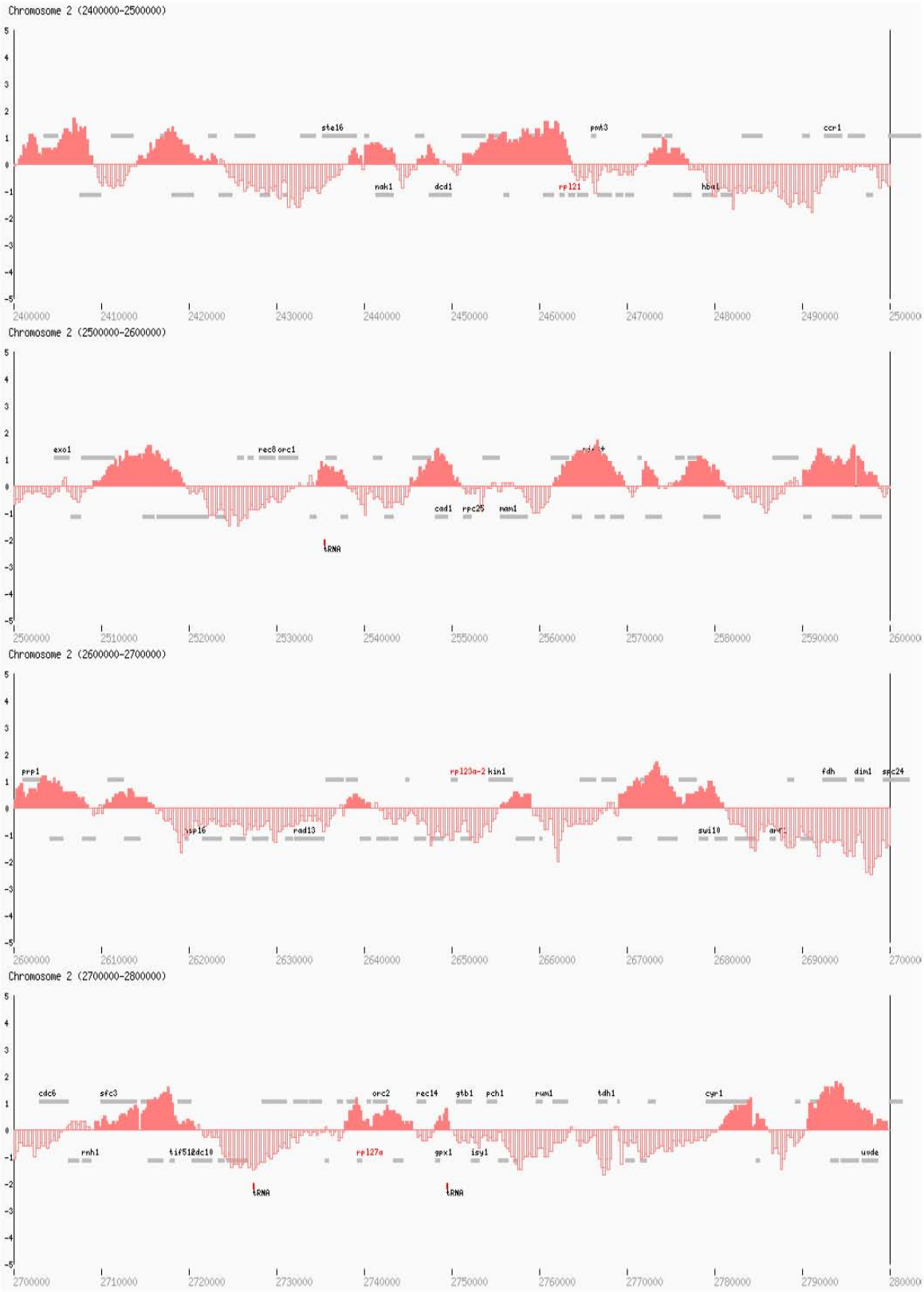

Rad21-Pk$_9$, G2 *(cdc25-22)*

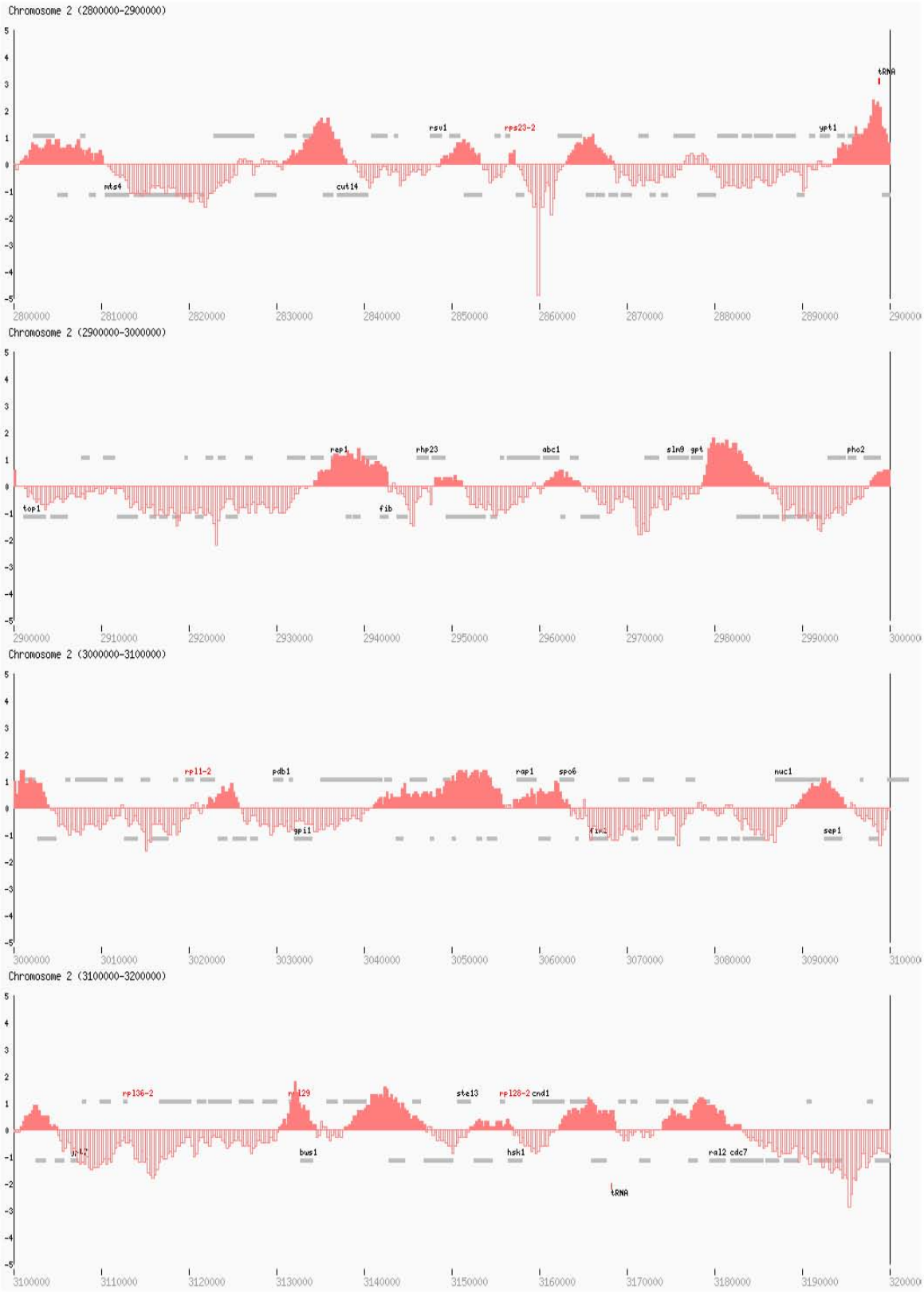

Rad21-Pk$_9$, G2 *(cdc25-22)*

Rad21-Pk$_9$, G2 *(cdc25-22)*

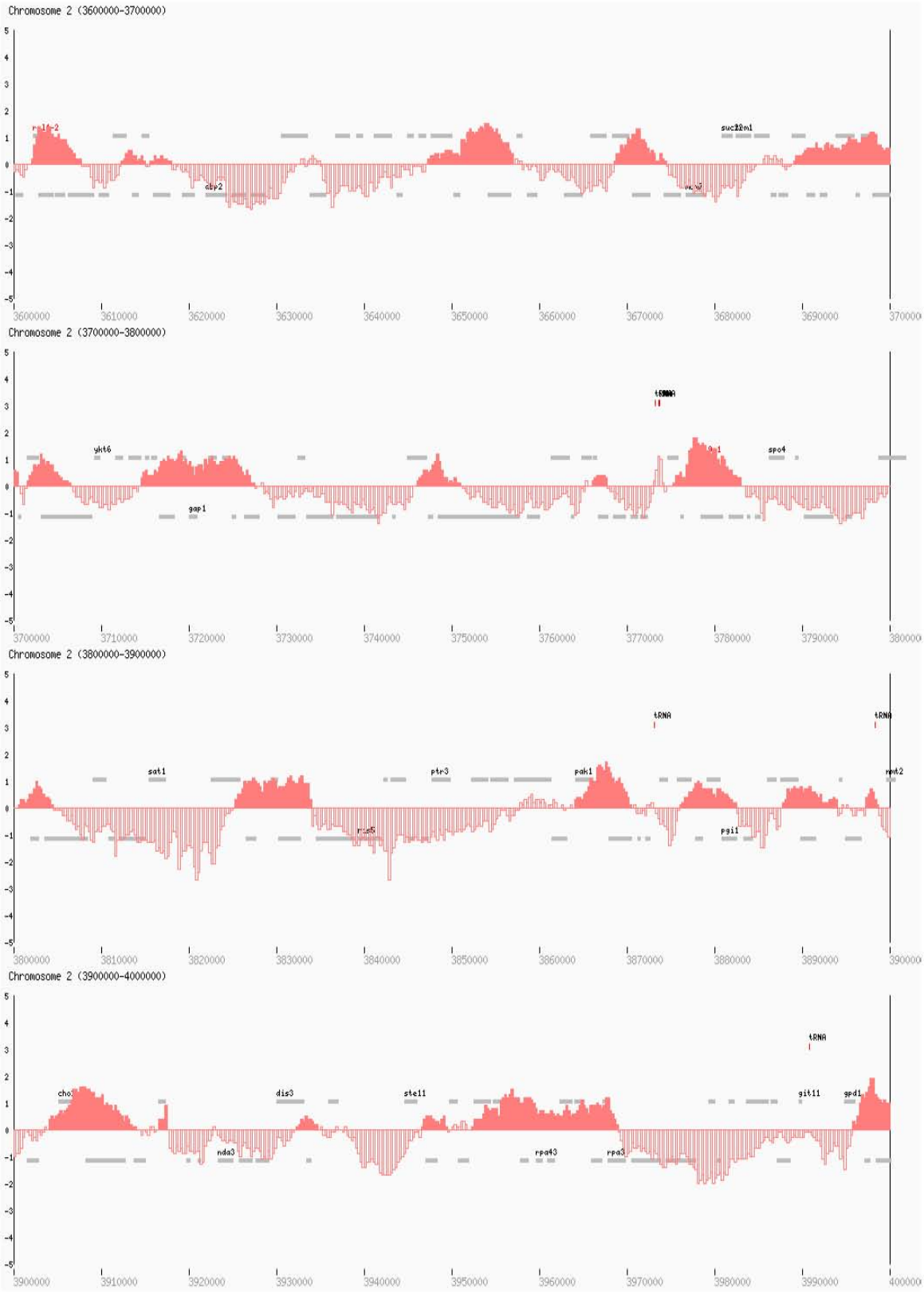

Rad21-Pk$_9$, G2 *(cdc25-22)*

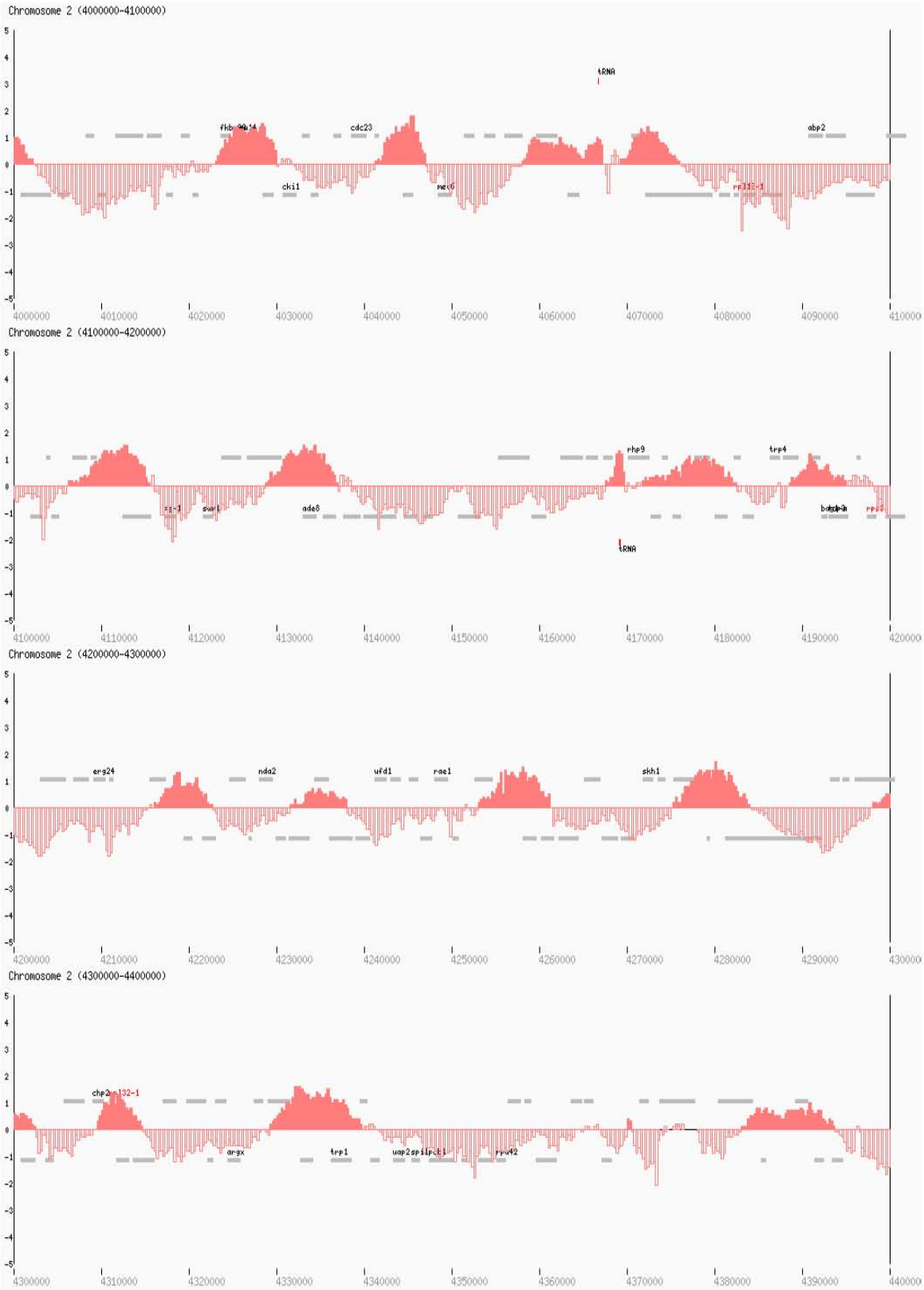

Rad21-Pk$_9$, G2 *(cdc25-22)*

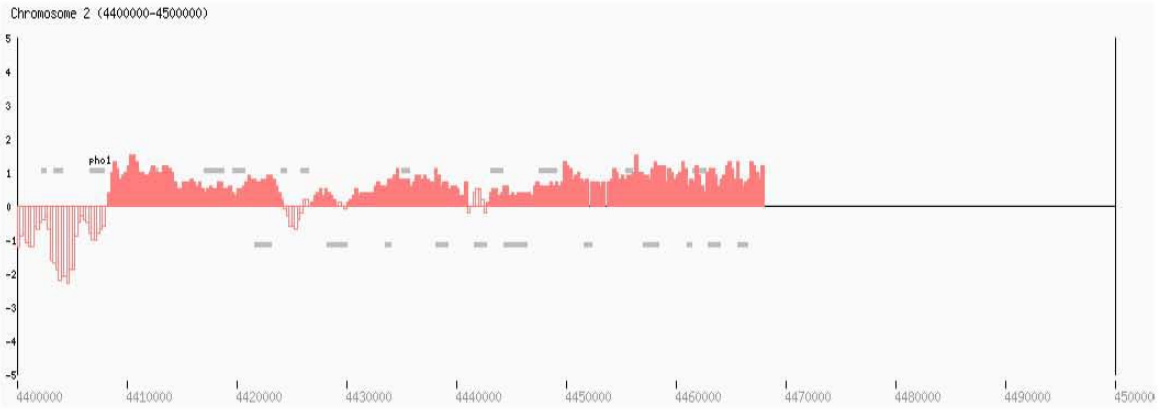

7.1.2 Peak list of the cohesin subunit Rad21

The positions of the midpoints (bp), the average heights and the widths (bp) of the 228 Rad21 peaks, as assigned in 7.1.1**,** are listed below.

Peak	Midpoint/bp	Avg height	Width/bp
1	7251	0,74	13000
2	28251	0,76	6000
3	57751	0,62	3500
4	79751	1,11	9000
5	137876	0,57	5750
6	154376	0,85	6250
7	177501	1,19	4000
8	189751	0,63	5000
9	204001	0,84	5000
10	213501	0,30	6000
11	237126	0,42	6250
12	246126	0,78	1750
13	256751	0,95	5500
14	270501	0,46	5500
15	286876	0,51	4750
16	317876	0,80	7250
17	343751	0,93	6500
18	356376	0,66	6750
19	390376	0,63	10250
20	428626	0,53	4250
21	438626	0,78	4250
22	450501	0,57	5500
23	466876	0,70	11750
24	494376	0,30	750
25	523251	0,96	7500
26	541876	0,28	3250

Peak	Midpoint/bp	Avg height	Width/bp
115	2320501	0,21	2000
116	2363626	0,41	9250
117	2375251	0,91	4500
118	2391251	0,41	4000
119	2404626	0,89	8250
120	2418501	0,61	9000
121	2440751	0,55	5000
122	2447126	0,36	2250
123	2457376	0,98	12250
124	2474501	0,54	4500
125	2514126	0,88	10250
126	2536126	0,63	3250
127	2548001	0,74	5500
128	2565501	0,96	8000
129	2572501	0,64	1500
130	2578126	0,65	5750
131	2594251	0,89	8500
132	2604126	0,72	8250
133	2613001	0,43	5500
134	2639126	0,33	2750
135	2657126	0,39	3250
136	2674876	0,80	11750
137	2714876	0,65	11250
138	2741501	0,54	7500
139	2748751	0,50	1500
140	2783126	0,63	5250

27	564001	0,75	3500
28	572751	0,39	4000
29	588001	0,71	5000
30	636626	0,48	3250
31	639501	0,43	1000
32	652126	0,49	2750
33	657751	0,50	3500
34	676751	0,97	7000
35	719876	0,68	6250
36	729501	1,06	6000
37	784876	0,98	8250
38	793501	0,32	3500
39	830751	0,81	11000
40	850001	0,93	7500
41	865126	0,28	1750
42	875376	0,61	9750
43	888751	0,29	4000
44	921751	1,00	7500
45	935626	0,55	5750
46	942501	0,74	7000
47	958126	0,51	2750
48	978251	0,26	2500
49	989376	0,28	2250
50	1007126	0,86	11250
51	1041251	0,59	13500
52	1062751	0,65	4000
53	1079751	0,76	6000
54	1089126	0,44	8750
55	1104376	0,48	5250
56	1140376	0,44	4750
57	1154876	0,95	8250
58	1169626	0,51	4250
59	1193501	0,52	5500
60	1199251	0,35	4000
61	1213251	0,70	6000
62	1229376	0,30	1250
63	1236876	0,61	5250
64	1262501	0,81	7000
65	1283126		250
66	1290876	0,81	6250
67	1349501	0,65	4500
68	1378501	0,48	7000
69	1407876	0,80	3750
70	1433376	0,94	4250
71	1494251	0,61	8000
72	1508251	0,76	7500

141	2795001	1,00	9000
142	2805376	0,59	9250
143	2834251	0,91	7000
144	2850876	0,55	4250
145	2856751	0,40	500
146	2865626	0,64	5250
147	2896751	1,20	6500
148	2938376	0,89	8250
149	2949501	0,27	3000
150	2962501	0,35	4000
151	2982251	1,05	7500
152	3000751	0,78	6000
153	3023751	0,53	3500
154	3048376	0,78	14750
155	3060126	0,49	6250
156	3092001	0,69	5500
157	3102751	0,51	4000
158	3132251	0,77	4000
159	3142251	0,83	9000
160	3154376	0,23	4750
161	3165376	0,73	6250
162	3178376	0,63	8750
163	3231251	0,89	15500
164	3257751	0,29	2500
165	3266251	0,62	4500
166	3277876	0,98	6250
167	3299751	0,23	2500
168	3312376	0,79	6750
169	3323001	0,87	8000
170	3350626	0,62	5250
171	3366126	0,88	6250
172	3400251	0,93	6000
173	3441001	1,00	8000
174	3462876	1,05	6250
175	3488501	0,20	1500
176	3500751	0,76	12500
177	3525876	0,78	8250
178	3537876	0,31	4750
179	3551001	0,61	6500
180	3570251	0,93	4000
181	3579501	0,35	5000
182	3593501	0,71	6000
183	3599001	0,10	500
184	3604751	0,91	5500
185	3613501	0,31	2500
186	3616626	0,20	2250

73	1515876	0,64	2750
74	1527751	0,38	2500
75	1535376	0,37	2750
76	1558126	1,24	13250
77	1571876	0,71	12750
78	1600001	1,17	23000
79	1633626	0,73	7250
80	1654626	0,74	8750
81	1668501	0,79	5000
82	1678126	0,61	5750
83	1692251	0,40	1000
84	1698876	0,94	7750
85	1733751	1,03	4000
86	1741876	0,52	5250
87	1759751	0,40	2500
88	1787126	0,61	4750
89	1792376	0,64	4750
90	1805876	0,90	7750
91	1842501	0,97	6000
92	1869876	0,23	1250
93	1887626	0,65	6750
94	1933251	1,16	4500
95	1946126	0,63	5750
96	1976126	0,86	5250
97	1987626	0,43	3250
98	1991251	0,40	1000
99	2011501	0,58	8000
100	2019876	0,49	2250
101	2035376	0,50	3250
102	2041001	0,60	1000
103	2078501	1,13	71500
104	2127001	0,86	13500
105	2141126	0,53	2250
106	2149626	1,00	3750
107	2174251	0,87	6500
108	2188626	0,42	9250
109	2210126	0,61	5250
110	2222876	0,51	5750
111	2250626	0,90	13250
112	2268751	0,63	4000
113	2292876	0,64	7750
114	2303751	0,80	13000

187	3652001	0,84	9500
188	3671376	0,67	5750
189	3694626	0,71	11250
190	3703876	0,61	4750
191	3720876	0,80	12750
192	3748376	0,49	4750
193	3766751	0,38	1500
194	3773376	0,85	750
195	3779001	0,99	7500
196	3802376	0,49	3750
197	3829501	0,91	8500
198	3867126	0,97	6250
199	3879126	0,58	6250
200	3890751	0,53	6000
201	3897876	0,53	1250
202	3908876	0,93	9750
203	3916876	0,40	750
204	3933376	0,34	2250
205	3947876	0,40	2750
206	3960501	0,83	16500
207	3998876	0,99	6250
208	4026376	1,10	6750
209	4044001	1,06	5500
210	4062501	0,68	9000
211	4072501	0,79	6500
212	4110751	0,87	9000
213	4132751	0,95	8000
214	4168501	0,73	2000
215	4177001	0,61	10500
216	4191626	0,56	6250
217	4219251	0,70	6500
218	4234626	0,43	6250
219	4257001	0,87	8000
220	4279501	0,97	8500
221	4300126	0,40	4250
222	4312001	0,85	5000
223	4334376	1,01	10250
224	4388251	0,57	10500
225	4416126	0,80	15750
226	4427751	0,39	2000
227	4435376	0,63	10750
228	4455251	0,81	25000

7.2 Mis4 and Ssl3 binding pattern along fission yeast chromosome 2

7.2.1 ChIP on chip map of the cohesin loader Mis4/Ssl3

Mis4 (green) and Ssl3 (blue) overlap along fission yeast chromosmes. Mis4-Pk_9 (Y2468) and Ssl3-Pk_9 (Y3071) cells were grown exponentially in rich YE4S medium at 25°C. ChIP was performed against the cohesin loading factor subunits Mis4-Pk_9 (green) and Ssl3- Pk_9 (blue). The graphic map shows an overlap of the binding patterns of the two proteins along fission yeast chromosome 2, relative to a whole genome DNA sample. Significant peaks are indicated as solid bars and were assigned according to the following criteria: Signal intensities were smoothed using a sliding 2.25 kb window. Local maxima were identified, and those with a smoothed signal intensity above 0.5 were chosen as a peak. Peaks reach from their maximum to both sides until the raw signal $\log_2$ ratio falls below a value of 0. The peak position was defined as the midpoint within the peak. Using this method 133 Mis4 peaks were assigned along chromosome 2. Cells containing no epitope-tagged proteins (Y2460; purple) were grown under identical conditions and processed in parallel with Mis4-Pk_9 (Y2468) cells for ChIP analysis, using anti-Pk antibodies. Identical peak-picking parameters were applied to the unspecific association pattern. All background peaks, assigned significant by this method that overlapped with Mis4 peaks, were subtracted from the 133 assigned Mis4 peaks, reducing the number from to 72 peaks specific for Mis4. Only these were used for statistical analyses. An accompanying list of the Mis4-specific peaks can be found in Appendix 7.2.2. The cohesin loading factor is known to be difficult to analyse by ChIP. Low yields of Mis4-bound DNA fragments might explain why the background pattern leaks through for some but not for other proteins. The actual number of Mis4/Ssl3 association sites might be higher, since some binding sites may not have been recognised by our peak-picking parameters. Further explanations of symbols in the maps can be found in Appendix 7.1.1.

Mis4-Pk$_9$, Ssl3-Pk$_9$, untagged Pk, cycling

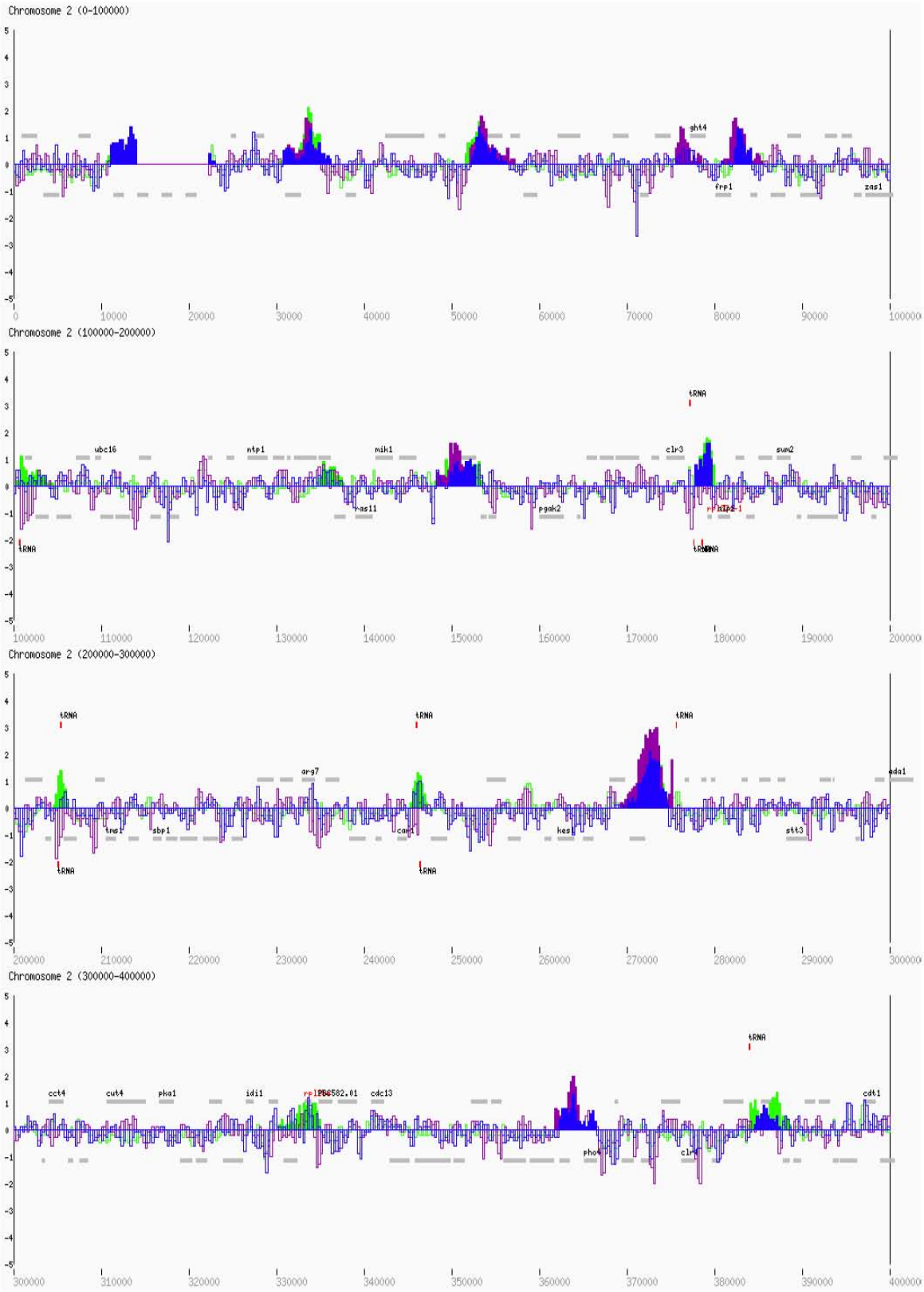

Mis4-Pk$_9$, Ssl3-Pk$_9$, untagged Pk, cycling

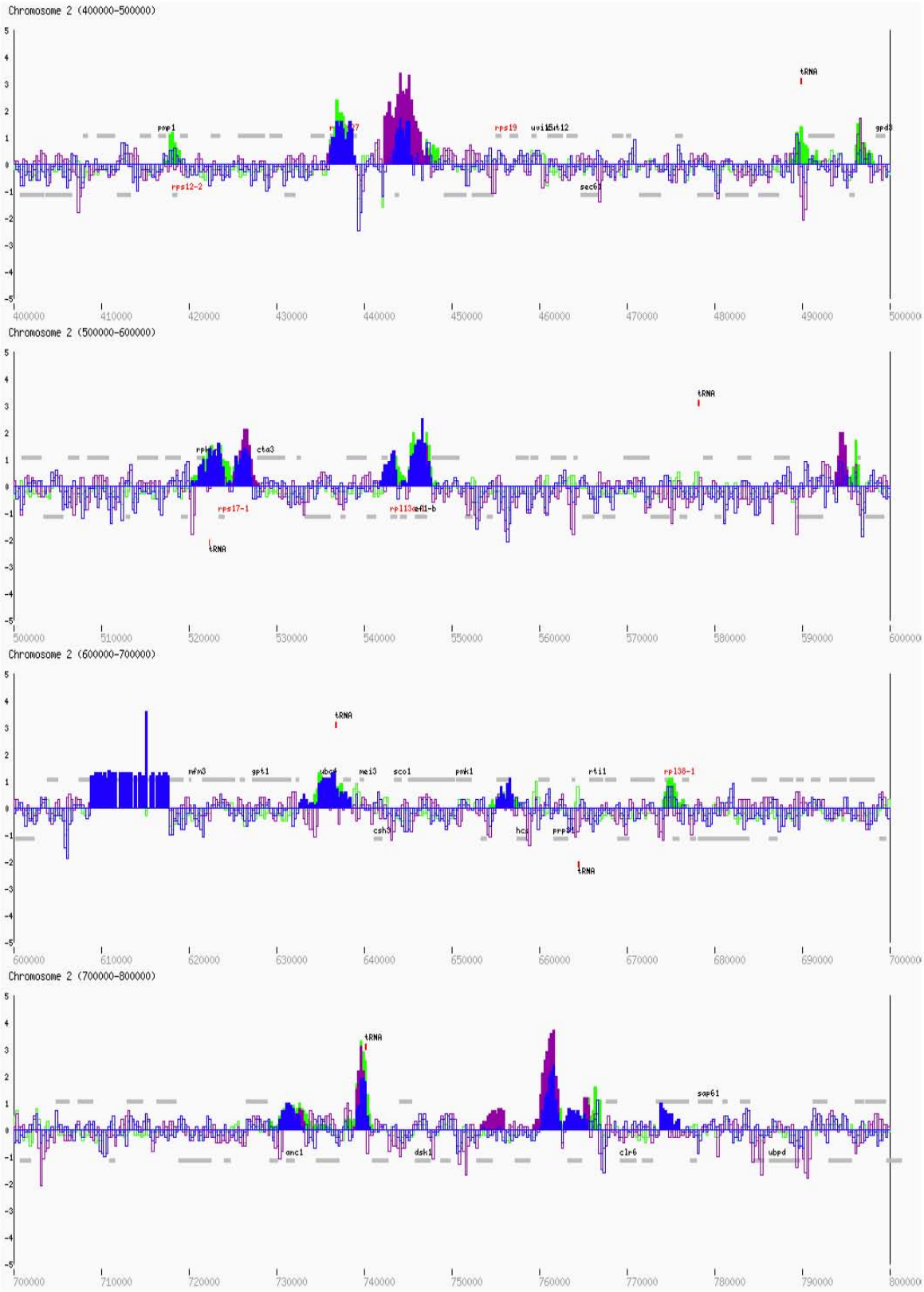

Mis4-Pk$_9$, Ssl3-Pk$_9$, untagged Pk, cycling

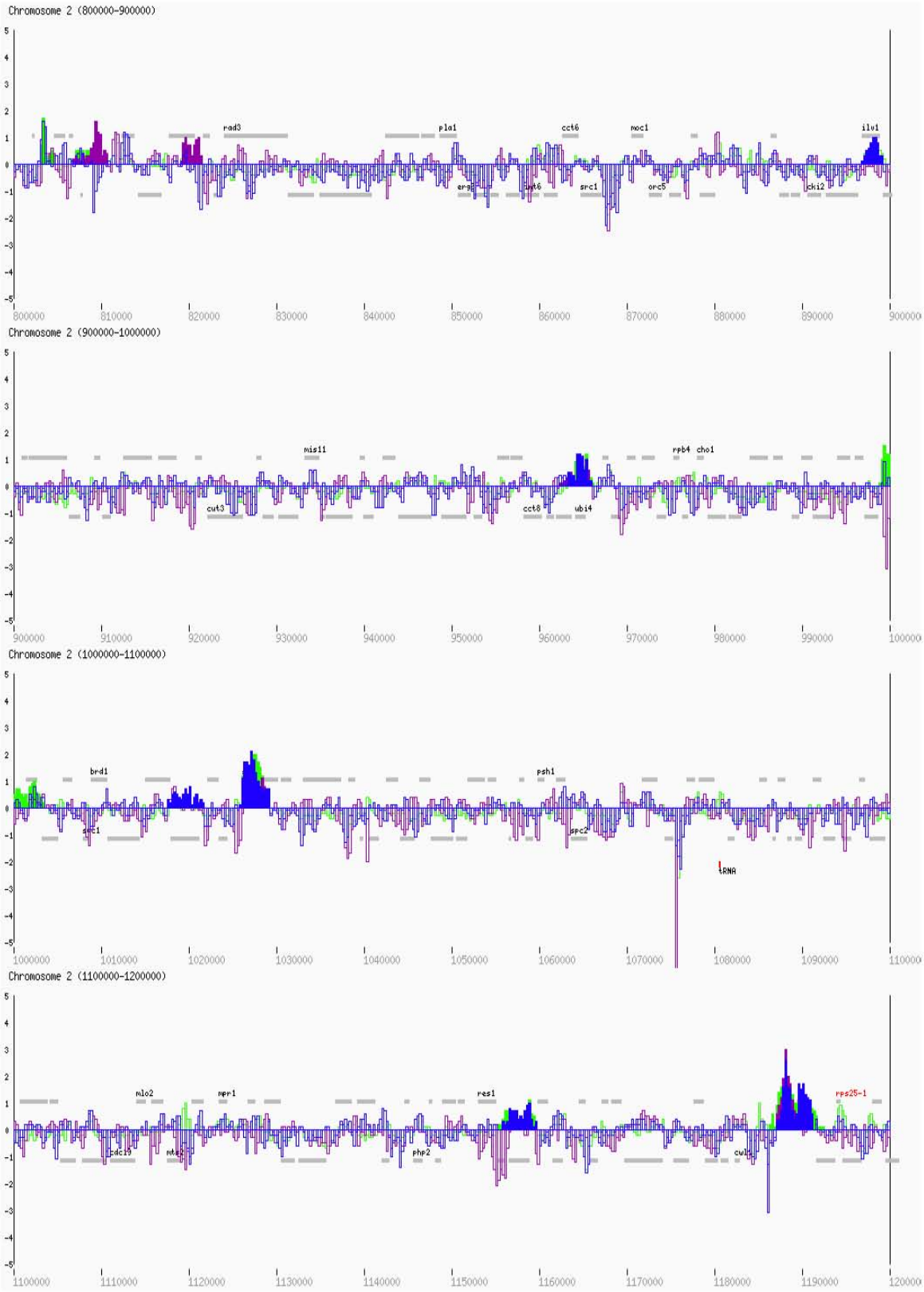

Mis4-Pk$_9$, Ssl3-Pk$_9$, untagged Pk, cycling

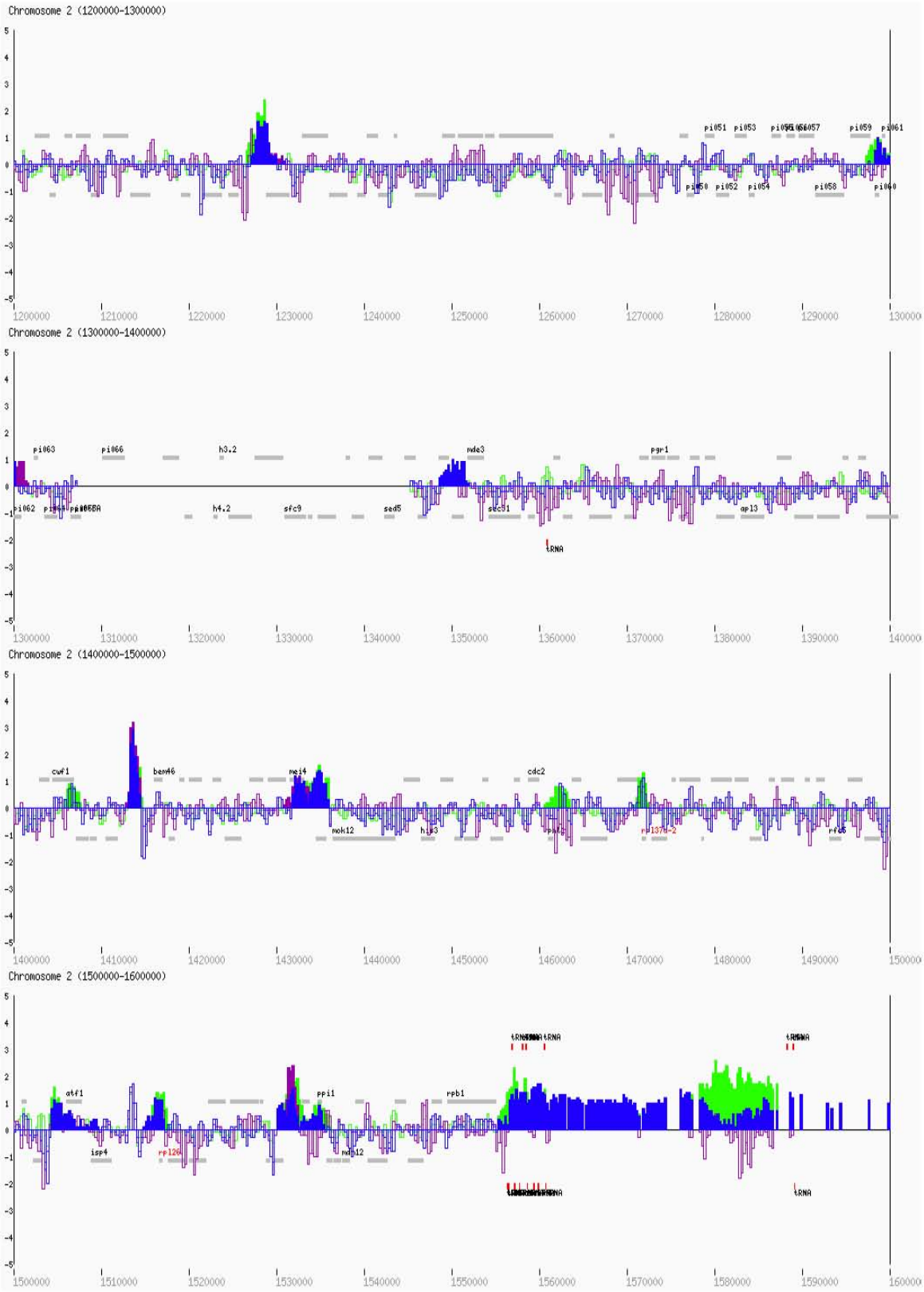

Mis4-Pk$_9$, Ssl3-Pk$_9$, untagged Pk, cycling

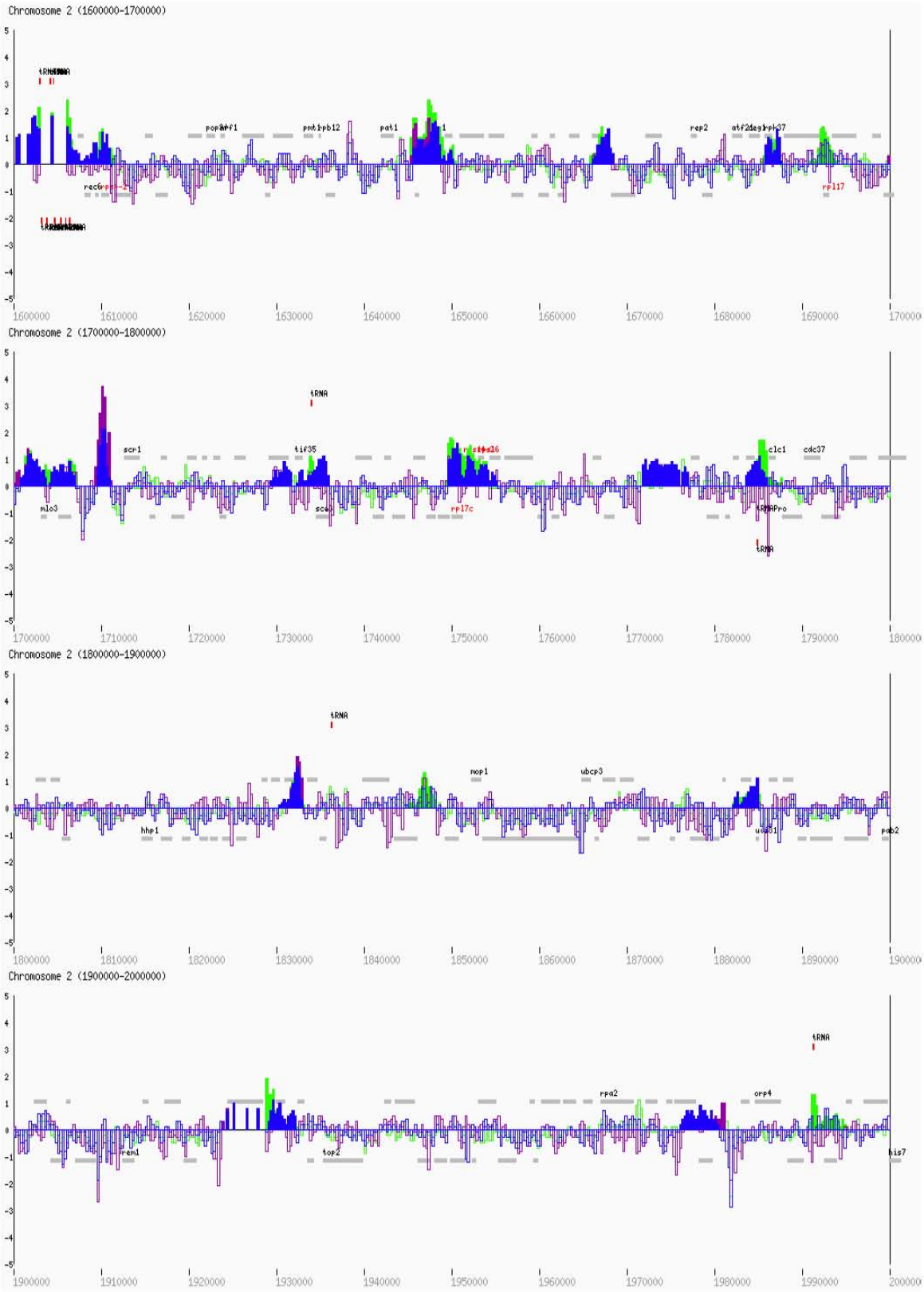

Mis4-Pk$_9$, Ssl3-Pk$_9$, untagged Pk, cycling

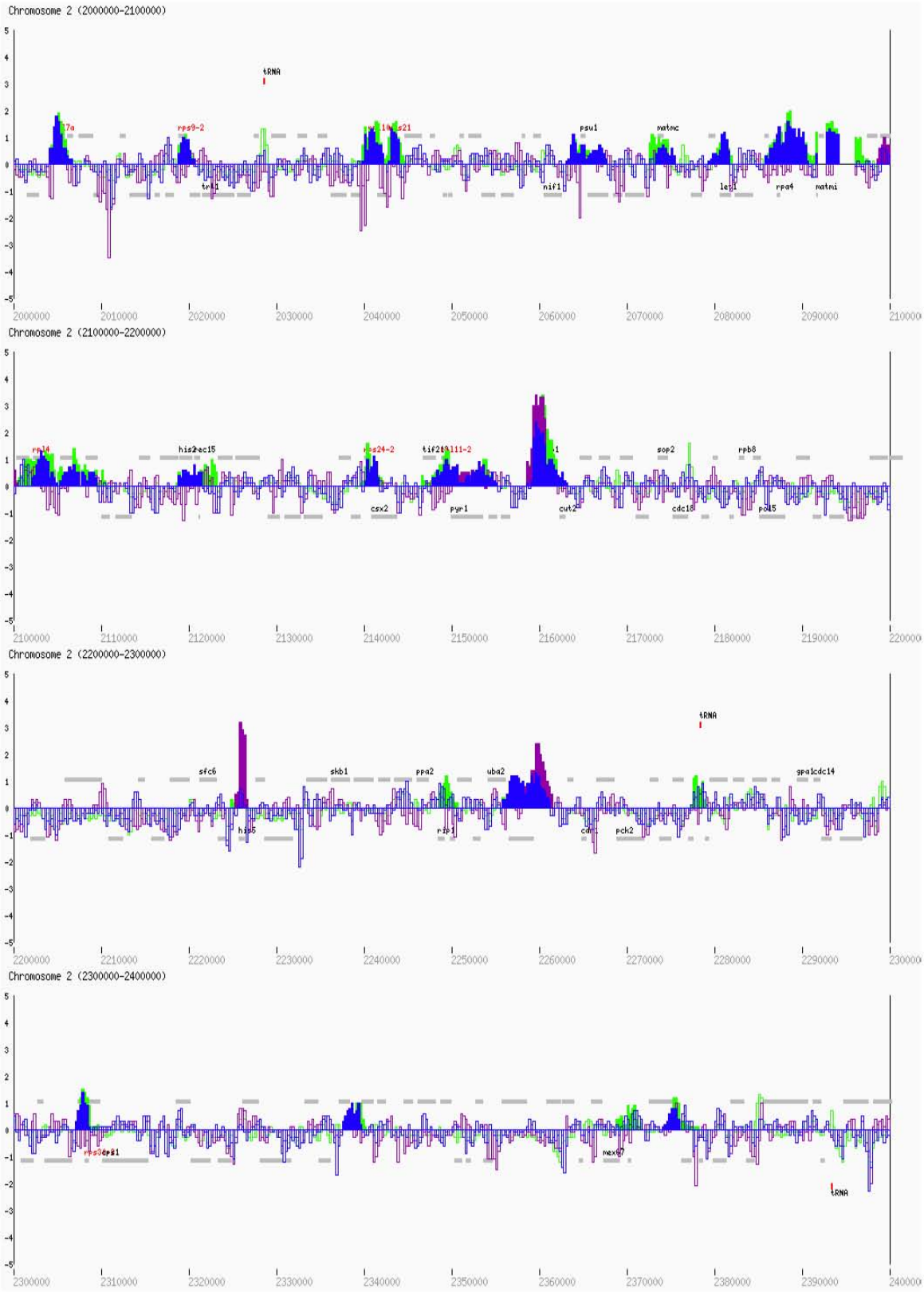

Mis4-Pk$_9$, Ssl3-Pk$_9$, untagged Pk, cycling

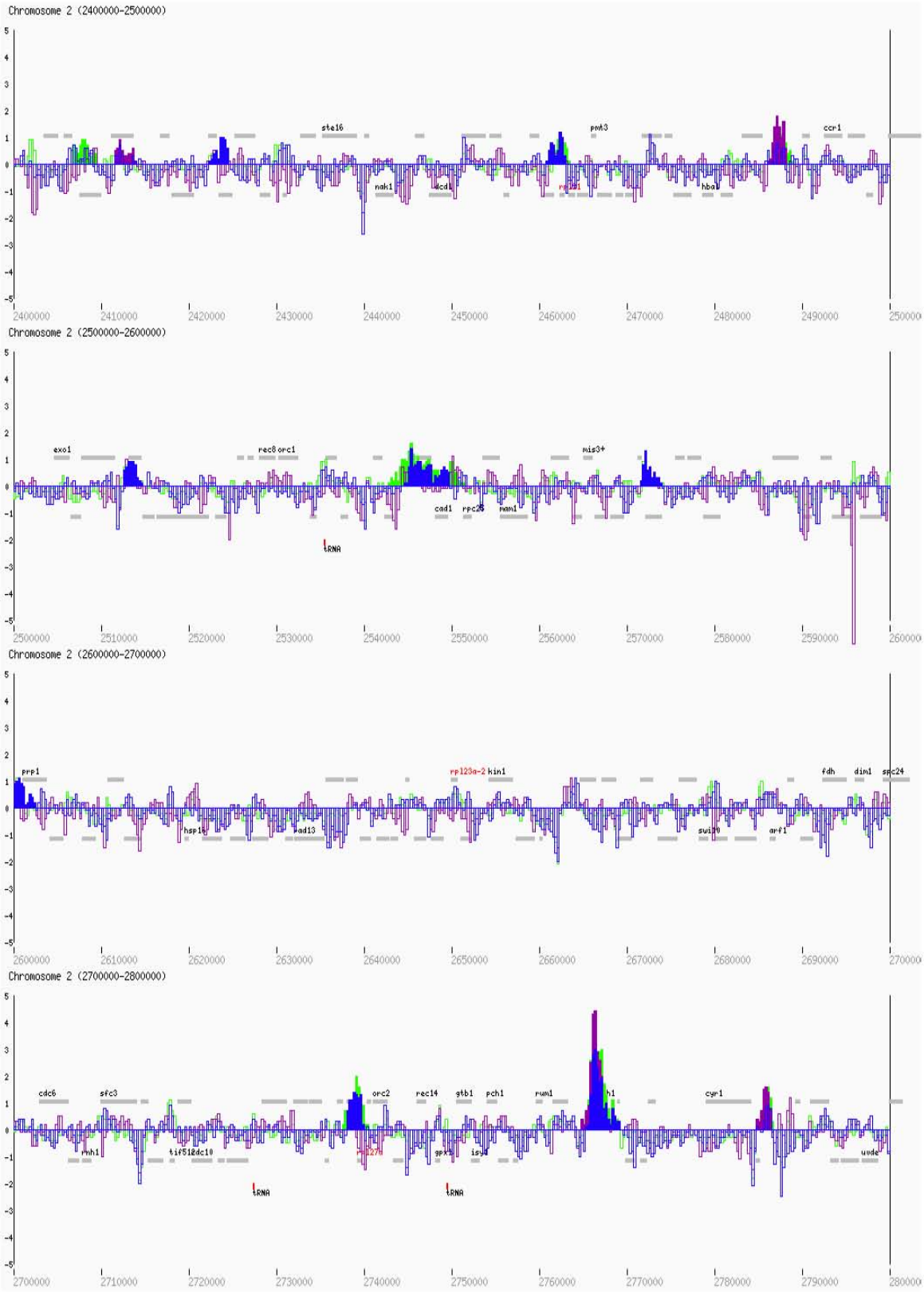

Mis4-Pk$_9$, Ssl3-Pk$_9$, untagged Pk, cycling

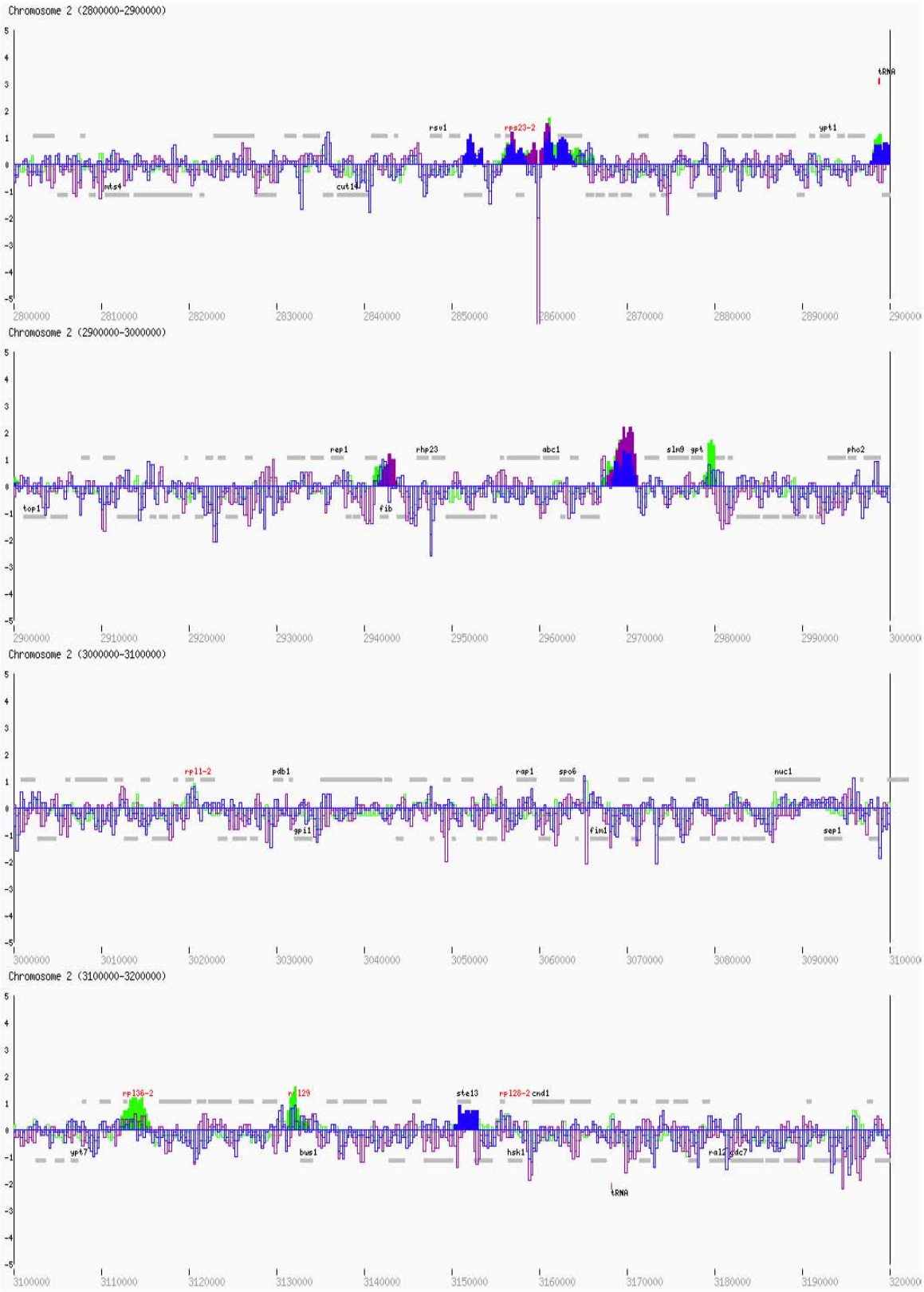

Mis4-Pk$_9$, Ssl3-Pk$_9$, untagged Pk, cycling

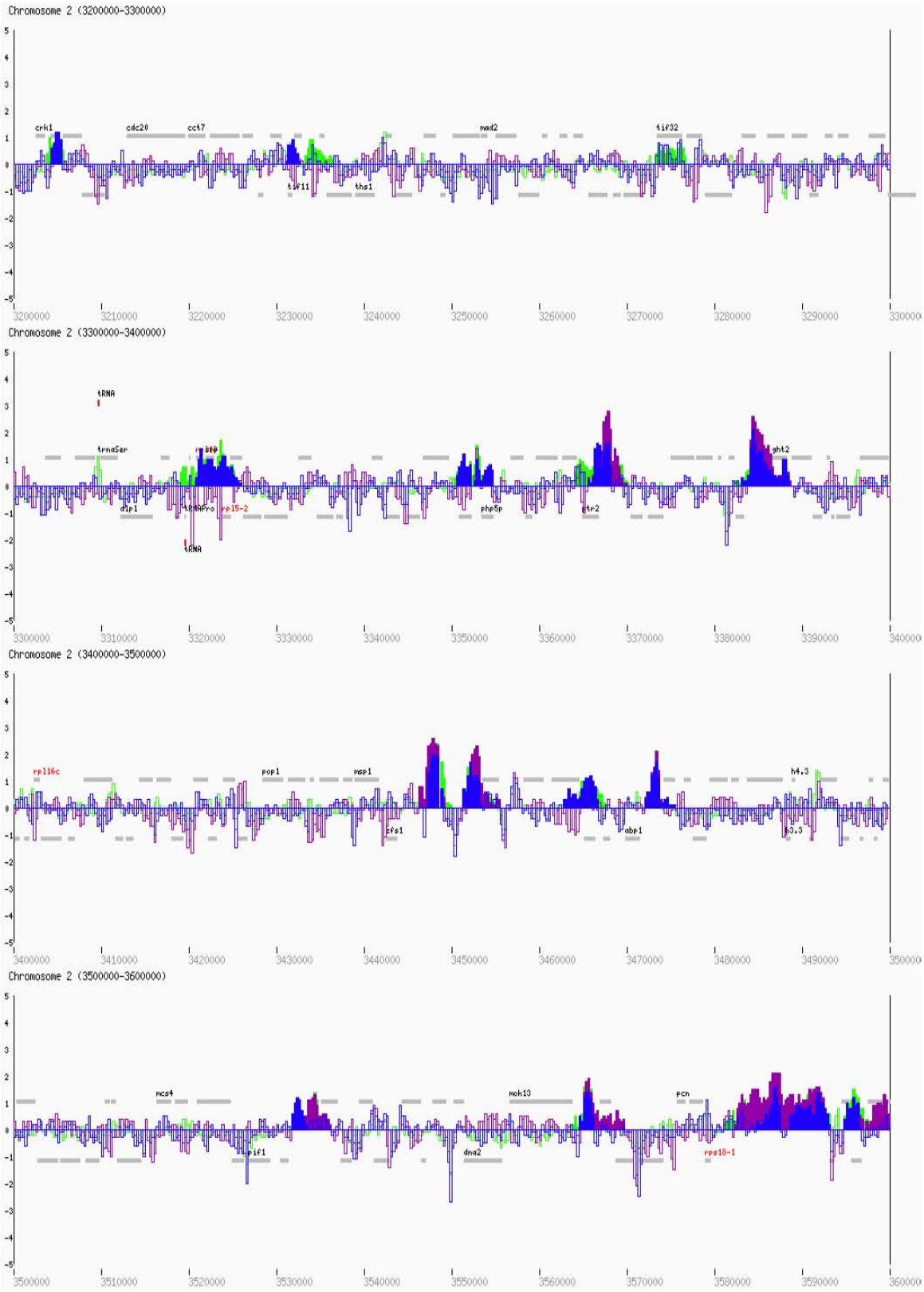

Mis4-Pk$_9$, Ssl3-Pk$_9$, untagged Pk, cycling

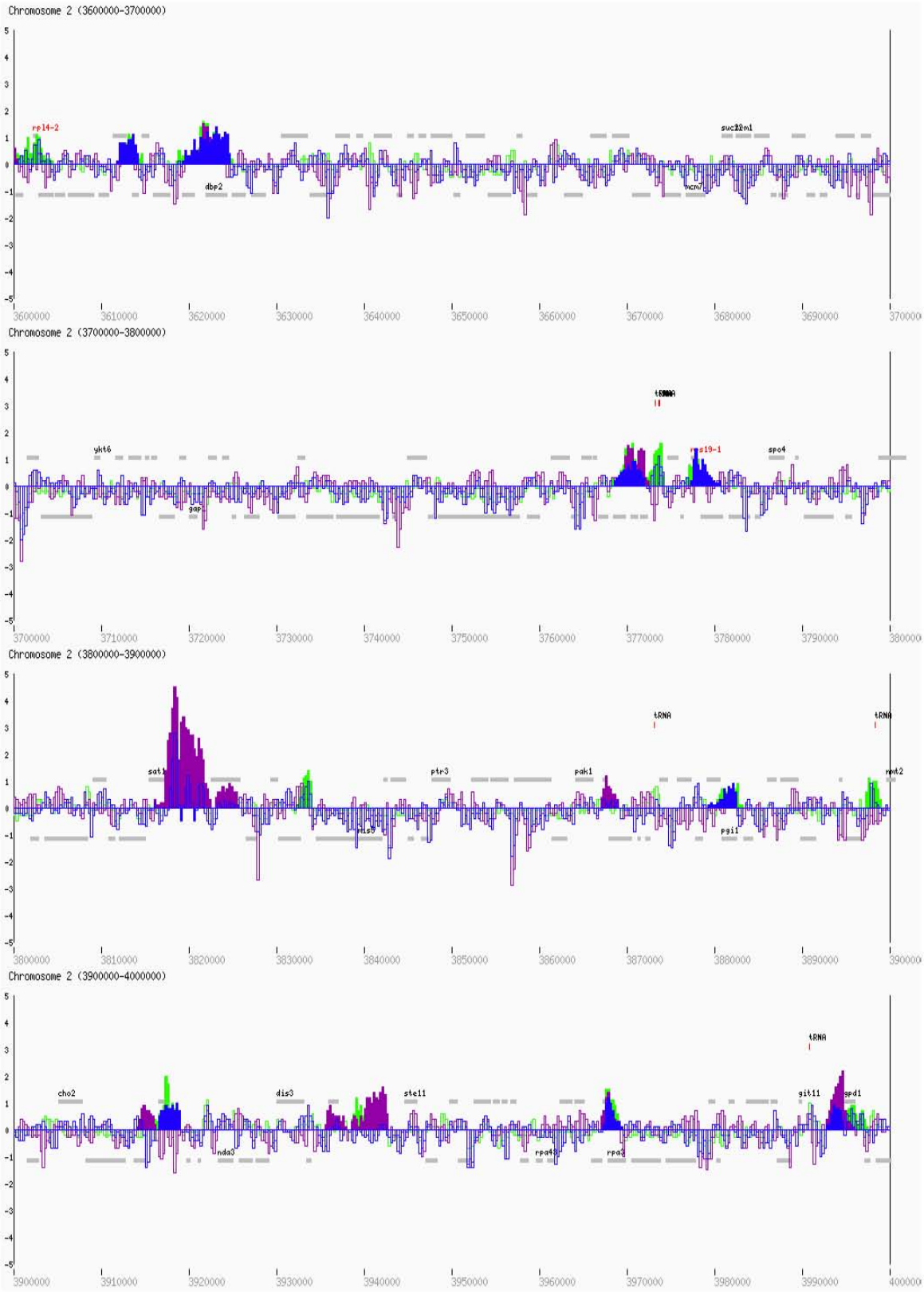

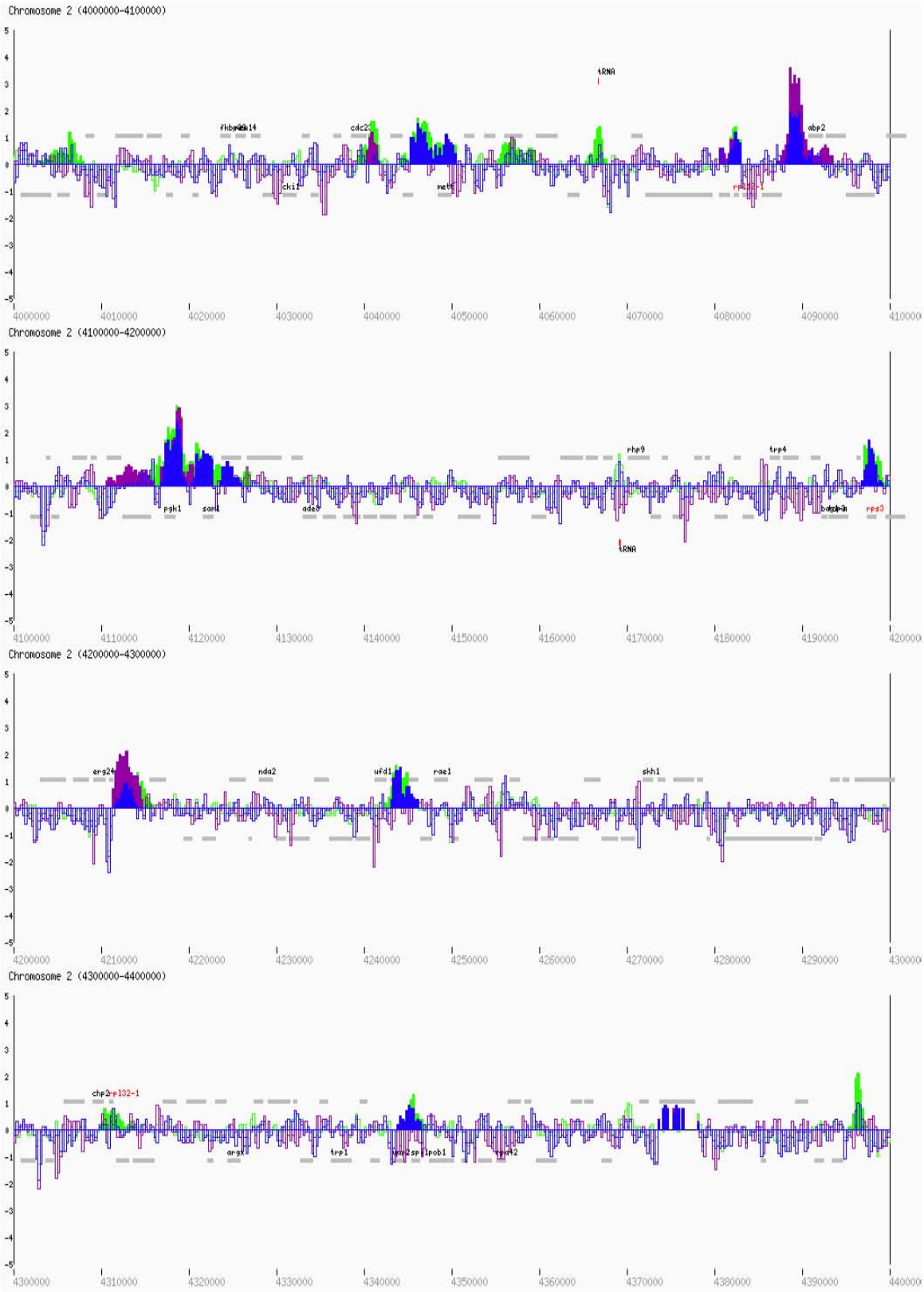
Chromosome 2 (4000000-4100000)
tRNA
cdc2
abp2
Chromosome 2 (4100000-4200000)
rhp9
trp4
pgk1
tRNA
Chromosome 2 (4200000-4300000)
erg24
nda2
ufd1
rae1
skh1
Chromosome 2 (4300000-4400000)
chp2-p132-1
trp1

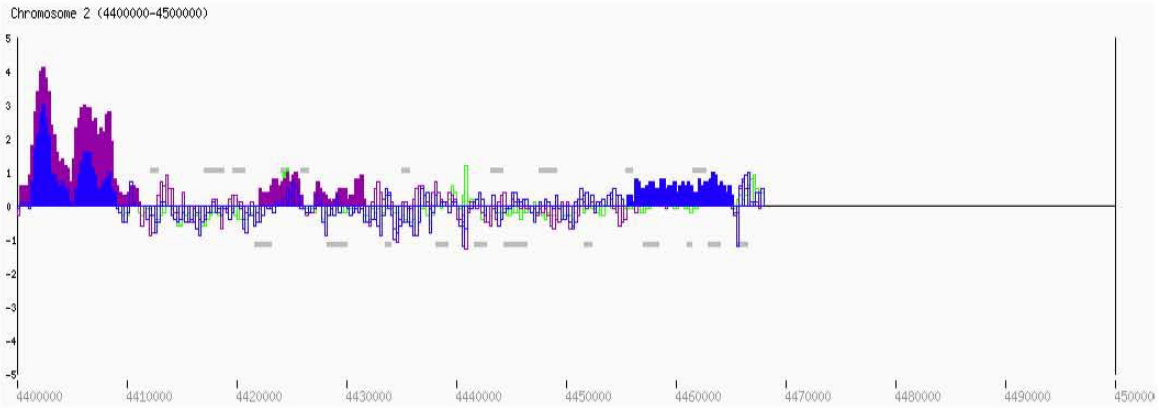

7.2.2 Peak list of the cohesin loader subunit Mis4

The positions of the midpoints (bp), the average heights (bp) and the widths (bp) of the 72 Mis4-specific peaks, as determined in Appendiy 7.2.1, are listed below.

Peak	Midpoint/bp	Avg height	Width/bp
1	12251	0,53	3500
2	101876	0,47	3750
3	136001	0,55	3000
4	178751	1,11	2500
5	205376	0,82	1750
6	246126	0,75	2250
7	332876	0,63	4250
8	385501	0,82	4000
9	490001	0,60	3500
10	496876	0,85	2250
11	636001	0,80	4500
12	656376	0,48	3250
13	675126	0,63	2750
14	803751	0,77	2000
15	1001126	0,71	4750
16	1157376	0,50	4750
17	1298626	0,60	3250
18	1462001	0,53	3000
19	1471626	0,83	1750
20	1505376	0,73	3250
21	1516376	0,88	2750
22	1610001	0,63	3000
23	1667001	0,74	3000
24	1686376	0,66	2250
25	1692626	0,86	2250

Peak	Midpoint/bp	Avg height	Width/bp
37	2104126	0,68	10750
38	2121626	0,58	3250
39	2140876	0,61	2750
40	2249501	0,64	2500
41	2278126	0,85	1750
42	2307751	1,03	2000
43	2338751	0,57	2500
44	2375626	0,58	2750
45	2408001	0,56	3000
46	2546876	0,73	8250
47	2738876	0,92	3250
48	2857376	0,53	3750
49	2899126	0,63	2750
50	2979376	1,00	1750
51	3113751	0,86	3500
52	3132376	0,73	2750
53	3204626	0,72	2250
54	3234751	0,45	3500
55	3322126	0,73	6750
56	3351751	0,64	3500
57	3465501	0,59	4000
58	3613251	0,55	3000
59	3777751	0,70	2500
60	3833126	0,98	1750
61	3881376	0,54	2750

26	1734501	0,64	2500
27	1751626	1,16	5250
28	1785376	0,90	2750
29	1847001	0,77	2500
30	2005001	1,18	2500
31	2019626	0,63	2250
32	2042001	0,97	5000
33	2065001	0,51	3000
34	2073501	0,90	2500
35	2080876	0,68	2250
36	2091251	0,96	11500

62	3898001	0,79	2000
63	3916876	0,79	3750
64	4005251	0,51	4000
65	4047751	0,94	5500
66	4057251	0,58	4500
67	4066501	0,64	2500
68	4197876	1,02	2750
69	4243876	1,11	2750
70	4311126	0,55	2750
71	4345626	0,64	2750
72	4396376	1,13	1750

7.3 The condensin binding pattern along fission yeast chromosome 2

Cnd2-Pk_9 *nda3-KM311* cells (Y252) were grown in rich YE4S medium at 32°C and arrested in metaphase by shifting the culture for 6 hours to 20°C, the restrictive temperature of the *nda3-KM311* allele. ChIP was performed against the Pk-tagged condensin subunit. Peak-picking parameters were as described in the 'Mis4 and Ssl3 binding pattern along fission yeast chromosome 2' in Appendix 7.12. Significant peaks are depicted as solid blue bars. Explanations of symbols in the maps can be found in Appendix 7.1.1. The map can be viewed on the following pages.

Cnd2-Pk$_9$, metaphase (*nda3-KM311)*

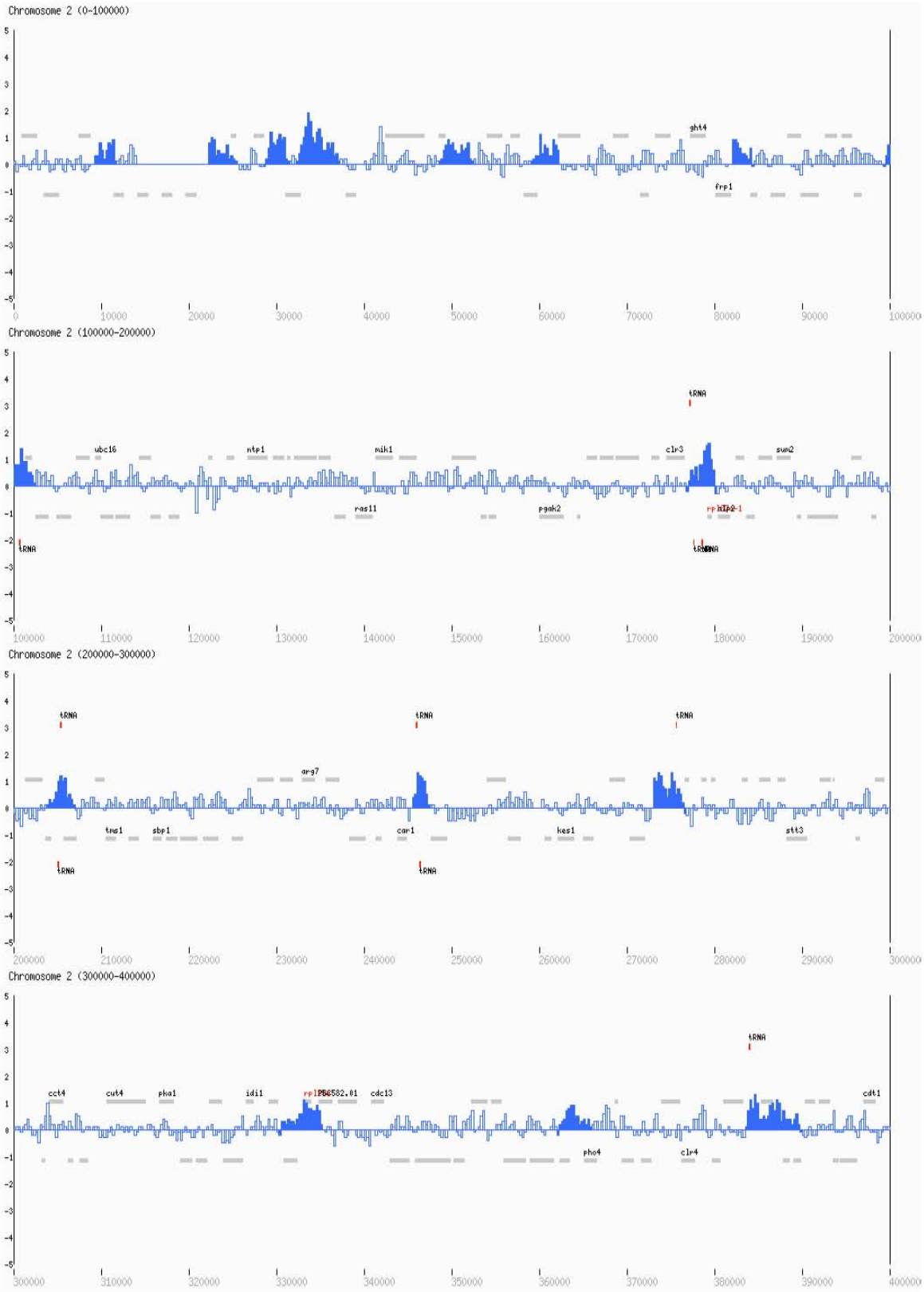

Cnd2-Pk$_9$, metaphase (*nda3-KM311)*

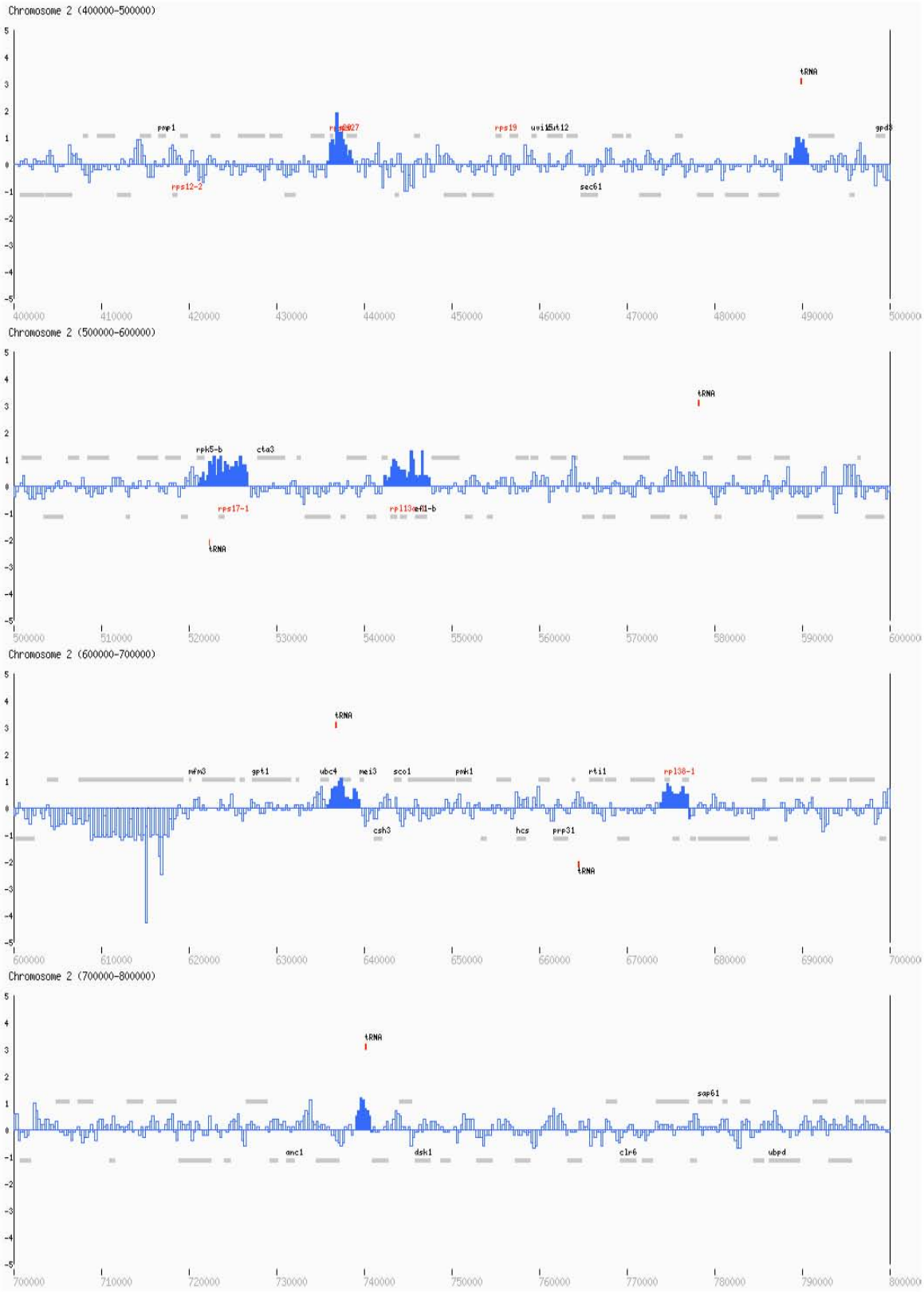

Cnd2-Pk$_9$, metaphase (*nda3-KM311)*

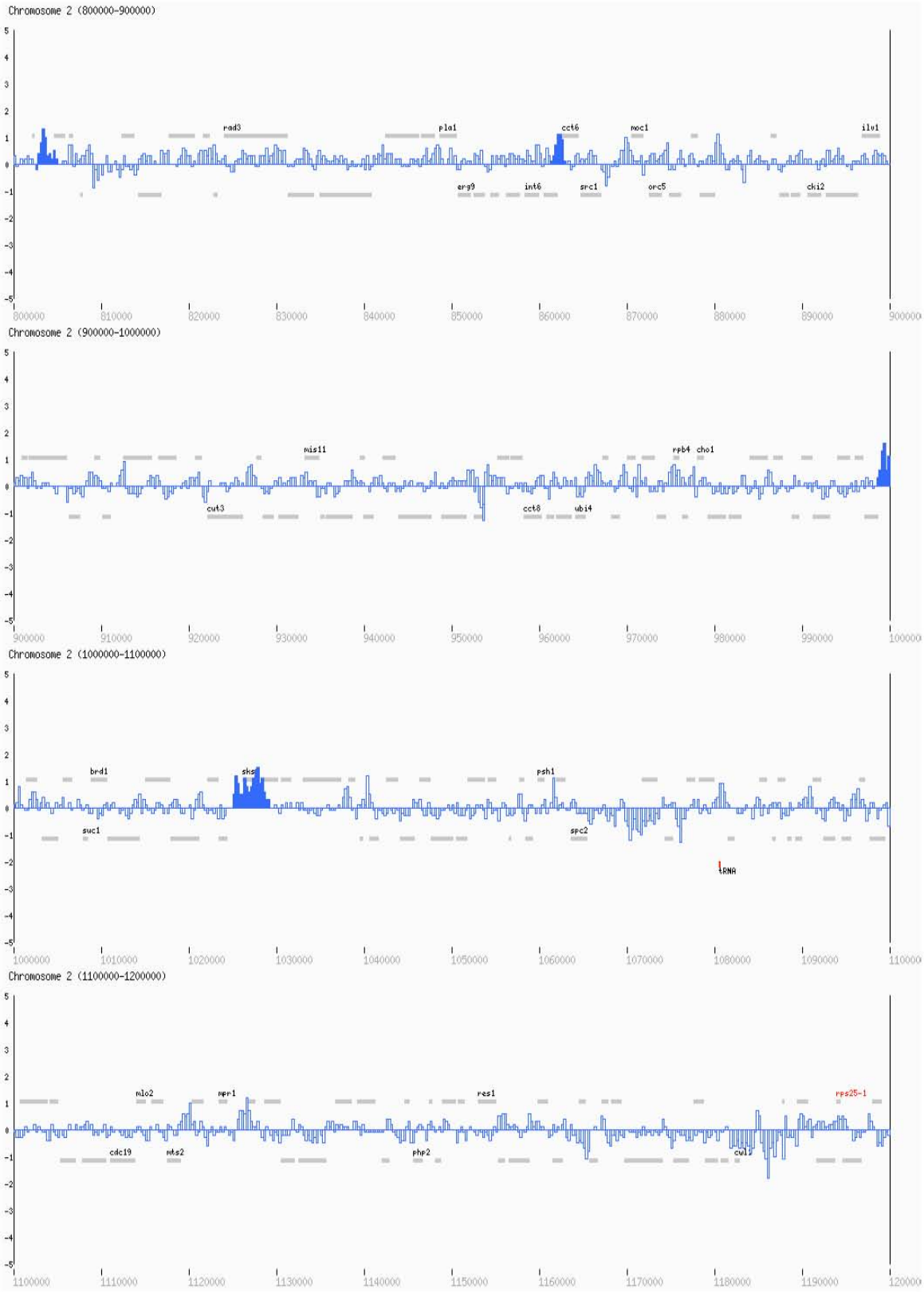

Cnd2-Pk$_9$, metaphase (*nda3-KM311)*

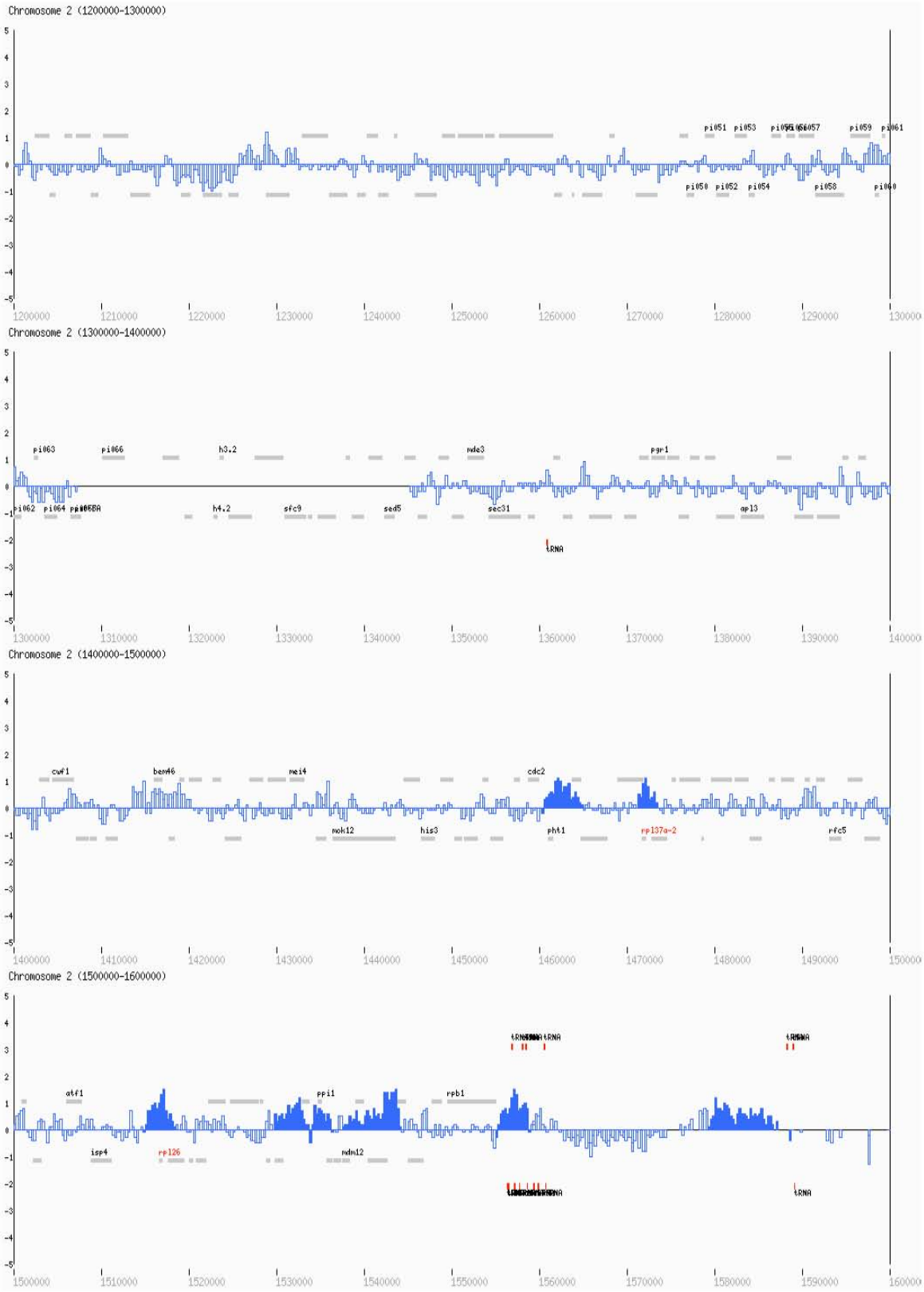

Cnd2-Pk$_9$, metaphase (*nda3-KM311)*

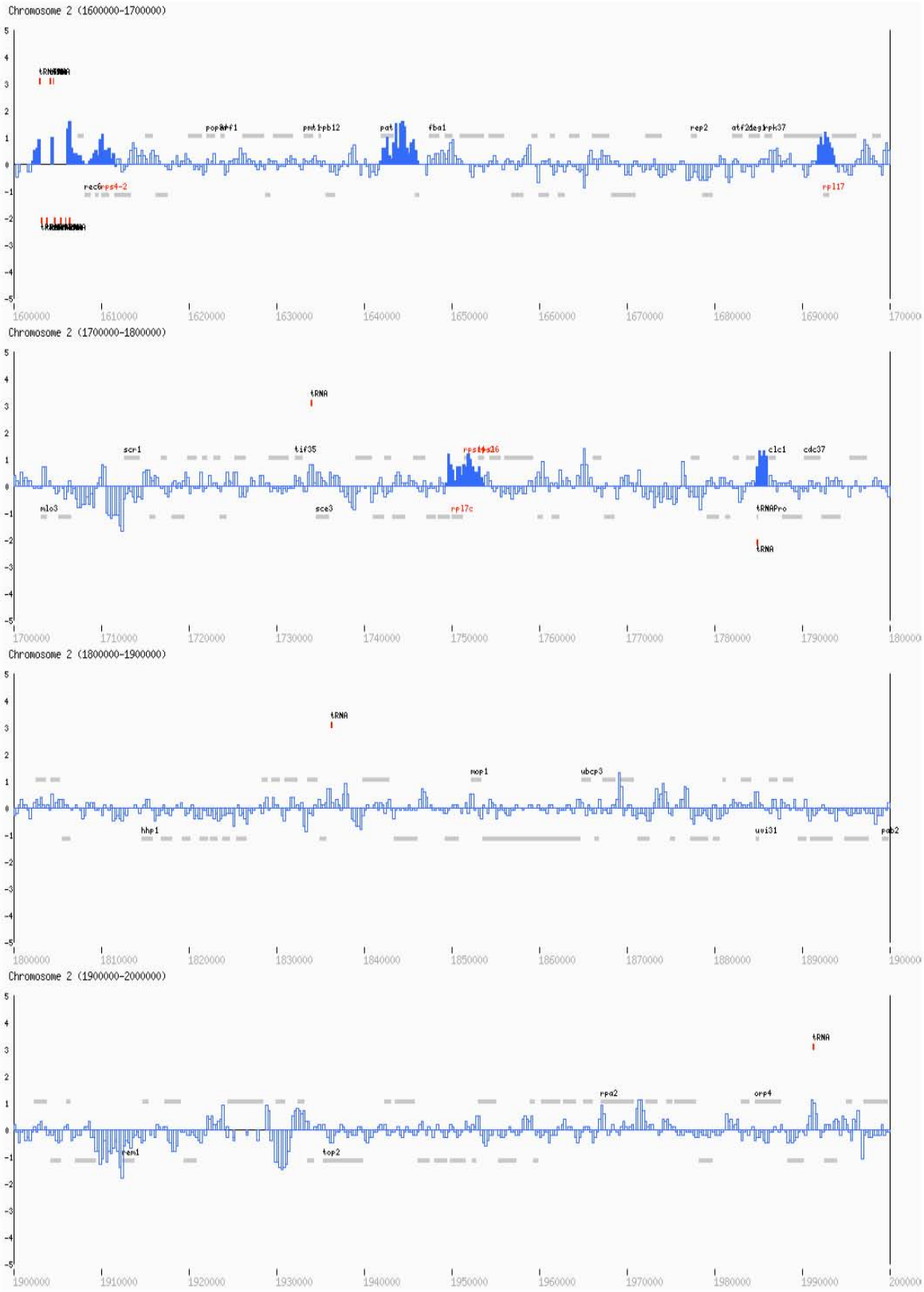

Cnd2-Pk$_9$, metaphase (*nda3-KM311)*

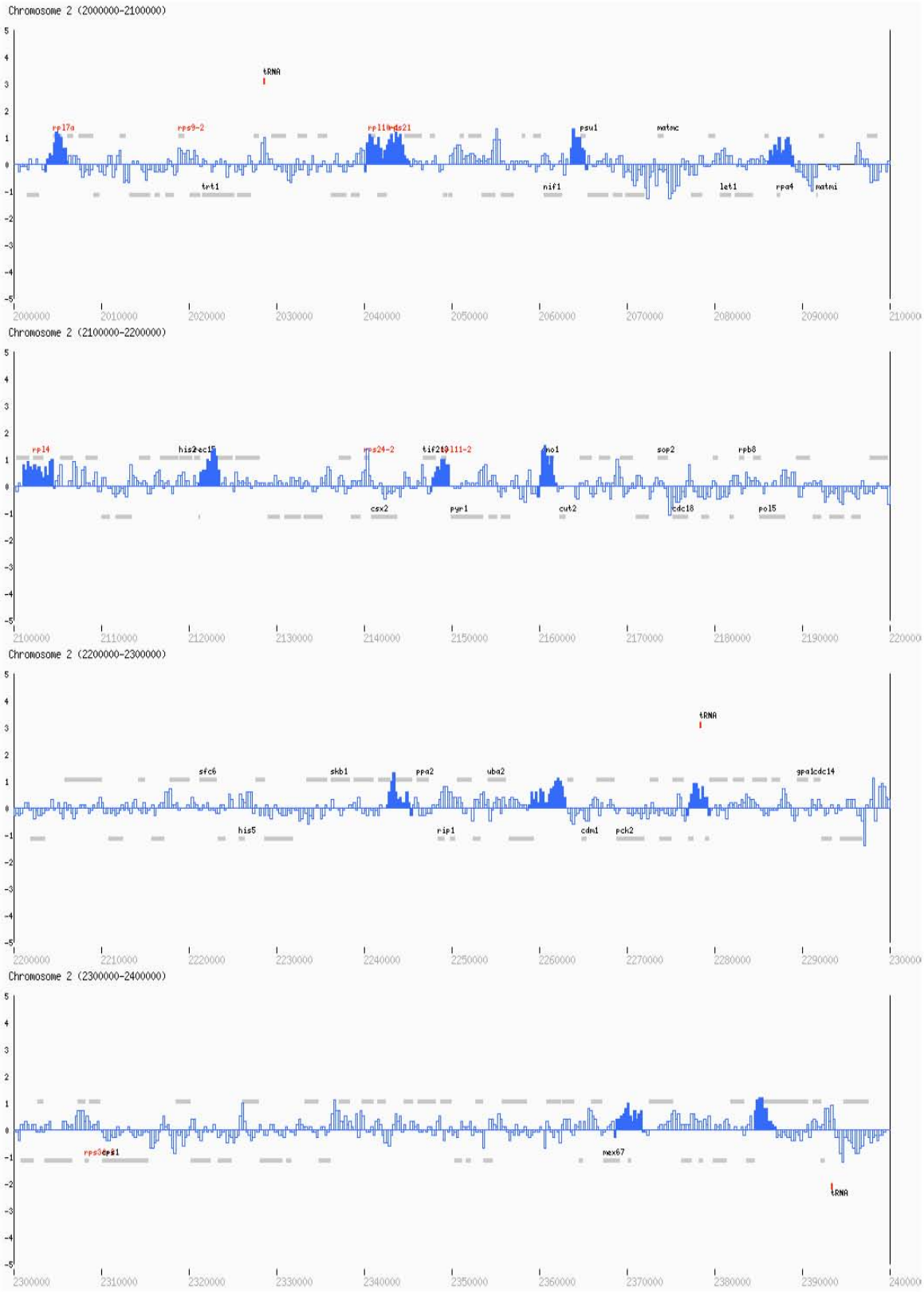

Cnd2-Pk$_9$, metaphase (*nda3-KM311)*

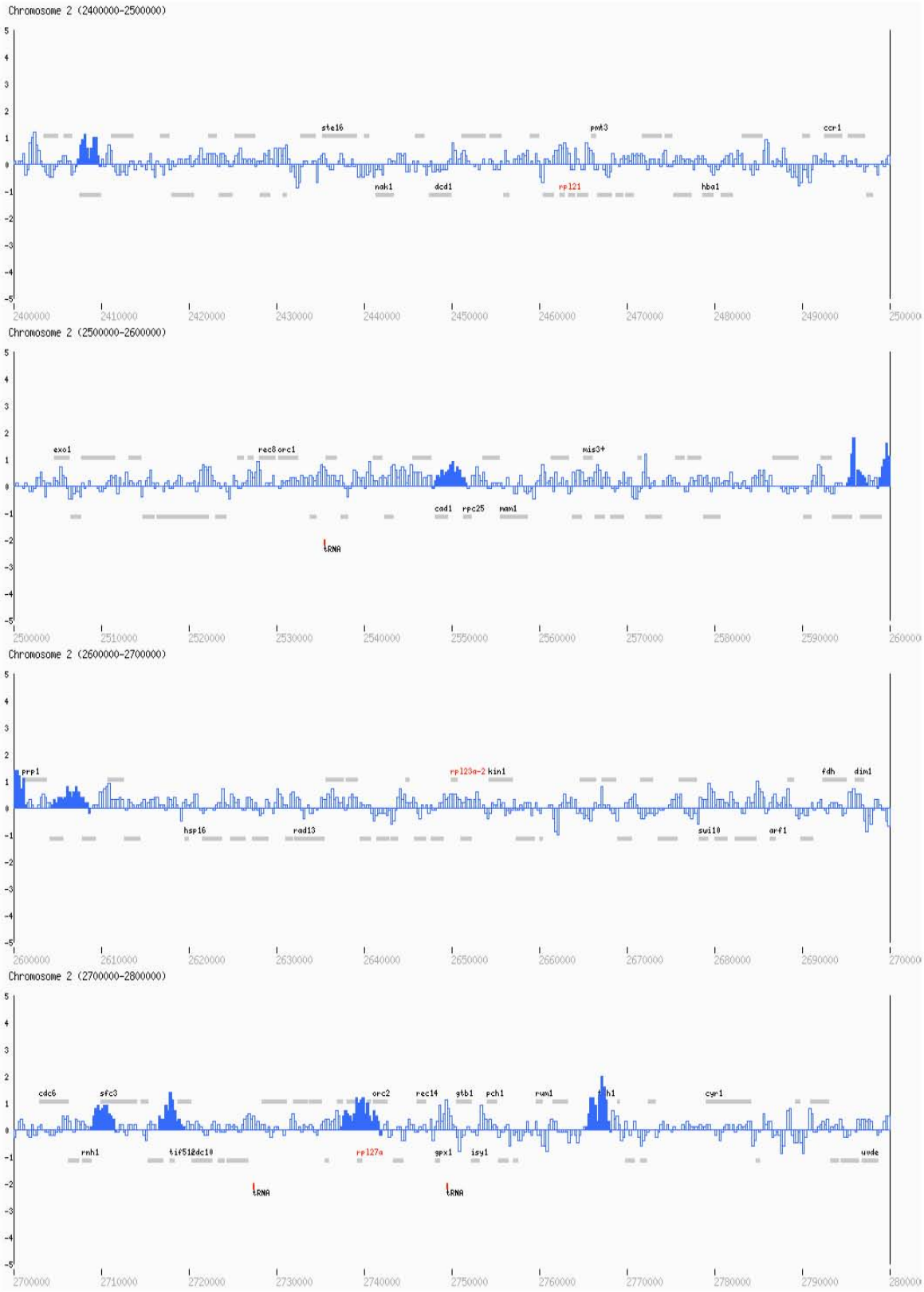

Cnd2-Pk$_9$, metaphase (*nda3-KM311)*

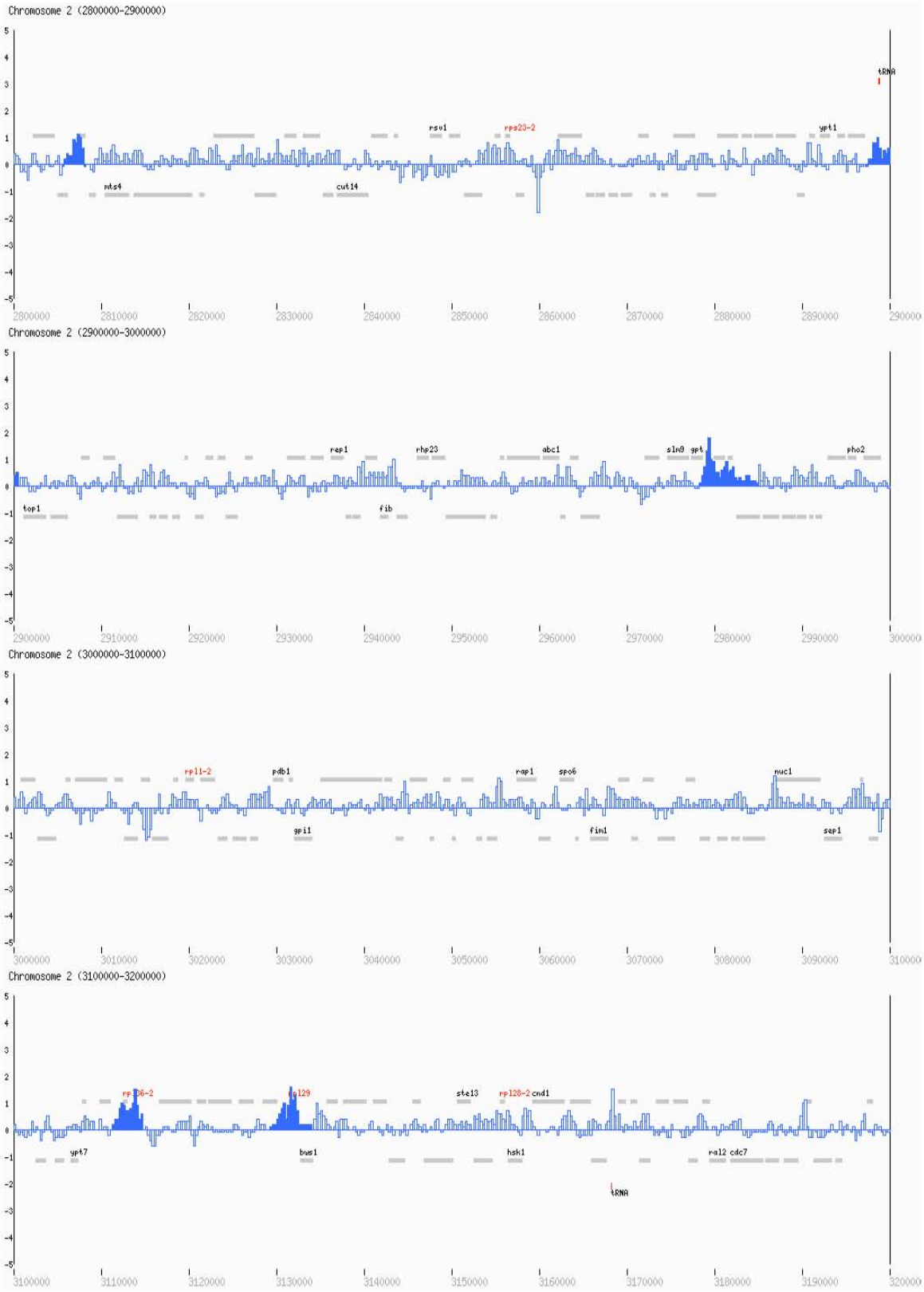

Cnd2-Pk$_9$, metaphase (*nda3-KM311)*

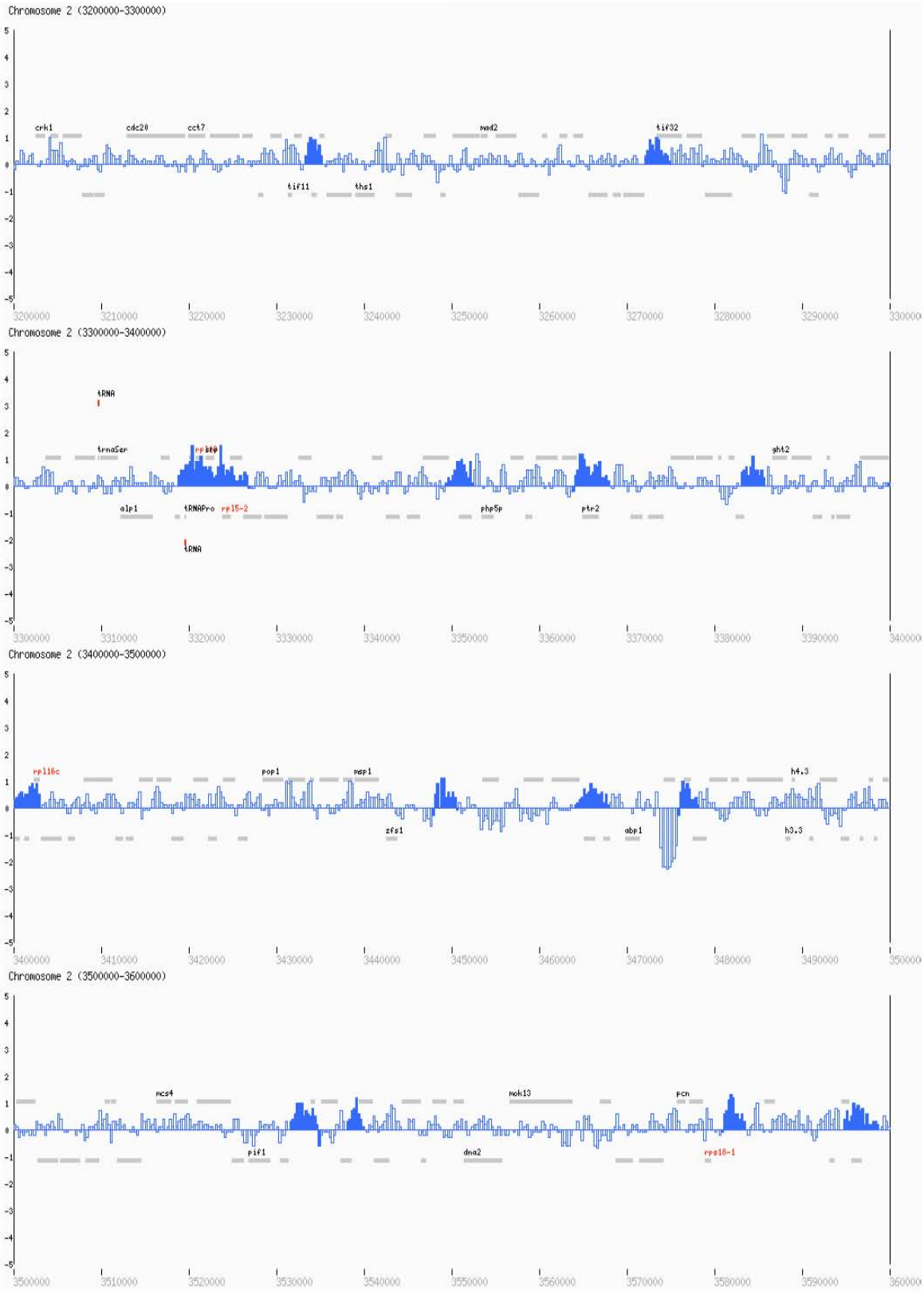

Cnd2-Pk$_9$, metaphase (*nda3-KM311)*

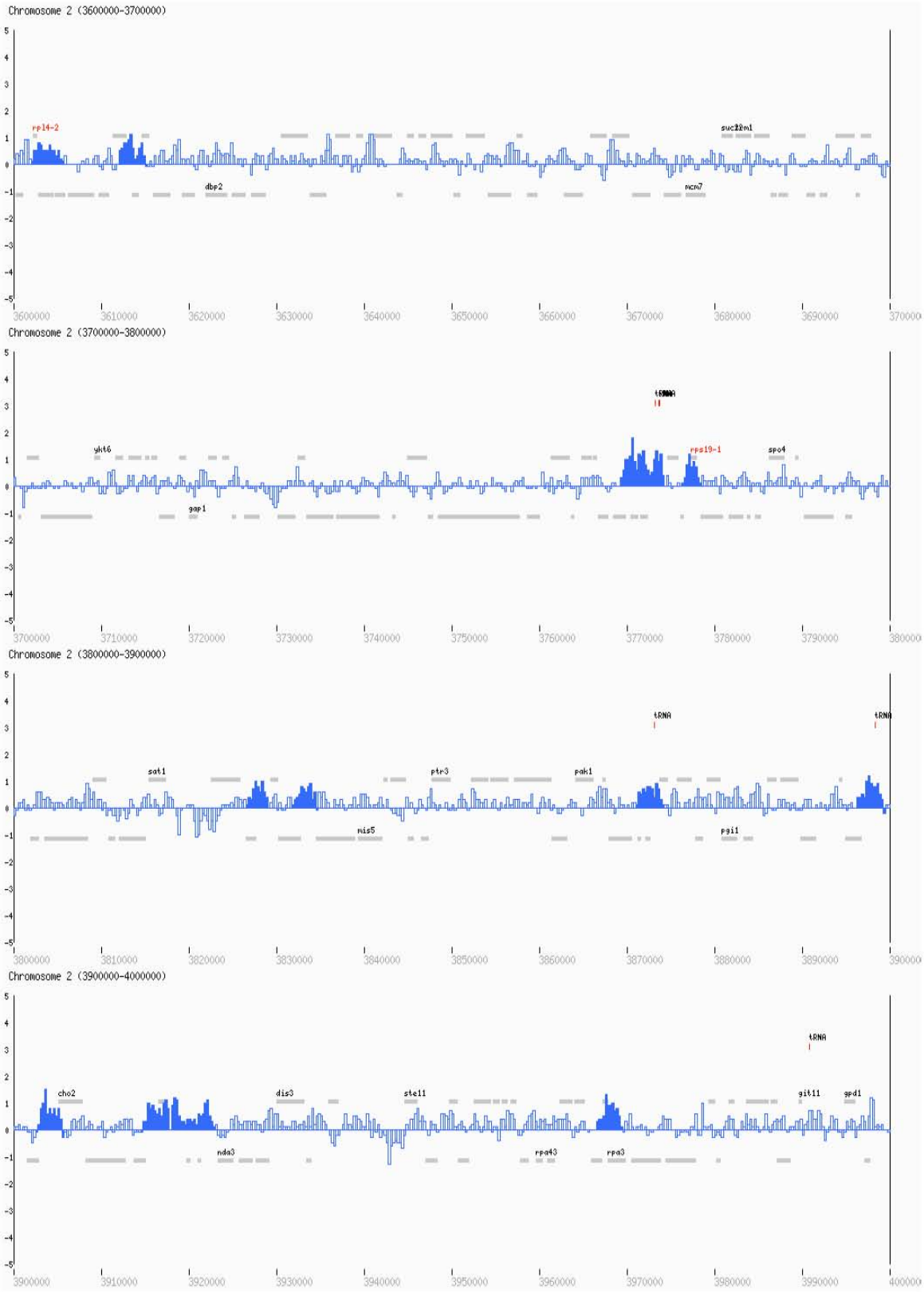

Cnd2-Pk$_9$, metaphase (*nda3-KM311)*

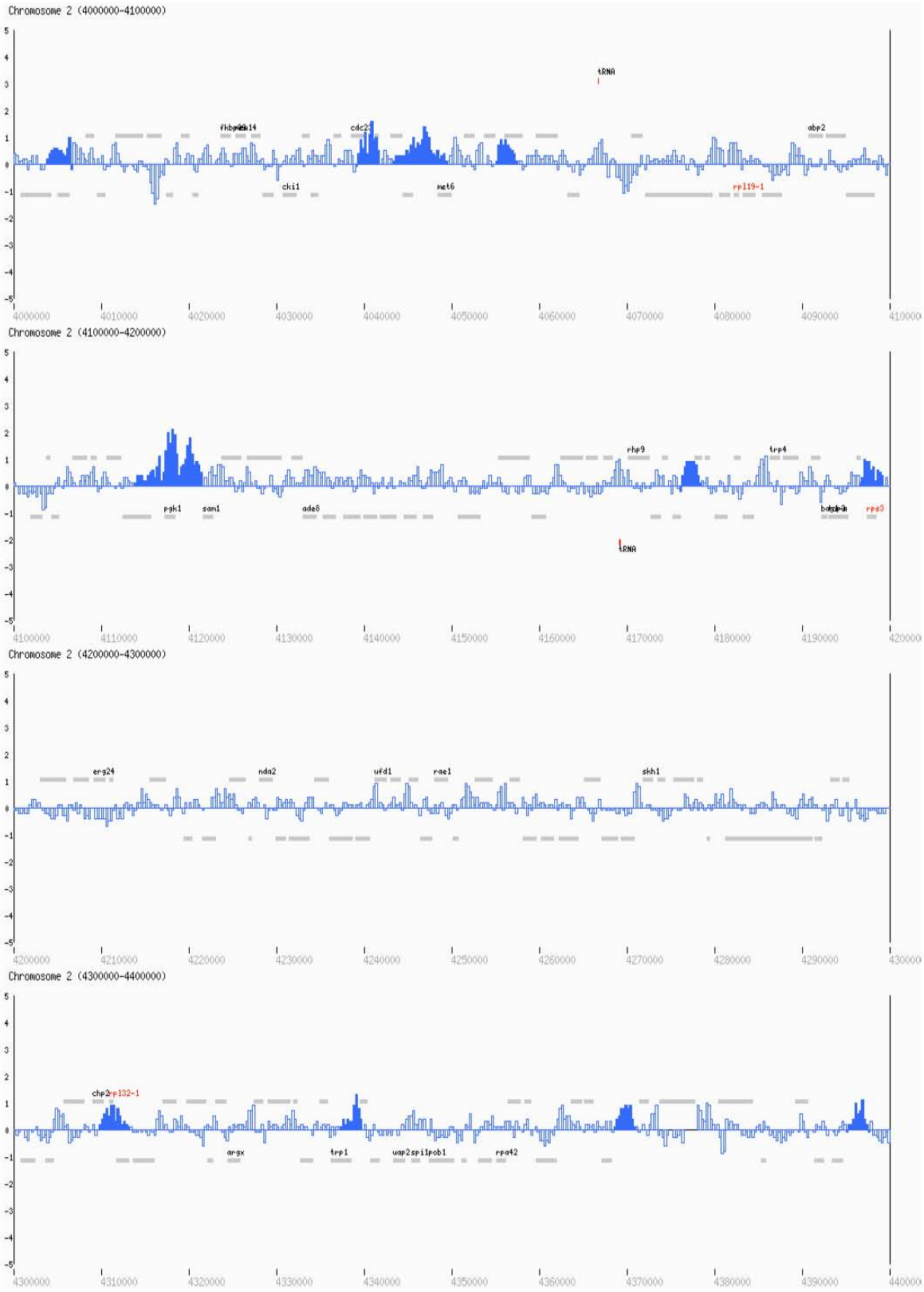

Cnd2-Pk$_9$, metaphase (*nda3-KM311)*

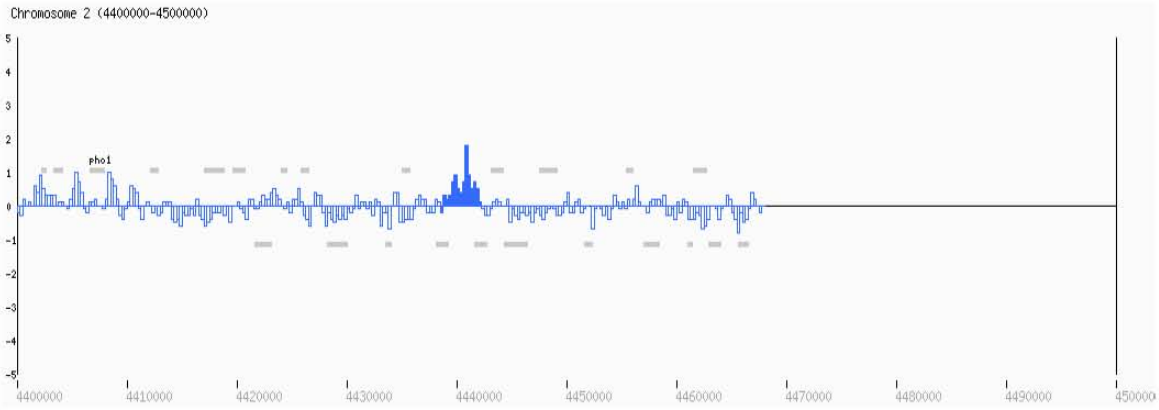

7.4 Sfc6 binding pattern along fission yeast chromosome 2

Sfc6-Pk_9 cells (Y3359) were grown exponentially in rich YE4S medium at 25°C and processed for ChIP against the Pk-tagged Sfc6 subunit of the TFIIIC RNA Pol III transcription factor. Symbols and peak-picking parameters were as described in the ‘Mis4 and Ssl3 binding pattern along fission yeast chromosome 2’ in Appendix 7.1. Further explanations of symbols in the maps can be found in Appendix 7.1.1. Significant peaks are marked as solid turquoise bars and can be viewed on the following pages.

Sfc6-Pk$_9$, cycling

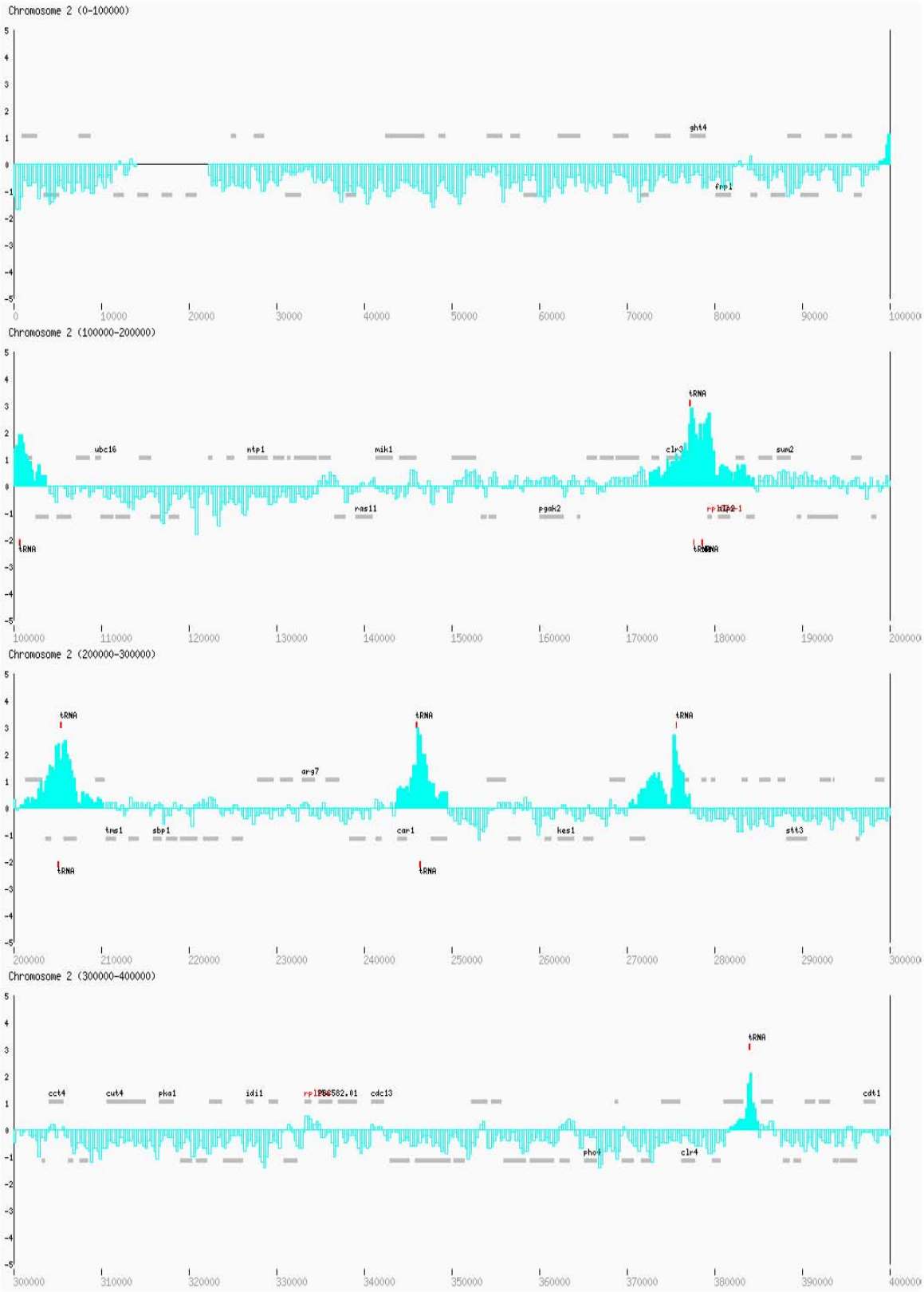

Sfc6-Pk$_9$, cycling

Sfc6-Pk$_9$, cycling

Sfc6-Pk9, cycling

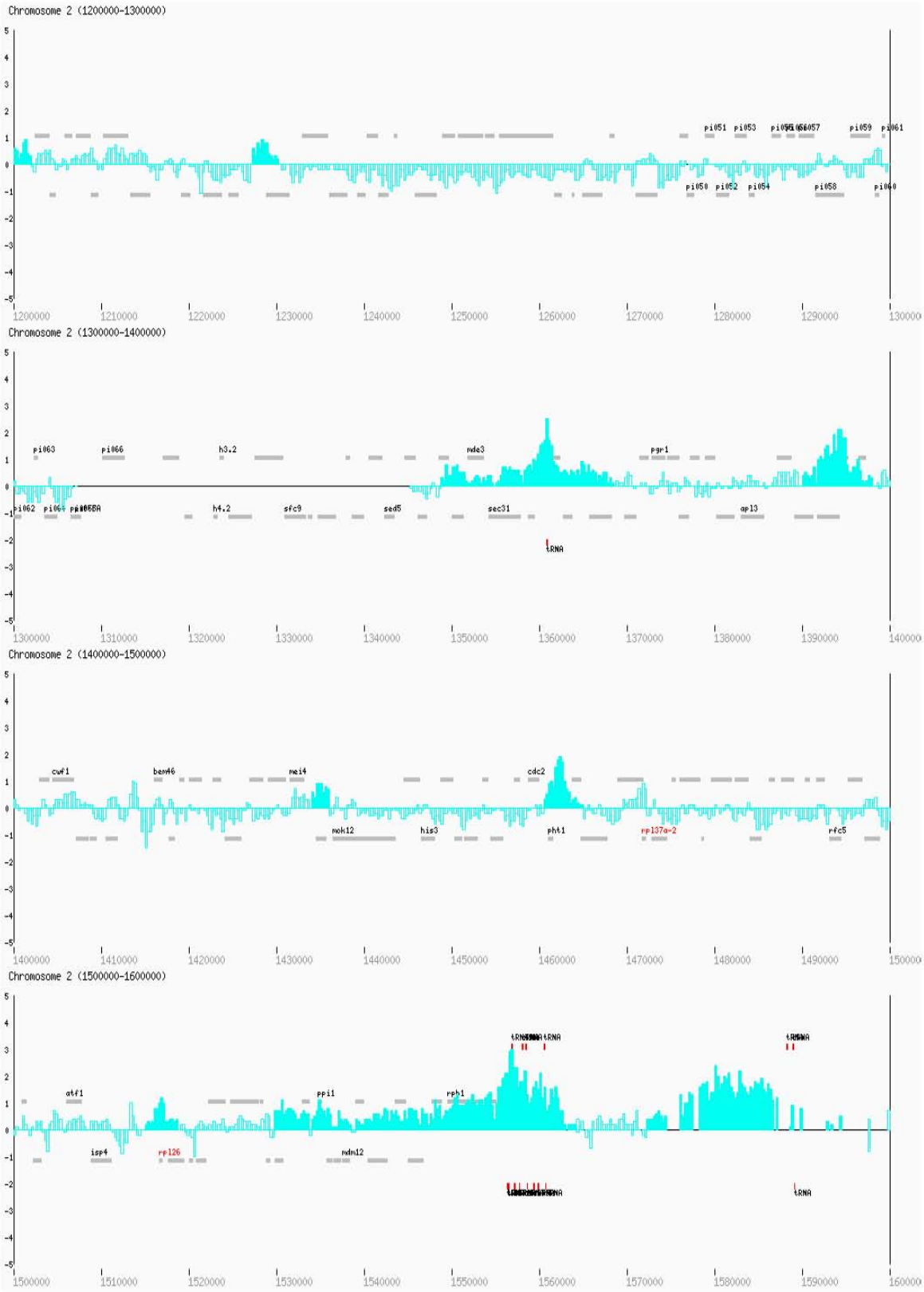

Sfc6-Pk9, cycling

Sfc6-Pk$_9$, cycling

Sfc6-Pk$_9$, cycling

Sfc6-Pk9, cycling

Sfc6-Pk9, cycling

Sfc6-Pk$_9$, cycling

Sfc6-Pk$_9$, cycling

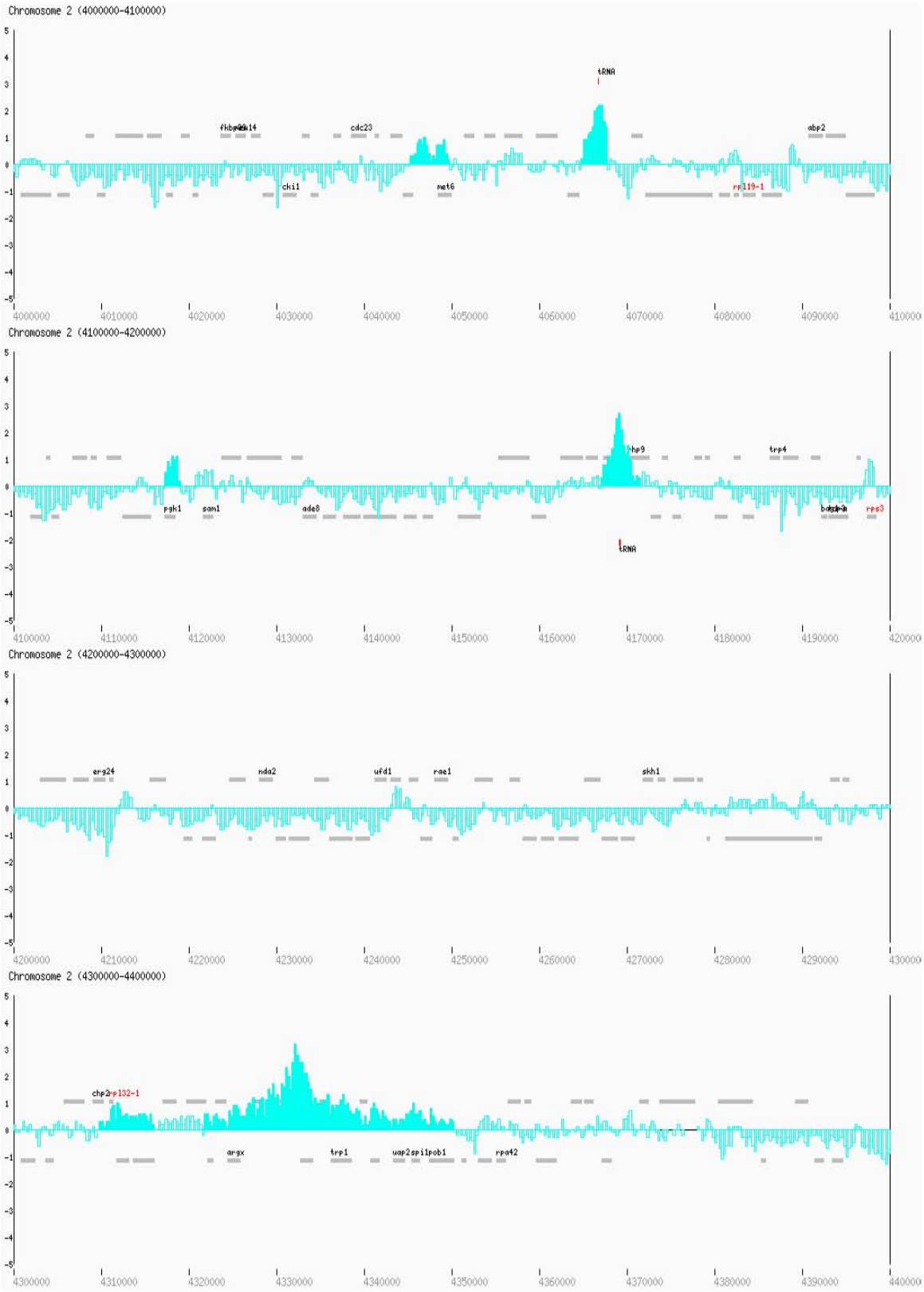

Sfc6-Pk9, cycling

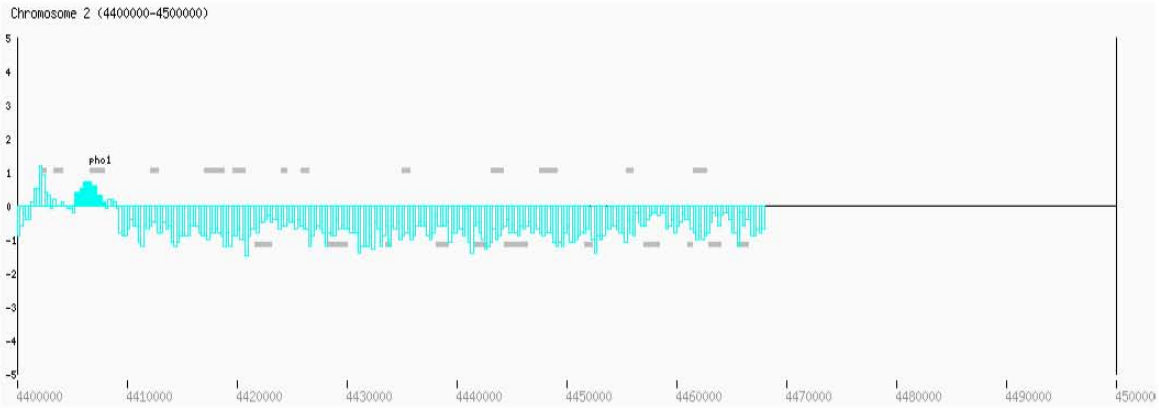

7.5 Fhl1 binding pattern along fission yeast chromosome 2

Fhl1-Pk_9 cells (Y3403) were grown exponentially in rich YE4S medium at 25°C and processed for ChIP against the Pk-tagged protein. Peak-picking parameters were as described in the ‘Mis4 and Ssl3 binding pattern along fission yeast chromosome 2’ in Appendix 7.2. Explanations of symbols in the maps can be found in Appendix 7.1.1. Significant peaks are shown as solid yellow bars. The entire chromosome 2 map can be viewed on the following pages.

Fhl1-Pk$_9$, cycling

Fhl1-Pk$_9$, cycling

Fhl1-Pk$_9$, cycling

Fhl1-Pk$_9$, cycling

Fhl1-Pk$_9$, cycling

Fhl1-Pk$_9$, cycling

Fhl1-Pk$_9$, cycling

Fhl1-Pk$_9$, cycling

Fhl1-Pk$_9$, cycling

Fhl1-Pk$_9$, cycling

Fhl1-Pk$_9$, cycling

Fhl1-Pk9, cycling

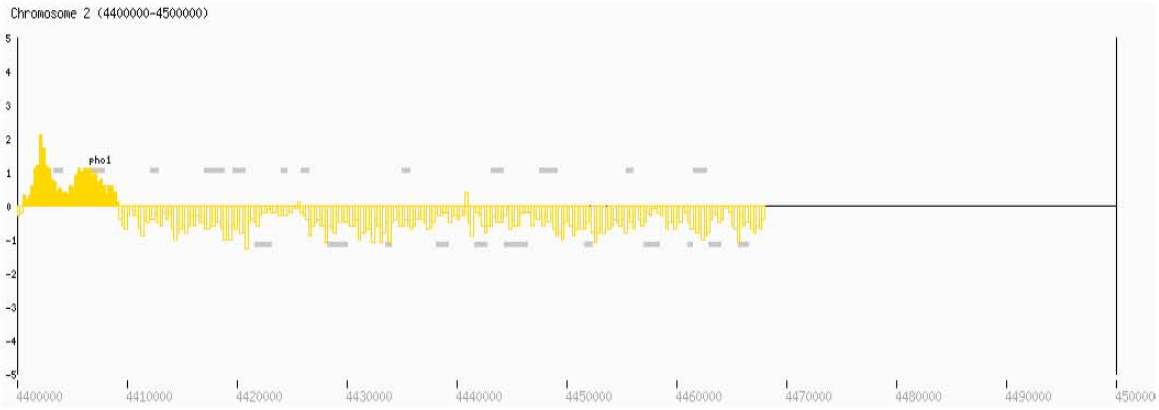

8 Acknowledgements

First of all, I would like to thank my supervisor Frank Uhlmann for continuous support of this project throughout the last 4 years. It has been a very stimulating experience working in the Chromosome Segregation Lab and has widened my scientific horizon to a great extent. I very much appreciated, that I could always walk into the office and immediately get helpful opinions and suggestions on any problem no matter how big or small, if of theoretical or of practical nature (and there were quite a few of all of them ☺). This has helped a lot - thanks very much!

I would next like to thank all the people in the lab - present members as well as past members. It was a great pleasure sharing a lab with you, and I hope I will stay in touch with many of you in the future. Special thanks to Chris who has been magnificent in organising the lab and who has always been extremely helpful no matter what problems had to be solved - thanks a lot for that! Thanks to Julia, Chris and Maria for proof-reading parts of this thesis. Armelle, I would like to thank, for introducing me to the ChIP on chip procedure in the beginning.

I would also like to thank all the people in the surrounding fission yeast labs - Julie Cooper's, Jacky Hayles' and Takashi Toda's lab - without whom it would have been impossible to establish the various fission yeast techniques and get the first strains to start the project. Special thanks go to Miguel who took a lot of time especially in the beginning to explain the basics. I would like to thank Kazu for tips and tricks and for strains and plasmids, all of which was and is very much appreciated. All the great discussions with Thomas have been very refreshing - thank you!

A very big thank you goes to Igor for his help, especially in the last couple of weeks. It would not have been the same without this support, and I will almost miss working late hours together at the desk.

Last but not least, I would like to thank my parents. Through all the years they have been of incredible support, and it was great to be able to share the hard as well as the good times. Thank you very, very much for that - I appreciate every single bit of it!